

FEBRUARY 15, 1990

# Analytical CHEMISTRY

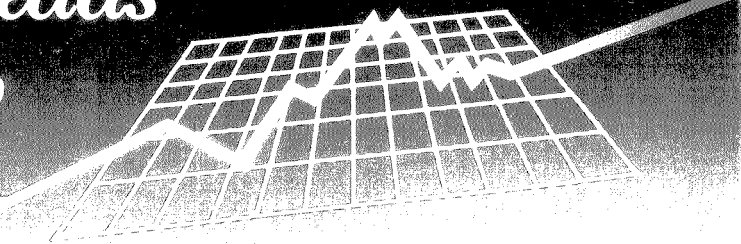


## ULTRAFAST SPECTROSCOPY

270 A

# Spectroscopy for Research..

## SLM Leads the Way



SLM Instruments is the leader in the innovative design and manufacture of spectrophotometers and spectrofluorometers for research. From our introduction of fluorescence polarization and time-resolved spectroscopy using the T-Optics™ lightpath, to our patented dual wavelength system, to the world's only multi-harmonic fast Fourier-transform fluorometer, we continue to explore and expand the frontiers of spectroscopy.

*Our comprehensive line of instruments and accessories answers the demands of the widest range of research applications:*

### *Fluorescence Polarization and Lifetime Spectroscopy*

Highest sensitivity in its class

- T-Optics polarization
- Dual emission wavelengths
- Simultaneous multiparameter measurements
- Photon counting, analog, and millisecond kinetics on each of three channels
- **SLM 8000C™ Photon Counting Spectrofluorometer**

Circle 124

Picosecond lifetimes • Dynamic depolarization • Phase resolved spectroscopy • Three-frequency, continuous, and multi-harmonic fast Fourier-transform instruments

- **SLM 4800C™ and SLM 4800S™ Lifetime Spectrofluorometers and SLM 4800MHF™ Multi-harmonic Fourier Fluorometer**

Circle 125

### *Fluorescence in an Integrated Package*

Outstanding sensitivity and resolution • Complete scanning, ratio-metric, and timebase capabilities

- Keyboard or computer control
- **SPF-500C™ Spectrofluorometer**

Circle 126

### *Dual Wavelength UV-Visible Spectrophotometry*

Simplifies difficult analyses such as turbid samples, highly scattering samples, whole tissue preparations, and other complex systems • Dual wavelength and split beam modes • Millisecond reaction rate studies • Stand-alone operation or computer control

- **DW-2000™ Dual Wavelength UV-Visible Spectrophotometer**

Circle 127

### *Intracellular Calcium Measurements*

Designed for dual wavelength fluorescent probes • Simultaneous multiple probe measurements

- Unmatched specifications
- **DMX-1000™ Multiparameter Cation Measuring Spectrofluorometer**

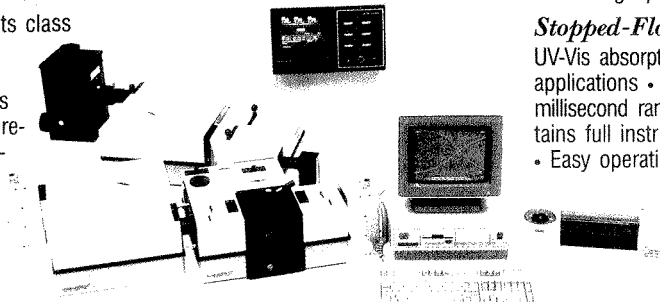
Circle 128

### *Stopped-Flow Kinetics*

UV-Vis absorption and fluorescence applications • For reactions in the millisecond range or longer • Maintains full instrument capabilities

- Easy operation

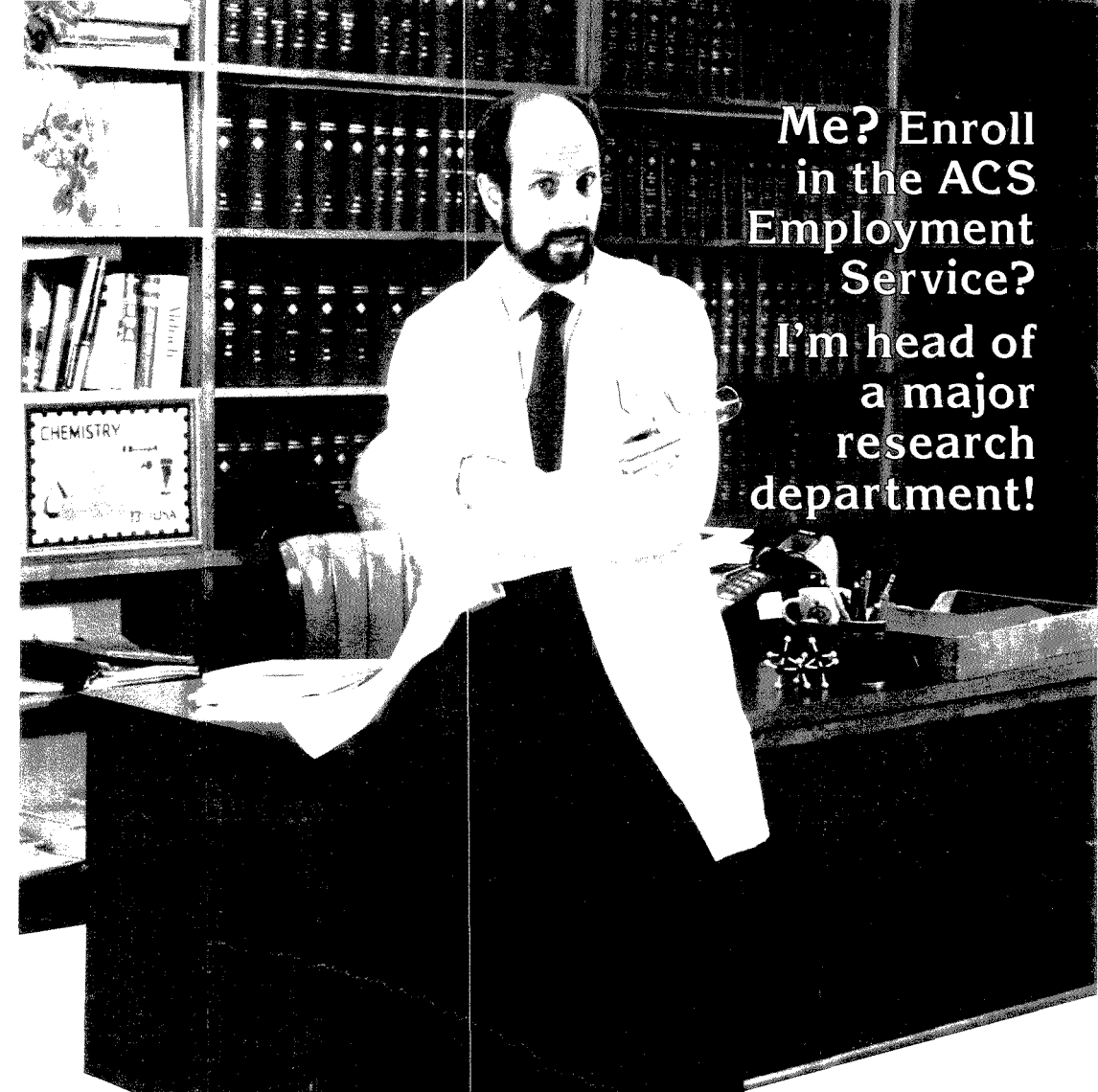
Circle 129



*Use the Reader Service Numbers, or call or write to us for more information on any SLM products.*

# SLM AMINCO®

SLM Instruments, Inc., 810 West Anthony Drive, Urbana, IL 61801  
(217) 384-7730 • (800) 637-7689 • Telex 206079 • FAX (217) 384-7744



**Me? Enroll  
in the ACS  
Employment  
Service?  
I'm head of  
a major  
research  
department!**

Even for the successful chemist or scientist in an allied field, sometimes the best way to get ahead is to make a change.

The ACS Employment Service offers the opportunity to investigate the possibilities discreetly—and at very low cost.

Our Employment Service is free to all ACS members. If you request confidentiality from current employers or other designated organizations there is a nominal charge.

For more information write, use coupon, or CALL TOLL FREE 800-227-5558

Employment Services Office,  
American Chemical Society  
1155 Sixteenth Street, NW,  
Washington, DC 20036

Yes. I am a member of ACS and I would like to learn how the ACS Employment Service can help me advance my career.

Name (please print) \_\_\_\_\_

Membership # \_\_\_\_\_

Address \_\_\_\_\_  
\_\_\_\_\_

City \_\_\_\_\_

State \_\_\_\_\_

ZIP \_\_\_\_\_

# For Over Six Decades...



## The Leader in the Field.

*ANALYTICAL CHEMISTRY*, the world's foremost publication in the vital field of measurement science, comes to you semi-monthly packed with *more* research articles, special features and application papers.

Keeping pace with the changes has continued to make *ANALYTICAL CHEMISTRY* the pinnacle of publications in the field . . . for over 6 decades.

For your personal subscription:

**CALL TOLL FREE (800) 227-5558 (U.S. only)**  
**Outside U.S. (202) 872-4363**

**Telex: 440159 UI**  
**89 2582 ACSPUBS**



American Chemical Society  
1155 16th St., NW  
Washington, DC 20036

Registered in U.S. Patent and Trademark Office;  
 Copyright 1990 by the American Chemical Society

ANALYTICAL CHEMISTRY (ISSN 0003-2700) is published semimonthly by the American Chemical Society at 1155 16th St., N.W., Washington, DC 20036. Editorial offices are located at the same ACS address (202-872-4570; FAX 202-872-4574; TDD 202-872-8733). Second-class postage paid at Washington, DC, and additional mailing offices. Postmaster: Send address changes to ANALYTICAL CHEMISTRY Member & Subscriber Services, P.O. Box 3337, Columbus, OH 43210.

Claims for missing numbers will not be allowed if loss was due to failure of notice of change of address to be received in the time specified; if claim is dated (a) North America: more than 90 days beyond issue date, (b) all other foreign: more than one year beyond issue date, or if the reason given is "missing from files."

**Copyright Permission:** An individual may make a single reprographic copy of an article in this publication for personal use. Reprographic copying beyond that permitted by Section 107 or 108 of the U.S. Copyright Law is allowed, provided that the appropriate per-copy fee is paid through the Copyright Clearance Center, Inc., 27 Congress St., Salem, MA 01970. For reprint permission, write Copyright Administrator, Publications Division, ACS, 1155 16th St., N.W., Washington, DC 20036.

Registered names and trademarks, etc., used in this publication, even without specific indication thereof, are not to be considered unprotected by law.

**Advertising Management:** Centcom, Ltd., 500 Post Rd. East, Westport, CT 06880 (203-226-7131)

1990 subscription rates include air delivery outside the U.S., Canada, and Mexico

	1 yr	2 yr
<b>Members</b>		
Domestic	\$ 29	\$ 49
Canada and Mexico	64	119
Europe	96	163
All Other Countries	118	227
<b>Nonmembers</b>		
Domestic	59	100
Canada and Mexico	94	170
Europe	186	336
All Other Countries	208	380

Three-year and other rates contact: Member & Subscriber Services, ACS, P.O. Box 3337, Columbus, OH 43210 (614-447-3776 or 800-333-9511).

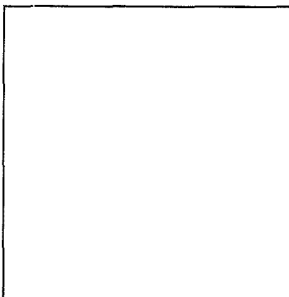
**Subscription orders by phone** may be charged to VISA, MasterCard, Barclay card, Access, or American Express. Call toll free 800-ACS-5558 in the continental United States; in the Washington, DC, metropolitan area and outside the continental United States, call 202-872-8065. Mail orders for new and renewal subscriptions should be sent with payment to the Business Management Division, ACS, P.O. Box 28597, Central Station, Washington, DC 20005.

**Subscription service inquiries and changes of address** (Include both old and new addresses with ZIP code and *recent mailing label*) should be directed to the ACS Columbus address noted above. Please allow six weeks for changes to become effective.

**ACS membership information:** Lorraine Bowlin (202-872-4567)

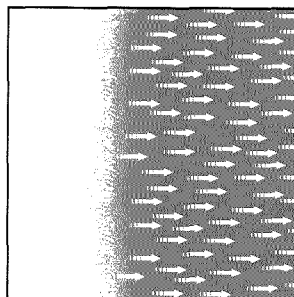
**Single issues**, current year, \$8.00 except review issue, \$14.00, and LabGuide, \$49.00; **back issues and volumes and microform editions** available by single volume or back issue collection. For information or to order, call the number listed for subscription orders by phone; or write the Microform & Back Issues Office at the Washington address.

**Nonmembers rates in Japan:** Rates above do not apply to nonmember subscribers in Japan, who must enter subscription orders with Maruzen Company Ltd., 3-10 Nihonbashi 2-chome, Chuo-ku, Tokyo 103, Japan. Tel: (03) 272-7211.



**REPORT 265 A**

**Preparative LC.** The goal of preparative LC is to separate mixtures so that the purified compounds can be used for other purposes. Maurits Verzele of the State University of Gent (Belgium) compares the technique with conventional LC and provides practical information for performing preparative separations



**INSTRUMENTATION 270 A**

**On the cover.** Ultrafast spectroscopy is receiving increasing attention from the analytical chemistry community, although it is far from being commonplace. Mary J. Wirth of the University of Delaware discusses spectroscopy on the ultrafast time scale (10 fs-100 ps) and predicts future developments in this area

**BRIEFS 258 A**

**NEWS 263 A**

EAS awards to Bard and Armstrong. ▶ Bower Science Award. ▶ Unpredictable earthquakes

**MEETINGS 279 A**

Conferences. ▶ Short courses and workshops. ▶ Call for papers

**BOOKS 281 A**

**Critical reviews.** Recently released books on electron microscopy and applied FT-IR spectroscopy are reviewed

**NEW PRODUCTS & MANUFACTURERS' LITERATURE 282 A**

**AUTHOR INDEX 321**

## Articles

### Nonionic Surfactants Used as Exact Mass Internal Standards for the 700–2100 Dalton Mass Range in Fast Atom Bombardment Mass Spectrometry 322

Low concentrations of monosubstituted poly(ethylene glycol) and poly(propylene glycol) nonionic surfactants and isolated oligomer fractions of monosubstituted poly(ethylene glycols), adulterated with alkali-metal salts, are routinely used as exact mass internal standards in the FAB peak matching mode for the mass range 700–2100 daltons.

**Marshall M. Siegel\***, **Rushung Tsao**, and **Steven Oppenheimer**, American Cyanamid Company, Medical Research Division, Lederle Laboratories, Pearl River, NY 10965 and **T. T. Chang**, American Cyanamid Company, Chemical Research Division, Stamford, CT 06902

### Chromatographic Oligomer Separation of Poly(oxyethylenes) on $K^+$ -Form Cation-Exchange Resin 327

A separation method for poly(oxyethylene) chains based on the number of oxyethylenes and complexation with  $K^+$  is proposed. The complex formation constants are also chromatographically determined.

**Tetsuo Okada**, Faculty of Liberal Arts, Shizuoka University, Shizuoka 422, Japan

### Evaluation of the Effect of Organic Modifier and pH on Retention and Selectivity in Reversed-Phase Liquid Chromatographic Separation of Alkaloids on a Cyclodextrin Bonded Phase 332

A mathematical model is developed using a basic equilibrium-driven approach to explain the effect of mobile-phase composition on the relative retention of ionizable solutes. Three specific cases involving different organic modifiers, different pHs, and different solute  $pK_a$ s as well as one general case are considered.

**Daniel W. Armstrong\***, **Gary L. Bertrand**, **Karen D. Ward**, and **Timothy J. Ward**, Department of Chemistry, University of Missouri—Rolla, Rolla, MO 65401 and **Henry V. Secor** and **Jeffrey I. Seeman\***, Philip Morris Research Center, P.O. Box 26583, Richmond, VA 23261

### Development of a Method for the Sampling and Analysis of Sulfur Dioxide and Nitrogen Dioxide from Ambient Air 338

Triethanolamine-impregnated filters and ion chromatography are used to sample  $SO_2$  and  $NO_2$  with sub-ppb detection limits. Precision estimates better than  $\pm 15\%$  are found, and accuracy within  $\pm 10\%$  is observed.

**Joseph E. Sickles, II\***, **Peter M. Grohse**, **Laura L. Hodson**, **Cynthia A. Salmons**, **Kelly W. Cox**, **Ann R. Turner**, and **Eva D. Estes**, Research Triangle Institute, Research Triangle Park, NC 27709

### Non-Steady-State Gas Chromatography Using Capillary Columns 347

Limiting activity coefficients are measured for diverse systems using non-steady-state GC with a wall-coated capillary column.

**Anatoly J. Belfer**, BP Research, Warrensville Research Center, 4440 Warrensville Center Road, Cleveland, OH 44128 and **David C. Locke\*** and **Isaac Landau**, Chemistry Department, Queens College and The Graduate School, CUNY, Flushing, NY 11367

### Pulse Voltammetric Techniques at Microelectrodes in Pure Solvents 349

Pulse voltammetry is applied to the reduction of decyl, butyl, and ethyl iodide at mercury microelectrodes in propylene carbonate without added electrolyte.

**Malgorzata Ciszowska** and **Zbigniew Stojek**, Department of Chemistry, Warsaw University, ul. Pasteura 1, 02-093 Warsaw, Poland and **Janet Osteryoung\***, Department of Chemistry, State University of New York, University of Buffalo, Buffalo, NY 14214

### Gas Sorption to Plasma-Polymerized Copper Phthalocyanine Film Formed on a Piezoelectric Crystal 353

Piezoelectric quartz crystals are covered with plasma-polymerized phthalocyanines. The possibility of a long-lived (more than 60 days) stable gas sensor with a sub-ppm level detection limit for various organic gases is demonstrated.

**Shigeru Kurosawa**, **Naoki Kamo\***, **Daijyu Matsui**, and **Yonosuke Kobatake**, Faculty of Pharmaceutical Sciences, Hokkaido University, Sapporo 060, Japan

### Binding Studies Using Ion-Selective Electrodes. Examination of the Picrate-Albumin Interaction as a Model System 360

ISEs are used to study the binding of ligands to macromolecules. A computer program that performs nonlinear least-squares fitting of the generalized Scatchard model is used to calculate the binding parameters.

**Theodore K. Christopoulos**, Laboratory of Analytical Chemistry, University of Athens, 104 Solonos Street, Athens 106 80, Greece and **Eleftherios P. Diamandis\***, Department of Clinical Biochemistry, Toronto Western Hospital, 399 Bathurst Street, Toronto, Ontario M5T 2S3, Canada

\*Corresponding author

---

---

---

---

---

*Backed by  
Matheson's  
more than 60 years  
of experience.*

Questionable quality of standard gases or calibration mixtures is intolerable. Purity and consistency are the by-words of the analytical chemist.

Matheson's experience and reputation as a supplier of the highest quality laboratory gases and mixtures eliminate uncertainty. Each Matheson UHP, Zero Gas, and Matheson Purity Gas is guaranteed to be exactly what the label says. Nothing more. Nothing less. Matheson Primary Standards are of the highest accuracy. Our complex calibration standards required in gas chromatography are the benchmark of the industry. And, our gas handling equipment will never jeopardize the integrity of our gases.

So whether your work is in the field of pharmaceuticals, petroleum, lasers, or aerospace... insist on quality. Insist on Matheson.

## APPLICATIONS

### Atomic Absorption Spectroscopy

### Calibration Standards

Primary Standards  
Certified Standards

### Gas Chromatography Detectors

DID Discharge Ionization Detector  
ECD Electron Capture Detector  
FID Flame Ionization Detector  
FPD Flame Photometric Detector  
GADE Gas Density Detector  
HECD Hall Electroconductivity Detector  
HID Helium Ionization Detector  
NPD Nitrogen Phosphorus Detector  
PID Photoionization Detector  
TCD Thermal Conductivity Detector  
TID Thermionic Ionization Detector

### Supercritical Fluid Chromatography

### Medical / Biological

Blood Gas Analysis  
Pulmonary Function  
Surgical Lasers  
Biological Atmospheres

### Flame Photometry

### Nuclear Counters

### Emissions Testing

E.P.A. Protocol

### Burner Calibration (BTU Verification)

### Leak Detection

 **Matheson®**  
**Gas Products**  
World Leader in Specialty Gases & Equipment  
30 Seaview Dr., Secaucus, NJ 07096-1587  
FAX: (201) 867-4572

**Transport of Catechols through Perfluorinated Cation-Exchange Films on Electrodes** 367

The influence of solution parameters (buffer concentration, pH, and methanol concentration) on the distribution constants and diffusion coefficients of catecholamines and related compounds in Nafion films on electrodes is studied. Diffusion coefficients in the film are in the  $10^{-7}$  cm<sup>2</sup>/s range. **Anna J. Tüdös, Wim J. J. Ozinga, Hans Poppe, and Wim Th. Kok\***, Laboratory for Analytical Chemistry, University of Amsterdam, Nieuwe Achtergracht 166, 1018 WV Amsterdam, The Netherlands

**Thin-layer Chromatography with Supersonic Jet Fluorometric Detection** 374

The sample, separated by thin-layer chromatography, is directly laser desorbed for jet expansion, allowing for the determination of the excitation spectrum and visualization of the chromatogram for chemical species directly on the TLC plate.

**Totaro Imasaka, Katsunori Tanaka, and Nobuhiko Ishibashi\***, Faculty of Engineering, Kyushu University, Hakozaki, Fukuoka 812, Japan

**Optimization of Separations in Supercritical Fluid Chromatography Using a Modified Simplex Algorithm and Short Capillary Columns** 378

A method development scheme for SFC is described that includes selection of response functions and optimization variables. Initial separations are performed on short capillary columns for rapid analysis and subsequently transferred to a longer column when necessary.

**Jeffrey A. Crow and Joe P. Foley\***, Department of Chemistry, Louisiana State University, Baton Rouge, LA 70803

**Determination of Iodine in Oyster Tissue by Isotope Dilution Laser Resonance Ionization Mass Spectrometry** 386

The concentration of iodine in SRM 1566a, oyster tissue, is 4.44 µg/g with an overall uncertainty of ±0.12 µg/g. Relative measurement precision is 1.4% for oyster tissue.

**J. D. Fasset\* and T. J. Murphy**, Center for Analytical Chemistry, National Institute of Standards and Technology, Gaithersburg, MD 20899

**Dual-Beam, Light-Scattering Interferometry for Simultaneous Measurements of Droplet-Size and Velocity Distributions of Aerosols from Commonly Used Nebulizers** 390

Dual-beam, light-scattering interferometry is used for the simultaneous measurement of droplet-size and droplet velocity distributions. The technique is tested by characterizing tertiary aerosols produced by five nebulization systems.

**R. H. Clifford, Izumi Ishii, and Akbar Montaser\***, Department of Chemistry, George Washington University, Washington, DC 20052 and **G. A. Meyer**, Analytical Sciences, Building 1897, Dow Chemical Company, Midland, MI 48667

**Kinetic Approach to the Measurement of Chemical Oxygen Demand with an Automated Micro Batch Analyzer** 395

An automated micro batch analyzer system continuously monitors the absorbance of Cr(VI) at 140 °C in 50% H<sub>2</sub>SO<sub>4</sub> and extrapolates results to produce final chemical oxygen demand values.

**Purnendu K. Dasgupta\* and Kaj Petersen**, Department of Chemistry and Biochemistry, Texas Tech University, Lubbock, TX 79409-1061

**Optimization of Multienzyme Flow Reactors for Determination of Acetylcholine** 402

Various immobilization methods are used to achieve improved detection limits for the determination of acetylcholine through optimized enzyme reactor performance.

**P. Chandrani Gunaratna and George S. Wilson\***, Department of Chemistry, University of Kansas, Lawrence, KS 66045

**Correspondence****Multichannel Electrochemical Detection System for Flow Analysis** 407

**Tomokazu Matsue\*, Atsushi Aoki, Eiji Ando, and Isamu Uchida\***, Department of Molecular Chemistry and Engineering, Faculty of Engineering, Tohoku University, Aoba, Sendai 980, Japan

**Lanthanum Hexaboride Electron Emitter for Electron Impact and Electron-Induced Dissociation Fourier Transform Ion Cyclotron Resonance Spectrometry** 409

**Eric L. Kerley, Curtiss D. Hanson, and David H. Russell\***, Department of Chemistry, Texas A&M University, College Station, TX 77843

**Technical Notes****Elimination of Power Line Noise from Transient Signals by Selective Triggering** 412

**Emilie Lassing and Vernon D. Parker\***, Department of Chemistry and Biochemistry, Utah State University, Logan, UT 84322-0300

**Real-Time Monitoring of Iodine in Process Off-Gas by Inductively Coupled Plasma-Atomic Emission Spectroscopy** 414

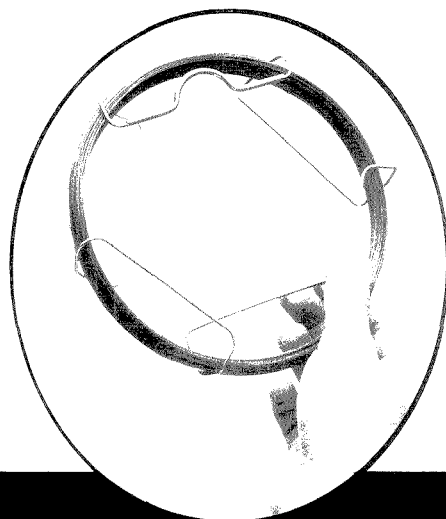
**Toshihiro Fujii\*, Takashi Uehiro, and Yukihiko Nojiri**, National Institute for Environmental Studies, Tsukuba, Ibaraki 305, Japan and **Yoshihiro Mitsutsuka and Hitoshi Jimba**, Department of Chemistry, The Meisei University, Hodokubo, Hino 191, Japan



*Now . . .*

## You Can Separate Complex Hydrocarbon Mixtures and Get . . .

- High Resolution
- High Efficiency
- Reproducibility



Our *Petrocol™ DH Column* is specifically designed and tested for detailed GC hydrocarbon analysis. You can separate closely eluting isomers and light hydrocarbon gases, or achieve detailed separations of highly complex mixtures.

Each 100M fused silica column is rigorously tested to ensure highly consistent polarity and film thickness. This testing includes retention index

measurements of key aromatic compounds (retention index tables are included with each column). Now you can be assured of consistent column-to-column performance.

For more information, call our Technical Service Department at 814-359-3041 and ask for our new *Petroleum/Chemical Applications Guide*.

Fused silica columns manufactured under HP US Pat. No. 4,293,415.

**To Order, Call: 800-247-6628**

**TWX: 510-670-3600 FAX: 814-359-3044**

CIRCLE 135 ON READER SERVICE CARD

Pittsburgh Conference Booth #s 4541 & 4542



**SUPELCO**

SEPARATIONS TECHNOLOGIES GROUP  
DIVISION OF ROHM AND HAAS

ENVIRONMENTAL SCIENCE & TECHNOLOGY

ES&T



**Editor, William H. Glaze**  
University of North Carolina,  
Chapel Hill

**Call TOLL FREE 800/227-5558**  
**Outside U.S. 202/872-4363**  
**Telex 440159 ACSP UI or**  
**89 2582 ACSPUBS**  
**TWX 710-822-0151**

**American Chemical Society**  
1155 Sixteenth Street NW  
Washington, DC 20036 USA

For nonmember rates in Japan, contact  
Maruzen, Co. Ltd.

**The premiere  
research  
publication in the  
environmental  
field.**

ES&T continues to give you the practical hard facts you need on environmental science . . . covering research, techniques, feasibility, products, and services.

Dealing with the chemical nature of water, air, and waste makes ES&T essential reading for environmental scientists both in the business and academic world.

Each monthly issue presents new knowledge and promotes scientific inquiry in such areas as the chemical nature of the environment and environmental changes through pollution or other modifications.

Also included are discussions on environmental analyses, governmental regulations, current environmental lab activities, and much more!

## EAS Awards

The Eastern Analytical Symposium (EAS) has announced two of the awards to be presented at its November meeting. Allen Bard will receive the Award for Outstanding Achievement in the Fields of Analytical Chemistry, and Daniel Armstrong will be given the Award in Chromatography.



**Allen Bard**, who is Hackerman/Welch Regents Chair at the University of Texas at Austin, received his B.S. degree (1955) from City College of New York and his M.A. degree (1956) and Ph.D. (1958) from Harvard University. His research interests include electroanalytical chemistry, electrode kinetics and mechanisms, electrogenerated chemiluminescence, photoelectrochemistry, and modified electrodes.

**Daniel Armstrong** received his B.S. degree (1972) from Washington & Lee University and his M.S. degree (1974) and Ph.D. (1977) from Texas A&M University. He is professor of chemistry and head of the Bioanalytical Research Institute and the Division of Analytical Chemistry at the University of Missouri—Rolla. His current work includes specific detection of enantiomers, computer modeling in molecular recognition, and the development of new analytical techniques.



## Franklin Institute's New Award

A \$7.4 million bequest to Philadelphia's Franklin Institute has established a new international award in science. The award is a bequest of Henry Bower, a one-time Philadelphia chemical manufacturer, and will be presented annually beginning this year. Institute officials hope the Bower Science Award will carry the same prestige as the Nobel prizes. Bower's bequest also establishes an award for business leadership.

The science awardee will be selected by a board of advisers drawn from 30 nations. The winner will receive at least \$250,000 and a gold medal.

Bower was the third generation to own and direct the Henry Bower Chemical Manufacturing Company (named for his grandfather) until his retirement in 1975. Having no heirs or other family members interested in the business, he sold the company and devoted himself to philanthropic causes until his death in 1988.

Nominations for the science award are accepted from institutions or individuals. For more information, contact Larry Tise, Executive Director, Benjamin Franklin National Memorial, The Franklin Institute, 20th and the Benjamin Franklin Parkway, Philadelphia, PA 19103 (215-488-1329). Deadline is April 17, the bicentennial of Benjamin Franklin's death.

## Unpredictable Quakes

Computer simulations by Cornell researchers suggest that earthquakes behave chaotically and therefore are inherently unpredictable. Jie Huang and Donald Turcotte found that their model of interconnected earthquake faults exhibited what is known as deterministic chaos, or behavior infinitely sensitive to initial conditions.

The two geologists studied earthquake faults with a well-known computer model that simulates the sticking and slipping as crustal plates slide past each other. The program mimics plate tectonics with two blocks, connected by springs, that slide on a surface driven back and forth by springs to a third driving block. To better model real faults, Huang and Turcotte ran the simulation with inhomogeneous friction. Because this system displayed chaos, the more complex system of actual earthquake faults will also be chaotic.

If the results hold up, then geologists may have to abandon their dream of predicting earthquakes. Explains Turcotte, "Earthquake prediction will have to be approached like the prediction of storms, from a probabilistic point of view."

## For Your Information

The American Institute of Chemical Engineers has established a **Center for Waste Reduction Technologies** to coordinate efforts to reduce rather than just treat pollution. The center will act as a focal point for research, information, and technology exchange among industries, government, and universities.

**Thomas Layloff**, director of the U.S. Food and Drug Administration's St. Louis Division of Drug Analysis, has been **elected president of the Association of Official Analytical Chemists**. Layloff received A.B. (1958) and M.A. (1961) degrees from Washington University and a Ph.D. (1963) from the University of Kansas.

**Ciba-Geigy** has announced that it **plans to sell Spectra-Physics and GRETAG**, a Swiss-based manufacturer of electronic and photo-finishing equipment.

The **National Institute of Standards and Technology (NIST)** has prepared a **new standard for measuring exhaust emissions from motor vehicles**. Each standard contains certified concentrations of propane, carbon monoxide, and carbon dioxide in nitrogen gas. For more information, contact the Office of Standard Materials, NIST, Rm. 204, Bldg. 202, Gaithersburg, MD 20899 (301-975-2762).

**Christopher Lowe**, director of Biotechnology at the University of Cambridge, has received the **Pierce Award in Affinity Chromatography**. The award for outstanding contributions to the field was presented at the International Symposium on Affinity Chromatography and Biological Recognition last year.

Here's Why Two Esteemed, Technical Societies Want *Your* Expertise...

The American Chemical Society & American Institute of Chemical Engineers  
Announce their 1990 co-publication of

# BIOTECHNOLOGY PROGRESS

Editor, Jerome S. Schultz, *University of Pittsburgh*

## SUBMIT YOUR PAPERS NOW TO THIS IMPORTANT "NEW" PUBLISHING MEDIUM

*Beginning January 1990 BIOTECHNOLOGY PROGRESS*, a well-established journal of the American Institute of Chemical Engineers, will become a joint publication of the American Chemical Society and AIChE. As a collaborative effort, several significant changes will occur, *providing enhanced editorial coverage and expanded readership*. These include:

- **Accelerated frequency** — from quarterly to bimonthly issues!
- **A redesigned format** which will better meet the needs of both new and current subscribers.
- **A redefined editorial focus** guaranteed to attract:
  - 1) additional topical papers and primary research findings
  - 2) an audience comprising the very experts *you* want to reach!

## ATTENTION CHEMISTS, LIFE SCIENTISTS, AND ENGINEERS!

*In bimonthly issues*, BIOTECHNOLOGY PROGRESS will provide the latest concepts — in genetics...microbiology and biochemistry...molecular and cellular biology...chemistry and chemical engineering — as they apply to the development of processes, products, and devices. Emphasis will be placed on the *application of fundamental engineering principles* to the *analysis* of biological phenomena involved.

BIOTECHNOLOGY PROGRESS will be of particular interest to *practitioners of R&D in process development, product development, and equipment/instrumentation design for the biotechnology/bioprocess industry*. Its coverage will encompass food, pharmaceutical, and biomedical arenas.

## LOOK FOR HIGHLY TARGETED TOPICS LIKE THESE

- **Applied Biochemistry:** Equilibrium data, protein conformations in solution, mapping of molecular surfaces.
- **Applied Molecular Biology:** Cell physiology, gene expression, protein transport, metabolic engineering.
- **Bioreactor Technology:** Reactor engineering, mechanical engineering, materials science, process control, biosensors.
- **Biocatalytic Processes:** Site specific mutagenesis, enzyme kinetics, cofactor regeneration, applied pharmaceutical kinetics.
- **Formulation and Product Delivery.**
- **Bioanalysis:** Online monitoring, containment, containment monitoring, offline analysis, statistical analysis (nonlinear regression, multifactor analysis).
- **Bioseparations.**

## ADDRESS YOUR MANUSCRIPT SUBMISSIONS & AUTHOR INQUIRIES TO:

Jerome S. Schultz  
Editor, BIOTECHNOLOGY PROGRESS  
Center for Biotechnology and Bioengineering  
University of Pittsburgh  
911 William Pitt Union  
Pittsburgh, PA 15260  
Telephone: 412/648-7956 Fax: 412/624-7145

To receive editorial updates please write:  
American Chemical Society, Marketing,  
BIOTECHNOLOGY PROGRESS, Room 609,  
1155 Sixteenth St., N.W., Washington, D.C. 20036  
FAX: 202/872-6005  
Telex: 440159 ACSP UI or 89 2582 ACSPUBS

## Preparative Liquid Chromatography

---

### Maurits Verzele

Laboratory of Organic Chemistry  
State University of Gent  
Krijgslaan 281 (S4)  
B-9000 Gent  
Belgium

---

Interest in preparative liquid chromatography (LC) is reflected by several recent events, including a series of international symposia, the seventh of which (Prep-90) will be held in Gent, Belgium, in April, and the appearance of a journal and several books devoted to the subject (1-3).

When Michael Tswett began to perform chromatography at the beginning of the century, he used an adsorbent as a stationary phase and a nonpolar solvent as the developing fluid. (This form of chromatography is known today as "normal-phase" LC.) The preparative aspects of Tswett's work were first exploited by organic chemists who used preparative LC to isolate natural compounds on a preparative scale. As it developed, chromatography became an analytical tool to identify and quantify compounds in mixtures, but preparative LC continued to be used extensively in organic and pharmaceutical research laboratories where organic compounds and natural products were synthesized.

The first preparative LC separations to attract more general attention, about 30 years after the discovery of chromatography, were those of Kuhn and Winterstein (4, 5), followed by

Zechmeister and Cholnoky (6), Strain (7), and Karrer and Strong (8). These researchers separated gram amounts of mixtures of plant pigments (chlorophylls, xanthophylls, and carotenes) and other natural products (pepper-pungent compounds and capsanthin). All of these separations involved colored substances that could be easily detected in glass columns. When the separation was complete, the column packing material was pushed out of the column and the visible bands cut apart and extracted with a suitable solvent.

After World War II preparative LC evolved slowly. Slight pressure (less than 1 bar) was often applied, and step gradient elution (rinsing the column with solvents of increasing polarity) was used rather than column extrusion. Preparative thin-layer chromatography (TLC) also was used extensively. During this period, silica gel was introduced as a new stationary adsorbent and the particle size of the column packing material—which during Tswett's time was very small (1-10  $\mu\text{m}$ )—was increased to 200-500  $\mu\text{m}$ . UV spectrometry or TLC of the collected fractions was used for off-line detection. Such preparative LC in glass columns is still in use in many laboratories.

Although some very large-scale moving-bed industrial separations (9), such as those used for molasses or xylenes, could be called chromatography, these procedures are inefficient for phase exchange and are clearly different from high-performance preparative LC.

Interest in instrumental high-per-

formance preparative LC is, of course, the result of the development of instrumental high-performance analytical LC. This technique developed rapidly after 1970 thanks to the introduction of reliable high-pressure pumps, efficient on-stream detectors, and the reintroduction of smaller, fully porous silica gel particles (10). Chemical derivatization of silica gel stationary-phase particles also made modern instrumental LC more reliable and accessible for both analytical and preparative applications (11).

### Preparative vs. analytical LC

Because the goal of preparative LC is to separate mixtures so that the purified compounds can be used for other purposes, the mass throughput of the chromatographic system must be optimized. The amount of sample that can be separated depends on the column size, the relative retention of the compounds, and the capacity of the two-phase system.

With good column technology, the sample size is linearly proportional to the column or stationary-phase size. Thus columns of increased size are used when large samples are to be separated. It is not always easy, however, to achieve good column technology.

Relative retention, or alpha value, is the most important parameter in determining possible sample size. It is therefore essential to maximize this value, and time devoted to optimizing it will always be well spent. A general relationship between the alpha value

and sample size cannot be used because too many variables are involved. Figure 1 shows the relationship between resolution, the required plate number, and the alpha value. Clearly, alpha values of 1.1 are readily acceptable for analytical separations. This is not the case, however, for preparative LC, which is never performed under linear chromatographic conditions and for which column efficiency can be reduced because of sample overloading.

Figure 2 relates column efficiency with sample size for standard LC conditions. Large-particle columns are practically unaffected by sample size but are inefficient and cannot handle difficult separations. Modern small-particle columns are significantly affected by sample size but can handle a wider range of separation problems. Optimization of relative retention is thus very important in preparative LC.

Different chromatographic modes have different capacities, which also influence the amount of sample that can be separated. The capacity difference between adsorption and partition chromatography is small but slightly favors adsorption LC. The capacity of an ion-exchange column depends exclusively on the exchange capacity of the stationary phase, which can be as high as 5 meq/g; small ion-exchange systems are thus able to accommodate very high sample loading. Size exclusion chromatographic columns generally have very small sample capacities.

In analytical LC, compounds do not affect each other's partition ratio. There is ample room on the surface of the stationary phase and in the mobile phase to allow partitioning of the compounds in the mixture to proceed independently. The unavoidable concentration changes involve primarily the linear portion of the adsorption isotherm of all compounds. In such linear LC, the alpha values do not change during the chromatographic run, the peaks are symmetrical, and fundamental LC theory applies.

In preparative LC, however, the column is actually overloaded, and the full range of the nonlinear (primarily Langmuir) adsorption isotherm is involved. The peaks are not symmetrical, and the compounds interfere with each other's partitioning process. Because the number of adsorption sites on the stationary phase is limited, the competition for these sites leads to displacement effects, and fundamental partitioning theory must be adapted.

Guiochon's group at the University of Tennessee is studying this important area of modern preparative LC (12). They have determined that displacement effects can be exploited to

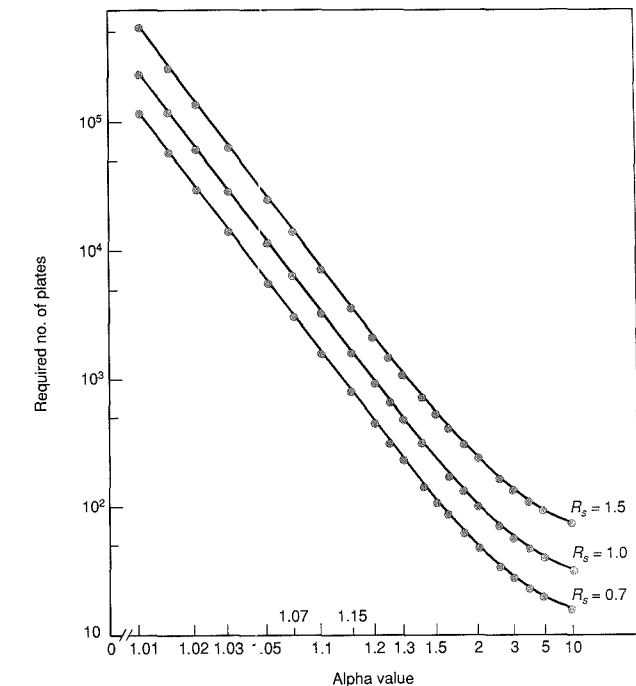


Figure 1. Relationship between the required plate number and the alpha value for different resolutions ( $R_s$ ).

increase the sample size that can be separated in each chromatographic pass (13). Displacement chromatography itself is very attractive for preparative applications, as shown by Horvath (14). For dedicated separations that must be performed repeatedly, the search for a displacement LC system can be most rewarding. Recently it has been shown that the synthesis of specific displacers is of potential general interest (15).

#### Practical preparative LC

Several forms of preparative LC have been developed according to various requirements for sample size and the difficulty of the separation (2). Analytical or laboratory preparative LC involves slightly enlarged column volumes obtained by either lengthening the column or enlarging its internal diameter. Longer columns allow difficult separations, but the back pressure and separation time soon become prohibitive. Enlarging the column diameter is thus the most practical means to achieve increased capacity.

High-performance laboratory preparative LC is currently performed primarily on columns 30–50 cm long with an i.d. of 7–10 mm. Such columns hold 10–20 g of silica gel and can handle sample loads from 1 to 1000 mg, depending on the difficulty of the separation. A larger column (20–30 cm long with an i.d. of 2–2.5 cm) that holds approximately 65 g of packing material is often used in the research laboratory. The optimum flow rate of such a column is 10–15 mL/min, which can easily be accommodated by most analytical LC instrumentation. This size column is the largest that can be packed with conventional packing methods and that will show reasonable column stability when handled carefully.

Even larger columns are needed for production-scale preparative LC, and two solutions to this problem have been developed. The first employs enlarged systems similar to those used in analytical LC with stainless steel columns filled with silica gel-based packing materials and high-pressure solvent delivery systems. The second,

used primarily in biotechnology, uses soft gels in glass or plastic columns under moderate pressure.

Analytical columns are usually packed by pumping a slurry of the packing material at pressures of up to 400–1000 bar. Packing fluid is forced at very high velocity through the column bed as it forms. This forces the stationary-phase particles into a more or less stable bed with a porosity that is still far from what is theoretically possible, making the stability of these columns uncertain. Under prolonged use, further settling of the stationary phase may occur, a void will appear at the top of the column, and the efficiency of the system will be reduced. ("Topping up" such deteriorated columns is a technique well known to most liquid chromatographers.) Column stability is also

affected by interaction of the packing material with the column wall, which has a stabilizing effect (16).

It is difficult, however, to pack large i.d. columns in this manner. Stainless steel columns of 10–60-cm i.d. can accommodate the necessary pressures only when the wall is prohibitively thick. Pumps that can generate the required pressures while delivering the necessary volume of solvent simply do not exist. Early preparative LC systems avoided this problem by using coarser stationary-phase particles; particles with an average size of 25  $\mu\text{m}$  can indeed be dry packed simply by pouring them evenly into the column. (Adding solvent to the particles without wetting them can improve dry packing results.) Glass or plastic columns can be used for such large-particle col-

umns, which have good stability because of the mild pressure drop and general chromatographic requirements of coarser particles.

The recent tendency in preparative LC, however, is toward high-efficiency columns using small particles with a diameter of 10–25  $\mu\text{m}$ . Packing problems are avoided by using compressed bed techniques in which dry packing material or a slurry is placed in the column, which is then compressed. Very little liquid is forced through the bed during packing.

Although bed compression was developed as a packing technique for large-scale columns, recent experience has shown that it is also important in maintaining columns in an efficient state during the chromatographic run (17). Friction heat is generated in the column as the solvent is forced through the packed bed. This appears to be a problem for the small-particle columns used in modern preparative LC. Such friction heat is a function of the linear flow velocity and viscosity of the solvent as well as the particle size and pressure drop over the column. With the larger particles and low-viscosity solvents used in normal-phase LC, friction heat is negligible. With smaller particle columns and the viscous solvents used in reversed-phase LC, however, friction heat becomes a serious problem. An opening appears at the column wall because of the difference in thermal expansion coefficients between the packed bed and column wall material. In a 20-cm i.d. column, packed efficiently with 15- $\mu\text{m}$  reversed-phase stationary phase, a visible opening of several tenths of a millimeter appears during the first chromatographic run. All solvent pumped through the column then passes along the wall and not through the packed bed, resulting in the "thermal wall effect" (16). This problem can be solved by continuous bed compression during the chromatographic run such that the volume of the space available to the packed bed is continuously corrected. Use of columns that have been removed from the compressed packing station can result in thermal wall effects for reversed-phase small-particle separations.

Bed compression can, in principle, be achieved axially, radially, or by a combination of the two. Axial compression can be exerted from the top of the column, the bottom of the column, or both together, and the piston can be actuated either mechanically or hydraulically. Because mechanical pistons require a lot of operating space, hydraulic pistons are preferable from an installation point of view.

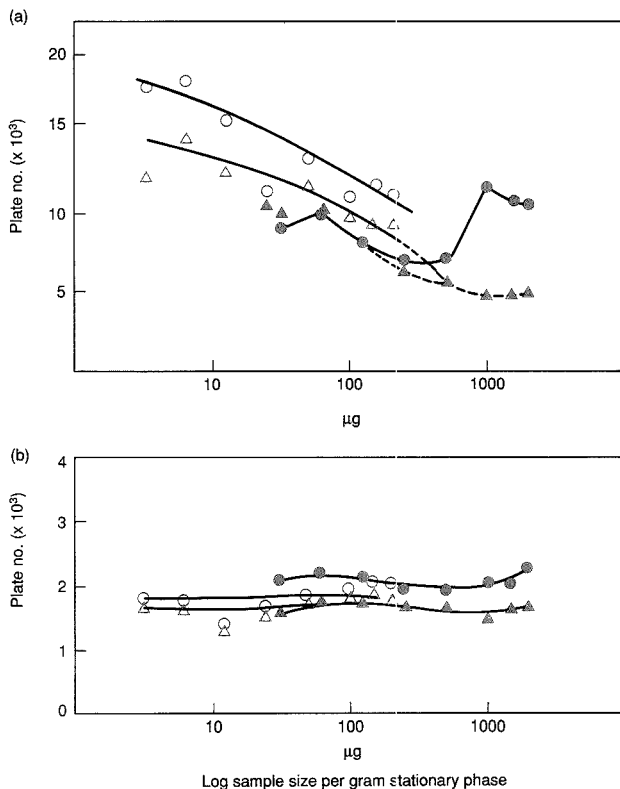


**Figure 2.** Plate number per meter as a function of sample size per gram of silica gel for normal-phase LC of 4-nitrophenol calculated from peak width or second moment.

Open circles = 10  $\mu\text{L}$ ; solid circles = 100  $\mu\text{L}$  (calculated from peak width).  $\Delta$ 's = 10  $\mu\text{L}$ ;  $\blacktriangle$ 's = 100  $\mu\text{L}$  (calculated from second moment). (a) 10- $\mu\text{m}$  particle size and (b) 40- $\mu\text{m}$  particle size. (Adapted with permission from Reference 17.)

Radial compression can be obtained by gas or liquid pressure on a flexible sheet against the column wall inside the metal column. The flexible wall obviously must be inert to the solvents used and must withstand frequent bending. Combined radial and axial compression is obtained by pressing a wedge-shaped shaft in the column. The term "dynamic axial compression" was recently introduced (18); such a term is useful in differentiating more clearly between "dynamic preparative LC" (continuous bed compression) and "static preparative LC" (without bed compression).

With the advent of commercially available large-scale compressed column instrumentation (17), this technique has become widely used in the pharmaceutical industry. Although very little information has been publicly disclosed, several pharmaceutical companies plan to present results of their work at Prep-90.

#### Economics of large-scale preparative LC

For large-scale industrial preparative LC, the economics of operation are important. Colin (18) estimates that the cost per kilogram of processed compound is between \$50 and \$500, depending on the difficulty of the chromatographic separation, which is not prohibitive for compounds of high commercial value. Solvent handling and recovery account for much of the operating costs for this type of large-scale system; other costs include instrumentation, installation, maintenance, and labor. Stationary-phase costs depend greatly on whether the silica gel must be derivatized. Although a large number of octadecylated silica gels are available commercially for large-scale preparative LC, all are different and will produce different alpha values for a given separation. It is thus extremely important to compare such materials on an analytical LC system to find the one that gives the most efficient separation.

Practically all analytical chromatography today is performed with mixtures of solvents, but it is almost impossible to recover large volumes of a ternary solvent without changing its composition in the distillate. This problem can be avoided by using a single solvent (no analysis required, no adjustment of composition), but a single solvent does not often provide the desired selectivity. The stationary phase is thus adapted to a particular separation problem by changing the degree of derivatization, changing the derivatization reagent, mixing different stationary phases, derivatizing with

mixed reagents, or sequentially using different derivatization reagents on the same phase. Such special stationary phases may be expensive at first, but in the final economic picture they may prove to be worthwhile.

Because stationary-phase packing material is expensive, particularly in the amounts required for large preparative LC columns, it is economically advantageous to regenerate used columns. Used packing materials can be dirtied by samples, lose bonded chains, or exhibit increased back pressure as a result of fine particles that are generated during packing or by continuous compression. Although some researchers believe that removal of fine particles by reclassification introduces unwanted changes in selectivity because new active surfaces are being generated, this does not appear to be the case.

**“Because proteins vary in molecular weight, hydrophobicity, isoelectric point, and thermal and chemical stability and reactivity, a generally applicable approach to their chromatographic separation is impossible.”**

The increase in surface area from compression is extremely small, and even if all the particles were halved, the surface area of a 20- $\mu\text{m}$  packing material would increase less than 1  $\text{m}^2/\text{g}$ , compared with a total specific surface area of  $\sim 200 \text{ m}^2/\text{g}$ . Regeneration of used packing materials is thus a viable proposition.

The feasibility of a production-scale LC process is, of course, determined by running the separation on analytical instrumentation first. It is, however, practically impossible to reproduce exact analytical LC data on a larger scale system. Even when the two columns are packed with the same stationary phase using the same packing material (which is normally not possible), wall effects will result in the columns having different packing densities, which in turn cause variations in retention data. Nevertheless, analytical results can be a great help in optimizing a preparative LC separation.

#### Preparative LC of proteins

Because proteins vary in molecular weight, hydrophobicity, isoelectric point, and thermal and chemical stability and reactivity, a generally applicable approach to their chromatographic separation is impossible.

Proteins cannot be chromatographed using isocratic conditions as can small and medium molecular-weight compounds, because the proteins are strongly adsorbed to the stationary phase (19, 20). Instead, size exclusion chromatography, in which there is no adsorption, or various forms of gradient LC, must be used. Such gradients include solvent gradients, in which the solvent composition eventually becomes strong enough to desorb the protein; buffer gradients; pH gradients; or salt concentration gradients, as in hydrophobic interaction chromatography.

Desorption of proteins from the stationary phase can also be promoted by addition of solvents or acids that modify the protein's conformation, such as trifluoroacetic acid, isopropyl alcohol, or acetonitrile. However, this can

sometimes cause denaturation of sensitive proteins. Weight recovery of the protein mass injected onto the LC system is important, but possible loss of biological activity of enzymes or hormones is even more important.

The pore size of the packing material also affects the recovery of the protein from the column; stationary phases with large pore sizes (30–100 nm) are used to avoid irreversible retention of proteins in the small pores of conventional packing materials. The pore size distribution of most stationary phases is large enough, however, that even large-pore stationary phases have some small pores, so there is always the possibility of some protein being retained on the column.

Most protein separations are performed on soft gels derived primarily from polysaccharides. Although these soft gels do not have the efficiency of silica gel-based small-particle stationary phases, they are more highly selective.

Another peculiarity of preparative protein chromatography is that the amount of sample necessary is sometimes quite small (21); many polypeptide enzymes and hormones of current pharmaceutical interest require only microgram dosages. A few grams of such proteins (a year's supply for the entire



world) can be chromatographed on analytical instrumentation.

Preparative LC of proteins can be difficult because of possible denaturation, difficult recovery from the collected fractions, solubility problems, and extreme sensitivity to even small variations in stationary-phase composition. The chromatographic separation, however, is often easy because of the very high selectivity that is readily available. Conditions under which one protein passes through the column while others are completely retained are not difficult to establish. There is a great future for preparative protein LC, but much remains to be done.

#### References

- (1) Hostettmann, K.; Hostettmann, M.; Marston, A. *Preparative Chromatographic Techniques*; Springer Berlin: Heidelberg, 1985.
- (2) Verzele, M.; Dewaele, C. *Preparative High Performance Liquid Chromatography. A Practical Guideline*; RSL Europe: Eke, Belgium, 1986.
- (3) Bidlingmeyer, B., Ed. *Preparative Liquid Chromatography*; Elsevier: Amsterdam, 1987.
- (4) Kuhn, R.; Brockmann, H. *Hoppe-Seyler's Z. Physiol. Chem.* 1932, 206, 41.
- (5) Winterstein, A.; Stein, G. *Hoppe-Seyler's Z. Physiol. Chem.* 1933, 220, 247.
- (6) Zechmeister, L.; Cholnoky, L. *Liebig's Ann. Chem.* 1934, 509, 269.
- (7) Strain, H. J. *Biol. Chem.* 1934, 105, 523.
- (8) Karrer, P.; Strong, F. *Helv. Chim. Acta* 1936, 19, 25.
- (9) Wankat, P. In *Preparative Liquid Chromatography*; Bidlingmeyer, B., Ed.; Elsevier: Amsterdam, 1987.
- (10) Majors, R. *Anal. Chem.* 1972, 44, 1722; 1973, 44, 88.
- (11) Halász, L.; Sebestian, I. *Chromatographia* 1974, 7, 371.
- (12) Golshan-Shirazi, S.; Guiochon, G. *J. Chromatogr.* 1988, 461, 19.
- (13) Newburger, J.; Guiochon, G. Presented at the Washington Symposium on Preparative Chromatography, Washington, DC, 1989.
- (14) Horvath, C.; Nahum, A.; Frenz, J. *J. Chromatogr.* 1981, 218, 365.
- (15) Camacho, P.; Geiger, E.; Farkas, G.; Bartha, A.; Vigh, G. Presented at the Washington Symposium on Preparative Chromatography, Washington, DC, 1989.
- (16) Verzele, M.; Dewaele, C.; De Weerd, M.; Abbott, S. *J. High Resolut. Chromatogr.* 1989, 12, 164.
- (17) Verzele, M.; De Coninck, M.; Vindevoel, J.; Dewaele, C. *J. Chromatogr.* 1988, 450, 47.
- (18) Colin, H. A. *Genetic Engineering News* 1988, 22; LC/GC 1989, in press; Presented at the Baden-Baden Symposium on Preparative Chromatography, Baden-Baden, FRG, 1988.
- (19) Snyder, L. R.; Stadalius, M. A.; Quarry, M. A. *Anal. Chem.* 1983, 55, 1412 R.
- (20) Verzele, M.; Yang, Y.-B.; Dewaele, C.; Berry, V. *Anal. Chem.* 1988, 60, 1329.
- (21) Sitrin, R. D.; DePhillips, P. Presented at the Washington Symposium on Preparative Chromatography, Washington, DC, 1989.



Maurits Verzele received a D.Sc. degree from the State University of Gent and was a member of the faculty there until his retirement in 1988. His research interests include column technology and stationary-phase synthesis for preparative and capillary gas and liquid chromatography. He is best known for his work in developing the static coating procedure for capillary GC columns.

# WONDERS SCIENCE

## Fun Physical Science Activities for Children and Adults to Do Together

- colorful comic book format
- useful at home or in classrooms
- reinforces language and math skills
- relates science concepts to technology
- aimed at 4th through 6th graders

Price per subscription (one-year, four-issues)	
To continental U.S. addresses	1-4 ..... \$4.00 each 5-19 ..... \$3.00 each 20 or more ..... \$2.00 each
To addresses outside the continental U.S.	50 or more ..... \$3.00 each (minimum)

For subscription information write or call:

American Chemical Society  
Prehigh School Science Program  
1155 Sixteenth St., N.W.  
Washington, DC 20036  
(202) 452-2113

# NEWEST!

## ELECTRONIC STIRRERS

AUTOMATIC TRANSMISSION

ONE OF A COMPLETE LINE OF LAB APPLIANCES

**N • E • W**  
ROTARY EVAPORATORS  
micro to 20 l capacities

**N • E • W**  
STIRRERS/HOT PLATES  
interchangeable baths

**N • E • W**  
PLATFORM MIXER  
asymmetric movement

**N • E • W**  
VORTEX MIXER  
interchangeable heads

NEW TECHNOLOGY BY

Cafamo

LIMITED

Warton, Ontario, Canada NOH 2T0

See what's new at the Pittsburgh Conference, Booth #5672.

CIRCLE 28 ON READER SERVICE CARD

## ULTRAFAST SPECTROSCOPY

Mary J. Wirth

Department of Chemistry & Biochemistry  
University of Delaware  
Newark, DE 19716

Time-resolved spectroscopy has been an active research area in analytical chemistry for more than 30 years. During this period, technological developments have improved time resolution from the millisecond to the subpicosecond range. Measurement of the temporal behavior of chemical systems has provided a new basis for selectivity. New technology has also allowed analytical spectroscopy to evolve beyond traditional boundaries to include the characterization of structurally heterogeneous systems such as surfaces and thin films, biological systems, electronic devices, and advanced materials. Time-resolved spectroscopy is now being used to provide structural and dynamic information to solve new types of chemical measurement problems and to improve qualitative and quantitative analyses.

Ultrafast spectroscopy is an interdisciplinary field that spans physics, chemistry, biology, and electrical engineering in the study of the fundamental nature of the myriad of relaxation processes. The field is an exciting one in which researchers pursue advances in short-pulse generation and applications. Recent applications in chemical physics (1), biology (2), and electrical engineering (3) have been reviewed, as

have methods of short-pulse generation (4). In even-numbered years, the Optical Society of America sponsors conferences on ultrafast phenomena, and Springer publishes these proceedings as a book series.

Ultrafast spectroscopy is receiving increasing attention from the analytical chemistry community, although it is far from being commonplace. The ultrafast time scale extends approximately from 10 fs ( $10^{-14}$  s) to 100 ps ( $10^{-10}$  s). The fast end of this range is marked by the limit of laser technology and the slow end by photomultiplier technology. Ultrafast techniques require multiple-beam optical methods for detection. The need for high sensitivity and the desire for general applicability and convenience have combined to limit much of analytical spectroscopy to the time scale of photomultiplier technology. Despite these disadvantages, analytical spectroscopists are devoting more time to working in the experimentally difficult area of ultrafast spectroscopy.

### Lifetime measurements using photomultipliers

In 1957 Keirs, Britt, and Watworth published the first analytical paper on time-resolved spectroscopy (5). At that time phosphorescence was known to originate from a transition between specific molecular states (6), and these workers expected that the phosphorescence lifetime,  $\tau_p$ , would be unique for a given molecule. They demonstrated

that  $\tau_p$  could be used as a parameter for chemical identification and for mixture analysis. The apparatus consisted of a pair of slotted wheels, one on each side of the sample, to mask the sample alternately from the arc lamp and the detector. By controlling the relative angular positions of the two slots, the emission was observed at a known delay time from the excitation. Their time resolution of 1 ms was limited by the sizes of the slots in the wheels and by the motor speed. Time-resolved spectroscopy thus began in the mechanical era.

The results of this first paper bear striking similarities to and differences from current work. Today much analytical research involves the same goal of using lifetimes for molecular identification. However, the time resolution has improved by 7 orders of magnitude, from 1 ms to 0.1 ns. Electronics and quantum electronics have replaced mechanical parts, due to the invention of the laser and mode locking; the development of repetitively pulsed lasers; and the availability of faster photomultipliers, particularly the microchannel-plate photomultiplier. Improvements in optical technology and continual advances in digital electronics and laboratory computers have made nanosecond fluorescence experiments routine.

These improvements in speed have permitted the study of fluorescence rather than phosphorescence. The use of phosphorescence is restricted to very viscous or solid media, whereas fluores-

cence is emitted by a wide variety of systems under less restrictive conditions. Faster time resolution was thus essential in making the original idea generally applicable. Fluorescence lifetimes can be determined rapidly enough to be implemented in chromatographic detection (7). Early efforts in time-resolved fluorescence spectroscopy involved the measurement of fluorescence decay times of laser dyes. With the many improvements in optical technology, fluorescence lifetime measurements have become generally applicable.

Impressive advances have been made in electronics at MHz and GHz frequencies, accelerating the development of frequency-domain techniques (8). The principle of frequency-domain techniques is that a decay function in the time domain can equivalently be determined in the frequency domain. By modulating the light beam at a variety of frequencies and measuring the amplitude demodulation and phase shift of the emission, the time decay is calculated from the simple Fourier transform relations. Deconvolution of the excitation pulse is intrinsic to the frequency-domain measurement and extends the effective time resolution of photomultiplier detection by about a factor of 10. Lifetime measurements by frequency-domain techniques are also very rapid and versatile. Multiple-component samples can be analyzed without prior knowledge of the lifetimes on an analytically useful time frame (9, 10).

#### Ultrafast relaxation processes

Now that the analytical utility of lifetime measurements has been vastly improved by the advancement from the millisecond to the nanosecond time scale, what can we expect from the advancement through the next 4 or 5 orders of magnitude? The technological barriers to measuring ultrafast processes can inhibit one's imagination about possible future applications. But suppose we had a photomultiplier with a rise time of 1 fs, along with a tunable laser with output pulses of 1 fs. Given this equipment, most spectroscopists would immediately go into the lab, put their most interesting fluorescent sample into the ultrafast fluorometer (perhaps one whose decay they have deconvoluted), and find out what the decay really looks like.

Figure 1 gives an educated guess as to what might be observed in a hypothetical femtosecond emission experiment, showing the decay plotted on different time scales. In part a, on the 10-ns time scale, the familiar fluorescence decay is shown. In part b, on the 100-ps

time scale, the intensity depends on which polarization is measured. This phenomenon, fluorescence anisotropy, results from the preferential excitation of solutes oriented with respect to the polarization of the laser beam. The decay of the anisotropy as a function of time is attributable to molecular reorientation. In part c, on the 1-ps time scale, the intensity increases with time. This represents the evolution of the

Stokes shift as the environment of the solute adjusts from ground-state solvation equilibrium to excited-state equilibrium (11).

As the time scale becomes increasingly shorter, other unfamiliar features of the fluorescence spectrum may be observed. One is unrelaxed fluorescence. Normally, fluorescence emission arises from a transition between the lowest excited electronic state to the ground state. Collisions with the environment cause extremely fast internal conversion, resulting in the same emission spectrum regardless of which wavelength is used for excitation. Fluorescence from vibronic states might be observed because vibrational relaxation can be slow on the femtosecond time scale.

A second observation might be that virtually everything fluoresces. According to the Heisenberg uncertainty principle, every transition having a bandwidth of a few hundred nanometers must be associated with a state having a lifetime at least as long as femtoseconds. Where there is absorption, there must be emission, albeit very small in some cases. Ultrafast spectroscopy could make fluorescence more universally applicable.

Raman emission is also interesting on the ultrafast time scale. Below 1 ps, resonance Raman emission emerges (12). In part d of Figure 1, on the time scale less than 100 fs, an intense and rapid decay resulting from resonance Raman emission appears. By selecting a narrow emission bandwidth, this peak could be larger than the fluorescence emission. The difference between resonance Raman and fluorescence is understood (13). On this time scale, the electronic states of the absorber are still in phase with the excitation, and the resulting temporally coherent emission process is referred to as resonance Raman. Collisions perturb the energies and, therefore, the phases of these states. The emission process after dephasing is referred to as fluorescence. On the 100-fs time scale, emission is also observed coincident with the laser pulse, as shown in part d. This is Raman emission without resonance enhancement, contributed by the solvent.

The value of such technology is evident for Raman spectroscopy. Raman spectra contain structural information, yet their use is limited because of low sensitivity and fluorescence interference. Our hypothetical experiment shows that all of the photons from the resonance Raman process are emitted before 1 ps, where little fluorescence interferes. One could use resonance enhancement with minimal interference

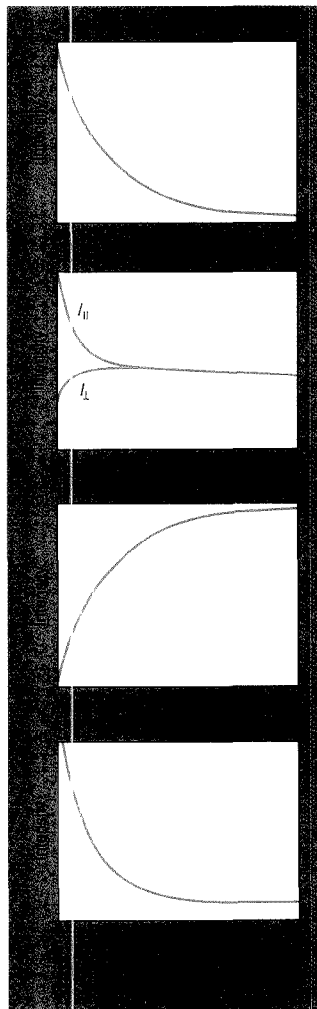


Figure 1. Emission behavior on different time scales.

(a) Fluorescence decay; (b) fluorescence anisotropy; (c) increase in fluorescence as the spectrum evolves; and (d) resonance Raman decay, with background fluorescence.

*inspires  
the innovator*

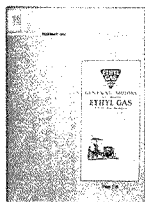
**Why do so many innovators in all chemical fields turn to CHEMTECH each month?**



... One of the best condensed technical news sources I get . . . Outstanding melding of social, political, and scientific literature . . . The fresh glibness and tongue-in-cheek style are unique and welcomed . . . I am impressed with the quality, scope and personal touch of the articles . . . I almost dread it when each issue arrives because I know I will take the time, whether I have it to spare or not, to read it from cover to cover.



**Join your satisfied colleagues and subscribe to the innovator's magazine . . .**



**Call now to order:  
800-227-5558**

## **INSTRUMENTATION**

from fluorescence. In fact, various techniques have been used to reject fluorescence from Raman emission based on temporal discrimination: time-domain methods with conventional photomultipliers (14) and microchannel-plate photomultipliers (15) and frequency-domain phase nulling with photomultiplier detection (16-18). These methods cannot push Raman spectroscopy to its fullest potential because they are a few orders of magnitude too slow. None has achieved rejection of fluorescence by more than a factor of about 200, and this is not good enough for wide applicability. Thus workers avoid fluorescence in Raman spectroscopy by excitation with near-IR (19), red (20), and UV (21) light.

One application of an ultrafast emission experiment is very close to achieving routine use in analytical chemistry: the measurement of fast fluorescence anisotropy decays. To be widely applicable, a time resolution of 10 ps is needed because the reorientation times of moderately small molecules in solvents of low viscosity can be as short as 10 ps. Although a commercial instrument with this time resolution does not exist, photomultiplier technology can now be pushed to this level of performance, particularly with frequency-domain spectroscopy. As with fluorescence lifetimes, early efforts in molecular reorientation measurements also involved the study of laser dyes. Short optical pulses can now be generated throughout the visible and UV, allowing applicability to virtually any fluorescent species of interest.

According to Debye (22), the reorientation time,  $\tau_{or}$ , of a solute is proportional to its molecular size. As a parameter for identification,  $\tau_{or}$  is potentially more valuable than either the fluorescence or the phosphorescence lifetime because it contains information pertaining more directly to solute structure. Anisotropy decays are multiple exponential (23), and their analysis also reveals the hydrodynamic shape of the solute as well as its size.

Anisotropy measurements contain a wealth of information. In addition to the structural parameters of size and shape, the symmetry of the excited state relative to the ground state is determined. Furthermore, the excited-state symmetry is wavelength dependent (24). Rather than just using the spectrum for identification, researchers will also routinely use the polarization dependence of the spectrum. The value of such a measurement has been demonstrated for a mixture analysis of anthracene derivatives (25).

The evolution of the fluorescence spectrum, vibrational relaxation, the

decay of Raman and resonance Raman emission, and the reorientation of molecules occur on ultrafast time scales. The amount of information that can be obtained by time resolution far exceeds the information in steady-state Raman and electronic spectra. These examples refer to an emission experiment, but many other types of experimental arrangements are used in ultrafast spectroscopy.

### **Beyond photomultipliers: techniques of ultrafast spectroscopy**

Although present ultrafast lasers can have pulse widths as short as 6 fs (26), 50 fs is more typical. What is lacking for the hypothetical femtosecond emission equipment to be a reality is an ultrafast photomultiplier. There are two general approaches to improving the time resolution of the experiment: make the detector faster or gate the light emitted from the sample.

**Streak cameras.** Photomultipliers are limited in speed by an inability to contain a collection of  $10^6$  electrons per pulse in closer spatial proximity. A streak camera, which is a distant relative of the photomultiplier, operates as fast as 0.6 ps at high repetition rates (27). What a streak camera has in common with a photomultiplier is a photocathode. When light strikes the photo-

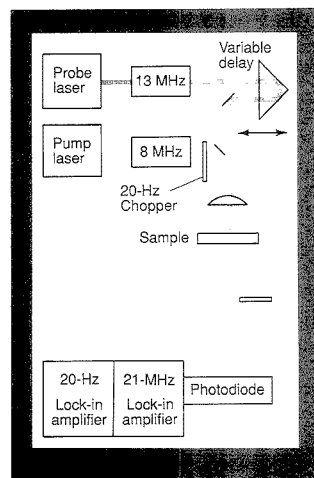


**Figure 2.** Schematic of a pump/probe experiment.

The pump and probe lasers are modulated at 8 and 13 MHz, with the pump laser chopped at 20 Hz. The arrival time of the probe laser is controlled by a variable delay line, and its intensity is detected with a photodiode. The signal at 21 MHz is isolated by a lock-in amplifier and is distinguished from any background contribution at 21 MHz by the low-frequency lock-in amplifier.

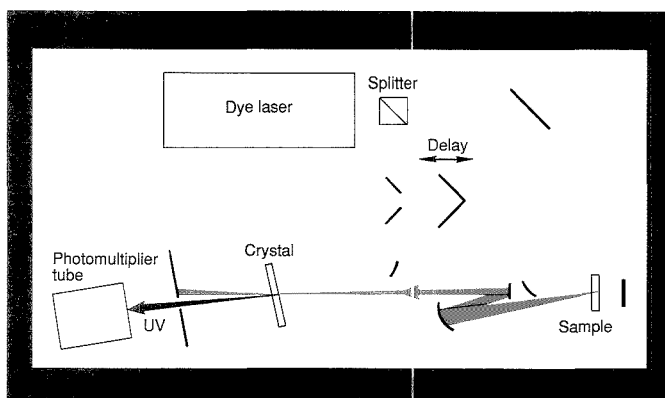


Figure 3. Schematic of an upconversion experiment.

The dye laser output is split. One arm is used to excite the sample. The other arm, variably delayed, is used for the upconversion process. The fluorescence, indicated as the red light, is shown to be collected with an off-axis curved mirror and is directed into the upconversion crystal. The UV output intensity of the crystal is proportional to intensity of the fluorescence at the particular delay time.

cathode of the streak camera, photoelectrons are emitted and then accelerated to pass between high-voltage plates. The deflection by these plates is rapidly swept in time. The photoelectrons strike a phosphorescent screen, and the spatial profile of the image on the plate is related to the temporal profile of the optical signal. Streak cameras have lower sensitivity and a lower dynamic range than photomultipliers, and they require careful calibration and tweaking. Their most notorious disadvantage is that they cost more than \$60,000.

**Pump/probe spectroscopy.** Scientists working in ultrafast spectroscopy today typically use optical rather than electronic methods of time resolution. The workhorse of these detection tools is pump/probe spectroscopy. The optical arrangement is illustrated in Figure 2. Two laser pulses are used: The pump pulse excites the sample, and the probe pulse stimulates emission. The stimulated emission intensity is proportional to the fluorescence intensity, provided that the probe pulse is not too intense. The arrival time of the probe pulse is controlled by the optical pathlength of the probe beam, and varying the arrival time allows construction of the temporal decay function.

It is the shortness of the laser pulses that allows pump/probe spectroscopy to work on ultrafast time scales. When the probe laser is tuned to an emission band, the same information that one would obtain from a fast fluorescence experiment is generated. The probe can also be tuned to an absorbance band, allowing the ground-state population to be probed. The change in-

tensity of the probe beam is very small, typically  $< 10^{-4}$ . To minimize low-frequency noise, the pump beam is modulated and the component of the probe beam at the pump modulation is detected.

The detection limit in pump/probe experiments is determined by the magnitude of the fluctuations on the probe beam. When pumped by a well mode-locked argon ion laser, the synchronously pumped dye laser has noise fluctuations on the order of its shot noise for measurements above 10-MHz modulation frequencies. This means that the noise on the laser intensity is attributable only to the fact that the beam is composed of discrete photons. For a 30-mW laser beam, this corresponds to 3 parts in  $10^9$ , which is extreme stability. This stability is valuable for pump/probe spectroscopy of dilute samples.

The first demonstrated use of shot-noise-limited pump/probe detection was for Raman gain spectra of surface monolayers without the need for surface enhancement (28, 29). A double-modulation scheme was used whereby the pump was modulated at both 10 MHz and 500 Hz. The component of the probe intensity at 10 MHz was detected. The 500-Hz chopping of the pump beam was used to reject background from rf pick-up.

A study of the sensitivity and detection capability of pump/probe fluorescence spectroscopy using triple modulation showed that the theoretical detection limit could be achieved in practice (30). The probe beam modulation,  $\Delta P_2$ , was shown to be proportional to concentration.

$$\Delta P_2 = \frac{1000(2.303)^2 \epsilon_1 \epsilon_2 bc P_1 P_2}{RKNA} \quad (1)$$

$R$  is the repetition rate of the laser;  $K$  is the photon energy;  $N$  is Avogadro's number;  $A$  is the beam area;  $\epsilon_1$  and  $\epsilon_2$  are the molar absorptivities of the pumped and probe transitions, respectively;  $P_1$  and  $P_2$  are the powers of the pump and probe beams; and  $c$  is the concentration of the sample. Under typical conditions, the detection limit is a few nanomolar. For rapid quantitative measurements of anisotropy decays, it is best to be about 1000X above the detection limit. This is sufficiently dilute for reorientation measurements, where the concentration must be low enough to avoid energy transfer.

**Upconversion.** An alternative method frequently used in ultrafast spectroscopy is upconversion (31), illustrated in Figure 3. The emission is collected with a lens, just as it would be in an emission spectrum, but then it is focused into a frequency-doubling crystal. The angle of the crystal is adjusted such that an intense laser beam focused to the same spot in the crystal will cause nonlinear generation at the sum of the frequencies of the laser and the fluorescence. Phase matching is required, which also prevents second harmonic generation from the laser beam alone. The upconversion process thus acts as a temporal gate. The signal can be derived from first principles to be

$$\text{Photons/s} = 2.3 \epsilon bc \frac{P}{J/\text{photon}} \times \Omega \gamma_f \gamma_{\text{pmt}} \delta_g \delta_t \gamma_{\text{uc}} \quad (2)$$

where  $\epsilon$  is the molar absorptivity and  $b$  the pathlength of the sample,  $c$  is the concentration,  $P$  is the laser power,  $\Omega$  is the collection efficiency of the lens,  $\gamma_f$  is the quantum yield for fluorescence,  $\gamma_{\text{pmt}}$  is the quantum yield of the photocathode,  $\delta_g$  is the fraction of the spectrum upconverted,  $\delta_t$  is the fraction of the decay upconverted, and  $\gamma_{\text{uc}}$  is the efficiency of the upconverter. Equation 2 differs from that for conventional fluorescence only by the factor  $\gamma_{\text{uc}}$ , which is typically  $10^{-4}$ . However, phase matching restricts  $\delta_t$  to a small value, and  $\delta_g$  is very small if the lifetime is on the nanosecond time scale. A substantial background also must be subtracted. Consequently, upconversion has a high detection limit but has the advantage of requiring only one laser.

The time resolution for upconversion experiments is as short as 200 fs. These experiments are nearly limited in time resolution by the uncertainty principle because of the narrow spectral width used for phase matching.

If upconversion were used for Raman

SPECIAL ISSUE  
 Advances in Materials for Electronics Packaging and Interconnection

EDITED BY  
 John H. Lupinski and  
 Robert S. Moore

## Polymeric Materials for Electronics Packaging and Interconnection

While there has been a number of books addressing packaging, and to some extent polymers, virtually none has emphasized the synthetic and physical chemistry of these systems. This new volume fills that gap, addressing the many aspects relating to the development of novel polymeric materials and processes. The emphasis is on chemistry and materials science, rather than circuitry, its electrical capabilities, or its design characteristics.

Covering a broad spectrum of subjects, this 38-chapter book focuses on four general areas:

- physical chemistry of materials
- properties and applications of encapsulants
- properties and applications of gels
- printed circuit board substrates and materials for circuit board substrates

Also included is a review of the marketing trends which drive packaging technology.

This unique volume will be helpful to scientists engaged in materials development for electronic packaging, electronic packaging engineers, and to technologists who monitor developments in the electronics industry and related fields.

John H. Lupinski, *Editor*, General Electric Company

Robert S. Moore, *Editor*, Eastman Kodak Company

Developed from a symposium sponsored by the Division of Polymeric Materials: Science and Engineering and of Polymer Chemistry of the American Chemical Society

ACS Symposium Series No. 407  
 512 pages (1989) Clothbound  
 ISBN 0-8412-1679-9 **\$99.95**

**O · R · D · E · R · F · R · O · M**

American Chemical Society  
 Distribution Office, Dept. 45  
 1155 Sixteenth St., N.W.  
 Washington, DC 20036

or CALL TOLL FREE

**800-227-5558**

(In Washington, D.C. 872-4363) and use your credit card!

emission,  $\delta_i$  in Equation 2 could approach unity and  $\delta_g$  could also be large as a result of the narrow bands. Upconversion would appear to be preferable to pump/probe measurements for Raman spectroscopy, although it has not yet been used. For resonance Raman, the resonance enhancement would be approximately offset by the inefficiency of upconversion, but fluorescence would be eliminated in the process.

**Effects of temporal dispersion.** Emission spectroscopy is not the same game on ultrafast time scales as it is in nanosecond spectroscopy. If you are holding this paper 12 in. away it takes 1 ns for the photons reflected from the paper to reach your eyes. The relationship between time and distance is crucial to ultrafast spectroscopy because the speed of light is comparatively slow on these time scales. An optical pulse is lengthened in time if any part of it travels a different optical distance than the rest of the pulse. This effect is called temporal dispersion. Despite short laser pulses and fast detection, the time resolution in an experiment can be destroyed by temporal dispersion from the optical layout of the experiment.

For any ultrafast emission method, temporal dispersion must be carefully diagnosed and eliminated. There are three causes of temporal dispersion. First, collecting light over a nonzero

solid angle with a lens or mirror results in a distribution of optical pathlengths (Figure 4a). Furthermore, passage through a thick lens can have a much greater effect than this distribution of pathlengths (Figure 4b). Either a larger  $f$ -number or reflective optics should be used; implementing both would give the best results.

Second, for excitation over a finite pathlength, molecules on one end of the path are excited at a different time than those on the other end (Figure 4c). This is a severe problem in an emission experiment but is absent in a pump/probe experiment. Finally, the refractive index of any material is wavelength dependent. A short pulse has frequency components greater than a few hundred nanometers, and the red wavelengths move faster than the blue wavelengths through typical optical materials (Figure 4d). The result is called pulse chirping because of what this signal would sound like if these were audio frequencies. Figure 4 illustrates that the temporal profile of the ultrafast pulse is easily lengthened by passage through commonly used optics.

A careful study of temporal dispersion in an upconversion measurement was recently detailed (32). From this study, one can appreciate that the resolution of 200 fs is a noteworthy accom-

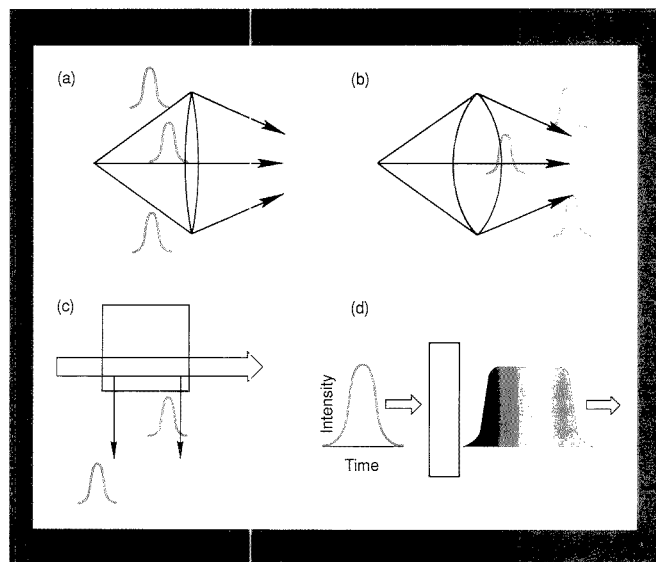


**Figure 4.** Pulse dispersion.

(a) Collection of light causes dispersion resulting from a distribution of pathlengths, (b) passage through a thick lens causes severe dispersion, (c) a long pathlength and perpendicular detection cause dispersion, and (d) passage through a material causes frequency chirp. Note that chirp would also be severe in part b but is neglected for clarity.

plishment because of the need to compensate for temporal dispersion. The hypothetical femtosecond emission experiment described earlier would be subject to the same problems, and the hypothetical emission decays of Figure 1 would not be resolved without a nearly diffraction-limited pathlength, reflective optics, and large  $f$  numbers.

### Analytical research in ultrafast spectroscopy

Despite the labor involved in ultrafast technology, several analytical research groups have used pump/probe spectroscopy for a variety of interesting applications.

**Ultrafast laser technology.** An early and significant contribution by analytical chemists to ultrafast spectroscopy was the invention of the synchronously pumped dye laser by Harris, Chrisman, Tobias, and Lytle in 1975 (33). This invention included cavity dumping to control repetition rate and was developed almost simultaneously with the continuously output version by two other research groups (34, 35). The name was coined by Harris et al. The significance of the synchronously pumped dye laser is that it routinely generated pulses of 4 ps with a high repetition rate.

Before this laser was developed, experiments were performed with "single-shot" lasers, where pulses of 6 ps were generated from Nd:glass lasers once every 2 min. Intense pulses were necessary, problems with nonlinearity were common, and control and characterization of the laser pulses were difficult. Synchronously pumped dye lasers are now able to generate pulses of < 50 fs. A more recently developed laser, the colliding-pulse ring dye laser, achieves shorter pulse widths, but the synchronously pumped dye laser is more widely tunable. The cavity-dumped version was able to generate pulses as short as 4 ps by the use of a saturable absorber in the cavity (36).

An elegant electronic means of scanning the time delay in pump/probe spectroscopy is the asynchronous optical sampling (ASOPS) method (37, 38). By synchronously pumping a pair of dye lasers with different Nd:YAG lasers, mode-locked at slightly different repetition rates, the pump and probe pulses are self-scanning. The applicability of ASOPS to the detection of species in harsh media has been demonstrated by a measurement of the emission lifetime of atomic sodium in a flame.

To generate laser pulses on the femtosecond time scale, a new technology has emerged: first, the bandwidth of the pulse is increased by using the non-

linearity in the refractive index of a material; second, temporal dispersion is used in reverse to compress the pulse. The result is a shorter pulse. Choi and Gustafson have accomplished the compressor of cavity-dumped synchronously pumped laser pulses down to 50 fs, with very high peak powers of 100 kW at a 2-MHz repetition rate (39). This is a valuable source for chemical applications in nonlinear spectroscopy because the high repetition rate minimizes saturation effects while the good beam quality allows for the tight focusing needed in obtaining the high-power density used in nonlinear spectroscopy.

**Molecular reorientation.** Pump/probe spectroscopy has been used to study molecular reorientation of cresyl violet in 1-dodecanol as a function of temperature (40). The reorientation time was constant below 30°C, jumped to a longer value by a factor of 2 at 30°C, and then behaved normally. Because heat usually speeds up rotation of molecules, the researchers were intrigued by the slowing of cresyl violet with increasing temperature. By using temperature-dependent NMR measurements of the  $T_1$  relaxation times, it was found that 1-dodecanol undergoes a liquid crystal phase transition at 30°C. This transition involves freeing the motional constraints of the last few carbons on the end of the chain that is opposite the OH group. The phase transition had not previously been observed and was undetectable by differential scanning calorimetry, polarization microscopy, and Raman spectroscopy. It was barely observable with NMR but was dramatically evident in the pump/probe anisotropy measurement. Molecular reorientation can be very sensitive to the short-range structure of a liquid.

The ability to sense the structure of the environment is one of the increasingly interesting uses of anisotropy measurements. The solvation of small molecules by long-chain alkyl groups is pertinent to bonded-phase applications in I.C. The motions of tetracene in 1-dodecanol have been studied using frequency-domain photomultiplier methods (41). The results indicate non-Debye behavior. The motions of acridine orange attached to sodium dodecyl sulfate (SDS) micelles have been studied (42). The decay could be quantitatively interpreted, owing to the symmetry of acridine orange. The study revealed that SDS-bound acridine orange rotates through an angle of 45°, with full rotation prevented by the attachment. The high sensitivity of the technique made it possible to study premicellar SDS. The results showed that premicellar aggregates were prev-

alent down to half of the critical micelle concentration and that these aggregates hold acridine orange more rigidly than do the micelles.

A comparison of the reorientation time of cresyl violet in its ground and excited states was undertaken using pump/probe spectroscopy to probe both states (24). The excited state has a significantly slower anisotropy decay; however, it was shown that a change in the transition symmetry introduced new exponential decay functions. The ground and excited states actually reorient with the same time constant. This experiment illustrates that reorientation behavior can only be interpreted by analyzing the full, multiexponential decay and determining the transition symmetry.

Blanchard has continued to pursue the question of whether ground states and excited states have the same reorientation behavior. This is an important question because the most common method of studying reorientation is fluorescence anisotropy, which inherently senses only the excited state, whereas the ground-state dynamics are often of interest. He has shown that the excited state reorients more slowly than the ground state for oxazine 725 (43). The excited-state reorientation time increases inordinately with increasing chain size of the alcohol solvent. Using studies of additional nitrogen-containing heterocycles and MNDO calculations of electron density for ground and excited states, Blanchard has shown that the excited state is a stronger Lewis base than the ground state; thus, the attachment to the solvent is stronger in the excited state (44). The quantitative amount of attachment, the equilibrium constant, can be determined experimentally using anisotropy measurements (45).

**The spectroscopy of transients.** A unique application of ultrafast spectroscopy is the determination of structures of transient species. Important applications include the understanding of vision and photosynthesis and the development of fast-switching photoconductors. Gustafson et al. were the first to accomplish a direct measurement of the transient Raman spectrum of an electronic excited state (46); they showed that *trans*-stilbene photoisomerizes into a distribution of conformations (47). These workers also applied the method to the study of the excited-state symmetry of diphenylbutadiene (48). The technique of transient Raman spectroscopy has generated intense interest in studies of structural changes on ultrafast time scales.

The development of fast switches is important to the communications in-

dustry. One type of device for switching optical signals would be based on the nonlinear response of conjugated polymers to a short pulse. The nonlinear response is determined by virtual states; thus, the switch would be open only for the duration of the optical pulse. Understanding the states that contribute to the nonlinear response is important to improvements in the efficiency of these switches. Blanchard et al. have used pump/probe inverse Raman spectroscopy to study the couplings of optical phonons to excitons in crystalline polydiacetylene (49). Their results reveal that the phonon-mediated optical Stark effect is an important contribution to the optical nonlinearity of polydiacetylene. For electronic signals, hydrogenated amorphous silicon is an important material in the development of photovoltaics and thin-film devices. An understanding of the nature of relaxation processes of the light-induced charge carriers is needed to evaluate the practical potential of this material. Gustafson et al. have measured the picosecond transient absorption of hydrogenated amorphous silicon to probe the transient, light-induced transport of electrons (50).

**Future potential**

Analytical spectroscopists will continue to explore applications of the large amounts of chemical information available on increasingly shorter time scales. Early studies on the nano- and picosecond time scales were technologically difficult and primarily involved dye molecules as test systems; however, these measurements evolved to become universally applied as technological advances were achieved. The technological advances that made nanosecond spectroscopy easy will most likely continue beyond the photomultiplier time scale, enabling femtosecond spectroscopy to be more widely applicable.

The newly emerging technologies will change the types of problems analytical spectroscopists solve. Today's new tools—such as supercomputers, scanning tunneling microscopy, and ultrafast lasers—and tomorrow's new tools—such as coherent X-ray sources, widely tunable lasers, ultrafast electronics, and technology yet to be determined—will lead to a further metamorphosis of the field. Continued expansion of the scope of analytical spectroscopy

and an embracing of the new technologies will allow analytical spectroscopists to continue to play a vital role in science and technology.

This work was supported by the National Science Foundation under grant CHE-14602.

**References**

- (1) Fleming, G. R. *Chemical Applications of Ultrafast Spectroscopy*; Oxford University Press: New York, 1986.
- (2) Hochstrasser, R. M. *Ber. Bunsenges. Chem.* **1989**, *93*, 239.
- (3) Miller, A.; Sibbett, W. J. *Modern Opt.* **1988**, *35*, 1871.
- (4) Fujimoto, J. G. *Photonics Spectra* **1988**, *22*, 95.
- (5) Keirs, R. J.; Britt, R. D., Jr.; Wentworth, W. E. *Anal. Chem.* **1957**, *29*, 202.
- (6) Lewis, G. N.; Kasha, M. *J. Am. Chem. Soc.* **1944**, *66*, 2100.
- (7) Desilets, D. J.; Kissinger, P. T.; Lytle, F. E. *Anal. Chem.* **1987**, *59*, 1830.
- (8) Lakowicz, J. R.; Lazco, G.; Gryczynski, I. *Rev. Sci. Instrum.* **1986**, *57*, 2499.
- (9) Nithipatikom, K.; McGown, L. B. *Appl. Spectrosc.* **1987**, *41*, 395.
- (10) Keating-Nakamoto, S. M.; Cherek, H.; Lakowicz, J. R. *Anal. Chem.* **1987**, *59*, 271.
- (11) Marcelloni, M.; Fleming, G. R. *J. Chem. Phys.* **1987**, *86*, 6221.
- (12) Myers, A. B.; Hochstrasser, R. M. *J. Chem. Phys.* **1987**, *87*, 2116.
- (13) Hochstrasser, R. M.; Novak, F. A. *Chem. Phys. Lett.* **1977**, *48*, 1.

**Choosing a graduate school?  
Need to know who's doing  
research critical to yours?**

**New  
edition!**

**The ACS  
Directory of  
Graduate Research  
1989**

**All the information you need on chemical research and  
researchers at universities in the U.S. and Canada . . .  
in a single source.**

- Contains a wealth of facts on 683 academic departments, 11,938 faculty members, and 68,276 publication citations.
- Includes listings for chemistry, chemical engineering, pharmaceutical/medical chemistry, clinical chemistry, and polymer science.
- Lists universities with names and biographical information for all faculty members, their areas of specialization, titles of papers published in the last two years, and telephone numbers, FAX numbers, and computer addresses.

1436 pages (1989) Clothbound  
Price: US & Canada \$55.00 Export \$66.00

Call toll free (800) 227-5558 and charge your credit card. In Washington, D.C., call 872-4363.

Please send me \_\_\_\_\_ copy(ies) of the ACS Directory of Graduate Research 1989.  
Price: US & Canada \$55.00, Export \$66.00.

Payment enclosed (make checks payable to American Chemical Society)

Purchase order enclosed. P.O.# \_\_\_\_\_

Charge my:  Master Card  American Express  Diners Club/Carte Blanche

Account # \_\_\_\_\_ Expires \_\_\_\_\_

Signature \_\_\_\_\_ Phone \_\_\_\_\_

Ship books to:

Name \_\_\_\_\_

Address \_\_\_\_\_

City, State, ZIP \_\_\_\_\_

Orders from individuals must be prepaid. Please allow 3-6 weeks for delivery. Prices are quoted in U.S. dollars.

Mail this order form with your payment to: American Chemical Society, Distribution Office Dept. 705,  
P.O. Box 57136, West End Station, Washington, D.C. 20037.

705



- (14) Harris, J. M.; Chrisman, R. W.; Lytle, F. E.; Tobias, R. S. *Anal. Chem.* 1976, 48, 1937.
- (15) Watanabe, J.; Kinoshita, S.; Kushida, T. *Rev. Sci. Instrum.* 1985, 56, 1195.
- (16) Demas, J. N.; Keller, R. A. *Anal. Chem.* 1985, 57, 538.
- (17) Bright, F. V.; Hieftje, G. M. *Appl. Spectrosc.* 1986, 40, 583.
- (18) Wirth, M. J.; Chou, S.-H. *Anal. Chem.* 1988, 60, 1882.
- (19) Hirschfeld, T.; Chase, B. *Appl. Spectrosc.* 1986, 40, 133.
- (20) Williamson, J. M.; Bowling, R. J.; McCreery, R. L. *Appl. Spectrosc.* 1989, 43, 372.
- (21) Asher, S. A.; Johnson, C. R.; Murtaugh, A. *Rev. Sci. Instrum.* 1983, 54, 1657.
- (22) Debye, P. *Polar Molecules*; Dover: New York, 1929.
- (23) Chuang, T. J.; Eisenthal, K. B. *J. Chem. Phys.* 1972, 57, 5094.
- (24) Blanchard, G. J.; Wirth, M. J. *J. Chem. Phys.* 1985, 82, 39.
- (25) Bright, F. V.; McGown, L. B. *Anal. Chem.* 1986, 58, 1424.
- (26) Fork, R. L.; Brito, C. H.; Becker, P. C.; Shank, C. V. *Opt. Lett.* 1987, 10, 609.
- (27) Finch, A.; Sleat, W. E.; Sibbett, W. *Rev. Sci. Instrum.* 1989, 60, 839.
- (28) Heritage, J. P.; Allara, D. P. *Chem. Phys. Lett.* 1980, 74, 507.
- (29) Levine, B. F.; Bethea, C. G. *Appl. Phys. Lett.* 1980, 36, 245.
- (30) Blanchard, G. J.; Wirth, M. J. *Anal. Chem.* 1986, 58, 532.
- (31) Shah, J. *IEEE J. Quantum Electron.* 1988, 24, 276.
- (32) Kał low, M. A.; Jarzeba, W.; DuBruil, T. P.; Barbara, P. F. *Rev. Sci. Instrum.* 1988, 59, 1098.
- (33) Harris, J. M.; Chrisman, R. W.; Lytle, F. E.; Tobias, R. S. *Appl. Phys. Lett.* 1975, 26, 16.
- (34) Chan, C. K.; Sari, S. O. *Appl. Phys. Lett.* 1974, 25, 403.
- (35) Mahr, H.; Hirsch, M. D. *Opt. Commun.* 1975, 13, 96.
- (36) Wirth, M. J.; Sanders, M. J.; Koskelo, A. C. *Appl. Phys. Lett.* 1981, 38, 295.
- (37) Elzinga, P. A.; Lytle, F. E.; Jaing, Y.; King, G. B.; Laurendeau, N. M. *Appl. Spectrosc.* 1987, 41, 2.
- (38) Kneisler, R. J.; Lytle, F. E.; Fiechtner, G. J.; Jiang, Y.; King, G. B.; Laurendeau, N. M. *Opt. Lett.* 1989, 14, 260.
- (39) Choi, K.-J.; Gustafson, T. L. *IEEE J. Quantum Electron.*, in press.
- (40) Blanchard, G. J.; Wirth, M. J. *J. Phys. Chem.* 1986, 90, 2521.
- (41) Wirth, M. J.; Chou, S.-H. In *Advances in Luminescence Spectroscopy*; Eastwood, D., Ed. ASTM: Philadelphia, in press.
- (42) Choi, K.-J.; Wirth, M. J. *J. Phys. Chem.* 1989, 93, 7694.
- (43) Blar chard, G. J. *J. Phys. Chem.* 1988, 92, 6303.
- (44) Blar chard, G. J.; Cihal, C. A. *J. Phys. Chem.* 1988, 92, 5950.
- (45) Blar chard, G. J. *Anal. Chem.* 1989, 61, 2394.
- (46) Gustafson, T. L.; Roberts, D. M.; Chernoff, D. A. *J. Chem. Phys.* 1983, 79(4), 1559.
- (47) Gustafson, T. L.; Roberts, D. M.; Chernoff, D. A. *J. Chem. Phys.* 1984, 81, 3438.
- (48) Gustafson, T. L.; Palmer, J. F.; Roberts, D. M. *Chem. Phys. Lett.* 1986, 127, 505.
- (49) Blanchard, G. J.; Heritage, J. P.; Von Lehman, A. C.; Kelly, M. K.; Baker, G. L.; Etemad, S. *Phys. Rev. Lett.* 1989, 63, 887.
- (50) Gustafson, T. L.; Scher, H.; Roberts, D. M.; Collins, R. W. *Phys. Rev. Lett.* 1988, 60, 148.



Mary J. Wirth is an associate professor of chemistry at the University of Delaware. She received her B.S. degree from Northern Illinois University (1974) and her Ph.D. from Purdue University (1978). At Purdue, her research on the quantitative aspects of two-photon spectroscopy was carried out under the guidance of Fred E. Lytle. Her research interests include the application of laser spectroscopic measurements to the understanding of solvation phenomena, specifically with regard to chemical separations.



## WHAT'S HAPPENING IN CHEMISTRY?

Within the pages of *What's Happening in Chemistry?* you'll find the wonder of discovery and the thrill of problem-solving. Sample topics are:

- Lightning May Fix More Nitrogen Than Bacteria
- A New Way to Clean Up Oil Spills
- Seesaw Battle Against the Common Cold

A valuable supplement to your textbook, this award-winning publication will bring the excitement of today's science to your students.

*What's Happening in Chemistry?* has received high praise from writers, teachers, and students. Here's what reviewers had to say about last year's edition:

*"What's happening in chemistry? A good way to find out would be to pick up a copy of the American Chemical Society's...journal of the same name."* **Science Teacher**

*"...accessible for readers who want to learn more about a broad range of current developments in chemical research."*

**Science Books & Films**

### WHAT'S HAPPENING IN CHEMISTRY?

ALL ORDERS MUST BE PREPAID

Charge My  VISA/MasterCard  American Express  
 Diners Club/Carte Blanche  Barclaycard  Access

Please Type or Print

Card # \_\_\_\_\_ Exp. Date \_\_\_\_\_

Interbank # \_\_\_\_\_ Signature \_\_\_\_\_

Name \_\_\_\_\_ Telephone \_\_\_\_\_

Organization \_\_\_\_\_

Address \_\_\_\_\_ City \_\_\_\_\_ State \_\_\_\_\_ Zip \_\_\_\_\_

(ACS 56170/7390/A113) American Chemical Society, Department of Public Communication, 1155 Sixteenth Street, N.W., Washington, D.C. 20036

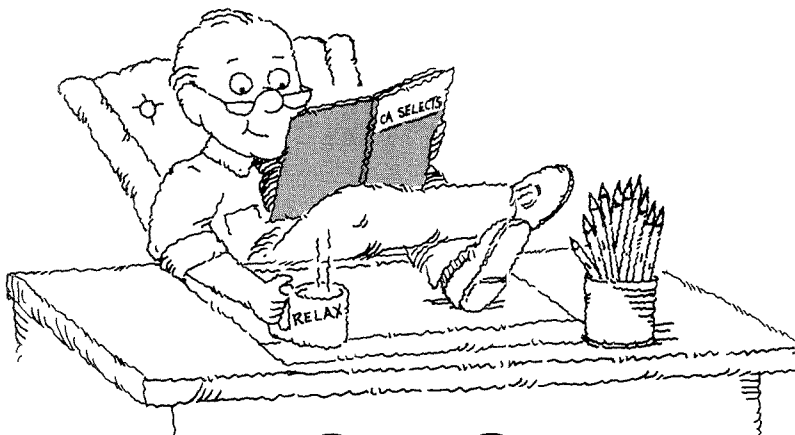
QUANTITY \_\_\_\_\_

COST \_\_\_\_\_

ISBN #0-8412-1649-5 @ \$5.00 \_\_\_\_\_

Foreign Add \$1.50 \_\_\_\_\_

TOTAL \_\_\_\_\_



## RELAX AND STAY CURRENT WITH CHEMICAL LITERATURE

CA SELECTS is a series of current awareness publications that are produced from the Chemical Abstracts (CA) database. *You can relax*, knowing that a profile will be run every other week to search all relevant current literature covered by CA for your area of interest. From our computer to you, a review of chemical literature in just 10–12 pages (on the average).

All this for just \$170.00—\$654 an issue, about 5 cents per abstract! Find out if CA SELECTS covers your research interests by sending for your FREE copy of all 215 topic descriptions.

Mail coupon to:  
Chemical Abstracts Service  
Marketing Dept. 31390  
2540 Olentangy River Road  
P.O. Box 3012  
Columbus, Ohio 43210, U.S.A.

Or call us at: (614) 447-3731;  
or 1-800-848-6538 (ask for Customer Service).

### CA SELECTS Catalog Coupon

YES! Please send me the descriptions of all 215 topics.

Name \_\_\_\_\_

Job Title \_\_\_\_\_

Organization \_\_\_\_\_

Address \_\_\_\_\_  
\_\_\_\_\_

City \_\_\_\_\_

State/Zip \_\_\_\_\_

Country \_\_\_\_\_

Phone Number \_\_\_\_\_

Chemical Abstracts Service is a division of the American Chemical Society.

## Conferences

■ **International Symposium on Characterization of Macromolecules Used as Pharmaceutical Excipients.** March 7-9. Gothenburg, Sweden. Contact: *Swedish Academy of Pharmaceutical Sciences, P.O. Box 1136, S-111 81 Stockholm, Sweden*

■ **22nd Annual Meeting of the National Committee for Clinical Laboratory Standards.** March 29-30. Bethesda, MD. Contact: *NCCLS, 771 E. Lancaster Ave., Villanova, PA 19085 (215-525-2435)*

■ **9th International Conference on Fundamental Aspects, Analytical Techniques, Processes, and Applications of Pyrolysis (Pyrolysis '90).** June 11-15. Noordwijkerhout, The Netherlands. Contact: *Louise Roos, FOM-Institute for Atomic and Molecular Physics, Kruislaan 407, 1098 SJ Amsterdam, The Netherlands*

■ **83rd Annual Meeting of the Air and Waste Management Association.** June 24-29. Pittsburgh, PA. Contact: *Air and Waste Management Association, P.O. Box 2861, Pittsburgh, PA 15230 (412-232-3444)*

■ **6th Annual Waste Testing and Quality Assurance Symposium.** July 16-20. Washington, DC. Contact: *American Chemical Society, Room 205, 1155 16th St., N.W., Washington, DC 20036*

■ **Inter/Micro-90.** Aug. 20-24. Chicago, IL. Contact: *Nancy Daerr, McCrone Research Institute, 2820 S. Michigan Ave., Chicago, IL 60616*

■ **10th International Symposium on HPLC of Proteins, Peptides, and Polynucleotides.** Oct. 29-31. Wiesbaden, F.R.G. Contact: *Secretariat, 10th ISPPP, P.O. Box 28, S-75103 Uppsala, Sweden*

## Short Courses and Workshops

For information on the following courses, contact *Toula Hionis, Pharmacia LKB Biotechnology, 800 Centennial Ave., Piscataway, NJ 08854 (201-457-8470)*

■ **Pilot Scale (from Milligrams to**

**Grams) Protein Purification.** March 6-9. Piscataway, NJ

■ **Validation Issues in Chromatographic Processes.** March 12. Piscataway, NJ

■ **Process Chromatography Techniques: Theory and Practice.** March 27-29. Piscataway, NJ

■ **Large-Scale Column Packing and Evaluation.** March 30. Piscataway, NJ

For information on the following courses, contact *Stat-Ease, 3801 Nicollet Ave. S., Minneapolis, MN 55409 (612-822-5574)*

■ **Experiment Design Made Easy.** March 13-22. St. Paul, MN

■ **Advanced Experiment Design.** April 23-26. St. Paul, MN

For information on the following courses, contact *Barbara Sherman, Professional Analytical and Consulting Services, 409 Meade Dr., Coraopolis, PA 15108 (412-262-4222)*

■ **Course on Inductively Coupled Plasma Spectrochemical Analysis.** March 2-22. Pittsburgh, PA

■ **Course on Quality Assurance of Chemical Measurements.** March 22-23. Pittsburgh, PA

■ **Courses on Supercritical Fluid Chromatography and 2D NMR.** April 19-20. Pittsburgh, PA

■ **Course on Infrared Spectrometry and Spectral Interpretation.** May 7-9. Pittsburgh, PA

For information on the following courses, contact *Tammy Morante, NUS Chemistry Training Center, Park West Two, Pittsburgh, PA 15275 (412-788-1080)*

■ **Advanced Gamma Spectroscopy.** March 26-29 and June 25-28. Pittsburgh, PA

■ **Power Plant Ion Chromatography.** April 30-May 4. Pittsburgh, PA

■ **Radiochemistry Principles and Applications.** May 7-18. Pittsburgh, PA

■ **Course and Workshop on Interpretation of IR and Raman Spectroscopy.** May 14-19. Nashville, TN. Contact: *Clara Craver, Fisk Infrared Institute, Box 15, Fisk University, Nashville, TN 37203 (314-962-5752)*

## Call for Papers

■ **International Conference on Ion-Exchange Processes (Ion-Ex '90).** July 9-11. Wrexham, U.K. Conference topics will include instrumental developments; environmental, inorganic, organic, biological, water, and pharmaceutical analysis; development of new materials; ion-exchange membranes; ion exclusion chromatography; ion chromatography and associated techniques; fundamental studies of ion-exchange processes and materials; and applications in the nuclear industry. Authors wishing to contribute poster presentations should submit 250-word abstracts by May 31 to Secretariat, Ion-Ex '90, Research Division, The North East Wales Institute, Deeside, Clwyd CH5 4BR, U.K.

■ **Euroanalysis VII.** Vienna, Austria. Aug. 26-31. The scientific program will consist of invited lectures and contributed oral and poster presentations on applications of analytical chemistry (environmental systems and food, pharmaceutical and biomedical science, biotechnology, materials science, and arts and archeology) and methodological developments in analytical chemistry (including atomic spectroscopy, molecular spectroscopy, separation techniques, electrochemical methods, sensors, radiochemical and nuclear techniques, thermal analysis, local and surface analysis, structure analysis of solids, and immunoassay). Special sessions are also planned on sample preparation for inorganic and organic trace analysis, computer-based analytical chemistry, quality assurance in analytical chemistry, and education and training in analytical chemistry. Prospective authors should request appropriate forms from M. Grasserbauer, Interconvention, Austria Center Vienna, A-1450 Vienna, Austria. Abstracts received after February 28 may not be considered.

---

These events are newly listed in the JOURNAL. See back issues for other events of interest.

---

**For state-of-the-art research and technology**

# Journal of Chemical Information and Computer Sciences

An American Chemical Society Publication

George W.A. Milne, Editor,  
National Institutes of Health

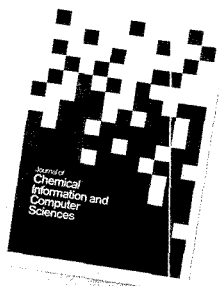
Edited for chemists, chemical engineers, and computer scientists, this international quarterly journal provides highly topical coverage of:

- data acquisition and analysis
- pattern recognition and artificial intelligence
- new algorithms and applications of existing algorithms
- interfacing techniques
- computer systems and components
- graphics, simulation, and modeling
- operations research
- econometric and management systems
- indexing classification and notation systems
- data correlation, information systems, nomenclature, and linguistics and communication
- information sources and services
- design and applications of computerized information and data systems.

The *Journal of Chemical Information and Computer Sciences* includes peer-reviewed research studies, programming innovations, software reviews, invited papers, and book reviews.

## Submit your original work!

Under new editorship, the *Journal of Chemical Information and Computer Sciences* is designed to attract the exact audience of experts whom you want to reach. For manuscript guidelines please contact: George W.A. Milne, Building 37, Room 5C28, National Institutes of Health, Bethesda, MD 20892, 301/496-3597.



### Associate Editors

W.A. Warr, ICI, UK  
R. Luckenbach, Beilstein Institute, Germany

### Software Editor

S. R. Heller, U.S.D.A.

### Advisory Board

B.A. Hohne, Rohm & Hass  
C.P. Jochum, Beilstein Inst., Germany  
G. Kramer, Purdue Univ.  
C.H. Lochmuller, Duke Univ.  
S.R. Lowry, Nicolet Analytical Instruments  
M. Munk, Arizona State Univ.  
F.A. Settle, Jr., Virginia Military Inst.  
W.G. Town, Hampden Data Services Limited, England  
T. Yamamoto, Univ. of Library Information Science, Japan

## 1990 Subscription Information

	U.S.	Canada and Mexico	Europe**	All Other Countries*
ACS Members*				
One year	\$ 18	\$ 22	\$ 24	\$ 26
Two years	\$ 32	\$ 40	\$ 44	\$ 48
Nonmembers	\$108	\$112	\$114	\$116

\*Member rates are for personal use only.  
\*\*Air service included.

For more information or to subscribe, write:

American Chemical Society  
Marketing Communications Department  
1155 Sixteenth Street, NW  
Washington, DC 20036  
1-800-227-5558 or (202) 872-4363  
TLX 440159  
FAX 202/872-4615

For nonmember rates in Japan contact Maruzen Co., Ltd.  
This publication is available on microfiche, microfilm, and online on CJO on STN International.

## Electron Microscopy and FT-IR

**Electron Microscopy and Analysis, 2nd Edition.** P. J. Goodhew and F. J. Humphreys. 223 pp. Taylor & Francis, 79 Madison Ave., New York, NY 10016. 1988. \$27

*Reviewed by M. V. Parthasarathy, Section of Plant Biology, 228 Plant Sciences Bldg., Cornell University, Ithaca, NY 14853*

Currently there are at least a dozen books on electron microscopy and analysis available on the market, and undoubtedly there are more in press. What then is different or new in this book by Goodhew and Humphreys? For one thing, it is one of the most affordable books available on the subject. Second, the authors have managed to cover a great deal of material within 223 pages (excluding the index). The book is primarily aimed at those interested in material sciences, but there is much information that can also be useful to others. The subject matter is well organized, and the authors have explained some of the difficult concepts in a lucid manner.

Five out of the seven chapters in the book are devoted to the principles and techniques of transmission and scanning electron microscopes. Basic principles and concepts of optics, electrons, and their interaction with specimens are very well presented and supplemented by carefully chosen figures. The chapter on electron diffraction, which has been added in this edition, is especially well covered.

The principles, designs, and techniques of transmission and scanning electron microscopes are explained well, if not in great detail. The use of computers to achieve digital beam control, image storage, and processing is also adequately described. Again, in this section the authors have used appropriate examples and figures very effectively.

Microanalysis in the electron microscope has become a powerful tool, and the authors' decision to add an entire chapter on chemical analysis for the second edition is commendable. Although this chapter is quite concise (44 pages), it covers most of the important principles of X-ray energy-dispersive spectrometry (EDS), X-ray wave-

length dispersive spectrometry (WDS), and electron energy loss spectrometry (EELS). The advantages and disadvantages of these techniques are well covered. Unfortunately, the use of ultra-thin windows in detectors of EDS systems has received only a passing remark. Ultra-thin window detectors, which are now used routinely in several laboratories, have solved most of the problems that are inherent in using windowless detectors and have extended the practical capability of EDS systems to the determination of light elements (e.g., C, N, and O). The last chapter offers an excellent summation of other techniques available for characterization of materials.

Because of the breadth of the subjects covered, the book is necessarily short on details. However, it is an excellent introduction for those who have little knowledge of electron microscopy or microanalysis.

**Advances in Applied Fourier Transform Infrared Spectroscopy.** M. W. Mackenzie, Ed. xii + 353 pp. John Wiley & Sons, 605 Third Ave., New York, NY 10158. 1988. \$95

*Reviewed by Bruce Chase, CRD 328/163, Du Pont Experimental Station, P.O. Box 80328, Wilmington, DE 19880-0328*

This book is essentially a collection of diverse chapters on various experimental techniques in IR spectrometry. The sole unifying feature is their dependence on interferometric instruments for enhanced signal-to-noise ratio or rapid data acquisition. For the reader who asks, "What are some of the different measurements I can now make with interferometers?", this volume will save the time involved in searching the literature. For those interested in polarization-modulation experiments in vibrational circular dichroism, for example, this is a good introduction, but it will not substitute for the current literature.

Chapter 1 stands alone since it is not related to any specific experiment but introduces the basic concepts in data analysis. Unfortunately, the very active

areas of resolution enhancement and multicomponent analysis are ignored. The concepts presented are not very relevant to the remainder of the volume, and it is not clear why the editors included it.

The second chapter reviews the development and current status of GC/IR. The relevant references are included, and the author gives a reasonable view of the future. The advent of the matrix isolation approach to GC/IR is well covered.

While the development and use of polarization-modulation techniques in FT-IR has not progressed past initial use in a few labs, the potential for the future is tremendous. Chapter 3 provides a sound basis for understanding the experimental requirements and difficulties in double (or triple) modulation experiments.

In Chapter 4 the authors do an excellent job reviewing potential approaches to analyzing solid samples. The strengths and weaknesses of microscopy, diffuse reflectance, and emission are well stated. For a beginning spectroscopist in an industrial laboratory, this is an excellent place to start.

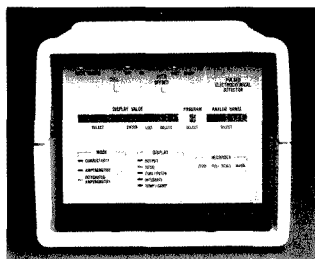
The limited amount of work done in rheo-optical FT-IR spectrometry is well reviewed in Chapter 5. The basis for looking at segment reorientation and the polarization measurements of orientation in polymers is explained quite clearly. The only aspect that is missing is the two-dimensional work recently discussed by Marcott and co-workers.

Chapter 6 stands apart from the remainder of the volume in that it is primarily a discussion of theoretical approaches to intensity and frequency calculation. The chapter also discusses the structure and dynamics of polyethylene chain systems.

The final chapter discusses IR spectrometry of catalyst systems under reactor conditions. Much of this chapter builds on the discussions of solid sampling techniques given earlier in the book. Transmission, emission, and photoacoustic approaches to catalyst studies are cited.

Most chapters have literature references through 1987 and provide reasonable introductions to the specific experiments discussed. As a desk reference I would give it a 5 out of 10.

# NEW PRODUCTS



**Pulsed electrochemical detector** features conductometric and amperometric capabilities. Applications include detection of inorganic anions and cations, organic acids, amines, alcohols, thiols, and carbohydrates. Dionex 401

**XRF.** Omicron X-ray microfluorescence spectroscopy system provides nondestructive small-area elemental and thickness analyses. Applications include multilayer, multielement film thickness and composition analyses at the microstructure level as well as contamination and failure analyses. KeveX Instruments 404

**Detector.** HP 1049A programmable electrochemical detector for LC features a built-in pulse mode that automatically keeps the electrode clean during a chromatographic run. Optional gold or platinum electrodes are available for special applications. Hewlett-Packard 405

**ICP.** Single-channel Plasma 1000 and dual-channel Plasma 2000 ICP emission spectrometers allow the selection of any emission line from a built-in 50,000-line wavelength table or any wavelength between 165 and 800 nm. The spectrometers are controlled by an industry standard 80386-based computer. Perkin-Elmer 406

**Gas analysis.** Odyssey 2001 is a portable, microprocessor-based analyzer that automatically measures and displays real-time gas concentrations in the 0–1000 ppb range. Applications include indoor pollution and personnel exposure monitoring. TRI 407

**Robotics.** Autolab 500 is a polar coordinate robot that allows control of sample preparation procedures or entire

assays, including tube- or plate-based immunoassays. Liquid-handling features include liquid-level sensing and dual probe sampling. Kemble Instruments 408

**MS.** GloQuad glow discharge mass spectrometer features a glow discharge source with cryo-cooling, a dual detector system with a linear dynamic range of > 7 orders of magnitude, multitasking software, and sample throughput of ~5 samples per hour. VG Instruments 409

**Digestion.** Büchi 420 Kjeldahl rapid digestion unit accommodates sample volumes of up to 10 g of powder or 200 mL of liquid. The unit, which can digest up to two samples simultaneously, features a built-in fan that cools the hot tubes and digested samples after they are automatically raised out of the heaters. Brinkmann Instruments 410

**LC.** Carlo Erba System 20 is a modular micro HPLC system that features isocratic and gradient capabilities. The high-pressure syringe pump provides flow rates in the 1–4000  $\mu\text{L}/\text{min}$  range and allows the user to purge or change solvents without removing the column. Fisons Instruments 411

**Oxygen.** Model 600 Oxan oxygen analyzer measures the percent concentration of oxygen in air and parts-per-million levels of dissolved oxygen in aqueous solutions in ranges of 0–100% and 0–20 ppm, respectively. The sensor can withstand pressures up to 25 psi. Engineered Systems and Designs 412

**Centrifuge.** Bench-top refrigerated centrifuge, which produces temperatures down to 1 °C with  $\pm 1$  °C accuracy, includes an automatic safety feature that prevents damage to the centrifuge and samples if unsafe speed, temperature, or rotor conditions develop. Wheaton 413

## Software

**Data handling.** DataTalk is a menu-driven software package that collects, manipulates, and formats data from laboratory instruments equipped with

an RS-232 port. Results can be exported to custom-designed reports or transferred to another computer. Labtronics 415

**Image analysis.** JAVA 1.3 video image analysis software, designed for IBM and compatible personal computers, features pseudocolor support and clear-field lighting equalization. Capabilities include densitometry, morphometric analysis, automatic line and edge digitizing, and automatic object counting. Jandel Scientific 416

## Manufacturers' Literature

**Process analysis.** Brochure discusses use of the Model 400 photometric analyzer in the pulp and paper industry. Applications at each stage of paper manufacturing are described. Du Pont 418

**LC.** *Chromatogram*, Vol. 10, No. 3, includes articles on metabolism, software, quality control, and foods and beverages. Recently published papers on HPLC are also discussed. 16 pp. Beckman Instruments 419

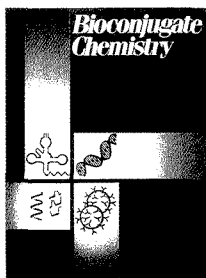
**GPC.** Brochure discusses the analysis of synthetic and natural polymers, environmental samples, and small organic molecules by gel permeation chromatography. 16 pp. HPLC Technology 420

**Electrophoresis.** Application notes describe use of the Model 230A high-performance preparative electrophoresis system for the purification of proteins, DNA, and synthetic oligonucleotides. Applied Biosystems 421

**Sample preparation.** Brochure describes the ASTED system for on-line preparation of biological and industrial samples prior to HPLC analysis. The system is based on a combination of dialysis and trace enrichment. Gilson Medical Electronics 423

For more information on listed items, circle the appropriate numbers on one of our Readers' Service Cards

**A long-awaited unifying medium for virtually any practitioner of conjugation chemistry**



# Bioconjugate Chemistry

Premiering January/February 1990.

**Editor:** Claude F. Meares,  
University of California, Davis

## Centralized Access Is Here!

In *bimonthly* issues, **Bioconjugate Chemistry** will bring together important research findings in the fast-developing discipline of conjugation chemistry. Now—in a *single, time-saving source*—you'll find information which otherwise might be scattered throughout broader-focus scholarly journals.

The central theme of **Bioconjugate Chemistry** is the joining of two different molecular functions by chemical or biological means. This includes:

### Conjugation of . . .

antibodies (and their fragments)  
nucleic acids and their analogs ( $\alpha$ -anomers, phosphonates, . . .)  
liposomal components  
other biologically active molecules (receptor-binding proteins, hormones, peptides, . . .)

### with each other or with any molecular groups that add useful properties . . .

drugs, radionuclides, toxins, fluorophores, photoprobes, inhibitors, enzymes, haptens, ligands, etc.

There is *no* journal with this precise focus published today.

## The Leading Edge In Biomedical Advances

**Bioconjugate Chemistry** will publish research at the core of many biotechnology enterprises, as well as of specific interest to biomedical firms, drug companies, and chemical laboratories.

Topics will emphasize the *chemical* aspects of conjugate preparation and characterization . . . *in vivo* applications of conjugate methodology . . . *molecular biological* aspects of antibodies, genetically engineered fragments, and other immunochemicals . . . and the relationships between conjugation chemistry and the biological properties of conjugates.

## Guided by a "Who's Who" in the Field

Editor: Claude F. Meares,  
Univ. of Calif., Davis

### 1990 Editorial Advisory Board

- V. Alvarez, Cytogen Corp.  
L. Arnold, Gen-Probe  
R. W. Atcher, Argonne Natl. Labs  
R. W. Baldwin, Univ. of Nottingham, England  
T. Burnol, Eli Lilly & Co.  
K. Chang, Immunomedics  
G. David, Hybritech, Inc.  
P. B. Dervan, California Inst. of Tech.  
D. Dolphin, Univ. of British Columbia, Canada  
T. W. Doyle, Bristol-Myers  
R. E. Feeney, Univ. of California, Davis  
D. Fitzgerald, Natl. Inst. of Health  
J. M. Frincke, Hybritech, Inc.  
A. Fritzbeg, NeoRx Corp.  
W. F. Goeckler, Dow Chemical Co.  
D. Goodwin, Stanford Univ.  
E. Haber, E.R. Squibb and Sons, Inc.  
T. Hara, Inst. for Biomedical Res., Japan  
R. Haugland, Molecular Probes, Inc.  
J. Hearst, Univ. of California, Berkeley  
N. Heindel, Lehigh Univ.  
C. Helene, Museum National D'Histoire Naturelle, France  
E. Hurwitz, Weizmann Inst. of Science, Israel  
D. Johnson, Abbott Labs  
D. Kaplan, Dow Chemical Co.  
B. A. Khaw, Massachusetts Gen. Hospital  
K. Krohn, Univ. of Washington  
P. Miller, Johns Hopkins Univ.  
H. Nagasawa, Univ. of Minnesota, Minneapolis  
P. Nielsen, Univ. of Copenhagen, Denmark  
A. Oseroff, Tufts New England Medical Ctr.  
M. Ostrow, The Liposome Co., Inc.  
G. Pietersz, Univ. of Melbourne, Australia  
R. Reisfeld, Scripps Clinic & Res. Fnd.  
S. Rocklage, Sealtar, Inc.  
J. Rodwell, Cytogen Corp.  
P. Schultz, Univ. of California, Berkeley  
P. Senter, Oncogen  
S. Srivastava, Brookhaven Natl. Lab.  
P. E. Thorpe, Imperial Cancer Res. Fund, England  
G. Tolman  
A. Tramontano, Scripps Clinic & Res. Fnd.  
J. Uppeslaci, Lederle Lab.  
R. S. Vickers, Sterling Drug Co.  
E. S. Vitetta, Univ. of Texas, Dallas  
S. Wilbur, NeoRx Corp.  
M. Wilchek, Weizmann Inst. of Science, Israel  
M. Zalutsky, Duke Univ.

## Attention Prospective Contributors!

**With its exclusive, focused readership, Bioconjugate Chemistry will attract the specific audience of experts whom you want to reach, and is committed to prompt publication of manuscripts.**

**For information on submitting your original work, please contact  
Dr. Claude F. Meares,  
Department of Chemistry,  
University of California, Davis, CA 95616  
(916/752-3360).**

## NEW PRODUCTS

**Detector.** Brochure highlights the AD-200 absorbance detector for HPLC and capillary electrophoresis. The double-beam system features a wavelength range of 190–700 nm and a bandwidth of 5 nm. SpectroVision 422

radiolabeled ligands for use in RIA, EIA, or fluorescent immunoassays. Sigma Immunochemicals 426

**Safety.** Catalog includes cabinets, clothing, drums, cans, eyewear, first aid products, gas cylinder apparatus,

gloves, labels, pumps, respirators, signs, and spill control products. 48 pp. Lab Safety Supply 427

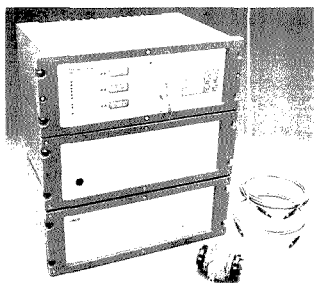
**Standards.** Catalog features GC/MS standards for environmental analysis, including carbon-13 labeled and native chlorodibenzo-*p*-dioxins, chlorodibenzofurans, polychlorinated biphenyls, bromodibenzofurans, and bromodibenzo-*p*-dioxins. Cambridge Isotope Laboratories 428

## Catalogs

**Standards.** Catalog lists chlorinated, brominated, and methylated chlorinated dibenzo-*p*-dioxins and dibenzofurans. Unlabeled, radioisotope-labeled, and stable-isotope-labeled compounds are included. Chemsyn Science Laboratories/Wellington Laboratories 431

**Chromatography.** Catalog features more than 5000 products for chromatography, including HPLC and GC columns, high-purity solvents, and EPA precleaned vials. Scientific Products Division, Baxter Healthcare 425

**Immunochemicals.** Catalog lists immunochemicals and related products, including antisera to drugs with matched enzyme, fluorochrome, or



LIMOR L is a near-IR multiple-component liquid analyzer that diffracts IR light into selected wavelengths without using moving parts. The system provides simultaneous analysis of up to four liquid components. Westinghouse Electric 402

**Environmental analysis.** Catalog describes reagents, high-purity solvents, and chromatography products for the analysis of organic and inorganic pollutants. Included are standards, sample preparation products, LC and vacuum pumps, replacement parts, a conductivity monitor, and test kits. 40 pp. EM Science 429

**Biotechnology.** Catalog lists products for chromatography, electrophoresis, filtration, sample preparation, and cell culture/fermentation. Immunoaffinity columns and packings and TLC accessories are included. 64 pp. Kontes Biotechnology 430

# LABORATORY SERVICE CENTER

Acetonedicarboxylic Acid & esters • Allyl-iso-Valerate • Aluminon  
DL-Aspartic Acid • Azelaic Acid • Benzoic Anhydride • Cesium Chloride  
Dihydroxyacetone • 3,5-Dihydroxybenzoic Acid • Dimethyl Adipate  
4-Dimethylaminobenzalrhodanine • Dimethylglyoxime • EGTA • Fluorenone  
Giemsa Stain • Glutaric Anhydride • Imidazole • Maltose • Methyl Acetam de  
3-Methylglutaric Anhydride • 4-Methylpentanoic Acid • Salicin  
Sodium Tetraphenylboron • Succinimide • Sulfosalicylic Acid • Thionin  
Trisodium Pentacynoamineferroate • iso- & o-Vanillin • Veratrole

Write for our Products List of over 3,000 chemicals

Tel: 516-273-0900 • TOLL FREE: 800-645-5565

Telefax: 516-273-0858 • Telex: 497-4275

**EASTERN CHEMICAL**  
A Division of UNITED-GUARDIAN, INC.

P. O. Box 2500  
DEPT. AC  
SMITHTOWN, N.Y. 11787

**Laboratory Service Center** (Equipment, Materials, Services, Instruments for Leasing). Maximum space — 4 inches per advertisement. Column width, 2-3/16"; two column width, 4-9/16". Artwork accepted. No combination of directory rates with ROP advertising. Rates based on number of inches used within 12 months from first date of first insertion. Per inch: 1" — \$165; 12" — \$160; 24" — \$155; 36" — \$150; 48" — \$145.

CALL OR WRITE JANE GATENBY

**ANALYTICAL CHEMISTRY**  
500 Post Road East  
P.O. Box 231  
Westport, CT 06880  
203-226-7131/FAX: 203-454-9939

## HELP WANTED ADS

ROP display at ROP rates. Rate based on number of insertions within contract year. Cannot be combined for frequency.

Unit	1-Ti	6-Ti	12-Ti
1" (25 mm)	\$190	\$170	\$160
	24-Ti	48-Ti	72-Ti
	\$150	\$140	\$130

CALL OR WRITE JANE GATENBY

**ANALYTICAL CHEMISTRY**  
500 Post Road East  
P.O. Box 231  
Westport, CT 06880  
203-226-7131  
FAX: 203-454-9939

## FREE DATA, FAST

To quickly amass data on all of the products you need, consult the Lab Data Service Section on our *Analytical Chemistry* reader reply card insert.



## INDEX TO ADVERTISERS IN THIS ISSUE

CIRCLE INQUIRY NO.	ADVERTISERS	PAGE NO.
28.....	Caframo, Ltd. ....	269A

**CENTCOM, LTD**  
*President*  
**James A. Byrne**

*Executive Vice President*  
**Benjamin W. Jones**

**Clay S. Holden, Vice President**  
**Robert L. Voepel, Vice President**  
**Joseph P. Stenza, Production Director**

75.....	*Leybold Vacuum Products, Inc. ....	OBC
	CD Werbeagentur GmbH	

500 Post Road East  
P.O. Box 231  
Westport, Connecticut 06880  
(Area Code 203) 226-7131  
Telex No. 643310  
FAX: 203-454-9939

ADVERTISING SALES MANAGER  
**Bruce E. Poorman**

90.....	*Matheson Gas Products .....	259A
	Kenyon Hoag Associates	

ADVERTISING PRODUCTION MANAGER  
**Jane F. Gatenby**

### SALES REPRESENTATIVES

	Philadelphia, PA . . . Patricia O'Donnell, CENTCOM, LTD., GSB Building, Suite 405, 1 Belmont Avenue, Bala Cynwyd, Pa. 19004. Telephone: 215-667-9666, FAX: 215-667-9353	
	New York, NY . . . John F. Raftery, CENTCOM, LTD., 60 East 42nd St., New York, N.Y. 10165. Telephone: 212-972-9660	
	Westport, CT . . . Edward M. Black, CENTCOM, LTD., 500 Post Road East, P.O. Box 231, Westport, Ct. 06880. Telephone: 203-226-7131, Telex 643310, FAX: 203-454-9939	
124-129.....	*SLM Instruments, Inc. ....	IFC
	Cleveland, OH . . . Bruce E. Poorman, John C. Guyot, CENTCOM, LTD., 325 Front St., Suite 2, Berea, Ohio 44017. Telephone: 216-234-1333, FAX: 216-234-3425	
	Chicago, IL . . . Michael J. Pak, CENTCOM, LTD., 540 Frontage Rd., Northfield, Ill. 60093. Telephone: 708-441-6383, FAX: 708-441-6382	
	Houston, TX . . . Michael J. Pak, CENTCOM, LTD. Telephone: 708-441-6383	
	San Francisco, CA . . . Paul M. Butts, CENTCOM, LTD., Suite 1070, 2672 Bayshore Frontage Road, Mountain View, CA 94043. Telephone: 415-969-4604	
	Los Angeles, CA . . . Clay S. Holden, CENTCOM, LTD., Newton Pacific Center, 3142 Pacific Coast Highway, Suite 200, Torrance, CA 90505. Telephone: 213-325-1903	
	Boston, MA . . . Edward M. Black, CENTCOM, LTD. Telephone: 203-226-7131	
135.....	*Supelco, Inc. ....	261A
	Atlanta, GA . . . John F. Raftery, CENTCOM, LTD. Telephone: 212-972-9660	
	Denver, CO . . . Paul M. Butts, CENTCOM, LTD. Telephone: 415-969-4604	
	United Kingdom	
	Reading, England . . . Malcolm Thiele, Technomedia Ltd., Wood Cottage, Shurlock Row, Reading RG10 0QE, Berkshire, England. Telephone: 073-434-3302, Telex #848800, FAX: 073-434-3848	
	Lancashire, England . . . Technomedia Ltd., c/o Meconomics Ltd., Meconomics House, 31 Old Street, Ashton Under Lyne, Lancashire, England. Telephone: 061-308-3025	
	Continental Europe . . . Andre Jamar, International Communications, Inc., Rue Mallar 1, 4800 Verviers, Belgium. Telephone: (087) 22-53-85, FAX: (087) 23-03-29	
	Tokyo, Japan . . . Sumio Oka, International Media Representatives Ltd., 2-29 Toranomon, 1-Chome Minato-ku Tokyo 105 Japan. Telephone: 502-0656, Telex #22633, FAX: 591-2530	

Directory section, see page 284A.

\* See ad in ACS Laboratory Guide.

Advertising Management for the American Chemical Society Publications



# JANAF THERMOCHEMICAL TABLES

## Third Edition

A Major Supplement from JOURNAL OF PHYSICAL AND CHEMICAL REFERENCE DATA

Presenting Reliable Data Utilized by Chemists, Chemical Engineers, and Materials Scientists from Around the World for Over 25 Years

JOURNAL OF PHYSICAL AND CHEMICAL REFERENCE DATA is very pleased to publish the Third Edition of the JANAF THERMOCHEMICAL TABLES.

Since the first version appeared 25 years ago, the JANAF THERMOCHEMICAL TABLES have been among the most widely used data tables in science and engineering.

You'll find:

- Reliable tables of thermodynamic properties of substances of wide interest
- A highly professional approach with critical evaluations of the world's thermochemical and spectroscopic literature
- A concise and easy-to-use format

This Third Edition presents an extensive set of tables including thermodynamic properties of more than 1800 substances, expressed in SI units. The notation has been made consistent with current international recommendations.

There is no other reference source of thermodynamic data that satisfies the needs of such a broad base of users.

Order your 2-volume set of the JANAF THERMOCHEMICAL TABLES today! You'll get over 1890 pages of valuable information that is crucial to your research—in two hardback volumes.

### SUBSCRIPTION INFORMATION

The JANAF THERMOCHEMICAL TABLES, THIRD EDITION is a two-volume supplement of *Journal of Physical and Chemical Reference Data*.

1896 pages, 2 volumes, hardcover  
ISBN 0-88318-473-7  
Supplement Number 1 to Volume 14, 1985

U.S. & Canada \$130.00  
All Other Countries \$156.00  
(Postage included.)

All orders for supplements must be prepaid.

Foreign payment must be made in U.S. currency by international money order, UNESCO coupons, U.S. bank draft, or order through your subscription agency. For rates in Japan, contact Maruzen Co., Ltd. Please allow four to six weeks for your copy to be mailed.

For more information, write American Chemical Society, Marketing Communications Department, 1155 Sixteenth Street, NW, Washington, DC 20036.

In a hurry? Call TOLL FREE **800-227-5558** and charge your order!



Published by the American Chemical Society and the American Institute of Physics for the National Institute of Standards and Technology

#### Editors:

**M.W. Chase, Jr.**  
National Institute of  
Standards and Technology

**C.A. Davies**  
Dow Chemical U.S.A.

**J.R. Downey, Jr.**  
Dow Chemical U.S.A.

**D.J. Frurip**  
Dow Chemical U.S.A.

**R.A. McDonald**  
Dow Chemical U.S.A.

**A.N. Syverud**  
Dow Chemical U.S.A.

ASSOCIATE EDITORS: Catherine C. Fenselau,  
Georges Guiochon, Walter C. Herlihy, Robert  
A. Osteryoung, Edward S. Yeung

**Editorial Headquarters**

1155 Sixteenth St., N.W.  
Washington, DC 20036  
Phone: 202-872-4570  
Telefax: 202-872-4574

Managing Editor: Sharon G. Boots

Assistant Managing Editor: Mary Warner

Associate Editor: Louise Voress

Assistant Editors: Grace K. Lee,  
Alan R. Newman

Editorial Assistant: Felicia Wach

Contributing Editor: Marcia Vogel

Director, Operational Support: C. Michael  
Phillippe

Head, Production Department: Leroy L.  
Corcoran

Art Director: Alan Kahan

Designers: Amy Meyer Phifer, Robert Sargent

Production Editor: Elizabeth E. Wood

Circulation: Claud Robinson

Editorial Assistant, LabGuide: Joanne Mullican

**Journals Dept., Columbus, Ohio**

Associate Head: Marianne Brogan

Journals Editing Manager: Joseph E. Yurvati

Senior Associate Editor: Rodney L. Temos

**Advisory Board:** Bernard J. Bulkin, Michael S.  
Epstein, Renaat Gijbels, William S. Hancock,  
Thomas L. Isenhour, James W. Jorgenson,  
Peter C. Jurs, Alan G. Marshall, Lawrence A.  
Pachla, John F. Rabolt, Debra R. Rollison, Ralph  
E. Sturgeon, Shigeru Terabe, George S. Wil-  
son, Mary J. Wirth, Richard N. Zare  
*Ex Officio:* Sam P. Perone

**Instrumentation Advisory Panel:** Daniel W.  
Armstrong, Bruce Chase, Thomas L. Chester,  
R. Graham Cooks, L. J. Cline Love, Sanford P.  
Markey, Brenda R. Shaw, Gary W. Small, R.  
Mark Wightman

Published by the  
**AMERICAN CHEMICAL SOCIETY**

1155 16th Street, N.W.  
Washington, DC 20036

**Publications Division**

Director: Robert H. Marks

Journals: Charles R. Bertsch

Special Publications: Randall E. Wedin

Manuscript requirements are published in the  
January 1, 1990 issue, page 89. Manuscripts  
for publication (4 copies) should be submitted  
to ANALYTICAL CHEMISTRY at the ACS Washing-  
ton address.

The American Chemical Society and its editors  
assume no responsibility for the statements  
and opinions advanced by contributors. Views  
expressed in the editorials are those of the  
editors and do not necessarily represent the  
official position of the American Chemical  
Society.

- Ando, E., 407  
Aoki, A., 407  
Armstrong, D. W., 332  
  
Belfer, A. J., 347  
Bertrand, G. L., 332  
  
Chang, T. T., 322  
Christopoulos, T. K., 360  
Ciszkowska, M., 349  
Clifford, R. H., 390  
Cox, K. W., 338  
Crow, J. A., 378  
  
Dasgupta, P. K., 395  
Diamandis, E. P., 360  
  
Estes, E. D., 338  
  
Fassett, J. D., 386  
Foley, J. P., 378  
Fujii, T., 414  
  
Grohse, P. M., 338  
Gunaratna, P. C., 402  
  
Hanson, C. D., 409  
Hodson, L. L., 338  
  
Imasaka, T., 374  
Ishibashi, N., 374  
Ishii, I., 390  
  
Jimba, H., 414  
  
Kamo, N., 353  
Kerley, E. L., 409  
Kobatake, Y., 353  
Kok, W. T., 367  
Kurosawa, S., 353  
  
Landau, I., 347  
  
Lasson, E., 412  
Locke, D. C., 347  
  
Matsue, T., 407  
Matsui, D., 353  
Meyer, G. A., 390  
Mitsutsuka, Y., 414  
Montaser, A., 390  
Murphy, T. J., 386  
  
Nojiri, Y., 414  
  
Okada, T., 327  
Oppenheimer, S., 322  
Osteryoung, J., 349  
Ozinga, W. J. J., 367  
  
Parker, V. D., 412  
Petersen, K., 395  
Poppe, H., 367  
  
Russell, D. H., 409  
  
Salmons, C. A., 338  
Secor, H. V., 332  
Seeman, J. I., 332  
Sickles, J. E., II, 338  
Siegel, M. M., 322  
Stojek, Z., 349  
  
Tanaka, K., 374  
Tsao, R., 322  
Tüdös, A. J., 367  
Turner, A. R., 338  
  
Uchida, I., 407  
Uehiro, T., 414  
  
Ward, K. D., 332  
Ward, T. J., 332  
Wilson, G. S., 402

# Nonionic Surfactants Used as Exact Mass Internal Standards for the 700–2100 Dalton Mass Range in Fast Atom Bombardment Mass Spectrometry

Marshall M. Siegel,\* Rushung Tsao, and Steven Oppenheimer

American Cyanamid Company, Medical Research Division, Lederle Laboratories, Pearl River, New York 10965

T. T. Chang

American Cyanamid Company, Chemical Research Division, Stamford, Connecticut 06902

**Monosubstituted poly(ethylene glycol) and poly(propylene glycol) nonionic surfactant mixtures and isolated monosubstituted poly(ethylene glycol) oligomer fractions were used, when adulterated with alkali-metal salts, as internal exact mass reference compounds in fast atom bombardment mass spectrometry for the mass range of 700–2100 daltons. Abundant  $[M + Metal]^+$  ions are produced with dithiothreitol/dithioerythritol and *m*-nitrobenzyl alcohol matrices for the monosubstituted poly(ethylene glycol) and poly(propylene glycol) surfactants, respectively. The uses of these internal mass standards for the determination of the exact masses of a number of pharmaceuticals in the manual and computerized peak matching modes are illustrated.**

## INTRODUCTION

Techniques reported for exact mass measurements in FAB (fast atom bombardment) mass spectrometry have included the successive insertion of a reference and a sample (1, 2) and the use of split targets for a reference and sample on stationary (3, 4), rotatable (3, 5), and wobble (6) probes. Because the reference and sample materials are separately analyzed, the reference material is referred to as an external standard. The mass measurement accuracy utilizing an external standard is not optimal due to nonreproducible mechanical, optical, and chemical factors in the successive experiments. More accurate mass measurements are obtained when the reference material is mixed together with the sample as an exact mass internal standard (7). A variety of reference standards have been suggested for exact mass measurements in FAB mass spectrometry including glycerol (8), triazines (1, 4), alkali-metal salts (4), peptides (3), phosphazines (3), perfluorokerocene (7), and the surfactants zonyl FSB (3), ethoquads (9), poly(ethylene glycols) (PEG's) (7, 10), and poly(propylene glycols) (PPG's) (6). Perhaps the most popular internal exact mass reference standards in use today are the PEG's and the PPG's which are used for manual peak matching and for computerized exact mass measurements. The advantages of the PEG's and PPG's are that they produce a series of very intense peaks 44 and 58 daltons apart, respectively.

In the FAB ionization mode, at resolutions greater than 6000, PEG mixtures are routinely useful (in our hands) up to ~750 daltons as internal standards utilizing either DTT/DTE (dithiothreitol/dithioerythritol, 5/1 (w/w)) or MNBA (*m*-nitrobenzyl alcohol) matrices for producing  $[M + H]^+$  or  $[M + Metal]^+$  ions. Above ~750 daltons, the ion abundances of the PEG's at high resolution are low. To remedy this situation, PPG's were proposed as exact high mass standards (6). PPG's work best with MNBA as a matrix; however, they tend to produce intense fragment ions and to suppress the sample intensity.

Because much of our work involves the mass spectral analysis of natural products of unknown structures with masses greater than 700 daltons, we sought reference materials that could be routinely used for FAB mass spectrometry over the mass range of 700–2100 daltons. Monosubstituted PEG and PPG surfactants were suggested (2), evaluated, and found to be very useful as exact mass internal standards for FAB mass spectrometry. The monosubstituted PEG's and PPG's change the physical properties and extend the mass range of their corresponding unsubstituted compounds.

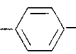
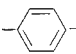
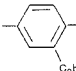
## EXPERIMENTAL SECTION

Octylphenyl, nonylphenyl, and dinonylphenyl groups constituted the different monosubstituents of the PEG surfactants used in these studies. These nonionic surfactants were obtained from the GAF Corp. (Wayne, NJ) and are commercially referred to as the IGEFAL CA, CO, and DM Surfactant Series, respectively. Each member of the IGEFAL Series is available over an oligomer range which is designated by the manufacturer by an average oligomer value,  $\bar{n}$ , where  $n$  is the number of repeating units. Likewise, a monosubstituted hexadecyl derivative of PPG was studied. This material is also available from the GAF Corp. and is referred to as EMULPHOGENE P-30. Table I lists all the surfactant structures used in this study and their corresponding elemental compositions and masses which can be used for generating tables of the exact masses of these reference compounds.

The pharmaceuticals used in this study, viz., LL-E19085 $\alpha$ , decapeptin, *N*-acetyl calicheamicin  $\delta_1^1$ , vancomycin, and avoparcin  $\alpha$ , were obtained from Lederle Laboratories (Pearl River, NY). The respective structures are listed in Table II. The isotopically enriched  $^{85}\text{RbCl}$  sample (99.5% enriched) was purchased from Oak Ridge National Laboratory (Oak Ridge, TN).

The surfactant series, described above, were used either as mixtures or as isolated fractions for the exact mass measurements. The isolated surfactant fractions were collected from the effluent of a high-performance liquid chromatography (HPLC) separation. For these separations, a Zorbax-CN analytical column (5- $\mu\text{m}$  particles, 4.6 mm  $\times$  25 cm), purchased from Du Pont, Wilmington, DE, was used. It operated at ambient temperature. The column was initially conditioned with THF followed by heptane, each at 2 mL/min for 30 min. Loop injections (20–50  $\mu\text{L}$ ) of surfactant solutions (1–5% in the initial HPLC solvent) were made on the column. The solvents used in the separations were (A) heptane and (B) 2-propanol/2-methoxyethanol (1/1 (v/v)). The linear gradient; generally used were as follows: for  $\bar{n} < 10$ , the initial A/B ratio was 100%/0% and the final ratio was 40%/60%; for  $\bar{n} = 10$ –30, the initial ratio was 80%/20% and final ratio was 40%/60%; for  $\bar{n} > 30$ , the initial A/B ratio was 65%/35% and the final ratio was 20%/80%. The analysis time was 40 min and the flow rates were either 2.0 or 2.5 mL/min. To reequilibrate the column, a 5-min linear gradient back to the initial conditions was used followed by pure heptane for 10 min, each at 2 mL/min. Resolved oligomers were individually collected from the HPLC effluent. Unresolved oligomers were collected at 1-min intervals. Waters Model 510 HPLC pumps, a Waters Model 680 gradient programmer, and a Kratos Model 773 UV detector, set at 280 nm, were used in these studies.

Table I. Nonionic Surfactants Used for Exact Mass Measurements in Fast Atom Bombardment Mass Spectrometry

chemical structure	commercial name	exact mass of oligomer $n$ (daltons)
$\text{HO}(\text{CH}_2\text{CH}_2\text{O})_n\text{H}$	poly(ethylene glycol)	$44.026215n + 18.010565 + \text{X}^a$
$\text{HO}(\text{C}_3\text{H}_6\text{O})_n\text{H}$	poly(propylene glycol)	$58.041865n + 18.010565 + \text{X}^a$
$\text{CH}_3\text{C}_6\text{H}_4(\text{CH}_2)_2\text{C}_6\text{H}_4\text{C}(\text{CH}_3)_2$  $\text{O}(\text{CH}_2\text{CH}_2\text{O})_n\text{H}$	etoxylated octylphenol (CAF IGEPAL CA Surfactant Series)	$44.026215n + 207.174891 + \text{X}^a$
$\text{C}_9\text{H}_{19}$  $\text{O}(\text{CH}_2\text{CH}_2\text{O})_n\text{H}$	etoxylated nonylphenol (CAF IGEPAL CO Surfactant Series)	$44.026215n + 221.190541 + \text{X}^a$
$\text{C}_9\text{H}_{19}$  $\text{O}(\text{CH}_2\text{CH}_2\text{O})_n\text{H}$	etoxylated dinonylphenol (CAF IGEPAL DM Surfactant Series)	$44.026215n + 347.331391 + \text{X}^a$
$\text{C}_{12}\text{H}_{25}\text{O}(\text{C}_2\text{H}_4\text{O})_n\text{H}$	propoxylated alcohol (CAF EMULPHOGENE P-30)	$58.041865n + 242.260966 + \text{X}^a$

<sup>a</sup> X is an adduct ion:  $\text{H}^+ = 1.007825$ ,  $\text{Na}^+ = 2.989770$ ,  $\text{K}^+ = 38.963708$ .

The FAB mass spectra were obtained on a VG ZAB-SE high-performance mass spectrometer equipped with a VG 11 250 data system. A cesium ion gun was used which operated at 35 kV and 5  $\mu\text{A}$ . The matrices used were DTT/DTE and MNBA. The spectrometer was operated at 10 000 resolution for the exact mass measurements. For weak signals, the data system was operated in the multichannel analyzer (MCA) signal-averaging mode. All samples were prepared and run at ambient temperature.

## RESULTS AND DISCUSSION

(A) FAB Properties of Oligomer Mixtures of the Monosubstituted Nonionic Surfactants. Under FAB ionization conditions, the IGEPAL surfactants produce intense spectra when adulterated with metal salts in DTT/DTE matrix. The relative sensitivities of the metal-adduct surfactant molecular ions (for the most abundant metal isotopes) are listed in Table III. These values were obtained from the FAB mass spectra produced from equal concentrations of surfactant adulterated with a series of binary mixtures of metal iodides of equal concentrations and computed relative to the potassium ion adduct. The surfactants are most sensitive as enriched rubidium-85 adduct ions. However, if an isotopically pure rubidium salt is not available, it is more practical to adulterate the samples with KCl in the DTT/DTE matrix to produce  $[\text{M} + \text{K}]^+$  ions, due to the complexity of the naturally occurring rubidium isotopic distribution of the rubidium-adduct ions.

The IGEPAL surfactants when neat or when dissolved in a FAB matrix do not produce  $[\text{M} + \text{H}]^+$  ions. Even when adulterated with 1  $\mu\text{L}$  of neat trifluoroacetic acid (TFA), the  $[\text{M} + \text{H}]^+$  ions are of very low abundance. This is characteristic of many compounds having low proton affinities containing only the elements C, H, and O (11). The IGEPAL surfactants when run at high concentrations contaminate the source reducing the overall instrument sensitivity. To restore instrument sensitivity, the source must be cleaned.

EMULPHOGENE P-30 produces intense spectra with MNBA as the matrix when adulterated with KCl and prepared as a 5% solution in  $\text{H}_2\text{O}/\text{CH}_3\text{OH}$  50/50 (v/v). EMULPHOGENE P-30 has a useful mass range of 1209–1907 daltons for nonsample limited work.

Typical low-resolution spectra for dilute samples of oligomeric mixtures of surfactants (approximately 5.0% (v/v) in  $\text{H}_2\text{O}/\text{CH}_3\text{OH}$  50/50 (v/v)) are illustrated in Figure 1 for IGEPALs CA 720 and CA 887 and EMULPHOGENE P-30. Note the high sensitivity of the compounds. The IGEPAL surfactant series with  $\bar{n}$  values up to 30 are useful as exact mass internal standards. (IGEPAI surfactants with  $\bar{n}$  values

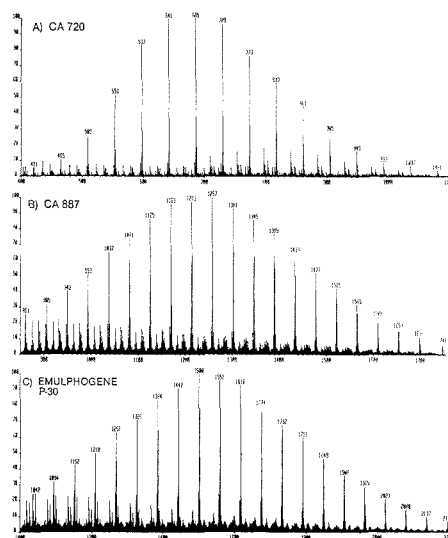
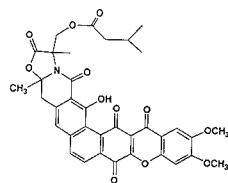


Figure 1. FAB mass spectra of oligomeric mixtures of monosubstituted nonionic surfactants (A) IGEPAL CA 720,  $\bar{n} = 12.5$  adulterated with KCl to produce  $[\text{M} + \text{K}]^+$  ions in DTT/DTE matrix, (B) IGEPAL CA 887,  $\bar{n} = 30$  adulterated with KCl to produce  $[\text{M} + \text{K}]^+$  and ions in DTT/DTE matrix, and (C) EMULPHOGENE P-30,  $\bar{n} = 30$  adulterated with KCl to produce  $[\text{M} + \text{K}]^+$  ions in MNBA matrix (experimental resolution, 2000).

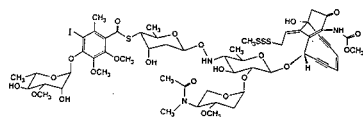
greater than 30 have very wide oligomer distributions and, therefore, the intensities in the FAB mass spectra of the individual oligomers are very weak.) The useful mass range of the different surfactant series are listed in Table IV. In nonsample limiting cases, exact masses of unknowns up to ~1400 daltons can be obtained by adulterating the unknown sample with a 1% KCl solution and the appropriate quantity of the IGEPAL surfactant. In practice, the appropriate amount of surfactant is determined by trial and error by stepwise addition of very low concentrations of surfactant until a surfactant signal of comparable size to that of the sample is observed. The unknown is peak matched, either by manual means or by computer, with the two closest surfactant reference peaks, chosen so that one is above and the other below the mass of the unknown compound. In the manual peak

**Table II. Structures of Pharmaceuticals Studied by Exact Mass High-Resolution FAB Mass Spectrometry**

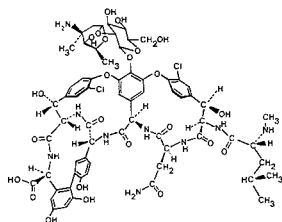
LL-E19085c (MW 669)

(pyro)Glu-His-Trp-Ser-Tyr-Trp-Lcu-Arg-Pro-Gly-NH<sub>2</sub>

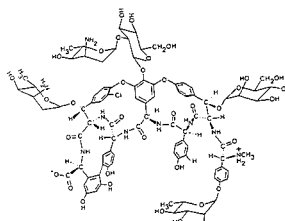
Decapeptyl (MW 1310)



N-Acetyl Calicheamicin 811 (MW 1395)



Vancomycin (MW 1447)

Avoparcin  $\alpha$  (MW 1907)

matching mode, when the peak matching unit and spectrometer are calibrated, only one reference peak is necessary for the exact mass measurement.

**(B) FAB Properties of Isolated Oligomer Fractions of the Monosubstituted Nonionic Surfactants.** For exact mass measurements in sample limited cases and for exact masses greater than ~1300 daltons, it is best to use the isolated oligomer fractions of the IGEFAL surfactants as the exact mass internal standards. These fractions are collected from the HPLC detector exit port. Figure 2 illustrates typical HPLC chromatograms obtained under the conditions described in the Experimental Section. For surfactant mixtures

**Table III. Relative Abundances of [M + Metal]<sup>+</sup> Ions for the  $n = 20$  Oligomer of the Nonionic Surfactant IGEFAL CA 887**

ion <sup>a</sup>	<i>m/z</i>	abundance relative to [M + <sup>39</sup> K] <sup>+</sup> <sup>b</sup>
[M + <sup>85</sup> Rb(enriched)] <sup>+</sup> <sup>c</sup>	1171	1.71
[M + <sup>85</sup> Rb] <sup>+</sup> <sup>c</sup>	1171	1.20
[M + <sup>39</sup> K] <sup>+</sup>	1125	1.00
[M + <sup>23</sup> Na] <sup>+</sup>	1109	0.67
[M + <sup>133</sup> Cs] <sup>+</sup> <sup>d</sup>	1219	0.60
[M + <sup>107</sup> Ag] <sup>+</sup>	1193	0.13
[M + <sup>14</sup> NH <sub>4</sub> ] <sup>+</sup>	1100	0.11
[M + <sup>7</sup> Li] <sup>+</sup>	1093	0.10

<sup>a</sup> All relative abundance measurements were made vs the [CA(*n* = 20) + <sup>39</sup>K]<sup>+</sup> ion except for the <sup>85</sup>Rb and <sup>133</sup>Cs adducts, as noted below. <sup>b</sup> The abundances are only due to the indicated isotope. No corrections are made for the abundances of the other naturally occurring isotopes. <sup>c</sup> The [CA(*n* = 20) + <sup>85</sup>Rb]<sup>+</sup> ion was measured vs the [CA(*n* = 20) + <sup>23</sup>Na]<sup>+</sup> ion because it is isobaric with the second isotope peak of the [CA(*n* = 21) + <sup>39</sup>K]<sup>+</sup> ion. <sup>d</sup> The [CA(*n* = 20) + <sup>133</sup>Cs]<sup>+</sup> ion was measured vs the [CA(*n* = 20) + <sup>85</sup>Rb]<sup>+</sup> ion because it is isobaric with the first isotope peak of the [CA(*n* = 23) + <sup>39</sup>K]<sup>+</sup> ion.

**Table IV. Useful Surfactants Mass Ranges for Exact Mass FAB Measurements**

surfactant ( $\bar{n}$ value)	useful mass range, <sup>b,c</sup> daltons	best FAB matrix
PEG 200-600	200-750	DTT/DTE or MNBA
PPG 1750	1566-2262 <sup>d</sup>	MNBA
PPG 2000	1624-2321 <sup>d</sup>	MNBA
CA 52 (5)	377-597	DTT/DTE
CA 72 (12.5)	597-905	DTT/DTE
CA 887 (30)	1037-1565	DTT/DTE
CA 897 (40)	~1100 to ~2500 <sup>e</sup>	DTT/DTE
CO 85 (20)	699-1007	DTT/DTE
CO 887 (30)	~1000 to ~1700	DTT/DTE
CO 897 (40)	~1100 to ~2500 <sup>e</sup>	DTT/DTE
DM 4:0 (7) <sup>f</sup>	516-869	DTT/DTE
DM 7:0 (15) <sup>f</sup>	605-1011	DTT/DTE
DM 7:0 (24) <sup>f</sup>	737-1221	DTT/DTE
P-30 (30)	1209-1907	MNBA

<sup>a</sup>  $\bar{n}$  values obtained from manufacturer. <sup>b</sup> The centers of the useful FAB mass ranges are less than the  $\bar{n}$  mass values by 100 to 300 daltons. <sup>c</sup> Only the PEG's produce abundant [M + H]<sup>+</sup> ions. All the other surfactants produce abundant [M + K]<sup>+</sup> ions. <sup>d</sup> The PPG's have a very abundant low mass ion series. <sup>e</sup> This broad mass range produces very low abundance ions. Abundant ions are only produced from isolated fractions. <sup>f</sup> The commercial DM series is actually a 50:50 mixture (from HPLC) of DM and CO components. However, the DM components dominate the FAB mass spectra. To separate the DM from the CO components, use of Zorbax CN column with a solvent program of 60%/40% → 70%/30% acetonitrile/H<sub>2</sub>O at 1 mL/min for 20 min.

with  $\bar{n}$  values less than or equal to 25, the individual surfactant components can be resolved and isolated (see Figure 3A). Above  $\bar{n}$  values of 25 the chromatographic resolution is poor and surfactant fractions were collected over 1-min intervals. These fractions tend to have two major oligomeric components (compare parts B and C of Figure 3). Two reference peaks are necessary for computerized peak matching. Therefore, sets of cuts obtained from surfactant mixtures with  $\bar{n}$  values less than 25 have to be mixed while surfactant cuts obtained from surfactant mixtures with  $\bar{n}$  values greater than 25 generally can be directly used. Typically, the collected surfactants were blown down to dryness and used after being prepared as 1% solutions with H<sub>2</sub>O/CH<sub>3</sub>OH 50/50 (v/v).

**Table V. FAB Ion Abundances of Drugs Adulterated with an Isolated Surfactant and a Surfactant Mixture When the Pure Drug Concentrations and the Reference Ion Abundances of the Unadulterated Surfactants Are Held Constant**

sample <sup>a</sup>		ion abundances, cm [m/z]		
surfactant	drug	surfactant alone surfactant ion <sup>b</sup>	mixture of surfactant and 1 μg of drug	
			surfactant ion <sup>b</sup>	drug ion <sup>c</sup>
(I) CA720 cut 9	LL-E19085 <sub>o</sub>	11.9 [729]	4.8 [729]	9.3 [710]
(II) CA720 mixture	LL-E19085 <sub>o</sub>	13.6 [729]	11.9 [729]	4.7 [710]
	ratio I/II	0.88 <sup>d</sup>	0.40	1.98 <sup>e</sup>
(III) CA887 cut 15	decapeptyl	20.0 [1389]	9.2 [1389]	55.0 [1349]
(IV) CA887 mixture	decapeptyl	23.8 [1389]	25.0 [1389]	6.0 [1349]
	ratio III/IV	0.84 <sup>d</sup>	0.37	9.17 <sup>e</sup>

<sup>a</sup> FAB matrix DTT/DTE adulterated with 0.3 μL of 0.2 M KCl. <sup>b</sup> m/z 729 is [CA(n = 11) + K]<sup>+</sup> and m/z 1389 is [CA(n = 26) + K]<sup>+</sup>. <sup>c</sup> For LL-E19085<sub>o</sub> m/z 710 is [M + H<sub>2</sub> + K]<sup>+</sup>, for decapeptyl m/z 1349 is [M + K]<sup>+</sup>. <sup>d</sup> This ratio would be exactly 1.00 if the ion abundances of the isolated surfactant and the surfactant mixture were equal. This precise mixture is experimentally difficult to achieve. <sup>e</sup> Enhancement of drug ion abundance in the isolated surfactant relative to the surfactant mixture.

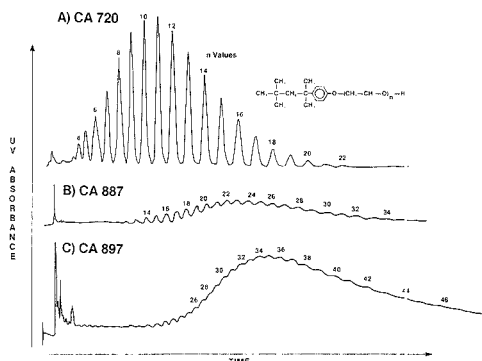


**Figure 2.** HPLC chromatograms generated from different members of the IGEPAL CA surfactant series: (A) IGEPAL CA 720,  $\bar{n} = 12.5$ , (B) IGEPAL CA 887,  $\bar{n} = 30$ , and, (C) IGEPAL CA 897,  $\bar{n} = 40$ . Note the degradation in chromatographic resolution with increasing  $\bar{n}$  values. Retention times for the same  $\bar{n}$  values in different surfactants differ because different solvent systems were used. Solvents used were (A) heptane and (B) 2-propanol/2-methoxyethanol (1/1 (v/v)). The flow rates were 2 mL/min with a linear solvent program of 30 min duration. The initial time and final time solvent mixtures were as follows: for CA 720, initial 85% A/15% B, final 60% A/40% B; for CA 887, initial 80% A/20% B, final 40% A/60% B; for CA 897, initial 62% A/38% B, final 20% A/80% B.

An advantage in the use of the isolated surfactants is that the signal of the unknown can be optimized by minimizing the amount of surfactant necessary for the reference signal. Typically, sample sensitivity enhancements of from 2 to 10 times are observed when the isolated surfactants are used as internal standards because the surfactant components not used as reference masses in the surfactant mixtures suppress the sample signal. These conclusions are based upon the sensitivity measurements, illustrated in Table V, for two drugs made with an isolated surfactant and with a surfactant mixture when the concentrations of the respective reference oligomer and drug were kept constant. The two drugs studied, LL-E19085<sub>o</sub> and decapeptyl, represent classes of compounds of extremely different structures and polarity typically studied by FAB mass spectrometry. The ion intensity of a specific oligomer in the surfactant mixture was maintained to be about equal to that of the same oligomer in the isolated surfactant (see Table V, "ratio" entries in "surfactant alone" column). Upon the addition of the drugs to the surfactant, the relative intensity of the [M + K]<sup>+</sup> ion of the respective drug: was 2 and 10 times more intense in the isolated surfactant versus the

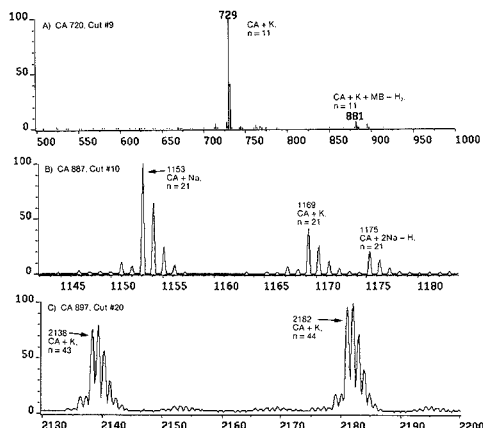


**Figure 3.** FAB mass spectra of isolated oligomeric fractions of monosubstituted nonionic surfactants (A) IGEPAL CA 720, cut 9 adulterated with KCl in DTT/DTE matrix, (B) IGEPAL CA 887, cut 10 adulterated with NaCl in DTT/DTE matrix, and, (C) IGEPAL CA 897, cut 20 adulterated with KCl in DTT/DTE matrix (experimental resolution, 2000).

surfactant mixture (see Table V, "ratio" entries in "drug ion" column). At the same time, the surfactant ion intensity was suppressed by about 30% in the isolated surfactant and unsuppressed in the surfactant mixture (see Table V, second vs first "surfactant ion" columns). These results are consistent with the surface ionization mechanism for FAB (12) in which the resulting spectra are representative of the surface solution and not the bulk sample. In both the isolated surfactant and the surfactant mixture experiments, the sample size was constant but the total surfactant concentration differed. Since the sample and the surfactant are competing for the surface, there is less competition for the surface with the isolated surfactant than with the surfactant mixture. Therefore, the sample can displace the isolated surfactant while the displacement of the surfactant mixture is negligible.

Additional benefits accrued by using the isolated surfactant are less background interference from other surfactant components and less likelihood of source contamination due to the low levels of surfactant needed as reference compounds.

**(C) Peak Matching Results Using Isolated Oligomer Fractions of the Monosubstituted Nonionic Surfactants.** Table VI summarizes computerized peak matching results obtained by utilizing isolated surfactant oligomers as exact

**Table VI. Typical High Mass Computerized Peak Matching Results Obtained by Utilizing Isolated Surfactant Oligomers as Internal Reference Mass Standards in FAB Mass Spectrometry<sup>a</sup>**

ref compound/ FAB matrix	low mass ref (oligomer)	high mass ref (oligomer)	exptl mass of "unknown", daltons	error $\Delta$ , <sup>b</sup> mmu	relative error, ppm	"unknown" elemental (M + H or M + K)	"unknown" compound name
CA 887, cut 15/ DTT/DTE + KCl	1345.7861 (n = 25 + K)	1389.8124 (n = 26 + K)	1349.5945 (M + K)	-0.1	-0.074	C <sub>84</sub> H <sub>82</sub> N <sub>18</sub> O <sub>13</sub> K	decapeptyl
CA 887, cut 16/ DTT/DTE + KCl	1433.8386 (n = 27 + K)	1434.8419 (n = 27 <sup>[13C]</sup> + K)	1434.2307 (M + K)	-2.2	-1.5	C <sub>86</sub> H <sub>74</sub> IN <sub>3</sub> O <sub>22</sub> S <sub>4</sub> K	N-acetylcalicheamicin $\delta_1^I$
CA 887, cuts 17 (n = 28) and 18 (n = 29)/ DTT/DTE + KCl	1477.8648 (n = 28 + K)	1521.8910 (n = 29 + K)	1486.3922 (M + K)	-1.7	-1.1	C <sub>86</sub> H <sub>78</sub> Cl <sub>2</sub> N <sub>9</sub> O <sub>24</sub>	vancomycin
Ca 897, cut 17/ DTT/DTE + TFA (1 $\mu$ L)	1902.1503 (n = 38 + Na <sup>c</sup> )	1918.1269 (n = 38 + K <sup>c</sup> )	1908.6133 (M + H)	-6.1	-3.2	C <sub>89</sub> H <sub>100</sub> ClIN <sub>9</sub> O <sub>26</sub>	avoparcin $\alpha$

<sup>a</sup>Resolution, 10 000. <sup>b</sup> $\Delta$  = experimental mass - predicted mass. <sup>c</sup>The surfactant cuts contain low levels of Na and K salts which are chelated to the surfactants. These salts principally originate from the Zorbax CN F-PLC column because surfactant-TFA mixtures do not produce significant Na or K adduct-molecular ions.

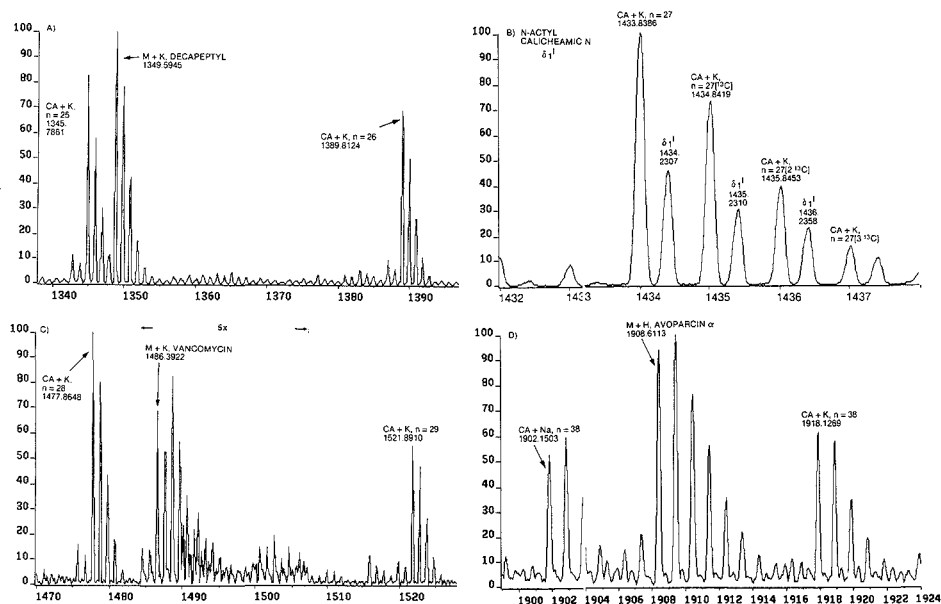


**Figure 4.** FAB computerized peak matching results for (A) decapeptyl, (B) *N*-acetylcalicheamicin  $\delta_1^I$ , (C) vancomycin, and (D) avoparcin  $\alpha$ . Note the ions of the reference compounds, isolated IGEAL CA oligomers, on each side of the sample ions (experimental resolution, 10 000).

mass internal standards in the FAB ionization mode. As described above, isolated surfactant fractions are useful in sample-limited situations, for low sensitivity compounds, when careful control of the quantity of internal standard is necessary to reduce the suppression of the sample signal and for most compounds in the mass range of 1300 to 2100 daltons.

The mass errors ( $\Delta$ ) listed in Table VI suggest a systematic error since all experimental masses are lower than that predicted. A possible explanation to account for this effect is that the  $[M + K]^+$  sample ions are contaminated with low levels of the second isotope peak from the corresponding  $[M - H_2 + K]^+$  sample ions. This latter ion, if due to two carbon-13 isotopes, is 7.96 mdaltons less than the mass of the

$[M + K]^+$  ion. If this type of contribution to the mass error is greater than the sample peaks than the reference peaks and the intensity of the  $[M - H_2 + K]^+$  ions increases with increasing mass, the mass errors should increase with increasing mass. Likewise, the first and second isotope peaks associated with the  $[M + K]^+$  ion can also lose  $H_2$  and produce weak ions which overlap on the low mass side of the  $[M + K]^+$  ion. A possible way to minimize this effect is to measure the peak centroids with the data close to the peak maximum rather than with the data from the peak half-height and above. We have measured more accurate peak centroids, with high signal-to-noise data, from the region of the peak top than with data from the peak half-height and above.



Typical computerized peak matching results obtained at 10 000 resolution are illustrated in parts A-D of Figure 4 for decapeptyl, *N*-acetylcalicheamicin  $\delta_1^I$ , vancomycin, and avoparcin  $\alpha$ , respectively. The isolated surfactant masses and the masses of the unknowns are clearly labeled. A limited amount of sample was available for the exact mass measurement for *N*-acetylcalicheamicin  $\delta_1^I$ . By coincidence, the nominal masses for the  $[M + K]^+$  ions for the reference and sample peaks were identical. Since in the high-resolution spectrum the peaks for the unknown fall between the peaks of the reference compound, all the peaks in the sample can be peaked matched with reference peaks within 1 dalton (See Figure 4B). *N*-Acetylcalicheamicin  $\delta_1^I$  was also manually peak matched with EMULPHOGENE P-30 as the reference material using the  $[M + K]^+$  ion at  $m/z$  1384.0201, corresponding to the  $n = 19$  oligomer, as the exact mass reference ion. The exact mass can be more accurately measured in the MCA computerized peak matching mode than in the manual peak matching mode.

A unique feature appears in the computerized peak matching results for avoparcin  $\alpha$  (Figure 4D) when adulterated with 1  $\mu$ L of neat TFA. The surfactants produced  $[M + Na]^+$  and  $[M + K]^+$  ions while the sample produced principally  $[M + H]^+$  ions. These results illustrate the relative selectivities of the reference material and sample for adduct formation with residual alkali-metal salts and available protons. When the sample was adulterated with 1  $\mu$ L of a 1% sodium chloride solution,  $[M + Na]^+$  ions were produced for the  $r = 38$  and  $n = 39$  isolated IGEPAL CA oligomers and the sample produced  $[M + H]^+$  and  $[M + Na]^+$  ions of equal intensity.

### CONCLUSIONS

Monosubstituted PEG nonionic surfactant mixtures and isolated oligomeric components have been successfully used as exact mass internal standards in the 700-2100 dalton mass range in FAB mass spectrometry. Abundant  $[M + K]^+$  ions are produced when the surfactant is adulterated with KCl in the DTT/DTE matrix. Similar results were obtained with

the monosubstituted PPG nonionic surfactant EMULPHOGENE P-30 with MNBA as the matrix. The advantages of the isolated surfactant oligomers versus surfactant mixtures as reference materials are the enhancement of the sample signal, reduction in chemical background, and drastic reduction in source contamination. These exact mass measurement techniques have been used in our laboratory for the last two years. By use of the HPLC methods described above, surfactant components above 2100 daltons could be isolated from higher mass oligomers to extend the upper mass limit beyond the 2100 daltons achieved in this work.

### ACKNOWLEDGMENT

The authors thank Joseph DeVasto for helpful suggestions for obtaining the HPLC chromatograms and the GAF Corp. for a generous supply of surfactant samples.

### LITERATURE CITED

- (1) Morgan, R. P.; Reed, M. L. *Org. Mass Spectrom.* **1982**, *17*, 537.
- (2) Chang, T. T.; Tsou, H.-R.; Siegel, M. M. *Anal. Chem.* **1987**, *59*, 614-617.
- (3) Gilliam, J. M.; Landis, P. W.; Occolowitz, J. L. *Anal. Chem.* **1983**, *55*, 1531-1533.
- (4) Heller, D.; Hansen, G.; Yergey, J.; Cotter, R. J.; Fenselau, C. *Annu. Conf. Mass Spectrom. Applied Topics* **1982**, 560-561.
- (5) "Accurate Mass Measurement Using a Newly Developed Dual Target Sample Introduction Probe for FAB-MS"; JEOL Application Note MS36; JEOL USA, Inc.; Peabody, MA, July, 1987; pp 16.
- (6) Rinehart, K. L., Jr. In *Mass Spectrometry in the Health and Life Sciences*; Eds., A. L. Burlingame, A. L., Castagnoli, N., Jr., pp. 119-148. Elsevier: Amsterdam, 1985;
- (7) Gilliam, J. M.; Landis, P. W.; Occolowitz, J. L. *Anal. Chem.* **1984**, *56*, 2285-2288.
- (8) Van Langenhove, A.; Costello, C. E.; Chen, H.-F.; Biller, J. E.; Biemann, K. *Annu. Conf. Mass Spectrom. Allied Topics* **1982**, 558-559.
- (9) DeStefano, A. J.; Keough, T. *Anal. Chem.* **1984**, *56*, 1846-1849.
- (10) Goad, L. J.; Prescott, C. M.; Rose, M. E. *Org. Mass Spectrom.* **1984**, *19*, 101-104.
- (11) Siegel, M. M.; McGahren, W. J.; Tomer, K. B.; Chang, T. T. *Biomed. Environ. Mass Spectrom.* **1987**, *14*, 29-38.
- (12) Ligon, W. V., Jr.; Dorn, S. B. *Int. J. Mass Spectrom. Ion Process.* **1986**, *78*, 99-113.

RECEIVED for review August 7, 1989. Accepted November 20, 1989.

## Chromatographic Oligomer Separation of Poly(oxyethylenes) on $K^+$ -Form Cation-Exchange Resin

Tetsuo Okada

Faculty of Liberal Arts, Shizuoka University, Shizuoka 422, Japan

Compounds having poly(oxyethylene) chains as a part of the structure were separated on a cation-exchange resin according to the number of oxyethylenes by utilizing a difference in the complexation with  $K^+$ . The retention strongly depended on properties of mobile phases, for example, dielectric constant of the solvent, the concentration of water, the concentration of  $K^+$ , etc. More than 30 oligomers were successfully separated with the gradient elution from pure methanol to methanol containing  $K^+$ . In addition, the formation constants of  $K^+$  complexes in methanol were chromatographically determined. Logarithms of formation constants linearly increased with increasing number of oxyethylene units.

### INTRODUCTION

Various surface-active compounds contain poly(oxyethylene) (POEs) as a part of the structure. POEs provide

hydrophilicity for most nonionic surfactants (1), which are one of the most generally consumed detergents, while ionic groups play the same role in ionic surfactants. Some of anionic surfactants also contain POEs together with ionic groups. These materials are used in a number of industries, e.g., food, oil, and textile industries. Useful methods for the analysis of these compounds are, therefore, often required for the process or the product control and environmental monitoring.

These surfactants are usually used as mixtures of poly-disperse POEs. Chromatographic methods are obviously a favorable choice of the analysis of such mixtures and the determination of the components. Supercritical fluid chromatography (SFC) is a useful mode for this purpose (2, 3). In spite of the high resolution, SFC is less common than liquid chromatography (HPLC) because of need of long analytical time and the special instrument. HPLC researches have focused on the separation concerning either the hydrophobic moieties or the oligomer distribution of POEs. Some re-

searchers (4, 5) developed methods for the separation of nonionic surfactants based on the difference in alkyl hydrophobic groups, wherein reversed-phase stationary phases were employed. Kudoh (4) found the combination of the octadecyl-bonded silica stationary phase and acetone-water mobile phases to be effective. The developed method was selective only to differences in the alkyl group but was not influenced by differences in the oligomer distribution of POE.

It appears that separation in terms of the POE distribution has attracted more research and is of importance in many cases. The normal-phase separation (6-9) has been usually utilized for the analysis of the POE distribution except for the case where the precolumn derivatization was carried out (10, 11). Ternary solvent systems, for example, composed of hexane, 2-propanol, and methanol or water, were employed in gradient elution schemes to separate POEs of wide distribution range (6-9). The successful normal-phase separation is attributed to the delicate cooperation of the hydrophilic partition and the hydrophobic absorption. The selection of mobile phases, therefore, is very complicated and difficult; it is usually based not on theories but on trial and error.

POEs adopt the 7/2 helix configuration and form the complexes with some Lewis acids such as metal cations similarly to cyclic ethers (1). This phenomenon is thought to be applicable to the separation of both metal ions and POEs. The purpose of the present work is to show the separation of POEs on a  $K^+$ -form cation exchanger and to chromatographically determine the formation constants of  $K^+$  complexes of POEs in a solution. Additionally, qualitative consideration on the complexation is presented on the basis of the structure of the complexes and nature of solvents used in mobile phase.

### EXPERIMENTAL SECTION

The chromatographic system was composed of a Tosoh computer-controlled pump (Model CCPD), a column oven (Model CO-8000, Tosoh), a UV-visible detector (Model UV-8000, Tosoh), a JASCO refractive index detector (Model 830-RI), and a Rheodyne injection valve equipped with a 100- $\mu$ L sample loop. A separation column was a TSK-gel IC-Cation-SW (4.6  $\times$  50 mm, packed with a silica-based cation-exchange resin with a particle size of 5  $\mu$ m, the ion-exchange capacity of which was 0.3 mequiv/g), which was developed for ion chromatography of cations by Tosoh. The column temperature was maintained at 25  $^{\circ}$ C. The flow rate was kept at 1 mL/min.

Mixtures of poly(ethylene glycols) (PEG) and poly(oxyethylated dodecyl alcohols) with six and eight repeating oxyethylenes (POE[6]D and POE[8]D) were purchased from Wako Chemicals. PEG[6] was purchased from Aldrich. Mixtures of POE and *p*-nonylphenols (POE(*n*)NP) were purchased from Tokyo Kasei. Mixtures of poly(oxyethylated dodecyl alcohols) (POE(*n*)D) were courteous gifts from Nikko Chemicals. The numbers in brackets represent numbers of oxyethylene units in monodisperse POEs, whereas those in parentheses refer to the average numbers of oxyethylenes in polydisperse POEs. All chemicals listed above were used as received.

Methanol of analytical reagent was distilled and stored with molecular sieves. Stored methanol was daily distilled again before the experiment. Water was deionized and distilled. KCl was dried at 110  $^{\circ}$ C under vacuum. Other solvents were also of analytical or HPLC grade.

### RESULTS AND DISCUSSION

**Choice of a Counter Cation for the Oligomer Separation of POE on a Cation-Exchange Resin.** The complexation of POEs with metal cations has been investigated in many ways and utilized for some analytical methods, namely gravimetric or volumetric determination of nonionic surfactants containing POEs (1), solvent extraction of metal cations (12-14), ion-selective electrodes (1), etc. However, POEs have not been used for HPLC separation of metal ions, whereas cyclic oxyethylenes such as crown ethers have been applied extensively. This is due to the poor selectivity and low for-

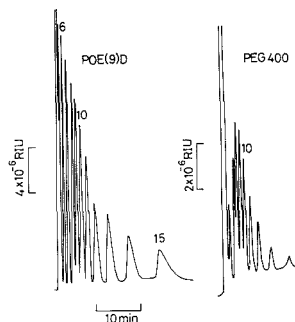


**Figure 1.** Oligomer separation of POE(9)D and PEG 400. The numbers on the chromatograms refer to the numbers of oxyethylenes in molecules. Sample concentration was 5 mg/mL. Mobile phase was methanol. Other conditions are given in the text.

mation constants of POE-metal complexes resulting from the flexible structures of the POE chains in comparison with the rigid structure of crown ethers. POEs form complexes with a number of metal ions, only if the circumstances are suitable for the reaction. POEs are likely to select  $K^+$ ,  $Ba^{2+}$ , or  $Hg^{2+}$  as a favorable partner of the complex rather than  $Li^+$ ,  $Na^+$ ,  $Ca^{2+}$ , or other alkaline-earth or transition-metal cations (1). Kraus and Rogers (15) described the effects of salts on the retention of PEG on size-exclusion chromatography and found that  $K^+$  salts more effectively influenced the retention of PEG than the other metal salts tested. This experimental fact was explained by the structure change of PEG resulting from the complexation with  $K^+$ . Studies conducted by Yanagida et al. (14) and Furger-Guerrisi and Tondre (16) also indicated that POEs showed strong coordination ability toward  $K^+$  and that the complexation moderately varied according to the number of oxyethylene units.

Thus,  $K^+$  is possibly an appropriate counter cation for the present purpose. A  $K^+$ -form cation exchange column was mainly used to investigate the effect of mobile phases; the results were compared with those obtained with  $Ba^{2+}$ ,  $Ca^{2+}$ ,  $Na^+$ ,  $Li^+$ ,  $H^+$ , and  $Pb^{2+}$ -form columns in the separation performance. Figure 1 shows examples of the oligomer separation of POE(9)D and PEG(9) on the  $K^+$ -form cation-exchange resin with methanol as a mobile phase. The elution was detected with refractive index (RI). The retention increases with an increase in oxyethylene units; the longer the POE chains, the higher the complexation ability (14). This shows that the separation is based on a difference in the complexation of POEs with  $K^+$  in the stationary phase.

$K^+$  sites in the stationary phase were easily saturated by injecting a large amount of POEs. This overloading caused the reduction of the retention of POEs. The concentration of a sample should be, therefore, kept as low as possible. The retention was constant when the sample concentration was kept lower than 0.5 mg/mL. However, since this concentration was too low for RI detection, 5 mg/mL samples were used for Figure 1.

Peaks were identified by mass spectrometric analysis of peak components and the comparison with the retention of POE[6]D, POE[8]D, or PEG[6]. As can be seen in Figure 1, compounds with six repeating oxyethylenes are separated as independent peaks. Also, compounds with five repeating oxyethylenes were slightly retained and separated from the void volume peak involving the elution of compounds containing less than four oxyethylene units. These results show that at least five or six oxyethylenes are required for the complexation with  $K^+$  bound on a cation-exchange resin and that the complexation ability of compounds containing four

oxyethylenes or less is so weak that we cannot evaluate it.

POE *p*-nonylphenyl ethers or POE *p*-isooctylphenyl ethers showed similar separation, albeit there were slight differences in the retention concerning the hydrophobic chains. For compounds with the same POE length, the retention increased in the following order: a dodecyl ether, *p*-nonylphenyl ether, *p*-isooctylphenyl ether, PEG. This order is the reverse of that predicted from hydrophobicity. In the present case, as will be discussed later, POEs were retained only on  $K^+$ - or  $Ba^{2+}$ -form stationary phase, but were not retained on the stationary phase preequilibrated with any other cations tested. This fact shows that the only separation mode is provided by metal cations bound on a resin and a cation-exchange resin itself does not have any effects on the separation. Therefore, we do not need to consider the contribution of hydrophobic interaction and interaction between POE and sulfonic groups to the retention. Thus, the difference in the retention between compounds with different hydrophobic chains is attributed not to the hydrophobicity of alkyl groups but to the complexation ability of entire molecules.

In the complexation of POE, it is a major determinant how facile oxygen atoms can move to the appropriate positions to provide coordination bonds through the configurational change. An alkyl chain affects the facility of this movement. Complexation accompanied by the movement of large alkyl chains is thought to be more endothermic. Additionally, the complexation on the stationary phase is more effectively affected by the steric hindrance than in a solution. These two factors make difficult the complexation of POEs having long alkyl chains and thus reduce the retention in the order of an increase in hydrophobicity.

Yanagida et al. (12) showed by studying the stoichiometry of POE- $K^+$  complexes that at least six or seven repeating oxyethylenes were necessary for complexation in methanolic solution. The results obtained in the present research show good agreement with their results. It was predicted that  $K^+$  bound on a cation-exchange resin would show a different property from  $K^+$  dissolved in a solution. Usually, the former appears to show the lower complexation ability than the latter because of steric hindrance of the cation-exchange sites and a decrease in the effective charge resulting from the ion-pair formation with a sulfonic group.  $K^+$  shows 6, 8, or 10 coordination numbers. In a solution, POEs should provide  $K^+$  with at least six coordination bonds for the stable complexation. However, in the present case, one of the coordination sites of  $K^+$  is already filled by a sulfonic acid in a cation-exchange resin. Additionally, the concentration of  $K^+$  in the stationary phase was rather high; the amount of  $K^+$  in the stationary phase was  $1.01 \times 10^{-4}$  mol. These factors permitted the complexation of POEs with five repeating oxyethylene units.

The oligomer separation was obtained only from the  $K^+$ -loaded column. The  $Ba^{2+}$  column showed very poor separation, and the other columns gave a single peak to a polydisperse POE sample with both aqueous and methanolic mobile phases. Complex formation of  $Na^+$  and  $Li^+$  with POEs was confirmed in acetone (14). Although the same condition was applied to the present separation, no retention was observed. This result will be explained on the basis of the effect of solvents as shown in the following part.

**Effect of the Mobile Phase Composition.** It is well-known that the complexation of POE with metal ions is strongly affected by nature of solvents; a high permittivity solvent is needed for the complexation, but water is not a preferable solvent because of its very high donor ability. The present separation based on the complexation ability of POE was also strongly influenced by the composition of mobile phases. Figure 2 shows the effect of water in mobile phases

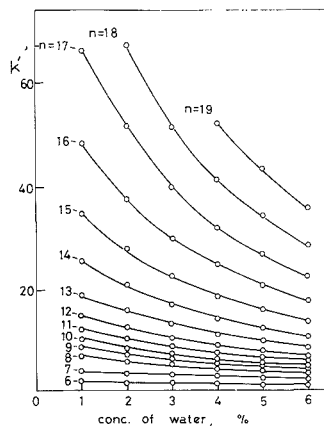


**Figure 2.** Effect of the concentration of water in a mobile phase on the retention of POE(*n*)NP: detection, UV (280 nm); sample concentration, 0.5 mg/mL.

on the retention of POE(*n*)NP. This result shows that the concentration of water should be precisely adjusted for the reproducible separation. However, this simultaneously indicates that the retention can be effectively modified according to the distribution range of oligomers in mixtures by changing the concentration of water in mobile phases.

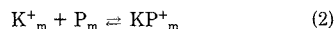
Ethanol, acetone, acetonitrile, and 1,4-dioxane were also examined on  $K^+$ -form resin. The retention became weaker in the order ethanol (24.6) > methanol (32.6) > acetonitrile (37.5) > acetone (20.7) = 1,4-dioxane (2.1) = water (78.3); the numbers in parentheses represent the relative dielectric constants. For solvents with relatively high dielectric constants, the retention can be discussed on the basis of a difference in the solvation to  $K^+$ ; that is, the strength of the solvation decreases in the order water > acetonitrile > methanol > ethanol. Acetonitrile shows relatively strong solvation to  $K^+$  in spite of the smaller donor number than methanol. Its small transfer free energy from water can be evidence of strong solvation to  $K^+$  (17). POEs form complexes with  $K^+$  as well as with  $Na^+$  and  $Li^+$  in acetone solutions (14). However, in the present case, a decrease in the effective charge of  $K^+$  resulting from the ion-pair formation with sulfonic groups in the cation-exchange resin is promoted in a low permittivity solvent such as acetone and 1,4-dioxane. This effect diminished the complexation at the resin surface and, thus, caused the weak retention.

The addition of  $K^+$  also reduced the retention of POE by stabilizing  $K^+$  complexes in the mobile phase, while the effect of solvent was based on changes in the complexation ability of POEs on the stationary phase. This effect of  $K^+$  in a mobile phase is evaluated by relating the complex formation in a mobile phase to the retention.

If no  $K^+$  is added to a mobile phase, a capacity factor ( $k'_0$ ) of POE can be written as

$$k'_0 = \phi[P]_s/[P]_m \quad (1)$$

where  $[P]_s$  and  $[P]_m$  represent the concentration of POE in the stationary and the mobile phases, respectively, and  $\phi$  represents the phase ratio. If  $K^+$  is added to the mobile phase, the following equilibrium will be established in the mobile phase:



where  $m$  as a subscript represents a mobile phase. Here, the formation of multiple complexes such as  $K^+(POE)_2$  or  $K^+_2(POE)$  was ignored. The former is possibly formed for short

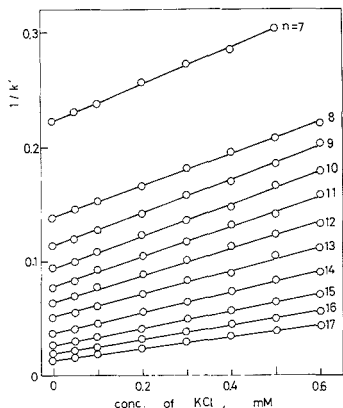


Figure 3. Plots based on eq 4.  $n$  refers to the number of repeating oxyethylenes in POE( $n$ )NP. Conditions are given in Figure 2.

Table I. List of Complex Formation Constants with KCl Obtained from the Plots Based on eq 4

no. of oxyethylenes	$\log K_f^a$	$\sigma^b$	$r^2$
7	2.86	8	0.999
8	2.99	38	0.994
9	3.05	50	0.994
10	3.15	33	0.999
11	3.18	22	0.997
12	3.27	29	0.997
13	3.32	40	0.995
14	3.40	24	0.999
15	3.45	26	0.999
16	3.51	23	0.999
17	3.57	22	1.000

<sup>a</sup> Eight points were used to calculate  $K_f$  values. <sup>b</sup> Standard deviation of  $K_f$ .

POEs but does not contribute to a decrease in the retention when  $[K^+] \gg [P]_m$  is valid. The formation of the latter is also negligible for compounds with less than 17 oxyethylene units longer retained on the stationary phase because of the lack of effective coordination sites and electrostatic repulsion between potassium ions (18). In this case, the capacity ratio ( $k'$ ) of a POE can be given by eq 3.

$$k' = \phi[P]_s / ([P]_m + [KP^+]_m) \quad (3)$$

If the concentration of  $K^+$  is much higher than that of POE in the mobile phase, the arrangement of eq 1 and 3 and the substitution of an equilibrium constant ( $K_f = [P]_m[K^+]_m / [KP^+]_m$ ) of reaction 2 give the useful equation

$$1/k' = 1/k'_0 (1 + K_f C_{K^+}) \quad (4)$$

where  $C_{K^+}$  is the concentration of  $K^+$  initially added in the mobile phase. This equation shows that the ratio of the slope to the intercept (equal to  $1/k'_0$ ) obtained from the linear plot of  $1/k'$  vs  $C_{K^+}$  will be equal to the formation constant of a POE with  $K^+$ . Figure 3 shows examples of the plot for POE( $n$ )NP ( $n = 7-17$ ). As predicted from eq 4, the linear relations are experimentally obtained for all oligomers.

On the basis of Figure 3, formation constants were calculated for 11 POE( $n$ )NP ( $n = 7-17$ ) and are summarized together with standard deviations in Table I. Apparently, logarithms of  $K_f$  values linearly increase with the number of oxyethylenes. The relation is represented by the following equation:

$$\log K_f = 0.0687n + 2.43 \quad (r^2 = 0.993) \quad (5)$$

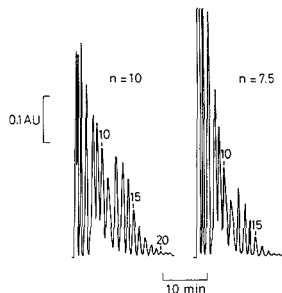


Figure 4. Oligomer separation of POE(7.5)NP and POE(10)NP: detection, UV (280 nm); sample concentration, 0.5 mg/mL. Linear gradient condition was as follows: methanol (0-7 min)  $\rightarrow$  methanol containing 5 mM KCl (25 min). Other conditions are given in the text.

These results show that longer POE chains are thermodynamically advantageous in complexation in comparison with shorter POE chains.

Formation constants of benzo-15-crown-5 (B-15-C-5) with  $K^+$  were determined and compared with literature values to examine the accuracy of the present method. It is known that B-15C-5 forms a sandwich-like 2:1 complex with  $K^+$ , but such multiple complexation is negligible for the present case as shown above.  $\log K_f$  for B-15-C-5 determined by the present method was 2.93; literature values range from 2.8 to 3.0 (19). There is good agreement between these values.

Formation constants have been determined for relatively short POEs by conductometry (15, 20) and nuclear magnetic resonance (13). Although monodisperse POEs are required for these methods, it is difficult to obtain pure compounds of a variety of POE lengths. The present method is applicable to polydisperse POEs, and can be used to evaluate complexation of each oligomer contained. This is an advantage of this developed method.

**Practical Separation of POE.** By seeing Figure 1, we can predict that a long analysis time is necessary to elute long POEs with a purely methanolic mobile phase. From a practical point of view, the effort should be made to reduce the analysis time without causing poor resolution. Isocratic elution with methanol-water or methanol containing  $K^+$  salts was effective for the separation of long POEs but resulted in poor resolution between short POEs. These results indicated that gradient elution was the best choice for the practical separation of POE derivatives of a wide distribution range as far as the gradient scheme did not influence the detection.

Gradient schemes from a purely methanolic mobile phase to methanol-water or to methanol containing  $K^+$  were concluded to be suitable for the present separation mode. Changing solvents often causes a change in the surface condition of the stationary phase, which induces the long reconditioning time for the following analysis. This is a general problem of gradient chromatography. However, changing the  $K^+$  concentration did not cause such a drawback. Therefore, pure methanol was employed as a starting solvent, and methanol containing 5 mM KCl was chosen as a final mobile phase. Figures 4 and 5 shows the oligomer separation of POE( $n$ )NP ( $n = 7.5-20$ ). Gradient conditions are given in the figure captions. POE[6]NP-POE[30]NP were separated within 35 min. Although the change in the composition of mobile phase was small, the gradient scheme caused drift of the base line in RI detection. Compounds without any chromophores, such as PEG or POE( $n$ )D, should be isocratically separated with a mobile phase; the composition of the mobile phase should be tailored for the oligomer distribution range of interest.

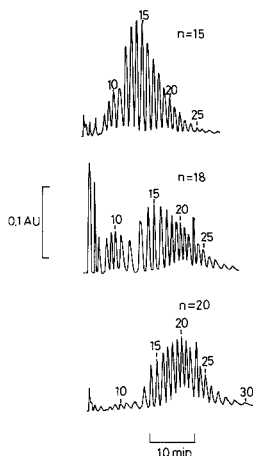


**Figure 5.** Oligomer separation of POE(15)NP, POE(18)NP, and POE(20)NP: detection, UV (280 nm); sample concentration, 0.5 mg/mL. Linear gradient condition was as follows: the same condition as for Figure 3 for POE(15)NP, methanol (1–10 min) → methanol containing 5 mM KCl (25 min) for POE(18)NP and POE(20)NP. Other conditions are given in the text.

In conclusion, the present method was useful not only for the separation of the compounds with POEs but also for the determination of the formation constants of  $K^+$  complexes. The detail studies on the formation constants of POE- $K^+$  complexes in various media and indirect conductometric detection of POEs separated on a cation-exchanger are now in progress in our laboratory and will appear in the near future.

## ACKNOWLEDGMENT

I thank Tosoh Co. for generous gifts of separation columns. I am grateful to K. Nozaki and M. Oyama for mass spectrometric measurements. I also acknowledge the courteous loan of an RI detector from my colleague D. Uemura.

## LITERATURE CITED

- (1) Cross, J. *Nonionic Surfactants*; Surfactant Science Series Vol. 19; Marcel Dekker: New York, 1987.
- (2) Richter, R. E. *HRC CC, J. High Resolut. Chromatogr. Chromatogr. Commun.* **1985**, *8*, 297–300.
- (3) Chester, T. L. *J. Chromatogr.* **1984**, *299*, 424–431.
- (4) Kudoh, M. *J. Chromatogr.* **1984**, *291*, 327–330.
- (5) Otuki, A.; Shiraishi, H. *Anal. Chem.* **1979**, *51*, 2329–2332.
- (6) Turner, L. P.; McCullough, D.; Jackewitz, A. *J. Am. Oil Chem. Soc.* **1976**, *53*, 691–694.
- (7) Aserin, A.; Garti, N.; Frenkel, M. *J. Liq. Chromatogr.* **1984**, *7*, 1545–1557.
- (8) Bear, G. R. *J. Chromatogr.* **1988**, *459*, 91–107.
- (9) Ernst, J. M. *Anal. Chem.* **1984**, *56*, 834–835.
- (10) McClure, J. S. *J. Am. Oil Chem. Soc.* **1982**, *59*, 364–373.
- (11) Desbene, P. L.; Desmazieres, B.; Basselier, J. J.; Desbene-Monvernay, A. *J. Chromatogr.* **1989**, *461*, 305–313.
- (12) Yanagida, S.; Takahashi, K.; Okahara, M. *Bull. Chem. Soc. Jpn.* **1977**, *50*, 1386–1390.
- (13) Yanagida, S.; Takahashi, K.; Okahara, M. *Bull. Chem. Soc. Jpn.* **1978**, *51*, 1294–1299.
- (14) Yanagida, S.; Takahashi, K.; Okahara, M. *Bull. Chem. Soc. Jpn.* **1978**, *51*, 3111–3120.
- (15) Kraus, S.; Rogers, L. B. *J. Chromatogr.* **1983**, *257*, 237–245.
- (16) Burger-Guerrisi, C.; Tondre, C. *J. Colloid Interface Sci.* **1987**, *116*, 100–108.
- (17) Popovych, O.; Tomkins, P. T. *Nonaqueous Solution Chemistry*; Wiley-Interscience: New York, 1981.
- (18) Okada, T., unpublished work.
- (19) Zollinger, D. Ph.; Buiten, E.; Christenhusz, A.; Bos, M.; van der Linden, W. E. *Anal. Chim. Acta* **1987**, *198*, 207–222, and references therein.
- (20) Ono, K.; Konami, H.; Murakami, K. *J. Phys. Chem.* **1979**, *83*, 2665–2669.

RECEIVED for review July 17, 1989. Accepted November 6, 1989. This work was partly supported by a Grant-in-Aid for Scientific Research (Grant No. 01740333) from the Ministry of Education Science and Culture, Japan.

# Evaluation of the Effect of Organic Modifier and pH on Retention and Selectivity in Reversed-Phase Liquid Chromatographic Separation of Alkaloids on a Cyclodextrin Bonded Phase

Daniel W. Armstrong,\* Gary L. Bertrand, Karen D. Ward, and Timothy J. Ward

Department of Chemistry, University of Missouri—Rolla, Rolla, Missouri 65401

Henry V. Secor and Jeffrey I. Seeman\*

Philip Morris Research Center, P.O. Box 26583, Richmond, Virginia 23261

A mathematical model is developed using a basic equilibrium driven approach to explain the effect of mobile-phase composition on the relative retention of ionizable solutes in a reversed-phase liquid chromatography (LC) separation. Three specific cases (i.e., different organic modifiers, different pHs, and different solute  $pK_a$ s) and one general case are considered. Twelve structurally related tobacco alkaloids and metabolites are separated under various conditions described by the model. The test solutes include anabasine, anatabine, cotinine, 2,3'-bipyridyl, *N'*-methylanabasine, myosmine, nicotine, the two nicotine *N'*-oxides, nicotyrine, norcotinine, and nornicotine. The basic model appears to explain the effects of pH and organic modifier on the relative retention of these solutes. The same general model should be applicable to most groups of ionizable solutes separated by reversed-phase LC.

"Optimizing the separation" is an important part of any methods development project involving liquid chromatography (LC). In doing this, one must choose the best stationary phase and mobile phase combination. There are several types of reversed-phase bonded stationary phases in liquid chromatography, including hydrocarbon-based materials (which include the well-known  $C_{18}$  and  $C_8$  phases as well as diphenyl and related bonded phases), cyclodextrin-based materials, internal surface reversed-phase materials, and others (1, 2). In classic reversed-phase LC, hydroorganic mobile phases are used, nonpolar solutes tend to be retained more than polar solutes, and retention of nonpolar solutes tends to decrease with increasing concentration of organic modifier in the mobile phase (provided solubility is not a problem).

Once a stationary phase is chosen, only the mobile-phase composition and temperature significantly affect the separation. Most researchers have focused attention on mobile-phase optimization, and with good reason, since this is the easiest way to control retention and selectivity in LC (1, 2). Obviously, the understanding and prediction of retention behavior in reversed-phase LC are of fundamental importance to chromatographers. Both empirical (3-6) and theoretical (7-9) approaches have been used to explain chromatographic retention.

The first goal of this work is to use a basic equilibrium driven approach to explain the relative retention behavior of ionizable solutes on a cyclodextrin bonded phase in three ideal situations. These include (1) the relative retention behavior of an ionizable solute when chromatographed with two different mobile phases in which the organic modifier is different

but the pH of the aqueous component is identical, (2) the relative retention behavior of different ionizable solutes in the same hydroorganic solvent at the same pH, and (3) the relative retention behavior of an ionizable solute in the same hydroorganic solvents at different pHs. A general theoretical treatment is given in the Appendix. The retention behavior expected from the theoretical treatment is compared to actual separation data for 12 naturally occurring tobacco alkaloids and metabolites (1-12, Chart I).

Qualitative and quantitative analysis are important for programs involving alkaloid isolation and phytochemistry (10-13) as well as for investigations involving metabolic, enzymatic, and chemical transformations (14-17). While an extensive literature is available on the quantitative determination of nicotine (7) (18-30), very few studies have been reported in which more than two or three of the other related tobacco alkaloids have been analyzed simultaneously (26, 29). The second goal of this study was to develop an LC method for 1-12 using a  $\beta$ -cyclodextrin ( $\beta$ -CD) bonded phase, which seemed to have the greatest selectivity for these compounds.

## EXPERIMENTAL SECTION

**Methods.** All separations were done at room temperature (21 °C) with Shimadzu LC-4A and 6A liquid chromatographs. The compounds were detected at 254 nm with a variable wavelength detector containing 13- and 8- $\mu$ L flow cells, respectively. All samples were dissolved in acetonitrile or methanol (depending on the mobile-phase composition) prior to injection. Typically, 5-10  $\mu$ L of solution (0.1-0.5% nicotine) was injected. Columns (25  $\times$  0.46 cm) containing  $\beta$ -cyclodextrin bonded to 5- $\mu$ m silica were obtained from Advanced Separation Technologies, Whippany, NJ. The void volume of the column was determined by injecting neat methanol. The peak-trough combination caused by the change in refractive index was used as a marker. Flow rates, solvent compositions, and pHs are given in the respective tables and figures.

**Materials.** High-performance liquid chromatography (HPLC) grade methanol, acetonitrile, triethylamine, and water were obtained from Fisher Scientific Co. Buffers were prepared by making a 1% solution of triethylamine in water and adding glacial acetic acid until the desired pH was obtained. Nicotine (7), cotinine (3), and 2,3'-dipyridyl (4) are available commercially (Aldrich). (1*R*,2*S*)-Nicotine *N'*-oxide (8) was prepared by sodium tungstate (Alfa Products)/hydrogen peroxide oxidation of nicotine following literature procedures (31) and isolated by chromatography on a 4-mm Chromatotron with sequential elution with chloroform followed by chloroform:ethanol:ammonium hydroxide (85/14/1) followed by chloroform:methanol:ammonium hydroxide (50/20/1). (1*S*,2*S*)-Nicotine *N'*-oxide (9) was prepared by *m*-chloroperbenzoic acid oxidation of nicotine (32) and purified by column chromatography. The other seven tobacco alkaloids were prepared by literature procedures: 1 (33-37), 2 (38, 39), 5 (37), 6 (33, 34), 10 (40), 11 (41), and 12 (33, 42).

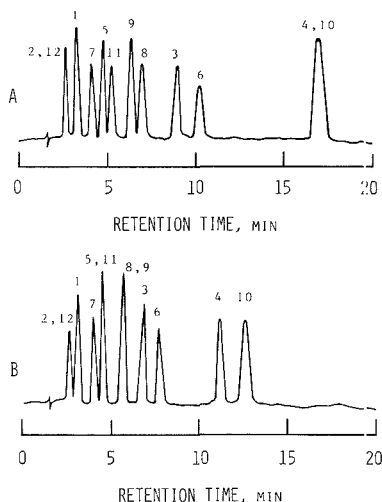


**Figure 1.** Separation of tobacco alkaloids and nicotine metabolites. A. Chromatographic conditions: 5% methanol, 95% aqueous triethylammonium acetate (1%) pH = 5.5, flow rate = 1.0 mL/min, one 25-cm  $\beta$ -cyclodextrin column. B. Chromatographic conditions were the same as in A except 5% acetonitrile was used.

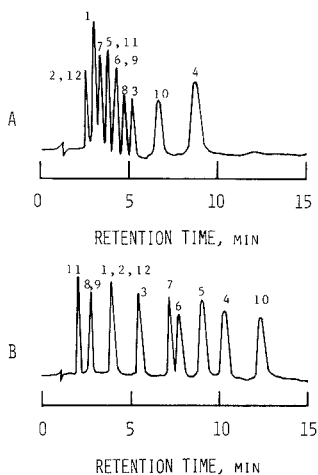


**Figure 2.** Separation of tobacco alkaloids and nicotine metabolites using a 5% acetonitrile, 95% triethylammonium acetate mobile phase: flow rate = 1.0 mL/min; one 25-cm  $\beta$ -CD column; (A) pH = 4.1 and (B) pH = 7.1.

## RESULTS AND DISCUSSION

The 12 naturally occurring tobacco alkaloids and metabolites (1–12) listed in Chart I cover a broad spectrum of structural types: imine, lactam, secondary and tertiary amine, amine oxide, and pyrrole. All are 3-substituted pyridine derivatives with either a pyrrolidine ring (nicotine family) or piperidine ring (anabasine family) substructure. The very close similarity of some of these compounds (e.g., 1, 2, and 12; 5 and 7; 8 and 9), the similarity of the basicity of these compounds, and the similar molecular size throughout the entire set makes the analytical challenge significant. We will first disclose our recent investigation using HPLC with improved  $\beta$ -cyclodextrin bonded phases to effect the optimum separations. We will then provide a discussion of an equi-

**Table I.** Retention Data for Tobacco Alkaloids and Nicotine Metabolites

compound	$k'$ with acetonitrile modifier at pH of			$k'$ with MeOH modifier at pH 5.5 <sup>a</sup>
	4.1 <sup>a</sup>	5.5 <sup>a</sup>	7.1 <sup>a</sup>	
1 (S)-(-)-anabasine	0.20	0.36	0.80	0.36
2 (R,S)-anatabine	0.15	0.30	0.80	0.22
3 (S)-(-)-continine	0.78	1.21	1.15	1.43
4 2,3'-dipyridyl	1.87	2.59	2.46	3.97
5 (S)-(-)-N'-methyl-anabasine	0.37	0.66	1.87	0.79
6 myosmine	0.60	1.48	1.60	2.03
7 (S)-(-)-nicotine	0.28	0.55	1.53	0.65
8 (1R,2S)-anti-nicotine N'-oxide	0.71	0.98	0.64	1.08
9 (1S,2S)-syn-nicotine N'-oxide	0.60	0.98	0.64	0.98
10 nicotyrine	1.41	2.87	2.94	3.97
11 (R,S)-norcotinine	0.37	0.66	0.56	0.83
12 (R,S)-nornicotine	0.15	0.30	0.80	0.22

<sup>a</sup>The mobile-phase composition was (5/95 (v/v)) acetonitrile:1% triethylammonium acetate (aq). The flow rate was 1.0 mL/min.

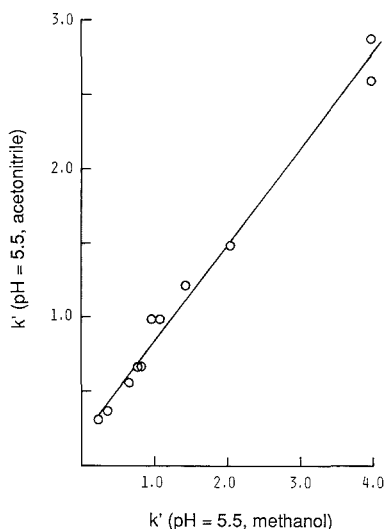


**Figure 3.** Relationship between  $k'$ 's with acetonitrile and methanol as modifiers at pH = 5.5 at the same flow rate, temperature, and column. See eq. 1.

ilibrium based model to explain relative retention behavior of ionizable solutes in reversed-phase HPLC.

Figures 1 and 2 show the separations obtained in this work by using either methanol or acetonitrile as the organic modifier with the aqueous phase buffered at pH = 4.1, 5.5 or 7.1. The data is summarized in Table I, where the  $k'$ 's can be directly compared, at different pHs, since differences in flow rate are normalized by using  $k'$ 's. At least one set of mobile-phase conditions could be found to separate all components except for anatabine (2) and nornicotine (12), the two secondary amines. As may be expected, significant changes in retention and selectivity could be obtained by altering the organic modifier and pH of the mobile phase. These figures demonstrate the capability of this reversed-phase LC method for the analysis of related alkaloids.

A comparison of Figures 1 and 2 indicates little change in the selectivity of the compounds at pH = 5.5 buffer. This is

Chart I. Structures of Tobacco Alkaloids and Nicotine Metabolites

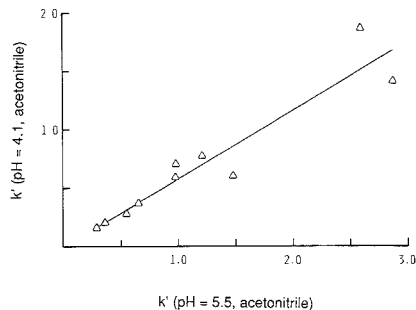
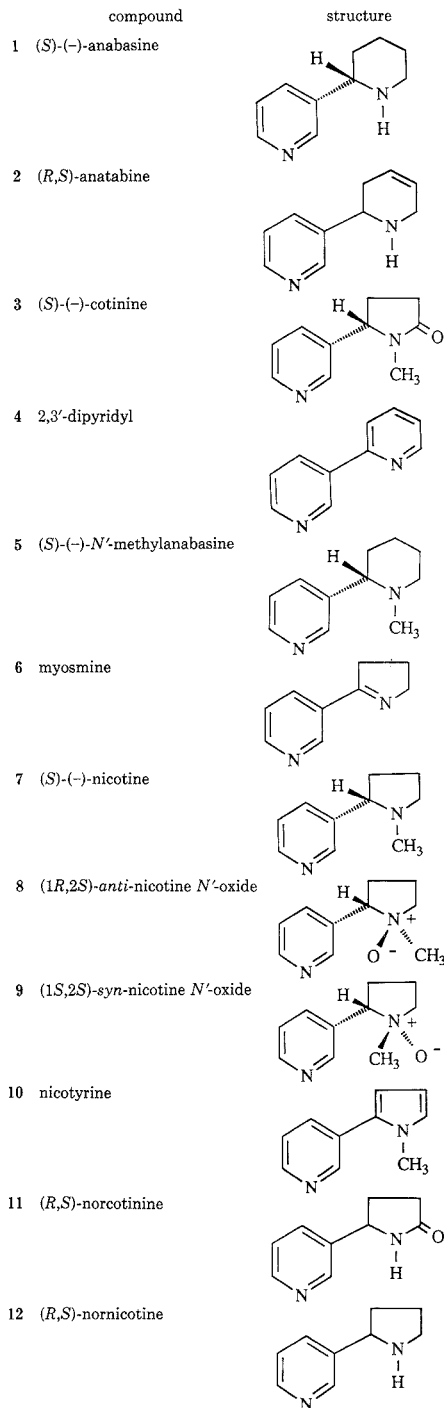


Figure 4. Relationship between  $k'$ 's at pH = 4.1 and 5.5 with acetoneitrile as modifier in both cases at the same flow rate, temperature, and column. See eq 2.

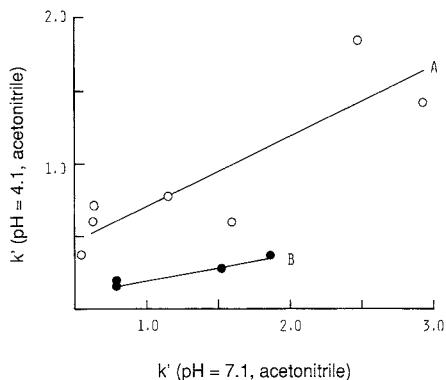


Figure 5. Relationship between  $k'$ 's at pH = 4.1 and 7.1 with acetoneitrile as modifier in both cases at the same flow rate, temperature, and column. The correlation line A (eq 3) describes the behavior for the seven less basic nicotinoids (types II and III, open circles). The correlation line B (eq 4) describes the behavior for the five more basic nicotinoids (type I, solid circles). The data was taken from Table I.

shown by an excellent correlation (Figure 3 and eq 1) between the  $k'$ 's with acetoneitrile vs methanol as modifier (note that pH, flow rate, temperature, and column remain the same).

$$k'(\text{acetoneitrile}) = 0.187 + 0.647k'(\text{methanol}) \quad (1)$$

pH = 5.5

$$r = 0.994, \quad \text{std dev of residuals} = 0.099,$$

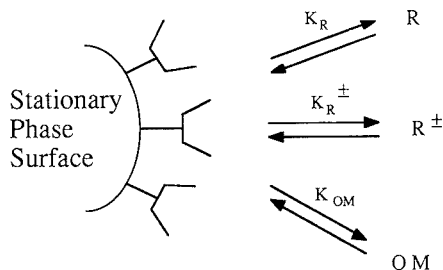
$$n = 12, \quad p < 0.0001$$

Figure 3

As the pH increases, three types of behavior are observed: type I (for 1, 2, 5, 7, and 12), where solute retention increases with pH; type II (for 8 and 9), where solute retention goes up from pH = 4.1 to pH = 5.5 and then decreases to less than the original retention at pH = 7.1; and type III (for 3, 4, 6, 10, and 11), where solute retention goes up and more or less stabilizes at pH > 5.5.

Examination of these three groups shows a structural clustering. All 12 substrates are 3-substituted pyridines. Type I compounds are moderately strong organic bases, all secondary or tertiary amines. At pH = 5.5, nicotine is >99% monoprotonated (43). Type III compounds are all far less basic, the second ring being part of a lactam, a pyrrole, an imine, or a pyridine. At pH = 5.5, these compounds exist primarily as their unprotonated free bases (44). The two compounds in type II are both *N'*-oxides of the methyl-





**Figure 6.** Basic model describing the equilibria involved in the HPLC retentions. R and R<sup>±</sup> refer to the solute being chromatographed, the former the amine free base and the latter the protonated species. OM is the organic modifier.

pyrrolidine ring. These structural features and basicity properties suggest that the protonated species does not complex strongly with the  $\beta$ -CD support.

Figure 4 illustrates that there is a linear correlation between the  $k'$ 's observed for 1–12 in acetonitrile at pH = 4.1 vs pH = 5.5 (eq 2). However, completely different behavior is found

$$k'(\text{pH} = 4.1) = -0.0099 + 0.588k'(\text{pH} = 5.5) \quad (2)$$

acetonitrile

$$r = 0.951, \text{ std dev of residuals} = 0.172,$$

$$n = 12, p < 0.001$$

Figure 4

when the  $k'$ 's are compared at pH = 4.1 vs pH = 7.1. As shown in Figure 5, a spread of points is observed. If the data is divided into two groups, one consisting of type I substrates and the second consisting of type II and type III substrates, two correlations are found, as indicated by eq 3 and 4 and the correlation lines A and B in Figure 5, respectively.

$$k'(\text{pH} = 4.1) = 0.225 + 0.477k'(\text{pH} = 7.1) \quad (3)$$

type II and type III substrates, acetonitrile

$$r = 0.851, \text{ std dev of residuals} = 0.307,$$

$$n = 7, p < 0.015$$

Figure 5, line A

$$k'(\text{pH} = 4.1) = 0.022 + 0.180k'(\text{pH} = 7.1) \quad (4)$$

type I substrates, acetonitrile

$$r = 0.971, \text{ std dev of residuals} = 0.026,$$

$$n = 5, p < 0.005$$

Figure 5, line B

Expressions can be derived that explain the observed elution profiles (vide supra) and can be used to predict relative retention behavior of other classes of acidic or basic solutes. The derivations are based on the simple model shown in Figure 6. There are a finite number of adsorption sites on the stationary phase on which the solute being chromatographed (R or R<sup>±</sup>) and the mobile-phase components (i.e., the organic modifier (OM) and water) can bind. It is assumed that the organic modifier has a greater affinity for the binding site than water has, and that the solute (R) has the greatest affinity for the adsorption site. If given sufficient time, there would be an equilibrium distribution of R, R<sup>±</sup> and OM between the mobile phase and the stationary-phase adsorption sites. It is further assumed that the equilibrium constants involving R and OM are independent of their concentration. Having made these assumptions, we point out that there can be secondary effects of concentration on both the thermodynamic equilibrium constants and activity coefficients. These could cause deviation from the ideal cases being outlined here and

will be considered subsequently.

Given the basic model shown in Figure 6, two equilibrium expressions can be written for the solute, R. The first will be referred to as the observed equilibrium expression (where  $(K_R)_{\text{obs}}$  is the equilibrium constant).  $(K_R)_{\text{obs}}$  actually is a distribution coefficient that takes into account all possible forms of R (i.e., ionized, un-ionized, associated, unassociated, etc).

$$(K_R)_{\text{obs}} = \frac{n_{R(s)}}{(n_s^\circ - n_{R(s)})[R]_{\text{total}}} \quad (5)$$

where  $n_{R(s)}$  is the number of adsorption sites occupied by solute R,  $n_s^\circ$  is the total number of adsorption sites, and  $[R]_{\text{total}}$  is the total concentration of R regardless of its form.

A true equilibrium expression for each form of R can be written as well:

$$(K_R)_{\text{true}} = \frac{n_{R(s)}}{(n_s^\circ - n_{R(s)} - n_{OM(s)})[R_{\text{aq}}]} \quad (6)$$

where  $n_{OM(s)}$  is the number of stationary-phase adsorption sites occupied by the organic modifier and  $[R_{\text{aq}}]$  is the concentration of R in bulk mobile-phase solution. The ratio of the observed to the true equilibrium constant (provided  $n_s^\circ \gg n_{R(s)}$ , which is the normal chromatographic condition) is

$$\frac{(K_R)_{\text{obs}}}{(K_R)_{\text{true}}} = \frac{n_s^\circ - n_{OM(s)} [R_{\text{aq}}]}{n_s^\circ [R]_{\text{total}}} \quad (7)$$

The equilibrium expression for the organic modifier (OM) is

$$K_{OM} = \frac{n_{OM(s)}}{(n_s^\circ - n_{OM(s)})[OM]} \quad (8)$$

where  $[OM]$  is the concentration of organic modifier in the mobile phase. Rearranging eq 8 gives

$$1 - \frac{n_{OM(s)}}{n_s^\circ} = 1 - \frac{K_{OM}[OM]}{1 + K_{OM}[OM]} \quad (9)$$

or

$$\frac{n_s^\circ - n_{OM(s)}}{n_s^\circ} = \frac{1}{1 + K_{OM}[OM]} \quad (10)$$

Equation 10 can be substituted into eq 7 to give

$$\frac{(K_R)_{\text{obs}}}{(K_R)_{\text{true}}} = \frac{[R_{\text{aq}}]}{[R]_{\text{total}}(1 + K_{OM}[OM])} \quad (11)$$

If R is a weak base (i.e.,  $R + H_2O \rightarrow RH^+ + OH^-$ ), then

$$(K_b)_R = \frac{[OH^-][RH^+]}{[R_{\text{aq}}]} \quad (12)$$

or

$$(K_b)_R = \frac{[OH^-]\{[R]_{\text{total}} - [R_{\text{aq}}]\}}{[R_{\text{aq}}]} \quad (13)$$

Equation 13 can be rearranged to

$$\frac{[R_{\text{aq}}]}{[R]_{\text{total}}} = \frac{1}{1 + (K_b)_R/[OH^-]} \quad (14)$$

If R is a weak acid, the analogous expression is obtained:

$$\frac{[R_{\text{aq}}]}{[R]_{\text{total}}} = \frac{1}{1 + (K_a)_R/[H^+]} \quad (15)$$

In general,  $[R_{\text{aq}}]/[R]_{\text{total}} = f(\text{pH}, \text{p}K_R)$ .

Taking the case where R is a weak base and substituting eq 14 into eq 11 yields

$$\frac{(K_R)_{\text{obs}}}{(K_R)_{\text{true}}} = \frac{1}{(1 + (K_b)_{R1}/[\text{OH}^-])(1 + K_{\text{OM}}[\text{OM}])} \quad (16)$$

For two different solutes ( $R_1, R_2$ ),  $(K_b)_{R1}/(K_b)_{R2}$  and  $(K_{R1})_{\text{true}}/(K_{R2})_{\text{true}}$  are fairly independent of small changes in pH and [OM] or the nature of the organic modifier.  $K_{\text{OM}}$  is independent of  $pK, [R]$ , and the nature of R.

**Special Case No. 1.** To evaluate the reversed-phase retention behavior of a solute, R, in two different mobile phases (i.e., in which the organic modifier is different) and with the pH of the buffer portion of the mobile phase identical, one must use eq 16. For the mobile phase containing the first organic modifier

$$(K_{R1})_{\text{obs}}^{\text{OM1}} = \frac{(K_{R1})_{\text{true}}}{(1 + (K_b)_{R1}/[\text{OH}^-])(1 + K_{\text{OM1}}[\text{OM}_1])} \quad (17)$$

For the mobile phase containing the second modifier

$$(K_{R1})_{\text{obs}}^{\text{OM2}} = \frac{(K_{R1})_{\text{true}}}{(1 + (K_b)_{R1}/[\text{OH}^-])(1 + K_{\text{OM2}}[\text{OM}_2])} \quad (18)$$

Dividing eq 17 by eq 18 gives

$$\frac{(K_{R1})_{\text{obs}}^{\text{OM1}}}{(K_{R1})_{\text{obs}}^{\text{OM2}}} = \frac{1 + K_{\text{OM2}}[\text{OM}_2]}{1 + K_{\text{OM1}}[\text{OM}_1]} \quad (19)$$

where both  $(K_{R1})_{\text{true}}$  and  $(1 + ((K_b)_{R1}/[\text{OH}^-]))$  have cancelled. In liquid chromatography, the capacity factor is directly proportional to the equilibrium constant of a solute between stationary and mobile phases (i.e.,  $k' \propto K_{\text{eq}}$ ). Therefore eq 19 also could be written as the ratio of the capacity factors. Thus, eq 19 can relate the relative retentions of a solute ( $R_1$ ) chromatographed with two different mobile phases. In order to compare the retention behavior (or  $k'$ ) of two or more different solutes chromatographed with two different mobile phases, the derivation that led to eq 19 must be repeated for the second solute, giving

$$\frac{(K_{R2})_{\text{obs}}^{\text{OM1}}}{(K_{R2})_{\text{obs}}^{\text{OM2}}} = \frac{1 + K_{\text{OM2}}[\text{OM}_2]}{1 + K_{\text{OM1}}[\text{OM}_1]} \quad (20)$$

Since the right sides of eq 19 and 20 are identical for any two different (but related) solutes, this quantity may be taken as a constant,  $\alpha$ , which is independent of solute.

$$(K_{R1})_{\text{obs}}^{\text{OM1}} = \alpha(K_{R1})_{\text{obs}}^{\text{OM2}} \quad (21)$$

According to eq 21, plots of  $k'$  or  $(K_R)_{\text{obs}}$  for different solutes in two different mobile phases (i.e., two different organic modifiers, all other conditions identical) should be a straight line with an intercept of zero. The slope of this line would vary with the type and concentrations of the organic modifiers. The intercept also can deviate from zero somewhat if other factors are operative, such as adsorption to residual silanol groups or deviations from the assumptions made for this derivation. An analogous plot of  $\ln(K_{R1})_{\text{obs}}^{\text{OM1}}$  vs  $\ln(K_{R1})_{\text{obs}}^{\text{OM2}}$  should produce a straight line of slope  $\sim 1$  and an intercept of  $\ln \alpha$ . An example of the type of behavior predicted by eq 21 is shown in Figure 3 in which the capacity factors of several alkaloids separated with two different mobile phases (at pH = 5.5) are plotted.

**Special Case No. 2.** To evaluate the reversed-phase retention behavior of a compound in the same mobile phase (i.e., the same organic modifier) but with the aqueous portion of the solution buffered at two different pHs, eq 16 again can be used. In this case eq 16 must be written for each of the two pH situations where

$$(K_{R1})_{\text{obs}}^{\text{pH1}} = \frac{(K_{R1})_{\text{true}}}{(1 + (K_b)_{R1}/[\text{OH}^-]_1)(1 + K_{\text{OM1}}[\text{OM}_1])} \quad (22)$$

and

$$(K_{R1})_{\text{obs}}^{\text{pH2}} = \frac{(K_{R1})_{\text{true}}}{(1 + (K_b)_{R1}/[\text{OH}^-]_2)(1 + K_{\text{OM1}}[\text{OM}_1])} \quad (23)$$

This time when the ratio of eq 22 and 23 is taken, both  $(K_{R1})_{\text{true}}$  and  $(1 + K_{\text{OM1}}[\text{OM}_1])$  cancel to give

$$\frac{(K_{R1})_{\text{obs}}^{\text{pH1}}}{(K_{R1})_{\text{obs}}^{\text{pH2}}} = \frac{1 + \{(K_b)_{R1}/[\text{OH}^-]_2\}}{1 + \{(K_b)_{R1}/[\text{OH}^-]_1\}} = \frac{[\text{OH}^-]_1 (K_b)_{R1} + [\text{OH}]_2}{[\text{OH}^-]_2 (K_b)_{R1} + [\text{OH}]_1} \quad (24)$$

Consider two limiting cases for eq 24. The first case is at a very high pH (relative to  $K_b$ ) where  $[\text{OH}^-]_1$  and  $[\text{OH}^-]_2 \gg (K_b)_{R1}$ . In this instance, eq 24 becomes

$$\frac{(K_{R1})_{\text{obs}}^{\text{pH1}}}{(K_{R1})_{\text{obs}}^{\text{pH2}}} = 1 \quad (25)$$

The second case is for a relatively strong base chromatographed with a mobile phase at lower pHs where  $(K_b)_{R1} \gg [\text{OH}^-]_1$  and  $[\text{OH}^-]_2$ . In this case one obtains

$$\frac{(K_{R1})_{\text{obs}}^{\text{pH1}}}{(K_{R1})_{\text{obs}}^{\text{pH2}}} = \frac{[\text{OH}^-]_1}{[\text{OH}^-]_2} \quad (26)$$

In plots of the limiting cases for a hypothetical series of strong and weak bases, the weak bases would fall along a line with a slope of 1, while the relatively strong bases would tend to fall along a line parallel to the x axis if this axis represents the high pH. Solutes of intermediate  $pK_b$ s would fall somewhere between these lines.

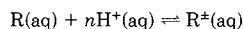
Indeed this type of behavior was observed for the alkaloids used in this study. Figure 5 is a plot of  $k'$  values for a series of the 12 alkaloids chromatographed at pH 4.1 and 7.1 (all other conditions were identical). Clearly two types of retention behavior are observed. One group of alkaloids (type I: anabasine, anatabine, *N'*-methylanabasine, nornicotine, and nicotine) approaches the retention behavior described by eq 26 while the other group (types II and III) approaches the behavior described by eq 25. The segregation of these alkaloids into two groups is a result of their relative  $pK_b$ s and the pH of the mobile phase as described by eq 24.

## CONCLUSIONS

The treatment derived in this work adequately explains the reversed-phase retention behavior of these alkaloids on a  $\beta$ -CD column. In fact, an analogous treatment should be able to explain the retention behavior of most ionizable compounds on any reversed-phase packing, given standard reversed-phase separation conditions (e.g., hydroorganic mobile phases; simple buffers; avoidance of temperature, flow, pressure, or concentration extremes; and so on). A general treatment describing the retention behavior of ionizable solutes in reversed-phase separations is given in the Appendix. The important procedure of optimizing a liquid chromatographic separation has been, at best, an empirical process. By providing a theoretical basis for this, one may be able to obtain a better separation and a more complete understanding of retention behavior.

## APPENDIX

Given the model in Figure 6, the following general equilibrium and associated constant can be written:



$$K_D = \frac{[R^+]}{[R][\text{H}^+]^n} \quad (27)$$

If

$$n = +1, \text{ R is a base} \quad K_D = K_b/K_w$$

$$n = -1, \text{ R is an acid} \quad K_D = K_a$$

The retention of R is determined by an effective equilibrium constant that does not distinguish between the various forms of R, R<sup>±</sup>, etc. Translation of retention volume to an equilibrium constant also assumes that all sites ( $n_s^0$ ) on the column are available to the analyte:

$$(K_R)_{\text{obs}} = \frac{\{n_{R(s)} + n_{R^{\pm}(s)}\}}{\{n_s^0 - n_{R(s)} - n_{R^{\pm}(s)}\}[\text{R}] + [\text{R}^{\pm}]}, \quad n_s^0 \gg n_{R(s)} + n_{R^{\pm}(s)} \quad (28)$$

However, the actual equilibria depend on the amounts of each form and the possible occupancy of sites by the organic modifier, OM:

$$K_{\text{OM}} = \frac{n_{\text{OM}(s)}}{\{n_s^0 - n_{R(s)} - n_{R^{\pm}(s)} - n_{\text{OM}(s)}\}[\text{OM}]} \quad (29)$$

$$K_R = \frac{n_{R(s)}}{\{n_s^0 - n_{R(s)} - n_{R^{\pm}(s)} - n_{\text{OM}(s)}\}[\text{R}]} \quad (30)$$

$$K_{R^{\pm}} = \frac{n_{R^{\pm}(s)}}{\{n_s^0 - n_{R(s)} - n_{R^{\pm}(s)} - n_{\text{OM}(s)}\}[\text{R}^{\pm}]} \quad (31)$$

Rearrangement of eq 29 gives

$$\frac{n_s^0 - n_{R(s)} - n_{R^{\pm}(s)} - n_{\text{OM}(s)}}{n_s^0 - n_{R(s)} - n_{R^{\pm}(s)}} = \frac{1}{1 + K_{\text{OM}}[\text{OM}]} \quad (32)$$

$$\frac{n_{R(s)}}{n_s^0 - n_{R(s)} - n_{R^{\pm}(s)}} = \frac{K_R[\text{R}]}{1 + K_{\text{OM}}[\text{OM}]} \quad (33)$$

$$\frac{n_{R^{\pm}(s)}}{n_s^0 - n_{R(s)} - n_{R^{\pm}(s)}} = \frac{K_{R^{\pm}}[\text{R}]}{1 + K_{\text{OM}}[\text{OM}]} \quad (34)$$

$$(K_R)_{\text{obs}} = \frac{\{K_R[\text{R}] + K_{R^{\pm}}[\text{R}^{\pm}]\}}{\{1 + K_{\text{OM}}[\text{OM}]\}[\text{R}] + [\text{R}^{\pm}]} \quad (35)$$

But

$$\frac{[\text{R}^{\pm}]}{[\text{R}]} = K_D[\text{H}^+]^n$$

$$(K_R)_{\text{obs}} = \frac{\{K_R + K_{R^{\pm}}K_D[\text{H}^+]^n\}}{\{1 + K_{\text{OM}}[\text{OM}]\}1 + K_D[\text{H}^+]^n} \quad (36)$$

Changing the organic modifier, [OM<sub>1</sub>] or [OM<sub>2</sub>], at low concentrations is not expected to have a great effect on  $K_R$ ,  $K_{R^{\pm}}$ , and  $K_D$  and in general will have similar effects on all analytes (R1, R2, ...) of a particular type. Therefore, two different cosolvents at the same pH will give

$$\frac{(K_{R1})_{\text{obs}}^{\text{OM1}}}{(K_{R1})_{\text{obs}}^{\text{OM2}}} = \frac{1 + K_{\text{OM2}}[\text{OM2}]}{1 + K_{\text{OM1}}[\text{OM1}]} \quad (37)$$

For a different analyte, R2

$$\frac{(K_{R2})_{\text{obs}}^{\text{OM1}}}{(K_{R2})_{\text{obs}}^{\text{OM2}}} = \frac{1 + K_{\text{OM2}}[\text{OM2}]}{1 + K_{\text{OM1}}[\text{OM1}]} = \frac{(K_{R1})_{\text{obs}}^{\text{OM1}}}{(K_{R1})_{\text{obs}}^{\text{OM2}}} \quad (38)$$

A plot of  $K_R$  values in solutions of OM1 vs those in solutions of OM2 will be linear with a slope of 1.

The effect of pH is more complex and depends on the values of  $K_D$ , the ratio  $K_{R^{\pm}}/K_R$ , and the pH range covered. For a given analyte at two pHs, pH1 = [H<sup>+</sup>] and pH2 = [H<sup>+</sup>]<sup>2</sup>

$$\frac{(K_R)_{\text{obs}}^{\text{pH1}}}{(K_R)_{\text{obs}}^{\text{pH2}}} = \frac{\{1 + K_D(K_{R^{\pm}}/K_R)[\text{H}^+]^n\} \{1 + K_D[\text{H}^+]^n\}}{\{1 + K_D(K_{R^{\pm}}/K_R)[\text{H}^+]^n\} \{1 + K_D[\text{H}^+]^n\}} \quad (39)$$

**Special Cases. I.** If  $(K_{R^{\pm}}/K_R) = 1$ , pH will have no effect.

$$\frac{(K_R)_{\text{obs}}^{\text{pH1}}}{(K_R)_{\text{obs}}^{\text{pH2}}} = 1 \quad (40)$$

**Special Cases. II. A.** If  $(K_{R^{\pm}}/K_R) \ll 1$

$$\frac{(K_R)_{\text{obs}}^{\text{pH1}}}{(K_R)_{\text{obs}}^{\text{pH2}}} = \frac{1 + K_D[\text{H}^+]^n}{1 + K_D[\text{H}^+]^n} \quad (41)$$

For a basic analyte, if pH1 < pH2,  $K_D[\text{H}^+] \gg K_D[\text{H}^+]^2$

$$\text{strong base } (K_R)_{\text{obs}}^{\text{pH1}} \ll (K_R)_{\text{obs}}^{\text{pH2}}$$

**Special Cases. II. B.** If base is very weak, or pHs are close together

$$\frac{(K_R)_{\text{obs}}^{\text{pH1}}}{(K_R)_{\text{obs}}^{\text{pH2}}} \sim 1 \quad (42)$$

**Registry No.** 1, 494-52-0; 2, 2743-90-0; 3, 486-56-6; 4, 581-50-0; 5, 24380-92-5; 6, 532-12-7; 7, 54-11-5; 8, 51020-67-8; 9, 51095-86-4; 10, 487-19-4; 11, 17708-87-1; 12, 5746-86-1; methanol, 67-56-1; acetonitrile, 75-05-8.

## LITERATURE CITED

- (1) Hamilton, R. J.; Sewell, P. A. *Introduction to High Performance Liquid Chromatography*; Halsted Press: New York, 1978; pp 78-84.
- (2) Armstrong, D. W.; Li, W. *Chromatography* **1987**, *2*, 43.
- (3) Trappe, W. *Biochem. Z.* **1940**, *305*, 50.
- (4) Strain, A. H. *Chromatographic Adsorption Analysis*; Interscience: New York, 1942.
- (5) Jacques, J.; Mathieu, J. P. *Bull. Soc. Chim. France* **1948**, *9*, 4.
- (6) Snyder, L. R. *Principles of Adsorption Chromatography*; Marcel Dekker: New York, 1968.
- (7) Carr, P. W. *J. Chromatogr.* **1980**, *194*, 105.
- (8) Martire, D. E.; Boehm, R. E. *J. Phys. Chem.* **1983**, *87*, 1045.
- (9) Karger, B. L.; Le Page, J. N.; Tanaka, N. In *High Performance Liquid Chromatography*; Horvath, C., Ed.; Academic Press: New York, 1980; Vol. 1, p 113.
- (10) Schmeltz, I.; Hoffmann, D. *Chem. Rev.* **1977**, *77*, 295.
- (11) Enzell, C. R.; Wahlberg, I.; Aasen, A. *J. Fortschr. Chem. Org. Naturst.* **1977**, *34*, 1.
- (12) Production of Quality Tobacco Leaf. Recent Advances in Tobacco Science, 37th Tobacco Chemists' Research Conference, October 11-13, 1983.
- (13) Enzell, C. R.; Wahlberg, I. In *Leaf Composition in Relation to Smoking Quality and Aroma*; Recent Advances in Tobacco Science, 34th Tobacco Chemists' Research Conference, October 27-29, 1980.
- (14) Seeman, J. I. *Heterocycles* **1984**, *22*, 165.
- (15) Strunz, G. M.; Findlay, J. A. *The Alkaloids*; Brossi, A., Ed.; Academic: New York, 1985; Vol. 26, Chapter 3, p 89.
- (16) Seeman, J. I. *Pure Appl. Chem.* **1987**, *59*, 1661.
- (17) Kasaki, T.; Maeda, S.; Kolwai, A.; Mikami, Y.; Sasaki, T.; Matsushita, H. *Beitr. Tabakforsch. Int.* **1978**, *9*, 308.
- (18) Barz, W.; Kettner, M.; Husemann, W. *Planta Med.*, *J. Med. Plant Res.* **1978**, *34*, 73.
- (19) Beckett, A. H.; Triggs, E. *J. Nature (London)* **1968**, *211*, 1415.
- (20) Berry, D. J.; Grove, J. *J. Chromatogr.* **1971**, *61*, 111.
- (21) Bluthgen, V. A.; Nijhuis, H.; Hamann, J.; Heeschen, W. *Milchwissenschaft* **1978**, *33*, 137.
- (22) Burns, D. T.; Collin, E. *J. Chromatogr.* **1977**, *133*, 378.
- (23) Bush, L. P. *J. Chromatogr.* **1972**, *73*, 243.
- (24) Clarke, E. G. C.; Hawkins, A. E. *J. Forensic Sci. Soc.* **1961**, *7*, 120.
- (25) Watson, I. D. *J. Chromatogr.* **1977**, *143*, 203.
- (26) Plade, J. J.; Hoffmann, D. *J. Liq. Chromatogr.* **1980**, *3*, 1505.
- (27) Saunders, J. A.; Blume, D. E. *J. Chromatogr.* **1981**, *205*, 147.
- (28) Sudan, B. J.; Brouillard, C.; Strehler, C.; Strub, H.; Sterboul, J.; Sainte-Laudy, J. *J. Chromatogr.* **1984**, *288*, 415.
- (29) Kyerematen, G. A.; Taylor, L. H.; de Bethizy, J. D.; Vesell, E. S. *J. Chromatogr.* **1987**, *419*, 191.
- (30) Mousa, S.; Van Loon, G. R.; Houdi, A. A.; Crooks, P. A. *J. Chromatogr.* **1985**, *347*, 405 and other papers in this series.
- (31) Phillipson, J. D.; Handa, S. *Phytochemistry* **1975**, *14*, 2683.
- (32) Craig, J. C.; Purushothaman, K. K. *J. Org. Chem.* **1970**, *35*, 1721.
- (33) Hu, M. W.; Bondinell, W. E.; Hoffmann, D. *J. Labelled Compd.* **1974**, *10*, 79.
- (34) Seeman, J. I. *Synthesis* **1977**, 498.
- (35) Alberici, G. F.; Adam, G.; Plat, M. M. *Tetrahedron Lett.* **1983**, 1937.
- (36) Mundy, B. P.; Larsen, B. R. *Syn. Commun.* **1972**, *2*, 197.
- (37) Buchel, K. H.; Korte, F. *Chem. Ber.* **1962**, *95*, 2438.
- (38) Ohno, K.; Ishikawa, H.; Kinjo, N.; Machida, M. *Heterocycles* **1986**, *25*, 276.

- (39) Quan, P. M.; Karns, T. K. B.; Quin, L. D. *J. Org. Chem.* **1965**, *30*, 2769.  
(40) Frank, R. L.; Holley, R. W.; Wikholm, D. M. *J. Am. Chem. Soc.* **1942**, *64*, 2835.  
(41) Glenn, D. F.; Edwards, W. B., III. *J. Org. Chem.* **1978**, *43*, 2860.  
(42) Seeman, J. I.; Secor, H. V.; Chavdarian, C. G.; Sanders, E. B.; Bassfield, R. L.; Whidby, J. F. *J. Org. Chem.* **1981**, *46*, 3040.  
(43) Seeman, J. I.; Secor, H. V.; Armstrong, D. W.; Timmons, K. D.; Ward, T. *J. Anal. Chem.* **1988**, *60*, 2120.

- (44) Yamamoto, I.; Soeda, Y.; Kamimura, H.; Yamamoto, R. *Agric. Biol. Chem.* **1968**, *32*, 1341.

RECEIVED for review May 16, 1989. Accepted October 18, 1989. Support of a portion of this work by the Smokeless Tobacco Research Council, Inc., to D.W.A. (Grant No. 0154-01) is gratefully acknowledged.

## Development of a Method for the Sampling and Analysis of Sulfur Dioxide and Nitrogen Dioxide from Ambient Air

Joseph E. Sickles, II,\* Peter M. Grohse, Laura L. Hodson, Cynthia A. Salmons, Kelly W. Cox, Ann R. Turner, and Eva D. Estes

Research Triangle Institute, Research Triangle Park, North Carolina 27709

A method has been developed to permit the simultaneous sampling of SO<sub>2</sub> and NO<sub>2</sub> from ambient air. Sulfur dioxide and NO<sub>2</sub> are collected on triethanolamine-impregnated glass fiber filters. After sampling, the filters are extracted, and the extract is analyzed for sulfate, nitrite, and nitrate using ion chromatography. Ambient concentrations are computed from the recovered nitrogen and sulfur and the sampled air volume. Laboratory tests were conducted to evaluate the performance of the method under various species concentrations and loadings, sampling rates, humidities, temperatures, flushing conditions, and interferences. Results of these tests are described. Field measurements using the developed method compared favorably with other established methods. On the basis of the precision of field blanks, SO<sub>2</sub> and NO<sub>2</sub> detection limits of 0.3 and 0.2 ppb for 24-h samples and 0.04 and 0.03 ppb for 7-day samples were estimated. Precision estimates of better than ±15% were found, and accuracy within ±10% was observed.

### INTRODUCTION

Assessment of ecosystem acidification resulting from air pollution requires monitoring the airborne concentrations of the contributing acidifying and neutralizing gaseous and particulate species. The offending constituents include the trace gases SO<sub>2</sub>, NO<sub>2</sub>, HNO<sub>3</sub>, HONO<sub>2</sub>, and NH<sub>3</sub> and particulate SO<sub>4</sub><sup>2-</sup>, NO<sub>3</sub><sup>-</sup>, NH<sub>4</sub><sup>+</sup>, and H<sup>+</sup>. A modular, multiconstituent, integrating sampler known as the transition flow reactor (TFR) has been designed and tested for selected pollutants (1). Although the initial TFR did not sample for SO<sub>2</sub> and NO<sub>2</sub>, its modular design provided for the addition of a module with that capability. As a result, the object of the current effort was to develop a method for the sampling and analysis of SO<sub>2</sub> and NO<sub>2</sub> from ambient air that could be incorporated in a modular form into a multiconstituent sampler such as the TFR.

Goals for the method were simultaneous determination of SO<sub>2</sub> and NO<sub>2</sub> at their nominal ambient (ppb) levels with ±20% accuracy, sampling durations ranging from one to several days, and use of ion chromatography (IC) as the analytical finish. Compatibility with IC was desirable to streamline laboratory operations for large numbers of samples (e.g., monitoring network applications), since IC was the method of choice for

most of the other constituents. The nominal 0.1 μg mL<sup>-1</sup> detection limit of the IC imposes a nominal 1 ppb detection limit for a 24-h integrated sample assuming a sampling rate of 1 L min<sup>-1</sup> and a 20-mL extract volume. This means that acceptable flow rates must be 1 L min<sup>-1</sup> or greater.

In an effort to identify existing methods that were either suitable or adaptable for our purposes, an extensive literature review was performed (2). Among the several types of samplers available, bubblers and impingers were judged to be unsuitable in view of their limited sampling times (due to evaporation of the collection solution) and their potential for handling, shipping, and freezing problems. These considerations narrowed the focus of our development efforts to sorbents and filters. Sulfur dioxide is relatively easy to collect and has been sampled successfully at stack concentrations using uncoated molecular sieves (MS) (3) and at ambient concentrations using various impregnated filters (4-10). The reported aqueous impregnating solutions usually contained the hydroxide, bicarbonate, or carbonate salts of sodium or potassium, along with glycerin or triethanolamine (TEA) as an humectant.

Uncoated silica gel (11, 12), MS (12), activated alumina (12-14), MnO<sub>2</sub> (13-15), and charcoal (13) have been used to collect NO<sub>2</sub> from air streams, but they were found to generate NO, especially under humid conditions (12, 13). Sorbents such as firebrick (12) and MS (16-18) coated with aqueous solutions of TEA have been used successfully to sample for NO<sub>2</sub>. Filters impregnated with TEA (19) or *p*-anisidine (20) have also been used to sample for NO<sub>2</sub>.

Only one method has been reported for the simultaneous sampling of SO<sub>2</sub> and NO<sub>2</sub> (21). This method uses 13X MS that have been coated with a solution containing primarily TEA (18, 21). The method uses an IC finish, has been reported to be applicable at SO<sub>2</sub> and NO<sub>2</sub> concentrations between 1 and 10 ppm, and was demonstrated at sampling rates of 30-200 mL min<sup>-1</sup> and sample durations of 5-120 min (21). These conditions are in contrast to the desired working concentration (i.e., ppb), sampling rate (i.e., 1 L min<sup>-1</sup>), and sample duration (i.e., 24 h) described earlier.

The current study was conducted in several phases, and this report is organized similarly. In the first phase, findings of other workers (2) as discussed above were used to guide our selection and subsequent preliminary laboratory testing of sorbents, filters, and coating/impregnating solutions. These tests were performed to identify a method suitable for more

comprehensive laboratory tests and led to the selection of a TEA-based solution for analyte collection. Preliminary testing of uncoated and coated sorbents and impregnated filters led to the selection of TEA-impregnated filters for comprehensive laboratory tests.

In the second phase, comprehensive laboratory tests were performed. These tests led to method refinement, the establishment of the bounds of applicability (i.e., species concentrations and loadings, sampling rates, capacities, humidity, temperature, and interferences), and definition of the method. The final phase of method development involved field tests where the method was deployed in a 13-day study, results were compared with accepted methods, and method precision and accuracy were established.

## EXPERIMENTAL SECTION

**General Procedures.** Challenge atmospheres containing  $\text{NO}_2$  and/or  $\text{SO}_2$  were prepared by using either permeation tubes or certified cylinders of compressed gas followed by dilution with clean air of controlled humidity. Ambient air was compressed and cleaned with catalytic chemical and sorption scrubbers to remove organics, ozone, nitrogen oxides, and sulfur oxides, but not  $\text{CO}_2$ , prior to introduction to the dilution system.

A TECO Model 14 B/E chemiluminescence (CLM)  $\text{NO}_x$  analyzer and a Monitor Labs Model 8450 flame photometric  $\text{SO}_2$  monitor were used to analyze the challenge atmosphere upstream and downstream of each sampler. An EG&G Model 880 was used to monitor the dew point (i.e., relative humidity (RH)) of the challenge atmosphere.

Tests were performed in the laboratory at temperatures of 25–27 °C or in a temperature-controlled 15-m<sup>3</sup> Sherer Environmental Test Chamber. The chamber can operate from 0 to 45 °C and maintain a constant temperature to within  $\pm 0.5$  °C.

Samplers were tested by using challenge atmospheres to evaluate collection efficiency (CE) and/or recovery efficiency (RE). CEs were determined by comparing the sampler inlet and outlet airborne concentrations of the challenge atmosphere as determined by the  $\text{NO}_x$  and  $\text{SO}_2$  monitors. REs were determined by comparing the amount of analyte recovered by extraction and IC analysis of the sample extract with the amount expected based on the gravimetrically or instrumentally determined airborne input.

The TEA solution used in the experiments performed in the current study was prepared by dissolving 25 g of TEA and 4 g of ethylene glycol in 25 mL of acetone and diluting to 100 mL with DI water (18, 21).

Samples were normally extracted in 20 mL of DI water, but sometimes IC eluent was used. When  $\text{SO}_2$  was present in the challenge atmosphere, 2 drops of 30%  $\text{H}_2\text{O}_2$  were added to the extract to ensure oxidation of any  $\text{SO}_3^{2-}$  to  $\text{SO}_4^{2-}$  and to prevent interference of the  $\text{SO}_3^{2-}$  with the  $\text{NO}_3^-$  IC peaks. The addition of  $\text{H}_2\text{O}_2$  was found to have no effect on the  $\text{NO}_2^-$  peak at the neutral to basic conditions of the extract.

All  $\text{NO}_2^-$ ,  $\text{NO}_3^-$ , and  $\text{SO}_4^{2-}$  analyses were performed on a Dionex Model 14 ion chromatograph. Analytical conditions were as follows: 3  $\times$  150 mm anion precolumn; 3  $\times$  500 mm anion separator column; anion fiber suppressor column; 0.005 M  $\text{NaHCO}_3/0.0024$  M  $\text{Na}_2\text{CO}_3$  eluent composition; 138 mL h<sup>-1</sup> flow rate; and 0.1-mL sample size. Standards covering the concentration range of the samples were run daily to prepare linear least-squares calibrations of concentration versus peak height. The nominal detection limit was  $0.1 \mu\text{g mL}^{-1}$ .

**Preliminary Experiments.** *Screening of Solutions for Collecting  $\text{NO}_2$ .* Several candidates for sorbent coatings or filter impregnation solutions were identified in a literature review (2) as having potential for collecting  $\text{NO}_2$ . These solutions include: DI water; tri-*n*-butyl phosphate/water (90/10%); 5 M NaOH;  $\text{K}_2\text{CO}_3$ /luminol (5.0/0.1%); TEA solution (as described previously); 0.2 M  $\text{Na}_2\text{SO}_3$ , 0.2 M NaOH; 0.4 M  $\text{Na}_2\text{SO}_3$ , 0.2 M  $\text{Na}_2\text{SO}_3$ , 0.2 M NaOH, 2% dimethyl sulfone; and 0.2 M  $\text{Na}_2\text{SO}_3$ , 0.2 M NaOH, 6  $\times 10^{-4}$ % Triton X-100. After preparation, these solutions were tested in impingers by bubbling gas streams containing  $\text{NO}_2$  at 0.4, 4.0, 200, and 2300 ppm at 1.2 L min<sup>-1</sup> through 20 mL of each solution for approximately 2 h and measuring the CEs at nominal 15-min intervals.

*Screening of Uncoated and Coated Sorbents and Impregnated Filters.* Both commercially prepared (SKC, Inc.; Eighty-Four, PA) and laboratory-prepared sorbent tubes were tested. The uncoated sorbents in commercially prepared tubes (nominal dimensions 6  $\times$  70 mm) that were tested include the following: Chromosorb 101 (0.105 g), 102 (0.099 g), 105 (0.112 g), 107 (0.112 g), and 108 (0.112 g); XAD 2 (0.13 g) and 7 (0.12 g); alumina (0.15 g); and 5A MS (0.217 g).

Laboratory-prepared tubes were loaded with a nominal 0.25 g of coated sorbent using 50-mm lengths of 6-mm-o.d. glass tubing with glass wool inserted at both ends to secure the sorbent. Several sorbents were coated with TEA solution following the method of Vinjamoori and Ling (21), tubes were loaded, and they were subsequently tested. These sorbents include 5A MS (SKC, Inc.), prewashed silica gel (Supelco, Inc., Bellefonte, PA), 45/60 mesh and 20/40 mesh 13X MS (SKC, Inc.), 20/40 mesh alumina (SKC, Inc.), and Soxhlet extracted (24-h in DI water) 20/40 mesh coconut-based charcoal (SKC, Inc.).

Filters used in the study were 47 mm in diameter. They were tested with Mace TFE Teflon filter holders providing an exposed filter diameter of 43 mm. Each filter was held in a separate holder when tests employing multiple filters were performed. Tested filters include Schleicher and Schuell fast flow no. 2 (cellulose) (S&S FF), Pallflex TX40 H 120 (Teflon-coated glass fiber), and Whatman 41 (cellulose), QM-A (quartz fiber), and GF/B, GF/C, and GF/F (glass fiber). In most cases, the TEA solution described previously was used to impregnate filters for testing, but in a few cases, filters were impregnated with aqueous solutions containing  $\text{K}_2\text{CO}_3$  (25% in 10% glycerin-water), alkaline  $\text{KMnO}_4$  (4% in 2% NaOH),  $\text{NaAsO}_2$  (1% in 1 M NaOH),  $\text{PbO}_2$  (25% in 10% glycerin-water), guaiacol (10% in 1 M NaOH), and TEA plus 2-naphthyl-3,6-disulfonate (1%).

Filters were prepared in batches of five by rinsing 4 times with DI water and a Büchner funnel. After drying under vacuum at 50–60 °C for 1 h, the filters were transferred to a beaker and covered with an aliquot of the appropriate impregnating solution. After a 5-min soak, they were transferred to the Büchner funnel where excess solution was removed by applying suction for 30–45 s. Filters were dried in a vacuum oven for 1 h at 50–60 °C, placed in a sealed, clean, polyethylene bag, and stored prior to use, in a desiccator containing silica gel and activated charcoal.

A second round of screening tests was conducted on selected sampling elements to measure pressure drop versus flow rate, CE versus flow rate at several temperatures, humidities, and analyte concentrations, and stability of collected  $\text{NO}_2$  and  $\text{SO}_2$  in loading and flushing tests. To determine pressure drop for tubes containing TEA-coated charcoal and TEA-impregnated filters, experiments were performed with a Heiss pressure gauge (+2500 to -760 mm,  $\pm 1$  mmHg), Tylan mass flow controllers, and an air supply/mover at dry (<2% RH) air flow rates between 0.5 and 10 L min<sup>-1</sup>. In a similar series of experiments, CEs for various TEA-coated sampling devices were determined at 5, 25, and 40 °C, under both dry and humid (75% RH) conditions at each temperature over the same range of flow rates. Nominal  $\text{NO}_2$  and  $\text{SO}_2$  concentrations were 170 and 130 ppb. Subsequent tests were also performed at flow rates between 0.5 and 6 L min<sup>-1</sup> using air containing 40 and 340 ppb  $\text{NO}_2$  with coated charcoal tubes sampling a dry atmosphere at 5 °C, with impregnated GF/B filters sampling dry atmospheres at 5, 25, and 40 °C, and with impregnated GF/B filters sampling a humid, 25 °C atmosphere. The filter experiments were conducted with two TEA-impregnated filters in series. The charcoal tube experiments, however, employed only one TEA-coated tube in line.

A series of loading and flushing experiments was conducted to investigate the stability of collected  $\text{NO}_2$  on TEA-coated charcoal and GF/B filters by providing exaggerated simulations of highly variable atmospheric conditions. In these experiments, four collectors were used simultaneously to sample a common atmosphere containing 50–100 ppb  $\text{NO}_2$  for 16–18 h at 1 L min<sup>-1</sup>. Subsequently, one sampler was flushed for 20 h with clean air at 40 °C, one at 27 °C, one at 5 °C, and one was not flushed. The samples were then analyzed to determine the stability of the collected  $\text{NO}_2$  and  $\text{SO}_2$ .  $\text{NO}_2$  and  $\text{SO}_2$  analyzers were used to monitor the atmosphere exhausted from the two types of samplers during both sampling and flushing. Three sets of experiments were performed with each sampler type: sampling from a humid

atmosphere and flushing with a dry atmosphere, sampling a dry atmosphere and flushing with a dry atmosphere, and sampling a humid atmosphere and flushing with a humid atmosphere.

**Laboratory Experiments to Refine Method.** Several tests were performed to determine the  $\text{NO}_2$  and  $\text{SO}_2$  capacities of single, TEA-impregnated GF/B filters. A dry atmosphere of  $\text{NO}_2$  at 190 ppb and  $\text{SO}_2$  at 300 ppb was sampled at  $30^\circ\text{C}$  at  $1.2\text{ L min}^{-1}$  until breakthrough was observed. Breakthrough was considered to have occurred when  $\text{NO}_2$  and  $\text{SO}_2$  concentrations monitored with instrumental analyzers in the exhausted atmosphere exceeded 10% of that for the delivered atmosphere. Capacities were computed based on the recovered masses of analytes expressed as loadings of  $\text{NO}_2$  and  $\text{SO}_2$  per area of exposed filter at the time of breakthrough.

Two types of liquid spiking experiments were performed. In the first, 10-mL aliquots of standard solutions containing  $50\ \mu\text{g mL}^{-1}$  of  $\text{NO}_2^-$ ,  $\text{NO}_3^-$ , and  $\text{SO}_4^{2-}$  were spiked with either 0.5 mL of TEA solution or an equivalent volume of DI water. Subsequent IC analyses were performed to determine if the presence of TEA acted as an interferent to alter the apparent ion concentrations. In the second type of spiking experiments, aliquots of standard solutions containing 12.5–200  $\mu\text{g}$  of each ion were added to: DI water in polyethylene bags; DI water in Nalgene bottles; uncoated GF/B filters; and TEA-impregnated GF/B filters. Recoveries were examined by using DI water extracts in bags versus bottles. Spiked filters were extracted by using DI water in bags for the uncoated filters, DI water in bags for a portion of the TEA-impregnated filters and IC eluent in bottles for the remainder of the impregnated filters.

A comprehensive series of experiments was performed to examine the influence of several variables on analyte recovery expressed as RE. Each experiment was conducted with two TEA-impregnated GF/B filters in series in each of four sampling trains to sample simultaneously a common challenge atmosphere containing both  $\text{NO}_2$  and  $\text{SO}_2$  at a nominal sampling flow rate of  $1.2\text{ L min}^{-1}$ . The variables that were examined include species concentration in the sampled atmosphere (5–400 ppb  $\text{NO}_2$  and 5–200 ppb  $\text{SO}_2$ ), species loading (10, 20, 50, and 200  $\mu\text{g}$ ), humidity (<2 and 50% RH), loading temperature (5, 30, and  $40^\circ\text{C}$ ), flushing and flushing temperature (0 and 18 h, and 5, 30, and  $40^\circ\text{C}$ ) at  $1.2\text{ L min}^{-1}$ , and interferences.

Interference tests were performed at  $30^\circ\text{C}$  using atmospheres containing  $\text{NO}$ ,  $\text{NH}_3$ ,  $\text{H}_2\text{S}$ ,  $\text{CH}_3\text{SH}$ ,  $\text{CS}_2$ ,  $\text{O}_3$ , peroxyacetyl nitrate (PAN), and  $\text{HNO}_2$ . The first five potential interferences were tested under dry (<2% RH) and nominal 50% RH conditions. Ozone was tested under 50% RH, PAN under dry and 60% RH, and  $\text{HNO}_2$  under 25% RH conditions. The  $\text{NO}$  was supplied from a certified cylinder of compressed  $\text{NO}$  in  $\text{N}_2/\text{NH}_3$  and the sulfides were supplied from gravimetrically calibrated permeation tubes; and  $\text{O}_3$  was produced by using dry air and a calibrated ultraviolet lamp  $\text{O}_3$  generator and verified by using a Bendix Model 8002 chemiluminescence  $\text{O}_3$  analyzer. PAN synthesized in isooctane (22) was used to prepare air mixtures in Teflon bags ranging in concentration from 100 to 500 ppb as determined by CLM (23) and by gas chromatography with electron capture detection (24). An  $\text{HNO}_2$  generator (25) was used to generate  $\text{HNO}_2$  concentrations ranging from 21 to 78 ppb as measured by CLM. Comparison of CLM responses to the  $\text{HNO}_2$  atmosphere and an atmosphere containing a similar amount of  $\text{NO}_2$  in the presence and absence of  $\text{Na}_2\text{CO}_3$ -impregnated filters along with IC analyses of filter extracts confirmed that the  $\text{HNO}_2$  atmosphere contained mostly  $\text{HNO}_2$  and negligible amounts of  $\text{NO}_2$ ,  $\text{NO}$ , and  $\text{HNO}_3$ .

**Field Studies.** The current method, as described subsequently in the method section of this paper, was incorporated into the TFR multiconstituent sampler as described by Knapp et al. (26) and evaluated in a field study (27). In this study, the samples were drawn through a PTFE Teflon cyclone and then passed at  $16\text{ L min}^{-1}$  through nylon- and Nafion-lined partial denuders, a 2- $\mu\text{m}$  Gelman Zefluor Teflon filter, a 1- $\mu\text{m}$  Gelman Nylasorb nylon filter, and an oxalic acid impregnated Gelman A/E glass fiber filter. At this point, the current method was introduced and a  $1.6\text{ L min}^{-1}$  stream was drawn through two TEA-impregnated Whatman glass fiber GF/B filters to collect  $\text{SO}_2$  and  $\text{NO}_2$ . This  $1.6\text{ L min}^{-1}$  and the remaining  $14.4\text{ L min}^{-1}$  stream then passed through mass flow controllers and were exhausted through a pump. The blank-corrected  $\text{SO}_4^{2-}$  recovered from the nylon filter

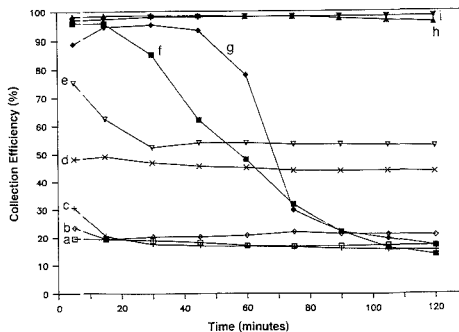


**Figure 1.**  $\text{NO}_2$  collection efficiency as a function of time for selected candidate coating solutions at  $1.2\text{ L min}^{-1}$  and  $0.4\text{ ppm NO}_2$ . Solutions are (a) DI water, (b) tri-*n*-butyl phosphate/water (90/10 wt %), (c) 5 M NaOH, (d)  $\text{K}_2\text{CO}_3$ /luminol (5/0.1 wt %), (e) TEA solution, (f) 0.2 M  $\text{Na}_2\text{SO}_3$ , 0.2 M NaOH, (g) 0.4 M  $\text{Na}_2\text{SO}_3$ , (h) 0.2 M  $\text{Na}_2\text{SO}_3$ , 0.2 M NaOH, 2 wt % dimethyl sulfone, and (i) 0.2 M  $\text{Na}_2\text{SO}_3$ , 0.2 M NaOH,  $6 \times 10^{-4}$  wt % Triton X-100.

was adjusted by the appropriate sample volumes and combined with the sum of blank-corrected  $\text{SO}_4^{2-}$  recovered from the TEA-impregnated filters to compute the TFR  $\text{SO}_2$  concentration. The sum of the blank-corrected  $\text{NO}_2^-$  and  $\text{NO}_3^-$  (expressed as  $\text{NO}_2^-$ ) recovered from the TEA-impregnated GF/B filters was used with the appropriate sample volume to compute the TFR  $\text{NO}_2$  concentration.

Field evaluation of the developed method for  $\text{SO}_2$  and  $\text{NO}_2$  was performed as part of a field comparison of methods for the measurement of selected trace air contaminants at an ambient air quality monitoring research site operated by the United States Environmental Protection Agency at Research Triangle Park, NC (27). Paired replicate daily (22-h) ambient sampling was performed over 13 consecutive days beginning 09/29/86 and ending 10/12/86.  $\text{SO}_2$  determinations obtained by using the current method were obtained for comparison with simultaneous  $\text{SO}_2$  determinations using the Canadian filter pack (FP) (28). The Canadian FP operated at a nominal flow rate of  $19\text{ L min}^{-1}$  and used three filters in series: a  $1\ \mu\text{m}$  pore size Gelman Zefluor Teflon, a  $1\ \mu\text{m}$  pore size Gelman Nylasorb nylon and a Whatman 41 cellulose filter impregnated with an aqueous solution of 10% (v/v) glycerin and 25% (w/v)  $\text{K}_2\text{CO}_3$ . The sum of the  $\text{SO}_4^{2-}$  recovered from the nylon and impregnated cellulose filters was used to compute the FP  $\text{SO}_2$  concentration. TFR  $\text{NO}_2$  measurements were obtained for comparison with composited  $\text{NO}_2$  measurements of a tunable diode laser absorption spectrometer (TDLAS) (29). TDLAS  $\text{NO}_2$  concentrations were determined by monitoring the extent of infrared absorption in the  $1600\text{-cm}^{-1}$  region, and the short-term (3-min) data provided by this instrument were composited to correspond to the daily sampling interval of the TFR.

## RESULTS AND DISCUSSION

**Preliminary Experiments. Screening of Solutions for Collecting  $\text{NO}_2$ .** Several solutions were identified in a literature review (2) as having potential for collecting  $\text{NO}_2$ . These solutions were tested for  $\text{NO}_2$  CE. In addition to DI water, which was chosen as a base-line material,  $\text{NO}_2$  CE results are depicted in Figure 1 for selected candidate coating/impregnating solutions as a function of time for a challenge atmosphere containing  $0.4\text{ ppm NO}_2$ . Analogous tests performed with challenge atmospheres containing 4, 200, and 2300 ppm  $\text{NO}_2$  showed similar behavior (30). The most effective solutions for collecting  $\text{NO}_2$  contained  $\text{Na}_2\text{SO}_3$ . Sulfite ions interfere with  $\text{NO}_3^-$  and  $\text{SO}_4^{2-}$  determinations by IC, and the presence of  $\text{SO}_3^{2-}$  ions prevents the reconciliation of absorbed  $\text{SO}_2$  which may be present in aqueous solution as  $\text{SO}_2 \cdot \text{H}_2\text{O}$ ,  $\text{HSO}_3^-$ , and  $\text{SO}_3^{2-}$  (31). In addition, the useful sampling duration of sulfite-based solutions is limited, since  $\text{SO}_3^{2-}$  is readily oxidized by atmospheric oxygen. These considerations rule

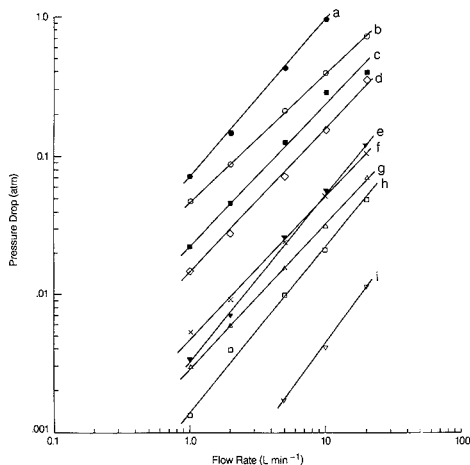


**Figure 2.** Pressure drop as a function of dry air flow rate for various sampling elements: (a) single tube containing TEA-coated 20/40 mesh charcoal; (b) two TEA-impregnated Whatman GF/F glass fiber filters; (c) two TEA-impregnated Whatman GF/B glass fiber filters; (d) two TEA-impregnated Whatman GF/C glass fiber filters; (e) two TEA-impregnated Whatman QM-A quartz fiber filters; (f) two TEA-impregnated Pallflex TX 40H 120 Teflon-coated glass fiber filters; (g) single uncoated 1- $\mu$ m Gelman Nylasorb nylon filter; (h) single uncoated 2- $\mu$ m Gelman Zefluor Teflon filter; and (i) single uncoated S & S FF cellulose filter.

out sulfite solutions for extended atmospheric sampling of  $\text{NO}_2$  and  $\text{SO}_2$ . Of the tested solutions that may be analyzed by IC, the TEA solution exhibited the highest and most stable CE for  $\text{NO}_2$  (i.e., 50 to 60%). This solution has also been reported to be effective for collecting  $\text{SO}_2$  (21); as a result, it was chosen as a coating/impregnating solution for subsequent testing.

**Screening of Uncoated and Coated Sorbents and Impregnated Filters.** A variety of tests was conducted to investigate the potential of several types of materials at collecting  $\text{NO}_2$  and  $\text{SO}_2$  for subsequent recovery. Results of selected experiments are summarized in Table I. These results indicate that, in general, uncoated sorbents are not suitable for sampling both  $\text{NO}_2$  and  $\text{SO}_2$ . They illustrate clearly that the method of Vinjamoori and Ling (21) (i.e., TEA-coated 13X MS) applied at a nominal sampling rate of  $1 \text{ L min}^{-1}$  fails under humid conditions. With TEA-coated 45/60 mesh MS under 70% RH, the sorbent became moist, the flow became restricted to less than  $1 \text{ L min}^{-1}$ , and the  $\text{SO}_2$  RE failed to exceed 50%. Similar low  $\text{SO}_2$  REs were found using the larger 20/40 mesh sorbent. Among the uncoated and coated sorbents that were tested, TEA-coated charcoal exhibited  $\text{SO}_2$  and  $\text{NO}_2$  CEs in excess of 90% and high  $\text{NO}_2$  REs under both dry and humid test conditions. Although TEA-coated charcoal displayed variable  $\text{SO}_2$  REs (i.e., 20–70%), it appeared to be the most promising of the sorbents at the conditions tested and was subjected to a second round of screening tests.

The results in Table I for coated filters indicate that several coating materials provide effective collection of  $\text{SO}_2$  and that  $\text{NO}_2$  is difficult to collect. Since the thicker QM-A filter retains more coating solution than the S & S FF and also displays increased  $\text{NO}_2$  CEs, several filters of various thicknesses manufactured from different materials were selected for a second round of screening tests.

The second round of screening tests involved TEA-coated charcoal and several TEA-impregnated filters. Since resistance to flow is an important consideration in the design of a sampling system, pressure drop versus flow rate results were

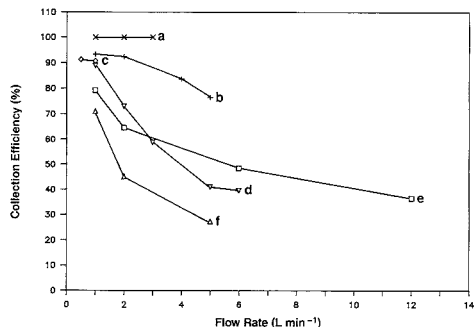


**Figure 3.**  $\text{NO}_2$  collection efficiency as a function of flow rate for various TEA-coated/impregnated sampling elements at an inlet  $\text{NO}_2$  concentration of 170 ppb and at 25 °C and 75% RH: (a) single tube containing 20/40 mesh charcoal; (b) two GF/B filters; (c) two GF/F filters; (d) two Pallflex TX 40H 120 filters; (e) two QM-A filters; and (f) two GF/C filters.

measured on both uncoated and coated sampling elements. Results for the selected coated elements, displayed in Figure 2, are higher than their uncoated counterparts. In addition, test results for single uncoated 1  $\mu$ m pore Gelman Nylasorb nylon, 2  $\mu$ m Gelman Zefluor Teflon, and S & S FF cellulose filters, commonly used filters in ambient air sampling, are included for comparison.

Collection efficiencies were measured at several temperatures, humidities, and analyte concentrations. Representative results are displayed in Figure 3 for one selected set of test conditions. At 170 ppb, the TEA-coated charcoal tubes and GF/B filters exhibited among the highest CEs for  $\text{NO}_2$ . CEs for the coated charcoal tubes at flow rates of  $2.5 \text{ L min}^{-1}$  and less were consistently greater than or equal to 92%. With the exception of the 5 °C tests, the CEs of TEA-impregnated GF/B filters at flow rates up to  $1.5 \text{ L min}^{-1}$  exceeded 90%. In the 5 °C tests, the  $\text{NO}_2$  CEs ranged from 78 to 90% at  $1.5 \text{ L min}^{-1}$ . The reduced  $\text{NO}_2$  CE of TEA with reduced temperature is consistent with observations of others (32) and with the 21 °C liquid–solid transition temperature for TEA. The  $\text{SO}_2$  CE for all of the tests exceeded 95%. In tests conducted at  $\text{NO}_2$  concentrations between 40 and 340 ppb, CEs were independent of  $\text{NO}_2$  concentrations across the flow rates tested.

In the loading and flushing tests with TEA-coated charcoal, the  $\text{NO}_2^-$  RE decreased with increasing flush temperatures—on the average, only 37% of the loaded  $\text{NO}_2^-$  could be accounted for after flushing with clean air at 40 °C. As the flush temperature increased, up to half of the collected  $\text{NO}_2$  was converted to nitrate ( $\text{NO}_3^-$ ) and an increasing portion of the collected  $\text{NO}_2$  was lost. The  $\text{SO}_2$  RE as  $\text{SO}_4^{2-}$  was generally less than 60%. Continuous monitoring of the exhausted atmosphere showed no  $\text{SO}_2$  breakthrough and increased liberation of NO and  $\text{NO}_2$  with flush temperature.

In the tests with TEA-impregnated GF/B filters, the  $\text{NO}_2^-$  RE exceeded 90% and was essentially independent of flush temperature. Less than 15% of the collected  $\text{NO}_2$  was converted to  $\text{NO}_3^-$ , and this portion was not associated with loading humidity or with flush temperature or humidity. The  $\text{SO}_4^{2-}$  RE generally exceeded 75%. Continuous monitoring of the exhausted atmospheres showed no  $\text{SO}_2$  breakthrough and negligible liberation of NO and  $\text{NO}_2$  under all test conditions.

**Laboratory Tests to Refine Method.** *General.* The previous experiments indicate that TEA-impregnated GF/B filters are preferred to TEA-coated charcoal and many other collection elements for ambient sampling. As a result, sub-

Table I. Results of Screening Tests of Uncoated and Coated Sorbents and Impregnated Filters

	coating/impregnating solution <sup>a</sup>	sampling		challenge atmosphere <sup>b</sup>		collection efficiency, %		recovery efficiency, %		comments	
		flow rate, L min <sup>-1</sup>	duration, h	humidity, %	[SO <sub>2</sub> ], ppb	[NO <sub>2</sub> ], ppb	SO <sub>2</sub>	NO <sub>2</sub>	SO <sub>2</sub>		NO <sub>2</sub>
Chromosorb 101	none	0.75	0.5	<2	Sorbent	140	<10	>90	ND <sup>d</sup>	ND <sup>d</sup>	floating, difficult to extract
Chromosorb 102	none	0.75	0.5	<2	100	140	<10	>90	ND <sup>d</sup>	ND <sup>d</sup>	floating, difficult to extract
Chromosorb 105	none	ND <sup>d</sup>	0.5	<2	100	140	ND <sup>d</sup>	ND <sup>d</sup>	ND <sup>d</sup>	ND <sup>d</sup>	fine particle size restricted flow
Chromosorb 107	none	0.75	0.5	<2	100	140	<10	<50	ND	ND	
Chromosorb 108	none	0.75	0.5	<2	100	140	<10	<50	ND	ND	
XAD2	none	0.75	0.5	<2	100	140	<10	<70	ND	ND	
XAD7	none	0.75	0.5	<2	100	140	<10	<70	ND	ND	
alumina	none	0.75	0.5	<2	100	140	>90	<50	ND <sup>d</sup>	ND <sup>d</sup>	high background NO <sub>3</sub> <sup>-</sup> and SO <sub>4</sub> <sup>2-</sup> levels
5A MS	TEA	0.75	0.5	<2	100	140	>90	<10	90	>90	
5A MS	TEA	0.4	15	<2	100	140	>90	>90	>90	>90	
silica gel	TEA	0.3	15	<2	100	140	>90	>90	ND	ND	n = 6
13X MS(45/60 mesh)	TEA	0.9	18	<2	40	55	ND	ND	>90	>90	n = 3
13X MS(20/40 mesh)	TEA	1.0	4	<2	40	55	ND	ND	>90	>90	flow restricted
13X MS(45/60 mesh)	TEA	ND <sup>d</sup>	2	60	40	55	>90	>90	<50	ND	visibly wet in 1 h
13X MS(20/40 mesh)	TEA	1.0	2	70	80	110	>90	ND	<50	ND	
alumina (20/40 mesh)	TEA	2.0	1	70	80	110	>90	>90	<20	ND	n = 3, SO <sub>2</sub> RE variable
alumina (20/40 mesh)	TEA	2.0	1	70	100	100	>90	>90	<70 <sup>d</sup>	>90	n = 3, SO <sub>2</sub> RE variable
charcoal (20/40 mesh)	TEA	2.0	1	<2	100	100	>90	>90	<70 <sup>d</sup>	>90	n = 3, SO <sub>2</sub> RE variable
					Filter <sup>e</sup>						
S & S FF	TEA	0.75	0.5	<2	100	140	>90	<10	ND	ND	
S & S FF	K <sub>2</sub> CO <sub>3</sub>	0.75	0.5	<2	100	140	>90	<10	ND	ND	
Whatman 41	K <sub>2</sub> CO <sub>3</sub>	0.75	0.5	<2	100	140	>90	<10	ND	ND	
S & S FF	PbO <sub>2</sub>	0.75	0.5	<2	100	140	>90	<10	ND	ND	
QM-A	KMnO <sub>4</sub>	4.0	1.0	<2	100	100	>90	<20	ND	ND	n = 2
QM-A	KMnO <sub>4</sub>	5.0	1.0	70	100	100	>90	<20	ND	ND	
S & S FF	NaAsO <sub>2</sub>	4.0	1.0	<2	80	110	<80	<20	ND	ND	
S & S FF	NaAsO <sub>2</sub>	5.0	1.0	70	80	110	>90	<20	ND	ND	
S & S FF	NiAsO <sub>2</sub>	4.0	1.0	<2	100	100	>90	<20	ND	ND	
S & S FF	K <sub>2</sub> CO <sub>3</sub>	4.0	1.0	70	100	100	>90	<20	ND	ND	
S & S FF	guaiacol	5.0	1.0	70	80	110	>90	<20	ND	ND	
S & S FF	TEA + NDS/	5.0	1.0	70	80	110	>90	<20	ND	ND	
S & S FF	TEA	4.0	1.0	70	100	100	>90	<20	>90	ND	n = 4
S & S FF	K <sub>2</sub> CO <sub>3</sub>	1.0	3.5 <sup>d</sup>	<2	90	70	>90	<10	ND	ND	breakthrough for SO <sub>2</sub> observed at 3.5 h
S & S FF	TEA	1.0	18 <sup>d</sup>	<2	90	70	>90	<30	ND	ND	breakthrough for SO <sub>2</sub> observed at 18 h
S & S FF	K <sub>2</sub> CO <sub>3</sub>	1.0	45 <sup>d</sup>	30	90	70	>90	<10	ND	ND	breakthrough for SO <sub>2</sub> not observed after 45 h
S & S FF	TEA	1.0	45 <sup>d</sup>	30	90	70	>90	<30	ND	ND	breakthrough for SO <sub>2</sub> not observed after 45 h
QM-A	TEA	1.0	13 <sup>d</sup>	30	90	70	>90	70	ND	ND	breakthrough for SO <sub>2</sub> not observed after 13 h
QM-A <sup>d</sup>	TEA	1.0	57 <sup>d</sup>	30	90	70	>90	>90	ND	ND	two-impregnated filters used; test terminated prior to breakthrough

<sup>a</sup>See Experimental Section for solution formulation. <sup>b</sup>Nominal temperature 25 °C. <sup>c</sup>ND = not determined. <sup>d</sup>See comment. <sup>e</sup>Single filter used in each test unless specified otherwise. <sup>f</sup>TEA solution + 2-naphthyl-3,6-disulfonate (1%).



**Table II. Summary of Results from NO<sub>2</sub> and SO<sub>2</sub> Recovery Efficiency (RE) Experiments Using Dual TEA-Impregnated GF/B Filters**

SO <sub>2</sub> and NO <sub>2</sub>		loading		flush		interferent		mean RE (SD, n = 4)			
concn <sup>a</sup>	loading, <sup>b</sup> μg	duration, h	temp, °C	duration	h	temp, °C	humidity <sup>c</sup>	species	loading, μg	NO <sub>2</sub> , %	SO <sub>2</sub> , %
H	20	0.33	30	0	—	—	D	—	—	75.0 (1.9)	89.1 (1.5)
H	50	1.0	30	0	—	—	D	—	—	81.8 (3.1)	87.9 (6.3)
H	50	1.0	30	0	—	—	D	—	—	80.3 (0.5)	—
H	50	1.0	30	0	—	—	D	—	—	—	89.8 (2.1)
L	10	0.83	30	0	—	—	D	—	—	86.3 (12.4)	104.8 (4.1)
H	10	0.18	30	0	—	—	H	—	—	73.7 (4.6)	79.3 (3.3)
L	20	0.34	30	0	—	—	H	—	—	74.2 (3.0)	72.9 (1.5)
L	10	6.2	30	0	—	—	D	—	—	64.6 (1.3)	77.0 (0.5)
H <sup>d</sup>	10	0.17	30	17.8	30	30	D	—	—	69.4 (5.3)	86.7 (3.8)
H <sup>d</sup>	200	3.4	30	17.8	30	30	D	—	—	79.4 (1.2)	92.1 (1.4)
H	50	0.85	30	0	—	—	H	—	—	88.3 (2.8)	83.3 (1.7)
L	20	2.4	30	0	—	—	D	—	—	79.9 (1.6)	97.1 (4.8)
H	10	0.17	30	0	—	—	D	—	—	90.1 (3.7)	81.1 (4.2)
H	200	3.4	30	0	—	—	D	—	—	91.2 (3.9)	91.9 (4.2)
H	10	0.17	30	0	—	—	H	—	—	85.1 (1.4)	74.9 (2.4)
H	200	3.4	30	0	—	—	H	—	—	90.9 (0.8)	81.5 (1.5)
L	10	1.2	30	0	—	—	D	—	—	104.4 (11.1)	83.6 (4.8)
L	50	5.7	30	0	—	—	D	—	—	86.6 (5.0)	80.3 (1.3)
L	200	23.0	30	0	—	—	D	—	—	82.4 (5.8)	82.8 (9.0)
L	200	23.0	30	0	—	—	H	—	—	97.6 (2.0)	77.8 (5.2)
L	10	1.2	30	0	—	—	H	—	—	92.6 (2.7)	83.7 (7.9)
H <sup>d</sup>	50	0.87	40	0	—	—	D	—	—	93.5 (2.6)	94.6 (3.5)
H	50	0.87	30	0	—	—	D	—	—	101.7 (2.8)	87.3 (7.8)
H <sup>d</sup>	50	0.87	5	0	—	—	D	—	—	81.6 (1.9)	87.8 (1.1)
H <sup>d</sup>	50	0.87	30	19.8	40	40	D	—	—	92.7 (1.8)	94.5 (2.2)
H <sup>d</sup>	50	0.87	30	17.3	30	30	D	—	—	91.2 (1.5)	94.4 (3.9)
H <sup>d</sup>	50	0.88	30	17.0	5	5	D	—	—	88.6 (5.2)	91.8 (3.0)
H	50	0.87	30	0	—	—	D	NO	50	92.4 (3.9)	88.9 (5.6)
H	50	0.88	30	0	—	—	H	NO	50	97.6 (2.0)	81.3 (2.1)
H	50	0.88	30	0	—	—	D	NO	50	—	85.7 (1.4)
VL <sup>d</sup>	50/90	48.8	30	0	—	—	H	—	—	91.4 (1.2)	86.0 (2.8)
VL <sup>d</sup>	50/150	90.8	30	0	—	—	D	—	—	88.8 (2.1)	89.5 (4.3)
H	50	0.9	30	0	—	—	D	—	—	84.5 (1.4)	85.9 (2.7)
H	50	0.9	30	0	—	—	H	—	—	90.9 (2.4)	79.8 (3.1)
H <sup>d</sup>	50	0.87	30	0	—	—	D	—	—	94.0 (-)	90.0 (-)
H <sup>d</sup>	50	0.87	30	0	—	—	D	NH <sub>3</sub> /S <sup>e</sup>	50	89.0 (-)	101.0 (-)
- <sup>d</sup>	0	0	30	0	—	—	D	NH <sub>3</sub> /S	50	0.0 (-)	0.0 (-)
H <sup>d</sup>	50	1.0	30	0	—	—	H	O <sub>3</sub>	50	86.3 (3.3)	—
H <sup>d</sup>	50	1.0	30	0	—	—	H	NH <sub>3</sub> /S	50	94.5 (1.0)	93.0 (1.8)
- <sup>d</sup>	0	0	30	0	—	—	H	NH <sub>3</sub> /S	50	0.0 (-)	0.0 (-)

<sup>a</sup> H = high concentration, nominal values 400 ppb NO<sub>2</sub> and 200 ppb SO<sub>2</sub>; L = low concentrations, nominal values 60 ppb NO<sub>2</sub> and 30 ppb SO<sub>2</sub>; and VL = very low concentrations, nominal values 5 ppb NO<sub>2</sub> and SO<sub>2</sub>. <sup>b</sup> Nominal loadings of NO<sub>2</sub> as nitrite and SO<sub>2</sub> as sulfate. <sup>c</sup> D = dry (<2% RH); H = humid (50% RH). <sup>d</sup> Experiments not considered in ANOVA. <sup>e</sup> NH<sub>3</sub>, CH<sub>3</sub>SH, CS<sub>2</sub>, and H<sub>2</sub>S, each loaded to approximately 50 μg.

sequent laboratory tests were limited to TEA-impregnated Whatman GF/B filters. These filters were thick (0.73 mm), exhibited a pressure drop of 0.01 atm at 1 L min<sup>-1</sup>, and retained approximately 0.43 g of impregnating material. This residual impregnating material was comprised primarily of TEA and ethylene glycol, since much of the acetone and water originally present in the impregnating solution was lost during the vacuum drying stage of filter preparation. Single-filter capacities of approximately 85 μg of NO<sub>2</sub> cm<sup>-2</sup> and 350 μg of SO<sub>2</sub> cm<sup>-2</sup> were observed.

At low loadings, the level and variability of sulfur and nitrogen on the blanks may influence the apparent airborne concentrations appreciably. Impregnated and uncoated blank GF/B filters were washed with DI water or washed with aqueous KOH solution and extracted in DI water or IC buffer solution. Washing with DI water reduced blank SO<sub>4</sub><sup>2-</sup> levels from 2 to approximately 1 μg filter<sup>-1</sup> but had no appreciable effect on blank NO<sub>2</sub><sup>-</sup> or NO<sub>3</sub><sup>-</sup> levels. The additional effects of KOH washing, TEA coating, and extract solution on blank levels could not be distinguished. It should be noted that KOH washing resulted in disintegration of the filters and, as a result, is not recommended. The mean (± standard deviation) background levels for NO<sub>2</sub><sup>-</sup>, NO<sub>3</sub><sup>-</sup>, and SO<sub>4</sub><sup>2-</sup> on 22 DI water-washed, TEA-impregnated GF/B filters are 0.87 ± 0.43,

0.66 ± 0.24, and 1.13 ± 0.32 μg.

**Spiking Experiments.** The first type of spiking experiments involved spiking standard solutions with TEA. In these tests, the presence of TEA did not influence the apparent species concentrations. In the second type of spiking experiments, standard solutions were spiked into various samples. Recoveries from spiked DI water in bags and bottles were greater than 95%, with those in bottles slightly exceeding those in bags. The differences in recoveries found between spiked, impregnated and uncoated filters using various containers and extract solutions were not significant ( $\alpha = 0.05$ ). For all spiked filters ( $n = 15$ ), the mean (± standard deviation) NO<sub>2</sub><sup>-</sup>, NO<sub>3</sub><sup>-</sup>, and SO<sub>4</sub><sup>2-</sup> recoveries were 88 ± 5, 94 ± 4, and 87 ± 5%. This indicates that 5 to 10% of loaded NO<sub>2</sub><sup>-</sup>, NO<sub>3</sub><sup>-</sup>, and SO<sub>4</sub><sup>2-</sup> may be retained by impregnated or uncoated GF/B filters.

**Analyte Recovery.** Experiments were conducted to examine the influence of several variables on analyte recovery. The variables that were examined are species concentration in the sampled atmosphere, species loading, humidity, loading temperature, flushing, and flushing temperature. Results from many of these analyte recovery tests performed under widely differing conditions are summarized in Table II. Each experiment was conducted with two TEA-impregnated GF/B filters in series in each of four trains to sample a common

challenge atmosphere simultaneously.

On the average, REs were  $87 \pm 9\%$  ( $n = 33$ ) for  $\text{NO}_2$  and  $86 \pm 7\%$  ( $n = 34$ ) for  $\text{SO}_2$ . The precision within any experiment was good, showing average standard deviations of 3% for both  $\text{NO}_2$  and  $\text{SO}_2$ . Examination of the distribution of collected nitrogen showed that most of the nitrogen was retained as nitrite; the average nitrate was only 2%. Most (96%) of the recovered nitrogen was found on the first filter. Sulfur dioxide was recovered as  $\text{SO}_4^{2-}$ , and most (99%) of the recovered sulfate was found on the front filter.

The results from the  $\text{NO}_2$  and  $\text{SO}_2$  recovery experiments were subjected to statistical analyses using an ANOVA on the reported mean REs adjusted for the unbalanced experimental design. Results from 25 of the experiments summarized in Table II were examined for effects from concentration, loading, and temperature. No significant differences ( $\alpha = 0.10$ ) were found between REs obtained at high species concentrations and those at low species concentrations. Although there was a significantly ( $\alpha = 0.10$ ) lower  $\text{NO}_2$  RE at a species loading of  $20 \mu\text{g}$  (RE = 76%), it is based on three experiments conducted early in the program compared to five or more experiments at the three other levels. The small sample size at  $20 \mu\text{g}$  can argue for considering only the 10-, 50-, and  $200\text{-}\mu\text{g}$  experiments. When results at these three loadings are considered, no significant differences ( $\alpha = 0.10$ ) were apparent among species REs obtained. Examination of the data for humidity effects revealed no significant differences ( $\alpha = 0.10$ ) between  $\text{NO}_2$  REs obtained at high and low levels. In contrast, there was a significant difference ( $\alpha = 0.05$ ) in  $\text{SO}_2$  RE associated with humidity. The mean  $\text{SO}_2$  RE under humid conditions was  $81 \pm 5\%$  ( $n = 11$ ), while under dry conditions, it was  $89 \pm 6\%$  ( $n = 23$ ). These findings may be compared with those for TEA-coated 13X MS, where 10% reductions in REs for both  $\text{NO}_2$  and  $\text{SO}_2$  were reported at 90% RH (21).

The results in Table II indicate that variation in species concentrations in the sampled atmosphere ranging from 5 to 400 ppb did not lead to different REs. REs were relatively constant across species loadings ranging from 10 to  $200 \mu\text{g}$ .  $\text{NO}_2$  REs were not appreciably different at 0 and 50% RH;  $\text{SO}_2$  REs were reduced at 50% RH in comparison to those observed under dry conditions. Loading temperature ranging from 5 to  $40^\circ\text{C}$  did not exert an appreciable effect on species RE except for  $\text{NO}_2$  at  $5^\circ\text{C}$ ; in this case, a small reduction in  $\text{NO}_2$  RE was indicated and the distribution of  $\text{NO}_2^-$  was shifted to the second filter. These observations are consistent with findings of some of the screening tests discussed previously. After loading at  $30^\circ\text{C}$ , flushing with clean dry air at temperatures from 5 to  $40^\circ\text{C}$  had no apparent effect on the species REs.

**Interference Tests.** The potential interference of eight common atmospheric trace gases on the determination of  $\text{NO}_2$  and  $\text{SO}_2$  using TEA-impregnated filters was studied. Test results for the first six potential interferents are summarized in Table II. Results for the remaining two, PAN and  $\text{HNO}_3$ , are discussed in subsequent paragraphs. Nitric oxide,  $\text{NH}_3$ , and the three tested sulfides showed negligible interference with  $\text{NO}_2$  or  $\text{SO}_2$  measurements. Ozone did not interfere with  $\text{NO}_2$  determinations at 50% RH. An instrumental malfunction prevented an assessment of  $\text{O}_3$  as an interferent for  $\text{SO}_2$  in the Table II experiments. Earlier experiments using a dry atmosphere of 10 ppb  $\text{NO}_2$ , 14 ppb  $\text{SO}_2$ , and 130 ppb  $\text{O}_3$  showed a mean  $\text{SO}_2$  RE ( $n = 4$ ) of 96.7% obtained by using TEA-coated S & S FF cellulose filters. These results suggest that  $\text{O}_3$  may not interfere with  $\text{SO}_2$  measurements obtained by using TEA-impregnated glass fiber filters.

At PAN concentrations of 500 ppb, TEA-impregnated filters showed recoveries of 15–25% of the delivered PAN as  $\text{NO}_2^-$  and 55–70% as  $\text{NO}_3^-$ . Thus, PAN should be considered

a major interferent with the determination of ambient  $\text{NO}_2$  using TEA-impregnated filters.

To test for  $\text{HNO}_2$  interference, atmospheres containing 21–78 fppb  $\text{HNO}_2$  and 170 ppb  $\text{NO}_2$  were employed. TEA-impregnated Whatman GF/B glass fiber filters, Gelman Nylasorb nylon filters,  $\text{Na}_2\text{CO}_3$  (25% in 10% glycerine-water)-impregnated Whatman 41 cellulose filters, oxalic acid (5% in methanol)-impregnated Whatman 41 filters, and Gelman Zefluor Teflon filters were tested separately. The gas mixture upstream and downstream of each filter was analyzed by using a chemiluminescent  $\text{NO}_x$  monitor, permitting estimates of CE by each filter type. Teflon and oxalic acid impregnated filters failed to collect either  $\text{HNO}_2$  or  $\text{NO}_2$ . The nylon filter appeared to retain  $\text{HNO}_2$  up to a point and saturate at approximately  $20 \mu\text{g}$ . This is consistent with reported findings: using nylon wool (33). No  $\text{NO}_2$  collection was noted with the nylon filter. On the basis of the chemiluminescent response, both the TEA-impregnated filters and the  $\text{Na}_2\text{CO}_3$ -impregnated filters collected all of the delivered  $\text{HNO}_2$ . The TEA-coated filter collected all the delivered  $\text{NO}_2$ , while the  $\text{Na}_2\text{CO}_3$ -impregnated filter collected only 4% of the  $\text{NO}_2$ . Since the collected  $\text{HNO}_2$  was recovered as  $\text{NO}_2^-$  by extraction and IC analysis of the TEA-coated filters,  $\text{HNO}_2$  acted as a direct interferent in the measurement of  $\text{NO}_2$  using TEA-coated filters.

**Method.** On the basis of previous findings, the recommended method employs two 47 mm diameter, TEA-impregnated Whatman GF/B glass fiber filters in series. The composition of the TEA-impregnating solution and the impregnating procedure were described previously. Other sizes and types of filters may also be suitable. Flow rates in excess of  $2 \text{ L} \cdot \text{min}^{-1}$  and temperatures at or below  $5^\circ\text{C}$  should be avoided. No known gaseous interferents exist for  $\text{SO}_2$ , although  $\text{O}_3$ , PAN, and  $\text{HNO}_2$  were not evaluated. Unless removed first, sulfate particles will act as direct interferents with this method. Both PAN and  $\text{HNO}_2$  will interfere with the determination of  $\text{NO}_2$ , and unless removed first, gaseous  $\text{HNO}_3$  as well as particulate nitrates will act as direct interferents. The maximum tolerable RH has not been sought; however, if operation at high humidities results in excessive accumulation of moisture, the temperature of the sampler could be elevated slightly to prevent the occurrence of 100% RH conditions within the sampler.

After sampling, the filters are extracted in 20 mL of DI water (or IC eluent solution), 2 drops of 30%  $\text{H}_2\text{O}_2$  are added to oxidize  $\text{SO}_3^{2-}$  to  $\text{SO}_4^{2-}$ , and the extract is analyzed for  $\text{NO}_2^-$ ,  $\text{NO}_3^-$ , and  $\text{SO}_4^{2-}$  using IC or another suitable method. By use of the extract volume, the ion loadings are determined. The  $\text{NO}_2^-$  and  $\text{NO}_3^-$  loadings are blank corrected and summed as  $\text{NO}_2^-$ . The blank-corrected  $\text{SO}_4^{2-}$  and  $\text{NO}_2^-$  loadings are then used with the sampled air volume to express the integrated sample air concentration in units of micrograms per cubic meter or parts per billion.

**Field Tests.** After development, the method was incorporated into a multiconstituent sampler for contributors to acidic deposition, known as the transition flow reactor (TFR). Results obtained by using the current method and assuming quantitative recoveries are compared in Figures 4 and 5 with simultaneous  $\text{SO}_2$  measurements using the Canadian FP and with composited  $\text{NO}_x$  measurements using a TDLAS. The median relative standard deviations (RSDs) for  $\text{SO}_2$  and  $\text{NO}_2$  in this study of 13 paired samples are 13 and 3%. Corresponding median RSDs in an earlier study (26) involving seven paired samples were 4% for both  $\text{SO}_2$  and  $\text{NO}_2$ .

Comparison of  $\text{SO}_2$  results obtained by using the current method with those of the FP are displayed in Figure 4 and show good agreement with a correlation coefficient of 0.99. The studywide mean ( $\pm 1$  standard deviation (SD))  $\text{SO}_2$  con-

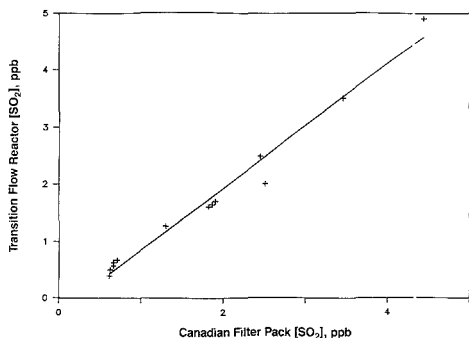


**Figure 4.** Comparison of ambient daily  $\text{SO}_2$  concentrations as determined by the transition flow reactor employing the currently developed method and by the Canadian filter pack. Linear regression analysis results ( $n = 13$ ):  $r = 0.99$ ; slope ( $\pm 95\%$  confidence intervals) =  $1.09 \pm 0.11$ ; and intercept ( $\pm 95\%$  confidence intervals) =  $-0.25 \pm 0.23$  ppb.

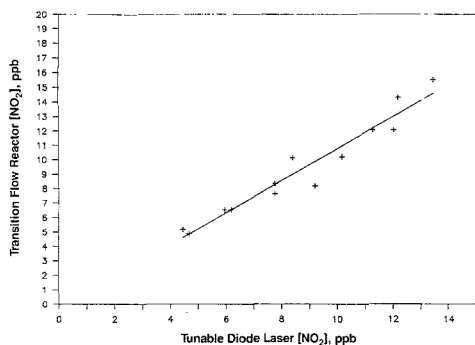


**Figure 5.** Comparison of ambient daily  $\text{NO}_2$  concentrations as determined by the transition flow reactor employing the currently developed method and by a tunable diode laser absorption spectrometer. Linear regression analysis results ( $n = 13$ ):  $r = 0.97$ ; slope ( $\pm 95\%$  confidence intervals) =  $1.11 \pm 0.19$ ; and intercept ( $\pm 95\%$  confidence intervals) =  $-0.33 \pm 1.74$  ppb.

centrations of  $1.68 \pm 1.33$  and  $1.77 \pm 1.21$  ppb as measured using the current and FP methods are in good agreement. The mean ( $\pm$ SD) daily ratio of TFR to FP  $\text{SO}_2$  concentrations is  $0.90 \pm 0.12$ , the difference between the two measures of  $\text{SO}_2$  concentration based on the paired Student's  $t$  test is not significant ( $\alpha = 0.05$ ). Linear regression analysis suggests a low constant bias for the current method. This low bias, if real, may be the result of less than quantitative  $\text{SO}_4^{2-}$  recovery from the TEA-impregnated filters or it may be associated with humidity. The average hourly RH for the study period was 73%, and the maximum hourly average RH exceeded 93% on 7 of the 13 days of the study. Excessive accumulation of moisture was not observed with the current method during this study. If humidity does exert an influence on  $\text{SO}_2$  recovery, even at the high RH present in this field study, the influence does not appear to be large. Recent laboratory tests (34) suggest that a portion of the  $\text{SO}_2$  retained by some nylon filters is unrecoverable. Since the sample passes through a nylon filter in both the FP and TFR, an absolute low bias may be present in the  $\text{SO}_2$  results but is not expected to influence the relative comparison of the two methods.

Comparison of  $\text{NO}_2$  results obtained by using the current method with those of the TDLAS are displayed in Figure 5 and show good agreement with a correlation coefficient of 0.97.

The studywide mean ( $\pm$ SD)  $\text{NO}_2$  concentrations of  $9.34 \pm 3.38$  and  $8.73 \pm 2.95$  ppb as measured using the current method and the TDLAS are in good agreement. The mean ( $\pm$ SD) daily ratio of TFR to TDLAS  $\text{NO}_2$  concentrations is  $1.07 \pm 0.09$ . Linear regression analysis does not reveal either a proportional or constant bias ( $\alpha = 0.05$ ). TFR results generally exceed those of the TDLAS, and the difference between the two measures of  $\text{NO}_2$  based on the paired Student's  $t$  test is significant ( $\alpha = 0.05$ ). Although the small difference (i.e., 7%) is within the  $\pm 15\%$  uncertainty of the TDLAS measurements and may not be of practical importance, it may have resulted from nitrogen-containing interferent gases (e.g., PAN or  $\text{HNO}_3$ ) which were not removed upstream of the TEA-impregnated filters.

The mean ( $\pm$ SD) background levels for  $\text{NO}_2^-$  ( $n = 8$ ),  $\text{NO}_3^-$  ( $n = 10$ ), and  $\text{SO}_4^{2-}$  ( $n = 8$ ) for TEA-coated GF/B filters used as field blanks in the previously mentioned field study (30) are  $1.19 \pm 0.30$ ,  $0.54 \pm 0.55$ , and  $1.51 \pm 0.79$   $\mu\text{g}$ . It should be noted that these field blank results are somewhat higher than previously noted laboratory blank results. Single-filter blank-corrected loadings of 3 times the SD for blank  $\text{NO}_2^-$  and  $\text{SO}_4^{2-}$  levels,  $0.90$   $\mu\text{g}$  of  $\text{NO}_2^-$  and  $2.37$   $\mu\text{g}$  of  $\text{SO}_4^{2-}$ , may be used to estimate the minimum detection limits (MDLs) for the current method (35). At a flow rate of  $1.6$   $\text{L min}^{-1}$  ( $0^\circ\text{C}$ ,  $760$  mmHg) MDLs may be computed for any sampling duration. For 24-h samples, MDLs for  $\text{SO}_2$  and  $\text{NO}_2$  are  $0.3$  and  $0.2$  ppb, and for 7-day samples they are  $0.04$  and  $0.03$  ppb.

## SUMMARY

A method has been developed to permit the simultaneous time-integrated sampling of  $\text{SO}_2$  and  $\text{NO}_2$  from ambient air. Triethanolamine-impregnated glass fiber filters are used to collect  $\text{SO}_2$  and  $\text{NO}_2$ . After sampling, the filters are extracted, and the extract is analyzed for sulfate, nitrite, and nitrate using ion chromatography. Ambient concentrations are computed from recovered nitrogen and sulfur and the sampled air volume.

To arrive at this method, preliminary experiments were performed to determine the suitability of selected sorbents, filters, and coating/impregnating solutions for collecting  $\text{SO}_2$  and  $\text{NO}_2$ . Candidate coating/impregnating solutions identified from the literature were tested in bubblers, and an aqueous solution of 25% (w/v) triethanolamine and 4% (w/v) ethylene glycol was chosen for subsequent testing. The uncoated sorbents that were tested proved unsuitable for sampling both  $\text{NO}_2$  and  $\text{SO}_2$ . Among the coated sorbents and filters that were tested, TEA-coated charcoal and TEA-impregnated filters appeared to be promising candidates and were subjected to a second round of screening tests. TEA-coated molecular sieves were eliminated because water accumulation from sampled humid atmospheres did not permit sampling at the minimum desired rate of  $1$   $\text{L min}^{-1}$ .

The second round of screening tests revealed that the thick GF/B glass fiber filters retained substantial amounts of the impregnating solution and exhibited the highest analyte CEs among the filters tested, generally exceeding 90% for  $\text{NO}_2$  at flow rates up to  $1.5$   $\text{L min}^{-1}$ . TEA-coated charcoal showed even better performance with  $\text{NO}_2$  CEs exceeding 92% at flow rates up to  $2.5$   $\text{L min}^{-1}$ . In subsequent tests where clean air was flushed through TEA-coated charcoal and TEA-impregnated filters that had been previously loaded with  $\text{NO}_2$ , REs obtained by using TEA-coated charcoal decreased to below 40% as the flush temperature was increased to  $40^\circ\text{C}$ , whereas REs obtained by using TEA-impregnated filters exceeded 90% and were independent of flush temperature.

As a result, a method incorporating TEA-impregnated GF/B glass fiber filters was chosen for refinement. Single filter capacities of  $85$   $\mu\text{g}$  of  $\text{NO}_2$  and  $350$   $\mu\text{g}$  of  $\text{SO}_2$   $\text{cm}^{-2}$  were measured. Laboratory tests showed average REs near 90%

for both NO<sub>2</sub> and SO<sub>2</sub>. In addition, laboratory tests suggested that REs are independent of NO<sub>2</sub> and SO<sub>2</sub> concentrations at high (i.e., 100's of ppb) and low (i.e., 10's of ppb) levels, that REs are independent of NO<sub>2</sub> and SO<sub>2</sub> loading at levels between 10 and 200 µg, that NO<sub>2</sub> RE is independent of humidity at <2 and 50% RH, but that SO<sub>2</sub> RE is reduced from approximately 90% under dry conditions to approximately 80% at 50% RH. Subsequent tests at loading temperatures of 5, 30, and 40 °C indicated a reduction in NO<sub>2</sub> RE at the 5 °C condition. Tests at 5, 30, and 40 °C using clean dry air to flush loaded filters did not reveal a flushing or flush temperature effect on REs. Tests with NO, NH<sub>3</sub>, CH<sub>3</sub>SH, CS<sub>2</sub>, and H<sub>2</sub>S showed no apparent interferences with NO<sub>2</sub> or SO<sub>2</sub> measurements. Ozone did not interfere with NO<sub>2</sub> measurements under the conditions tested. Although the potential interference with SO<sub>2</sub> measurements of O<sub>3</sub>, PAN, and HNO<sub>2</sub> was not examined, both PAN and HNO<sub>2</sub> were found to be strong interferences with NO<sub>2</sub> measurements using TEA-impregnated filters. Recommendations were made to avoid sampling particulate sulfates, particulate nitrates, and/or HNO<sub>2</sub> since they can act as direct interferences.

On the basis of the results of the previously described tests, a method using TEA-coated filters was defined. The bounds of applicability were described with respect to species concentration and loading, sampling rate, capacity, humidity, temperature, and interferences. Subsequently, the method was incorporated into a multiconstituent sampler (i.e., TFR) and deployed in a 13-day field study. On the basis of the precision of field blanks, and a sampling rate of 1.6 L min<sup>-1</sup>, SO<sub>2</sub> and NO<sub>2</sub> detection limits of 0.3 and 0.2 ppb for 24-h samples and 0.04 and 0.03 ppb for 7-day samples were estimated. Paired duplicate daily measurements showed median RSDs for SO<sub>2</sub> and NO<sub>2</sub> of 13 and 3%. TFR results were compared with those of accepted methods (i.e., Canadian filter pack (FP) for SO<sub>2</sub> and tunable diode laser absorption spectrometer (TDLAS) for NO<sub>2</sub>). These comparisons were in reasonable agreement with correlation coefficients above 0.95 in both cases. At the ambient SO<sub>2</sub> concentrations present (i.e., 0.5–5 ppb), although the TFR SO<sub>2</sub> measurements appeared to be biased slightly (i.e., 10%) lower than the FP measurements, the difference was not statistically significant ( $\alpha = 0.05$ ). At the ambient NO<sub>2</sub> concentrations sampled (i.e., 5–17 ppb), while the TFR NO<sub>2</sub> measurements were biased higher than the TDLAS measurements ( $\alpha = 0.05$ ), the magnitude of this bias was small (i.e., 7%). These findings demonstrate that TEA-impregnated filters can be used to sample ambient air for SO<sub>2</sub> and NO<sub>2</sub> sensitively (i.e., sub-part-per-billion detection limit) at commonly occurring levels, with good precision (i.e.,  $\pm 15\%$ ) and accuracy (i.e., 10%).

#### ACKNOWLEDGMENT

Appreciation is expressed to J. L. Durham, L. L. Spiller, and R. J. Paur of the United States Environmental Protection Agency for advice and guidance during the course of the methods development effort. We thank Dr. K. G. Anlauf and his colleagues at the Canadian Atmospheric Environment Service and Dr. G. I. Mackay of Unisearch Associates for making the FP SO<sub>2</sub> and TDLAS NO<sub>2</sub> data from the 1986 field study available to us for comparison.

**Registry No.** XAD2, 9060-05-3; XAD7, 37380-43-1; TEA, 102-71-6; SiO<sub>2</sub>, 14808-60-7; NO<sub>2</sub>, 10102-44-0; SO<sub>2</sub>, 7446-09-5; K<sub>2</sub>CO<sub>3</sub>, 584-08-7; PbO<sub>2</sub>, 1309-60-0; KMnO<sub>4</sub>, 7722-64-7; NaAsO<sub>2</sub>, 7784-46-5; chromosorb 101, 9003-70-7; chromosorb 105, 62852-91-9; chromosorb 107, 77641-01-1; chromosorb 108, 82905-08-6; guaiacol, 90-05-1; alumina, 1344-28-1; cellulose, 9004-34-6.

#### LITERATURE CITED

- (1) Durham, J. L.; Ellestad, T. G.; Stockburger, L.; Knapp, K. T.; Spiller, L. L. *J. Air Pollut. Control Assoc.* **1986**, *36*, 1228–1232.
- (2) Sickles, J. E., II; Grohse, P. M. Sampling and Analysis Methods for Sulfur Dioxide and Nitrogen Dioxide: A Literature Review. Research Triangle Institute Report No. RTI/2823/00-011. Research Triangle Institute: Research Triangle Park, NC, 1984.
- (3) Chiswell, C. D.; Gjerde, D. T. *Anal. Chem.* **1982**, *54*, 1911–1913.
- (4) Pate, J. B.; Lodge, J. P., Jr.; Neary, M. P. *Anal. Chim. Acta* **1963**, *28*, 34–36.
- (5) Hurlgen, C. *Anal. Chim. Acta* **1963**, *28*, 349–360.
- (6) Adams, D. F.; Bamesberger, W. L.; Robertson, T. J. *J. Air Pollut. Control Assoc.* **1968**, *18*, 145–158.
- (7) Forrest, J.; Newman, L. *Atmos. Environ.* **1973**, *7*, 561–573.
- (8) Johnson, D. A.; Atkins, D. H. F. *Atmos. Environ.* **1975**, *9*, 825–829.
- (9) Levin, E.; Zachau-Christiansen, B. *Atmos. Environ.* **1977**, *11*, 861–862.
- (10) Fa'well, S. O.; Liebowitz, D. P.; Kagel, R. A.; Adams, D. F. *Anal. Chem.* **1980**, *52*, 2370–2375.
- (11) Van Mourik, J. H. C. *Am. Ind. Hyg. Assoc. J.* **1965**, *26*, 498–509.
- (12) Le'raggi, D. A.; Siu, W.; Feldstein, M.; Kothny, E. L. *Environ. Sci. Technol.* **1972**, *6*, 250–252.
- (13) Julekikis, H. S.; Siegel, S.; Stewart, T. B.; Hedgpeth, H. R. Heterogeneous: Reactions of Nitrogen Oxides in Simulated Atmospheres. U.S. EPA Publication EPA-600/3-77-028; Office of Research and Development: Cincinnati, OH, 1977.
- (14) Guddebeck, J. E.; Saltzman, B. E.; Burg, W. R. *J. Air Pollut. Control Assoc.* **1975**, *25*, 725–729.
- (15) Adams, K. M.; Japar, S. M.; Pierson, W. R. *Atmos. Environ.* **1986**, *20*, 1211–1215.
- (16) Le'raggi, D. A.; Siu, W.; Feldstein, M. *J. Air Pollut. Control Assoc.* **1973**, *23*, 30–33.
- (17) Blocker, J. H. *Am. Ind. Hyg. Assoc. J.* **1973**, *34*, 390–395.
- (18) Wiley, M. A.; McCammon, C. J., Jr.; Doemeny, L. *J. Am. Ind. Hyg. Assoc. J.* **1977**, *38*, 358–363.
- (19) Bourbon, P.; Alary, J.; Esclassan, J.; Lepert, J. C. *Atmos. Environ.* **1977**, *11*, 485–488.
- (20) Christie, A. A.; Lidzey, R. G.; Radford, D. W. F. *Analyst* **1970**, *95*, 519–524.
- (21) Vijjamoori, D. V.; Ling C.-S. *Anal. Chem.* **1981**, *53*, 1689–1691.
- (22) Holdren, M. W.; Spicer, C. W. *Environ. Sci. Technol.* **1984**, *18*, 113–116.
- (23) Winer, A. M.; Peters, J. W.; Smith, J. P.; Pitts, J. N., Jr. *J. Environ. Sci. Technol.* **1974**, *8*, 1118–1121.
- (24) Derley, E. F.; Kettner, K. A.; Stephens, E. R. *Anal. Chem.* **1963**, *35*, 589–591.
- (25) Braman, R. S.; de la Cantera, M. A. *Anal. Chem.* **1986**, *58*, 1533–1537.
- (26) Krapp, K. T.; Durham, J. L.; Ellestad, T. G. *Environ. Sci. Technol.* **1986**, *20*, 633–637.
- (27) Sickles, J. E., II; Hodson, L. L.; McClenny, W. A.; Paur, R. J.; Ellestad, T. G.; Muik, J. D.; Anlauf, K. G.; Wiebe, H. A.; Mackay, G. I.; Schiff, H. I.; Buback, D. K. *Atmos. Environ.* **1990**, *24*, 155–165.
- (28) Anlauf, K. G.; Wiebe, H. A.; Fellin, P. J. *J. Air Pollut. Control Assoc.* **1986**, *36*, 715–723.
- (29) Schiff, H. I.; Hastie, D. R.; Mackay, G. I.; Iguchi, T.; Ridley, B. A. *Environ. Sci. Technol.* **1983**, *17*, 352A–354A.
- (30) Sickles, J. E., II. Sampling and Analytical Methods Development for Dry Deposition Monitoring. Research Triangle Institute Report No. RTI/2823/00-15F; Research Triangle Institute: Research Triangle Park, NC, 1987.
- (31) Dellinger, B.; Groteloclos, G.; Fortune, C. R.; Cheney, J. L.; Homolya, J. B. *Environ. Sci. Technol.* **1980**, *14*, 1244–1249.
- (32) Girman, J. R.; Hodgson, A. T.; Robinson, B. K.; Traynor, G. W. "Laboratory Studies of the Temperature Dependence of the Palmes NO<sub>2</sub> Passive Sampler;" Proceedings of the National Symposium on Recent Advances in Pollutant Monitoring of Ambient Air and Stationary Sources. U.S. EPA Publication EPA-600/9-84-001; Office of Research and Development: Cincinnati, OH, 1984; pp 152–166.
- (33) Sanhueza, E.; Plum, C. N.; Pitts, J. N., Jr. *Atmos. Environ.* **1984**, *18*, 1029–1031.
- (34) Sickles, J. E., II; McClenny, W. A.; Paur, R. J.; Baumgardner, R. E. Internal Report on the Retrofit of NDDN Multiconstituent Samplers. Research Triangle Institute Report No. RTI/3993/09-02F; Research Triangle Institute: Research Triangle Park, NC, 1988.
- (35) A/S Committee on Environmental Improvement. *Anal. Chem.* **1980**, *52*, 2442–2449.

RECEIVED for review July 12, 1989. Accepted November 14, 1989. The research described in this paper has been funded in part by the United States Environmental Protection Agency under Contracts 68-02-3170 and 68-02-4079. The paper has not been subjected to Agency review and therefore does not necessarily reflect the views of the Agency. As a result, no official endorsement should be inferred.

# Non-Steady-State Gas Chromatography Using Capillary Columns

Anatoly J. Belfer

BP Research, Warrensville Research Center, 4440 Warrensville Center Road, Cleveland, Ohio 44128

David C. Locke\* and Isaac Landau

Chemistry Department, Queens College and The Graduate School, CUNY, Flushing, New York 11367

**Non-steady-state gas chromatography involves the use of a relatively volatile solvent phase that elutes slowly and continuously while solutes are injected. Application of the technique to the determination of limiting activity coefficients of solutes in the solvent is shown to provide useful data when the solvent is condensed onto the walls of an uncoated fused silica capillary column. Activity coefficients of *n*-hexane, *n*-heptane, and benzene solutes are determined in *n*-nonane and *p*-xylene solvents at 40, 50, and 60 °C, and of acrylonitrile and methyl methacrylate in water in the range of 35–60 °C. Compared with packed column non-steady-state gas chromatography, capillary columns require smaller solvent and sample volumes, and measurement times are substantially reduced.**

Non-steady-state gas chromatography (NSGC) has been shown to be an efficacious method for the determination of physicochemical properties of nonelectrolyte solutions (1–3). For this application, NSGC has the particular advantage over normal gas chromatography in that it is useful for determining limiting activity coefficients and other thermodynamic properties of volatile solutes in volatile solvents. The criterion is that the volatility, the product of the vapor pressure and the activity coefficient, of the solute must be greater than the volatility of the solvent. In normal gas chromatography (GC), a stationary solvent of low volatility is used, which limits study to systems that are primarily of theoretical interest. Volatile compounds have served as solvent phases in GC (4–7), but presaturation of the carrier gas with the solvent is required, and the exact weight of the solvent present in the column is always uncertain.

In NSGC, the volatile solvent phase is injected into the hot injection port, evaporates, is allowed to equilibrate in the column, and bleeds out at a steady rate dependent on its vapor pressure at the column operating temperature. Solute is more volatile than the solvent are injected repetitively while the solvent is eluting, over the life of the column, and elute with ever-decreasing retention times as the weight of solvent diminishes linearly with time. An analysis of the system (1, 2) leads to a remarkably simple equation relating the infinite dilution (limiting) activity coefficient,  $\gamma_1^\infty$ , of the solute in the volatile solvent to the ratio of their vapor pressures,  $P_1^\circ/P_2^\circ$ , and the rate at which retention time decreases with the time of injection,  $\Delta t_R/\Delta t$ :

$$\gamma_1^\infty = -(P_1^\circ/P_2^\circ)(\Delta t_R/\Delta t) \quad (1)$$

Solutes of lower volatility than the solvent will elute at the tail of the solvent band, and cannot be studied from this point of view.

Heretofore all NSGC work (1–3) was done by using a column packed with only a solid support material. We report here the use of a capillary column in which the solvent is condensed onto the walls of the column. The primary advantage of a capillary column in NSGC is the small volume of solvent that is required, which facilitates the study of rare, expensive, and/or toxic compounds as solvents. In addition, the time required to equilibrate the column and to make measurements is reduced substantially compared to that required for packed columns. A more uniform coating of the solvent film and consequently a more constant rate of evaporation of the film will also result. The thin liquid film and the short lateral diffusion distance improve solute mass-transfer characteristics.

With packed column NSGC, thermal conductivity detector base-line stabilization is assisted by using dual columns, into both of which are injected equal volumes of solvent. For the capillary columns, we used a Hewlett-Packard modulated thermal conductivity detector (11). This detector is quite sensitive, and once solvent equilibration has been achieved, a flat base line results, enabling detection of solute quantities small enough to ensure effectively infinite dilution solutions.

## EXPERIMENTAL SECTION

A Hewlett-Packard 5890A gas chromatograph (GC) equipped with a Hewlett-Packard modulated thermal conductivity detector and splitless injector was used with a 30 m × 0.53 mm i.d. uncoated Hewlett-Packard fused silica capillary column. The carrier gas was He at flow rates in the range of 2–10 mL/min. Carrier gas flow rate was set to provide a column lifetime of at least 15 min, which is sufficient to allow at least five solute injections. The injector and detector were maintained at 200 and 250 °C, respectively. Measurements were made at column temperatures in the range of 35–60 °C. Without cryocooling, for which the GC used was not equipped, the oven gave unstable temperature control below about 30 °C. Chromatographic data were recorded on a Hewlett-Packard 3392A recording integrator. The attenuator setting was 5 or 6 for injections of 0.2  $\mu$ L of solute mixtures.

To load the column with a presumably uniform and relatively thick film of solvent, the column temperature was set to a value slightly greater than the boiling point of the solvent. Injection of 25–50  $\mu$ L of solvent into the Grob injector produced a temporary surge in pressure at the head of the column. As the vapors passed into the column, the pressure dropped back to normal. At this time the column was filled with the saturated vapor of the solvent. Condensation of solvent onto the walls of the capillary column was achieved by opening the door of the GC oven and setting the temperature down to the desired operating value. Liquid nitrogen cryocooling would presumably serve the same function in a more elegant fashion. The base line stabilized in about 5–6 min. If the rapid cooling was started before the inlet pressure had dropped to normal, a liquid plug formed at the column inlet, which led to an excessively long equilibration time and a shorter effective column lifetime. On the other hand, cooling should not be delayed lest elution of solvent vapor leave an amount of solvent insufficient to produce a long-lived column. When the temperature descended to the operating value, the oven door was closed gradually to maintain the temperature. If the door was closed at once, residual

\* Author to whom correspondence should be addressed

Table I. Activity Coefficients in *n*-Nonane and *p*-Xylene

solvent	temp, °C	activity coeff of solute		
		<i>n</i> -hexane	<i>n</i> -heptane	benzene
<i>n</i> -nonane	40	0.76	0.77	0.97
	50	0.80	0.80	0.96
	60	0.85	0.84	0.96
<i>p</i> -xylene	40	1.25	1.22	0.91
	50	1.20	1.17	0.88
	60	1.14	1.10	0.85
	20 <sup>a</sup>	1.39	1.38	0.98
	20 <sup>b</sup>	1.44	1.40	0.99

<sup>a</sup> Extrapolated. <sup>b</sup> Reference 7.

heat in the oven components caused a sharp rise in temperature followed by a slow equilibration back to the set value.

As soon as base-line stabilization was noted, solutes could be injected, neat or in solution or in mixtures if the components were separated. Peak shapes were generally symmetrical, except for the solutions in *n*-nonane, in which the peaks tended to front, indicative of overload. Injection times were noted on the recorder chart by using the event marker on the integrator. It is not necessary to wait for complete elution of a sample before making a new injection, if elution times allow a separation. Indeed, the more solute injections made over the life of the column, the better the definition of the slope of the retention time/injection time plot. For example, for *n*-nonane solvent at 40 °C, the column lifetime was about 65 min, which allows time for at least 12 injections of a mixture of *n*-hexane and *n*-heptane solutes. The complete evaporation of solvent is noted by a sharp drop in the base line, which signals the need to inject fresh solvent. One need not wait for loss of all solvent; a new solvent injection can be made at any time, and once equilibration has been achieved, solute injections can be resumed.

## RESULTS AND DISCUSSION

From eq 1,  $\gamma_1^\circ$  is calculated from the slope of a plot of retention time vs injection time and from the ratio of solute-to-solvent vapor pressures. Vapor pressures for all compounds except H<sub>2</sub>O were calculated by using the Fortran program of the Design Institute for Physical Property Data (12). The vapor pressure of H<sub>2</sub>O was calculated from the Chebyshev polynomials given by Ambrose and Lawrenson (13). Corrections for vapor-phase nonideality, calculated from the truncated virial equation of state using second virial coefficients calculated according to Reid, Prausnitz, and Poling (14), were insignificant compared with the estimated experimental error ( $\pm 10\%$ ). Activity coefficients are listed in Table I for *n*-hexane, *n*-heptane, and benzene solutes in *n*-nonane and *p*-xylene solvents. Values for acrylonitrile and methyl methacrylate solutes in water are given in Table II.

There are few data in the literature for comparison with the values listed in Tables I and II. For *p*-xylene solvent, Thomas et al. (7) give  $\gamma_1^\circ$  values for benzene and *n*-hexane at 20 °C. Extrapolation of their data for *n*-pentane and *n*-hexane yields a value for  $\gamma_1^\circ$  of *n*-heptane in *p*-xylene at 20 °C. Extrapolation of our data to 20 °C yields the values on the next to last line of Table I; on the line below are the values of Thomas et al. (7). The agreement is quite good. The activity coefficient of acrylonitrile in H<sub>2</sub>O at 25 °C has been calculated by Banerjee using UNIFAC (15). This value, 45.3, is in reasonable agreement with our extrapolated value, 48.4.

It is of interest to calculate the average liquid film thickness on the walls of the capillary tubing, assuming a uniform film. This value,  $d_L$ , can be calculated from the initial solvent volume,  $V_L$ , which in turn is estimated from the specific retention volume of a solute,  $V_G$ , the net retention volume per gram of stationary phase

$$V_G = RT/p_1^\circ \gamma_1^\circ M_s$$

where  $M_s$  is the molecular weight of the solvent. From the

Table II. Activity Coefficients in Water

temp, °C	activity coeff of solute	
	acrylonitrile	methyl methacrylate
35	44.4	431
40	45.2	388
50	42.0	376
60	38.4	338
25 <sup>a</sup>	48.4	
25 <sup>b</sup>	45.3	

<sup>a</sup> Extrapolated. <sup>b</sup> UNIFAC-calculated, ref 15.

experimentally determined  $\gamma_1^\circ$  value for a solute of vapor pressure  $p_1^\circ$ ,  $V_G$  can be calculated. For an injection of this solute early in the column life, the retention time and flow rate are measured. The total column volume is measured at the end of the column life from the retention time of air and the flow rate. From these values can be estimated the initial weight and volume of solvent present in the column, and assuming a uniform film on the walls of the capillary tube,  $d_L$  can be calculated. For example, for the acrylonitrile/water system at 50 °C,  $V_L = 24 \mu\text{L}$  and  $d_L = 1.2 \times 10^{-3} \text{ cm}$ .  $V_L$  is consistent with the volume of water injected, which was 25  $\mu\text{L}$ .

Film thicknesses of this magnitude lead one to raise the obvious question as to whether the solutions are sufficiently dilute to give effectively infinite dilution activity coefficients. An estimate of the most dilute concentration of the solute in the chromatographic solution can be made by using the maximum permissible sample size calculation of Conder and Young (5), assuming the solvent film is uniformly distributed. According to this calculation, the column plate number,  $N$ , is related to the total column length,  $L$ , and to the length of the column occupied by the solute,  $d_s$ , when it begins to elute:

$$N = 5.545(L/d_s)^2$$

For example, for acrylonitrile in H<sub>2</sub>O,  $N = 16070$ , from which  $d_s = 930 \text{ mm}$ . The 24  $\mu\text{L}$  of solvent initially present in the column is 1.3 mmol; i.e. the solute is dissolved in 1300  $\mu\text{mol} \times (d_s/L) = 25 \mu\text{mol}$  of H<sub>2</sub>O. Since 0.05  $\mu\text{L}$  of acrylonitrile (1  $\mu\text{mol}$ ) is injected, the mole fraction of solute in solvent at the end of the column is about 0.03. For *p*-xylene solvent, the solute mole fraction is about 0.05, and for *n*-nonane, 0.1. The precise upper limit of solute mole fraction consistent with effectively infinite dilution solutions is somewhat arbitrary (5). In any case, the concentration of the solution in *n*-nonane is rather high, all the more so when one considers that this calculation refers to the most dilute conditions, i.e. just before the solute elutes from the column. The bandwidth on injection should be quite narrow, producing a substantially higher concentration, and that concentration will decrease with the square root of the length of column traveled; the bandwidth will increase in the same way, finally reaching the value  $d_s$  at the outlet of the column (16). The apparently low values of the activity coefficients of *n*-hexane and *n*-heptane in *n*-nonane could be accounted for in terms of their solutions being at finite concentrations; the fact that the peaks fronted substantiates this. In current work we inject solutions containing only 1–10  $\mu\text{g}$  of each solute, 0.01–0.1 times the quantity injected to obtain the data reported here.

Although the theory of NSGC does not require a uniform liquid film as long as the rate of evaporation is constant over time, a second question can be raised regarding whether the solvent wets the capillary tube. If a solvent does not wet the surface, presumably it forms globules and droplets on the surface of the silica (17). According to Grob (18), untreated glass capillary tubes are wet by nonpolar solvents but not by polar solvents, presumably including water. Fused silica

should behave in a similar fashion (19). One way to compare the uniformity of liquid films would be through the measured plate numbers. Uniform films should produce more efficient chromatographic behavior. However, although more plates were generated in the hydrocarbon solvent systems, since  $k'$  values and flow rates were different, a meaningful comparison cannot be made.

It is not obvious either what the effect of nonwetting would be on the derived activity coefficients, or how to circumvent the problem if the effect is detrimental to their accuracy. One could start with a fused silica column containing a cross-linked polar phase such as a polyethylene glycol or a propylcyanosiloxane, which should be wet by polar solvents such as water, but these phases would of course change solute retention behavior and obfuscate interpretation of the data. This problem is currently under investigation by us.

#### ACKNOWLEDGMENT

We thank C. Wysocki of BP Research for technical assistance.

#### LITERATURE CITED

- (1) Belfer, A. I. *Neftekhimiya* 1972, 12, 435; *Chem. Abstr.* 1973, 78, 20591.
- (2) Belfer, A. J.; Locke, D. C. *Anal. Chem.* 1984, 56, 2485.
- (3) Yang, Y.; Xiao, S.; Li, H.; Fu, Y. *J. Chengdu Univ. Sci. Technol.* 1988, No. 1, 35; *Chem. Abstr.* 1988, 109, 157451.

- (4) Locke, D. C. *Adv. Chromatogr.* 1976, 14, 87.
- (5) Conder, J. R.; Young, C. L. *Physicochemical Measurements by Gas Chromatography*; Wiley: New York, 1979.
- (6) Laub, R. J.; Pecsok, R. L. *Physicochemical Applications of Gas Chromatography*; Wiley: New York, 1978.
- (7) Thomas, E. R.; Newman, B. A.; Long, T. C.; Wood, D. A.; Eckert, C. A. *J. Chem. Eng. Data* 1982, 27, 399.
- (8) Eckert, C. A.; Newman, B. A.; Nicolaides, G. L.; Long, T. C. *AIChE J.* 1981, 27, 33.
- (9) Terasawa, S.; Itsuki, H.; Yamaki, H. *Anal. Chem.* 1986, 58, 3021.
- (10) Itsuki, H.; Terasawa, S.; Yamana, N.; Ohtaka, S. *Anal. Chem.* 1987, 59, 2918.
- (11) Craven, J. S.; Clauser, D. E. *Analisis* 1980, 8(1), 1.
- (12) American Institute of Chemical Engineers, Design Institute for Physical Property Data. *Project 801, DCAP II Users Guide*; The Pennsylvania State University: University Park, PA, 1983.
- (13) Ambrose, D.; Lawrenson, I. J. *J. Chem. Thermodyn.* 1972, 4, 755.
- (14) Reid, R. C.; Prausnitz, J. M.; Poling, B. E. *The Properties of Gases and Liquids*, 4th ed.; McGraw-Hill: New York, 1987.
- (15) Banerjee, S. *Environ. Sci. Technol.* 1985, 19, 369.
- (16) Littlewood, A. B. *Gas Chromatography*; Academic Press: New York, 1967; p 127.
- (17) Jennings, W. *Gas Chromatography with Glass Capillary Columns*, 2nd ed.; Academic Press: New York, 1980; p 21.
- (18) Grob, K. *Helv. Chim. Acta* 1965, 48, 1362.
- (19) Jennings, W. *Gas Chromatography with Glass Capillary Columns*, 2nd ed.; Academic Press: New York, 1980; p 33.

RECEIVED for review September 1, 1989. Accepted November 22, 1989. This work was supported in part at QC by grants from the National Science Foundation (CHE-8420326) and the PSC-CUNY FRAP Program.

## Pulse Voltammetric Techniques at Microelectrodes in Pure Solvents

Malgorzata Ciszowska and Zbigniew Stojek

Department of Chemistry, Warsaw University, ul. Pasteura 1, 02-093 Warsaw, Poland

Janet Osteryoung\*

Department of Chemistry, State University of New York, University at Buffalo, Buffalo, New York 14214

**Experimental conditions are described for application of pulse voltammetric techniques with microelectrodes in solvents containing no deliberately added supporting electrolyte. Elimination of supporting electrolyte was found to be advantageous in the case of alkyl iodides, for which supporting electrolyte strongly influences the voltammetric curves. The primary reduction waves obtained at mercury microelectrodes were free from phenomena due to adsorption and following chemical reaction. The heights of both linear scan reduction and reverse pulse oxidation curves were linearly dependent on ethyl, butyl, and decyl iodide concentration.**

Research on microelectrodes is focused on the ways of preparation, properties, theory, and application of these electrodes (1, 2). One of the important properties of microelectrodes is a very low level of current flowing through the electrochemical cell. Consequently, the ohmic drop ( $iR$ ) may be very small despite large resistance of the solution. Therefore it is possible, with the proper instrumentation, to monitor electroactive species in solvents containing virtually no added supporting electrolyte (3-8). These conditions can be interesting, since any salt used as the supporting electrolyte can be a source of unwanted impurities in trace analysis and

a source of unwanted water in nonaqueous solvents.

The first published papers on this subject proved that obtaining a curve in a pure solvent and measuring its height are possible. However, many bothersome questions remain. First of all, how does ion migration current contribute to the total current? For large-area electrodes it is well-known that at low supporting electrolyte concentrations the reduction signal of positively charged species can be appreciably higher than that at high concentrations. An experimental study done with microelectrodes showed minor changes of the limiting reduction current for  $\text{Fe}(\text{CN})_6^{3-}$  with a change in supporting electrolyte concentration in water (6). This result is linked to substantially enhanced diffusional transport to electrodes of very small area. On the other hand, it is not surprising that uncharged molecules give wave heights virtually independent of the electrolyte level (3, 4, 6). A recent paper by Oldham deals with theory of microelectrode steady-state voltammetry with various ratios of reactant to supporting electrolyte (9). At a hemispherical electrode, for reactions that engender an increase in ionic strength at the microelectrode interface, the faradaic redistribution of ions is predicted to diminish the ohmic overvoltage. Simultaneously the counterions will be brought into the neighborhood of the microelectrode so effectively that a very low electrolyte concentration can behave as "excess" supporting electrolyte. In the present case of no

deliberately added electrolyte, local departure from electro-neutrality may shift the autodissociation reaction of the solvent to the right (10).

Another problem is choosing the optimal scheme for potential control and current measurement. Since the currents are very small, a two-electrode system can be used (4, 8). In such a system all electrodes exhibit the same ohmic potential drop at steady state (11). Such a simple electrical circuit can be employed for amperometry (12, 13) or other simple electroanalytical techniques. A pulse voltammetric technique in a solvent containing no supporting electrolyte would seem to be much more demanding. First, it is convenient to use a commercial instrument based on a high input impedance potentiostat; second, one has to take into account the cell time constant, to make sure the working electrode has been polarized to the desired potential during the (usually short) pulse time. There are apparently only two reports of pulse techniques applied in a pure solvent, square wave voltammetry of ethylenediaminetetraacetic acid in pure water (7) and differential pulse voltammetry of ferrocene in acetonitrile (14).

A special reason for abandoning addition of a supporting electrolyte is strong interaction of the electrolyte with the substrates or products of the electrode reaction, which complicates the interpretation of the results. This is a common circumstance, particularly in the study of organic molecules. We have previously examined the reduction of several alkyl iodides at mercury electrodes under conventional voltammetric conditions (15). The mechanism of the reduction was investigated by employing reverse pulse voltammetry. This provides a particularly challenging case, for the potential range of interest requires pulse amplitudes of up to 3 V. Thus the test compounds for these investigations were chosen to be decyl, butyl, and ethyl iodide.

Numerous papers have been devoted to electrochemistry of alkyl halides. Those dealing with alkyl iodides at mercury electrodes have been reviewed critically in ref 15 and the references therein. Alkyl iodides are known to produce poorly defined staircase and normal pulse polarographic waves. A large maximum generally appears on the plateau of the waves, and the half-wave potentials shift toward positive potentials with a decrease in the size of the cation in tetraalkylammonium supporting electrolytes. The two-electron process consists of one or two steps, depending on the supporting electrolyte used. Although the electrochemistry of this class of compounds has been studied extensively, some aspects of the electrode process still are not clear.

Mercury electrodeposited on a platinum disk was chosen as the working electrode in the present work, as we had used this electrode successfully previously in aqueous solution without supporting electrolyte (7).

Our first specific objective was to identify solvents that would yield reproducible results. Second, we wished to see if the mercury microelectrode would behave reasonably with large pulse amplitudes in nonaqueous solvent. Third, we wished to test the practical range of pulse amplitude, pulse duration, and analyte concentration over which quantitative results without obvious distortions could be obtained. Finally, recognizing deficits in basic physical understanding of such systems, we wished to see what quantitative results could be obtained from these preliminary experiments.

## EXPERIMENTAL SECTION

Normal pulse, reverse pulse, and linear scan voltammetric measurements (NPV, RPV, LSV) were carried out with a three-electrode system. Mercury deposited on a platinum microdisk, a saturated calomel electrode (SCE), and a platinum wire served as the working, reference, and auxiliary electrodes, respectively. Bare platinum and gold microdisk electrodes were also used in preliminary experiments. The SCE was separated from the cell by a bridge containing pure solvent. A two-electrode

system was also used in some experiments. A number of instruments were used, but mostly a Laboratori Pristroje P-03 pulse polarograph, a PARC 173 potentiostat, and a BAS-100 electrochemical analyzer. The measurements of very low currents were done by connecting a Keithley 427 current amplifier to the electrochemical instrumentation by the way described in either ref 7 or ref 16. An IBM/XT Turbo computer (10 MHz) served as a storage device for the purpose of background subtraction. Background curves were obtained in the absence of analyte and subtracted point-by-point. The cathodic waves for the alkyl iodides are not well-separated from the solvent reduction. In the worst case the background current was as large as 50% of the current for reduction of the alkyl iodide.

Two platinum microdisk electrodes of radius  $r = 12.5$  and  $1 \mu\text{m}$  were employed. The platinum wires were sealed into glass capillaries according to published procedures (2). Mercury was plated from 0.01 M Hg(I) solution at  $-0.5$  V vs SCE. To control the amount of mercury on the platinum surface, the charge required to oxidize the mercury was determined after each series of experiments. Usually, the amount of mercury plated on the platinum microdisk ( $r = 12.5 \mu\text{m}$ ) was  $48 \mu\text{C}$ , which corresponds to  $0.49$  n.mol. (Note that the amount of mercury must be large enough so that the amount removed by anodization is negligible.) We assume this electrode is a segment of a sphere, the radius of the planar intersection being the radius,  $r$ , of the platinum substrate. The volume of mercury corresponding to  $48 \mu\text{C}$  is  $7.34 \times 10^{-9} \text{ cm}^3$ . The volume of the segment of a sphere of radius  $R = (h^2 + r^2)/2h$  is  $V = \pi h(3r^2 + h^2)/6$ , where  $h$  is the height of the segment. Comparison with the experimental volume yields  $R = 13.3 \times 10^{-4} \text{ cm}$  and  $h = 17.84 \times 10^{-4} \text{ cm}$ . The area of this spherical segment is  $A = \pi(h^2 + r^2) = 1.49 \times 10^{-5} \text{ cm}^2$ . It is necessary to deal with this geometry rather than the simple hemisphere because the spherical segment with  $h > r$  is more stable than that with  $h = r$  and because it is experimentally impractical to deposit quantitatively each time the amount of mercury equivalent to a hemisphere.

It has been shown empirically that the diffusion-limited steady-state current at such an electrode is described by  $i_{ss} = knFDCr$  where  $k$  is an empirical constant, a function of  $h/r$  that has the value 4 when  $h = 0$  and  $2\pi$  when  $h = r$  (hemisphere) (17). The time dependence of the current is given approximately by

$$i = (nFADC/r)(2/(\pi\tau)^{1/2} + 1), \quad \tau \leq 1 \quad (1)$$

$$i = knFDCr(1 + k/\pi^{3/2}\tau^{1/2}), \quad \tau \geq 1 \quad (2)$$

where  $\tau = 4Dt/r^2$ . These equations are correct for the hemisphere and correct in first order for a disk. Thus they should be a reasonable approximation for the spherical segment. For  $r = 12.5 \mu\text{m}$  and  $h = 17.84 \mu\text{m}$ ,  $k = 3.245$  (17).

Before the Hg/Pt electrode was inserted into the cell, it was dried by washing with ethyl alcohol and acetone. Mercury electrodes based on a platinum substrate can cause problems in cases where certain metal amalgams are formed, due to formation of intermetallic compounds. However, for the purposes of this paper, which does not involve any metal deposition, such electrodes appear to function reliably (7).

Propylene carbonate (Fluka AG) was distilled under vacuum before use. Alkyl iodides were stabilized with metallic copper.

## RESULTS AND DISCUSSION

**Preliminary Experiments.** Certainly, not all solvents can be used in electrochemical experiments without supporting electrolyte. There is a limit, which can be expressed in terms of dielectric constant,  $\epsilon$ , below which a certain amount of supporting electrolyte is necessary to measure a current response. This limit depends on the electrode area (4, 6, 18) and should also depend on the type of the instrument used. In these terms electrochemistry without supporting electrolyte has its roots in the measurements in highly resistive media of Lines and Parker, who examined some aromatic compounds in benzene and chlorobenzene solutions also containing tetrahexylammonium salts (19).

Water-dioxane mixtures can cover a wide range of  $\epsilon$ , so this medium was chosen in this work to determine the experimental limits in pure solvents for the particular electro-



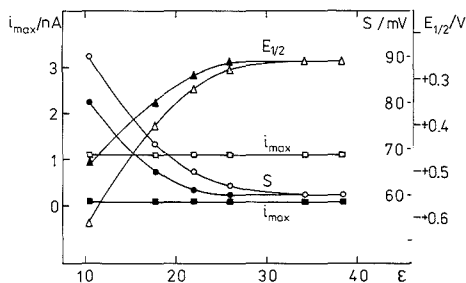


**Figure 1.**  $E_{1/2}$  (triangles),  $i_{\max}$  (squares), and slope (circles) of LSV curves plotted vs dielectric constant of water-dioxane mixtures: 0.5 mM ferrocene; Pt microdisk radius, 12.5  $\mu\text{m}$  (empty marks) and 1  $\mu\text{m}$  (filled marks);  $T = 25^\circ\text{C}$ .

chemical instrumentation used. Ferrocene served as the depolarizer. Examining  $i_{\max}$ ,  $E_{1/2}$ , and the slope,  $\log((i_d - i)/i_d)$ , of the ferrocene wave, we have found that a 12.5- $\mu\text{m}$  electrode can be used in solvents of  $\epsilon$  not lower than 10. For  $\epsilon$  greater than 30 all three measured quantities changed negligibly. In the range  $10 < \epsilon < 30$ , the limiting current was still constant, but  $E_{1/2}$  shifted toward positive potentials and the slope increased with decreasing  $\epsilon$ , as illustrated in Figure 1. Substituting a 1- $\mu\text{m}$  Pt disk for a 12.5- $\mu\text{m}$  electrode widened the useful range of  $\epsilon$ . These results agree with the earlier results of Bond, Fleischmann, and co-workers (4, 18), who applied electrodes of radius even smaller than 1  $\mu\text{m}$ . Based on these experiments, propylene carbonate (PC), a nontoxic liquid with  $\epsilon = 64.9$ , appears to be an excellent solvent, and it was used in the following investigations. It should be emphasized that these comments apply only for a potentiostat with a suitably high input impedance electrometer ( $Z > 10^{11} \Omega$ , e.g., PA 03, PARC 173, 174A, and 273). The measurements are impossible otherwise.

**Linear Scan Voltammetry.** Linear scan voltammetric curves obtained in pure propylene carbonate containing decyl iodide are presented in Figure 2. Since the curves are close to the cathodic limit of the potential window, the background had to be subtracted. We assume the dimensionless time for a linear scan experiment is  $\tau = D/nf\nu r^2$ , where  $\nu$  is scan rate and  $f = F/RT = 38.9 \text{ V}^{-1}$ . For the conditions of Figure 2, the non-steady-state contribution to the maximum current is approximately 19%, based on theory for a disk (20). The reduction wave is split, but it exhibits no maximum on the plateau. In fact neither adsorption nor convection maxima appear in the steady state, due to substantial flux at the surface of the electrode.

The heights of the first and second waves in Figure 2 depend linearly on DecI concentration over the entire range investigated. The ratio of the height of the second wave to that of the first is approximately unity (1.09), which is evidence for two one-electron reduction steps. This clear situation is the result of the unique property of microelectrodes: The influence of surface phenomena and following chemical reactions is insignificant under these conditions. Although LePerriese et al. (21) have found conditions in mixed solvent that yield well-shaped normal pulse waves for DecI, this regular behavior is strikingly different from the typical complex response at a conventional mercury drop electrode (5, 21).

Similar behavior is observed for BuI and EtI. Under the conditions of Figure 2, the corresponding calibration plots for the total wave height have slopes  $\partial i/\partial C$  ( $\text{nA mM}^{-1}$ ) = 7.51, 7.09, and 5.78 for EtI, BuI, and DecI, respectively. The diminishing slope of the lines in the sequence EtI, BuI, and DecI corresponds to decreasing values of the respective dif-

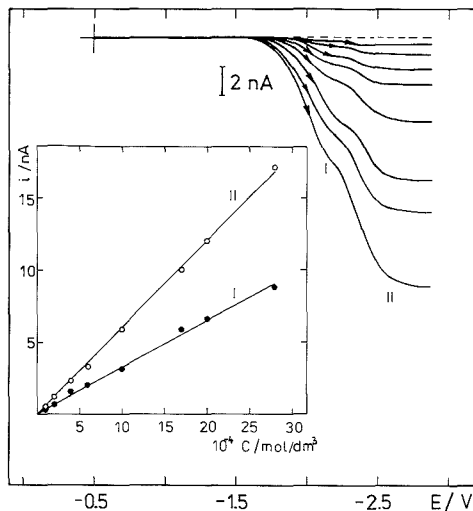


**Figure 2.** LSV curves of DecI in PC containing no supporting electrolyte:  $C_{\text{DecI}}$ , 0.1, 0.2, 0.4, 0.6, 1.0, 1.7, 2.0, 2.8 mM; Pt/Hg microelectrode;  $\nu = 20 \text{ mV/s}$ ;  $T = 25^\circ\text{C}$ . Inset: first wave height (I) and total height of two waves (II) plotted vs  $C_{\text{DecI}}$ . Electrode: 48  $\mu\text{C}$  of Hg on 12.5- $\mu\text{m}$ -radius Pt.

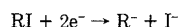
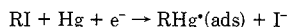
**Table I.** Diffusion Coefficients and  $E_{1/2}$  Values of Two LSV Reduction Waves of Ethyl, Butyl, and Decyl Iodide in Pure Propylene Carbonate

	$E_{1/2}(1)$	$E_{1/2}(2)$	$10^6 D, \text{cm}^2 \text{s}^{-1}$
EtI	-2.28	-2.59	3.12
BuI	-2.16	-2.54	2.93
DecI	-2.03	-2.48	2.34

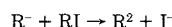
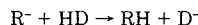
fusion coefficients. From the limiting LSV currents, diffusion coefficients of alkyl halides could be determined. To do this, the amount of mercury plated on a 12.5- $\mu\text{m}$ -radius Pt disk was set exactly at 26.8  $\mu\text{C}$  so that an ideal hemisphere could be formed, and experiments were carried out at a very low scan rate to achieve a steady-state limiting current. We assume the equation describing the limiting steady-state current at this electrode is  $i_{\text{ss}} = 2\pi n F C D r$ . The diffusion coefficients calculated in this way and the corresponding  $E_{1/2}$  values are presented in Table I.

According to the discussion above, we formulate the steady-state current on the 48- $\mu\text{C}$  electrode as  $i_{\text{ss}} = 8.245 n F D C r$ , from which the slope of the calibration curve at steady state is predicted to be ( $n = 2$ ) 6.21, 5.83, and 4.65  $\text{nA/mM}$  for ethyl, butyl, and decyl iodide, respectively. The experimental values are about 17% higher than the predicted steady-state values, in good agreement with the estimate of non-steady-state diffusion for Figure 2.

**Reverse Pulse Voltammetry.** According to Bilewicz and Osteryoung (15), the electroreduction of alkyl iodides at mercury electrodes can be described by the reactions



The radical  $\text{RHg}^*$  can dimerize to form  $\text{HgR}_2$  and can react with RI to produce  $\text{I}^-$ . The anion  $\text{R}^-$  can react with proton donors (13, 22) or with reactant:



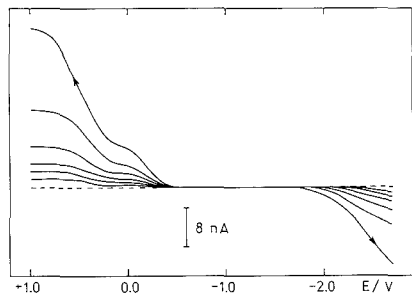


**Figure 3.** Reverse pulse voltammetry of DecI in PC containing no supporting electrolyte:  $C_{\text{DecI}}$ , 0.1, 0.2, 0.3, 0.5, 1, 2 mM;  $t_p$ , 50 ms; delay time (at  $-2.7$  V) = 1 s. Electrode:  $48 \mu\text{C}$  of Hg on  $12.5\text{-}\mu\text{m}$ -radius Pt.

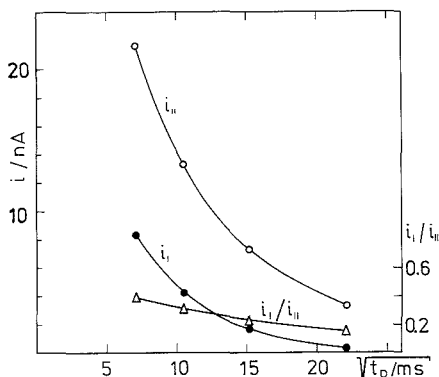


**Figure 4.** First and second reverse pulse wave heights and their ratio plotted vs  $t_p^{1/2}$ . The current  $i_2$  for the second wave is measured with respect to  $i_1$ . Other conditions are the same as in Figure 3.

If HD is a water molecule, then  $\text{D}^-$  is hydroxide ion. The species  $\text{I}^-$ ,  $\text{OH}^-$ ,  $\text{R}^-$  and  $\text{RHg}^*$  potentially can yield anodic waves, but in fact only in the presence of iodide and hydroxide ions is the Hg electrode oxidized at more negative potentials than the background oxidation. The adsorbed radical,  $\text{RHg}^*$ (ads), is also oxidized anodically in the presence of iodide. This situation favors choosing RPV as the appropriate technique for monitoring the reduction of RI. In addition, RPV can be accomplished easily at microelectrodes, since boundary conditions are readily renewed during the waiting periods between pulses (23). Note that because Hg is oxidized during the pulse period as the RPV curve advances, the size of the electrode and the pulse width must be chosen to avoid a significant decrease in the electrode area.

Typical RP voltammograms of DecI in pure propylene carbonate are presented in Figure 3. The curves are background corrected. The maximum pulse amplitude is 3.7 V. The shape of the curves and well-developed plateau indicate that the electrode was appropriately polarized during the pulses. The DC current (at  $-2.7$  V) is predicted, using the approximations given above, to give the slope  $\partial i_{\text{DC}}/\partial C = 7.53 \text{ nA mM}^{-1}$ . The experimental currents are linear in concentration with slope  $7.40 \text{ nA mM}^{-1}$ .

Two well-formed reverse pulse waves are seen in Figure 3. We deal first with the time dependence of these limiting currents as displayed in Figure 4. The height of the first wave decreases with respect to that of the second at longer times. This suggests that the first wave is due to the reaction of a

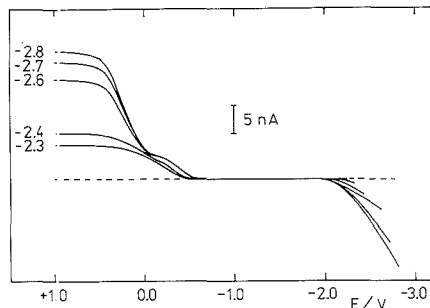


**Figure 5.** Reverse pulse voltammetry of 2 mM DecI obtained for various cationic potentials, as pointed out at the left side of the figure. Conditions are the same as in Figure 3.

species unstable on the time scale of the experiment, probably  $\text{RHg}^*$  (15). Detailed interpretation of the time dependence of the RPV data is not possible. However, a few further observations can be made. At a disk, the time dependence of the reverse pulse current for an uncomplicated process has the form  $(1/t_p^{1/2} - 1/(t_p + t_d)^{1/2})$ , where  $t_d$  is the time at the generating potential (here  $-2.7$  V) and  $t_p$  the pulse time. For the data of Figure 4, a plot of  $-i_{\text{RP}} \text{ vs } (1/t_p^{1/2} - 1/(t_p + t_d)^{1/2})$  is linear with slope  $6.22 \text{ nA s}^{1/2}$  and intercept  $-0.10 \text{ nA}$  for the second wave. The first wave also exhibits a linear plot, but the substantial negative intercept ( $-0.8 \text{ nA}$ ) suggests the same thing as Figure 4, that a coupled chemical reaction is removing the material responsible for the current at a rate commensurate with the experimental time scale.

The experimental values for the ratio  $i_{\text{DC}}/(i_{\text{DC}} - i_{\text{RP}})$  from the data of Figure 3 range from 0.332 (2 mM) to 0.417 (0.1 mM) ( $i_{\text{DC}}$  at  $-2.7$  V,  $-i_{\text{RP}}$  at  $+1.0$  V). As  $i_{\text{DC}}$  agrees well with theory,  $-i_{\text{RP}}$  is increasing with increasing concentration, as found previously for the same general range of time and concentration (15). We speculate that this is caused by the reaction of  $\text{R}^-$  with RI to form  $\text{R}_2 + \text{I}^-$ .

From the analytical point of view the key point is that the reverse pulse height is proportional to concentration of alkyl iodide. For the conditions of Figure 4, the slopes of the calibration plots are  $-\partial i_{\text{RP}}/\partial C$  ( $\text{nA mM}^{-1}$ ) = 13.12, 13.56, and 14.29 for decyl, butyl, and ethyl iodide, respectively, and the intercepts are 0.01, 0.07, and 0.31 nA, respectively ( $s_p = 0.34, 0.22, \text{ and } 0.06 \text{ nA}$ , respectively;  $r \geq 0.999$ ). The amount of iodide produced depends sensitively on impurity levels, and hence the slopes of these curves are sensitive to additions of supporting electrolyte. These results show that the limiting reverse pulse currents can be used analytically in the absence of supporting electrolyte.

Figure 5 displays reverse pulse voltammograms for the reduction of decyl iodide at various potentials. As the potentials made less negative, the limiting reverse pulse current decreases, as expected (15). Furthermore, the height of the second anodic wave decreases with respect to that of the first, and the two waves are no longer distinct. This is consistent with the increasing importance of the radical  $\text{RHg}^*$  at less negative reduction potentials. The prominence of the first anodic wave shown in both Figures 3 and 5 at rather high concentrations and long pulse widths suggests that the lifetime of the radical is much more longer under the present conditions than under the usual conditions employing excess supporting electrolyte.

These results demonstrate the feasibility of carrying out not only linear scan but also normal and reverse pulse voltammetry at platinum-based mercury microelectrodes in solvents of sufficiently high dielectric constant in the absence

of supporting electrolyte. The spherical segment electrode is well-behaved experimentally even with very large (3.7 V) pulse amplitudes. Furthermore, the limiting cathodic currents agree well with the semiempirical prediction for the spherical segment. The DC and reverse pulse limiting currents are also proportional to concentration, which suggests that this experimental approach could be useful for in situ monitoring of the composition of resistive liquids.

The quality of the experimental results also suggests that it would be worthwhile to develop the necessary models for studying reaction mechanisms by reverse pulse voltammetry in such systems. In the absence of supporting electrolyte the lifetime of unstable species is extended because the solvent medium is more inert. This can offer significant advantages in the study of complex reaction mechanisms. It may also improve reproducibility of experimental conditions. The voltammetric response in reverse pulse provides a picture of the reactions occurring (as does the response in cyclic voltammetry). The reverse pulse limiting currents, which are unaffected by  $iR$  drop, provide the accuracy and relatively simple interpretation characteristic of double potential step chronoamperometry. Particularly in the absence of supporting electrolyte, for which case complicated models are required, it would seem reasonable to focus on analysis of potential-independent currents. Thus reverse pulse voltammetry appears to be an attractive tool for investigating homogeneous reaction mechanisms under these conditions.

#### LITERATURE CITED

- (1) Pons, S.; Fleischmann, M. *Anal. Chem.* **1987**, *59*, 1391A.
- (2) *Ultramicroelectrodes*; Fleischmann, M., Pons, S., Rolison, D., Schmidt, P. P., Eds.; Datatech Science: Morganton, NC, 1987.
- (3) Howell, J. O.; Wightman, R. M. *Anal. Chem.* **1984**, *56*, E24.

- (4) Bond, A. M.; Fleischmann, M.; Robinson, J. J. *Electroanal. Chem. Interfacial Electrochem.* **1984**, *168*, 299.
- (5) Bond, A. M.; Fleischmann, M.; Robinson, J. J. *Electroanal. Chem. Interfacial Electrochem.* **1984**, *172*, 11.
- (6) Ciszowska, M.; Stojek, Z. J. *Electroanal. Chem. Interfacial Electrochem.* **1986**, *213*, 189.
- (7) Stojek, Z.; Osteryoung, J. *Anal. Chem.* **1988**, *60*, 131.
- (8) Bond, A. M.; Lay, P. A. J. *Electroanal. Chem. Interfacial Electrochem.* **1986**, *199*, 285.
- (9) Oldham, K. B. J. *Electroanal. Chem. Interfacial Electrochem.* **1988**, *250*, 1.
- (10) Bond, A. M.; Fleischmann, M.; Robinson, J. J. *Electroanal. Chem. Interfacial Electrochem.* **1984**, *172*, 11.
- (11) Bruckenstein, S. *Anal. Chem.* **1987**, *59*, 2098.
- (12) Bixler, J. W.; Bond, A. M. *Anal. Chem.* **1986**, *58*, 2859.
- (13) Ghoroghchian, J.; Sarfarazi, F.; Dibble, T.; Cassidy, J.; Smith, J. J.; Russel, A.; Dunmore, G.; Fleischmann, M.; Pons, S. *Anal. Chem.* **1986**, *58*, 2278.
- (14) Bond, A. M.; Henderson, T. L. E.; Thormann, W. J. *Phys. Chem.* **1986**, *90*, 2911.
- (15) Bilewicz, R.; Osteryoung, J. J. *Electroanal. Chem. Interfacial Electrochem.* **1987**, *226*, 27.
- (16) Huang, H.-J.; He, P.; Faulkner, L. R. *Anal. Chem.* **1986**, *58*, 2889.
- (17) Stojek, Z.; Osteryoung, J. *Anal. Chem.* **1989**, *61*, 1305-1308.
- (18) Pons, M. J.; Fleischmann, M.; Garrard, N. J. *Electroanal. Chem. Interfacial Electrochem.* **1987**, *220*, 31.
- (19) Lines, R.; Parker, V. D. *Acta Chem. Scan. Ser. B* **1977**, *31*, 369.
- (20) Aoki, K.; Akimoto, K.; Tokuda, K.; Matsuda, H.; Osteryoung, J. J. *Electroanal. Chem. Interfacial Electrochem.* **1984**, *171*, 219-230.
- (21) La Perriere, P. M.; Carroll, W. F., Jr.; Willett, B. C.; Torp, E. C.; Peters, D. G. *J. Am. Chem. Soc.* **1979**, *101*, 7561.
- (22) Andrieux, C. P.; Gilardo, J.; Saveant, J. M.; Su, K. B. *J. Am. Chem. Soc.* **1986**, *108*, 638.
- (23) Sinru, L.; Osteryoung, J.; O'Dea, J. J.; Osteryoung, R. A. *Anal. Chem.* **1988**, *60*, 1135.

RECEIVED for review September 12, 1989. Accepted November 14, 1989. This work was supported in part by the U.S. Office of Naval Research and by Grant 01.17.04.01 from the Polish government. Preliminary results were presented at Euroanalysis VI, Paris, 1987.

## Gas Sorption to Plasma-Polymerized Copper Phthalocyanine Film Formed on a Piezoelectric Crystal

Shigeru Kurosawa, Naoki Kamo,\* Daijyu Matsui, and Yonosuke Kobatake

Faculty of Pharmaceutical Sciences, Hokkaido University, Sapporo 060, Japan

Copper phthalocyanine was plasma-polymerized on piezoelectric quartz crystals. The film formed was very stable and resistant to chemical and physical treatment. Various spectroscopic data suggested that the essential properties of phthalocyanine remained after the polymerization. A variety of organic chemicals were examined to measure the sorption to the film from the gas phase (in the presence of air). Adsorption of gases to the film decreased the oscillating frequency. Sensitivity was defined as the frequency decrease per 1 part per million (ppm) of a certain gas, and the values ranged from 670 to 0.001 Hz/ppm. Chemicals showing high affinity are plane molecules with conjugate double bonds and some polar substituting groups or are higher alcohols, such as vanillin, benzoic acid, aniline, nitrobenzene, phenol, *n*-octyl alcohol, 1-nonanol, *n*-decyl alcohol, benzyl alcohol, DL-camphor,  $\beta$ -ionone, naphthalene, and anthracene. The film on the piezoelectric crystals was proved to have a life as long as 60 days. The sensitivity to various chemicals was dependent on a central metal of phthalocyanine.

\* Author to whom correspondence should be addressed.

#### INTRODUCTION

The frequency of vibration of an oscillating piezoelectric crystal is decreased by adsorption of a foreign substance onto its surface. Sauerbrey (1) derived an equation describing the relationship between frequency decrease and the weight of substances attached to a surface. The detection limit of a 9-MHz oscillating crystal has been estimated to be as low as  $10^{-9}$  g. By coating the crystal with some adsorbent substances, it is possible to construct gas sensors. Since King (2) reported the use of piezoelectric crystals for gas sensors, their features of low detection limit, broad application range, and continuous operation mode have attracted interest (3-14).

Phthalocyanines (Pc) are known to be good adsorbents for various chemicals. In addition, they work as a p-type semiconductor in the presence of oxygen, and adsorption of electronegative gases changes their electric resistance appreciably (15-18). Using this interesting nature of Pc, Barandasz, et al. (19, 20), Ricco et al. (21), and Roberts et al. (22) fabricated a surface acoustic wave (SAW) device covered with a thin Pc film and succeeded in obtaining a highly selective and sensitive response to halogen gases and NO<sub>2</sub> gases. The device was operated at 150 °C, and gradual loss of the film

occurred, due perhaps to sublimation (19). Thus, a stable coating with long life is necessary.

Plasma polymerization (23) is a promising technique for the making of an ultrathin film on substrata. The coating film formed adheres strongly to the substratum and is highly resistant to chemical and physical treatments. In fact, Cu Pc plasma-polymerized membrane was subjected to repeated use without any loss in the photoinduced reduction of methylviologen (24). An ion-selective electrode made by plasma polymerization showed a long lifetime (25).

These facts imply that the plasma-polymerized membrane works as a long-lived functional thin membrane. Unfortunately, Pc cannot be plasma-polymerized because it is not gaseous in the condition employed for usual plasma polymerization. Osada and his colleagues (24, 26-29), however, developed a method for plasma polymerization using solid chemicals instead of gaseous monomers, provided that a monomer can be sublimed. This technique is the first to sublime a monomer under low pressure and is followed by glow discharge. Pc (24, 26), D-camphor (27), L-menthol (27), anthracene (28), dicyclohexyl-18-crown-6 (29), and ammonium tetraphenylborate (25) are reported to be polymerizable. In addition, the plasma-polymerized dicyclohexyl-18-crown-6 membrane showed the same cation selectivity as did the monomer (29). The membrane of plasma-polymerized tetraphenylborate had a negative charge of boron and worked as a good selective membrane electrode for hydrophobic cations (25). This technique of Osada et al. thus broadened the selection of substances to be plasma-polymerized.

In this communication, we report preparation of a plasma-polymerized film of Cu Pc on piezoelectric quartz (bulk acoustic wave (BAW) device) by the method of Osada et al. (24) and measurement of the sorption of 77 organic chemicals, which were evaporated at 25 °C in the presence of air. Although Pc is thought to be a good adsorbent, few detailed data on the sorption of various chemicals are available, as far as we know. Hence, we measured sorption of various gases to a plasma-polymerized film on a piezoelectric quartz crystal that is very sensitive to a weight change due to adsorption. Results obtained may serve as basic data for constructing a gas sensor using Pc. Response sensitivity was defined as the frequency decrease per 1 ppm of gas, and the values ranged from 670 to 0.001 Hz/ppm, depending on the species of gas used. Chemicals with high sensitivity were vanillin, benzoic acid, aniline, nitrobenzene, phenol, *n*-octyl alcohol, 1-nonanol, *n*-decyl alcohol, benzyl alcohol, DL-camphor,  $\beta$ -ionone, naphthalene, and anthracene. They are plane molecules having conjugate double bonds and some polar substituting groups or are higher alcohols. If a frequency decrease of 10 Hz is taken as the limit of detection, a response sensitivity of 670 means that 0.015 ppm of gas can be detected. The plasma-polymerized film was proved to be long-lived: For as long as 60 days, no change in the response was observed, while the response of an evaporated film was reduced during the same period of operation. Results in this paper indicate that a piezoelectric quartz crystal covered with plasma-polymerized Pc may be a good device for detection of various organic gases. Preliminary results of a study of the effect of a central ion of Pc on the adsorption of chemicals are reported.

#### EXPERIMENTAL SECTION

**Materials.** Piezoelectric crystals used were AT-cut quartz, 8 mm  $\times$  8 mm  $\times$  0.18 mm, with a basic resonant frequency of 9 MHz (Yakumo Tushin, Tokyo). The relationship between frequency decreases and amounts adsorbed on surfaces was examined by application of known amounts of polystyrene or poly(vinyl chloride), and it was found that a decrease of 1 Hz corresponded to 1.58 ng of adsorption, 0.63 Hz/ng. The Cu Pc used was an ultrapure  $\alpha$ -type (data of elemental analysis agreed with theoretical values) supplied by Toyo Ink Co. (Tokyo); other Pc having central

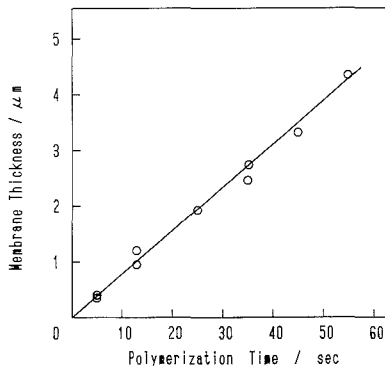


**Figure 1.** Membrane thickness vs period of plasma polymerization. Pc was sublimed at 300-400 °C under an atmosphere of 10.7 Pa of argon, and the discharge power was 100 W at 13.56 MHz. The distance between two electrodes was 3.5 cm.

metals different from Cu were the gift of Asada Kagaku Co. (Tokyo). Reagents used were of analytical or guaranteed grade and were purchased from Wako Pure Chemicals (Osaka) or from Tokyo Kasei Co. (Tokyo). The purity of benzoic acid, vanillin, *n*-decyl alcohol, and  $\beta$ -ionone, to which this system was highly responsive, was checked by the melting point (which agreed with those of refs 30-32). Further, benzoic acid was subjected to a vacuum at 25 °C overnight to remove any volatile contaminating impurities.

**Plasma Polymerization.** Cu Pc was plasma-polymerized by a method essentially the same as that described by Osada et al. (24). The polymerization was performed in a bell-jar reactor in which internal electrodes were installed (Type BP-1, Samuco International, Kyoto, Japan). This apparatus was modified so that it contained a ceramic crucible of 3-mL capacity and a manually operated shutter located above the crucible. Both were positioned between two electrodes. The crucible was heated with coiled tungsten wire. The temperature was controlled by adjusting the voltage of the heater. The shutter was kept closed prior to sublimation, and sublimation was begun when the temperature reached 300-400 °C at 10.7 Pa of argon. This temperature, however, was at the outer surface of the crucible and thus was not equal to that of solid Pc. Without the shutter the film formed was sometimes granulated and was not uniform. Immediately after the shutter was opened, glow discharge was started. Typical conditions for the discharge were a distance between electrodes of 3.5 cm and a discharge power of 100 W at 13.56 MHz. Membrane thickness was measured by a laboratory-made multiinterference thickness meter (the use of which was through the generosity of Professor S. Kuriki, Institute of Applied Electronics, Hokkaido University). The thickness was linearly proportional to the period of polymerization, and 75 nm/s was observed (see Figure 1). As described below, the thickness of film was also estimated from the frequency difference before and after the polymerization. A film of about 0.5- $\mu\text{m}$  thickness was synthesized on the quartz surface.

**Apparatus.** The electric circuit for the quartz oscillator was made with TTL (33). Frequency output was measured by a universal counter (Iwatsu, Model SC7021) that was controlled by a microcomputer (NEC, PC9801), and the signals were also stored in the microcomputer. The detection limit of the frequency change of the counter was 1 Hz, and the time base was 1 s.

The cell employed was either batch or flow type, the batch type having a volume of 19.2 mL. After an appropriate volume of organic chemicals (typically 20  $\mu\text{L}$  or 10 mg) was introduced, the vessel was closed with a glass-ground lid and heated with hot air, followed by incubation in an air bath controlled at 25 °C for 3-6 h to attain equilibrium between gaseous and liquid or solid phases. A plasma-polymerized crystal fixed to the glass-ground lid was inserted to start the measurement. The concentration of organic compounds in the gaseous phase was calculated from the ideal gas law by using data of saturated vapor pressure taken

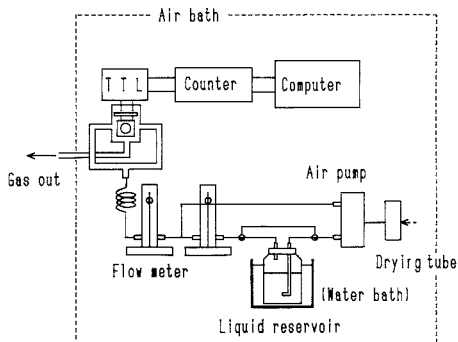


Figure 2. Scheme for flow-type cell experiments.

from refs 30–32. A similar method was employed by Okahata et al. (10).

The flow type cell was constructed in accordance with the method of Guilbault and colleagues (8, 9), and an experimental setup is shown schematically in Figure 2. An air stream containing organic compounds flowed directly onto both surfaces of the crystal. Air used as carrier gas was supplied by a vibrating diaphragm air pump and bubbled through a desired organic solvent to make an air stream containing test organic compounds. The experiment was performed in an air bath controlled at 25 °C, and a reservoir for the organic compounds was immersed in a water bath controlled at 25 °C. The flow rate was measured with a flowmeter and 2.7 L/min was usually employed. No significant effect was observed by the change of flow rate. The concentration of organic compounds in the air stream was calculated from the loss of organic compounds in the reservoir divided by the volume of air bubbled through the reservoir. A desired concentration of evaporated organic compounds was prepared by mixing the air stream containing organic solvent and fresh air.

**Calculation of Partition Coefficient,  $K$ .** The partition coefficient  $K$  was defined as

$$K = C_m / C_v$$

where  $C_m$  and  $C_v$  stand for the concentration of a chemical in the adsorbent film and in the gaseous phase, respectively.  $C_v$  can be

calculated by assuming the ideal gas law.  $C_m$  can be calculated as follows:

$$C_m = W / V_m = \frac{(\Delta F / M_w) / C}{(\Delta F^0 / \rho) / C} = \frac{\Delta F / M_w}{\Delta F^0 / \rho}$$

where  $W$  stands for the number of moles adsorbed to the membrane on the quartz crystal and equals  $(\Delta F / M_w) / C$ .  $\Delta F$ ,  $M_w$ , and  $C$  are the frequency changes due to adsorption of chemicals, the molecular weight of the chemicals, and the constant describing the relation of the amount of adsorbed chemical to the frequency change of 1 Hz (1.58 ng/1 Hz), respectively.  $V_m$  stands for the volume of the Pc film,  $\Delta F^0$  is the frequency change before and after the polymerization on the crystal, and  $\rho$  is the density of the film (taken to be unity);  $V_m$  is estimated from the amounts of polymerized Pc. The validity that  $\rho$  is taken to be unity is shown as follows: When 20  $\mu\text{g}$  was polymerized on a surface area of 0.392  $\text{cm}^2$ , the thickness was 0.5  $\mu\text{m}$ . Hence  $\rho = 20 \mu\text{g} / (0.392 \text{ cm}^2 \times 0.5 \mu\text{m}) = 1.02 \text{ g}\cdot\text{cm}^{-3}$ .

## RESULTS AND DISCUSSION

### Characterization of the Plasma-Polymerized Film.

The film formed is not dissolved by concentrated  $\text{H}_2\text{SO}_4$  or pyridine, which are good solvents for the monomer. Elemental analysis of the film showed 64.86% C (that of the monomer is 66.72%), 2.75% H (2.80%), and 18.95% N (19.45%), indicating that the values of C and N were smaller than those of the monomer. Elemental analysis data of an evaporated film were not changed from those of the starting material, which were equal to the theoretical values within 0.1%. These facts suggest the formation of a network of polymer chains.

UV and visible spectra (Figure 3a) showed absorption near 550–700 nm (Davydov splitting) and 320 nm (Soret band), which is characteristic of Pc. The Soret band was not different from that of the vapor-deposited film, but the intensity of the Davydov splitting was reduced. This spectrum change implies that interaction between Pc molecules is weakened and/or the spacing of Pc is increased in comparison with the evaporated film.

Figure 3b shows Fourier transform infrared (FT-IR) data obtained with a Nicolet Model 5DX-S by the diffusion-reflection method, showing that the spectrum of plasma-polymerized film is essentially the same as that of the vapor-deposited Pc except for the broadening: Absorption bands

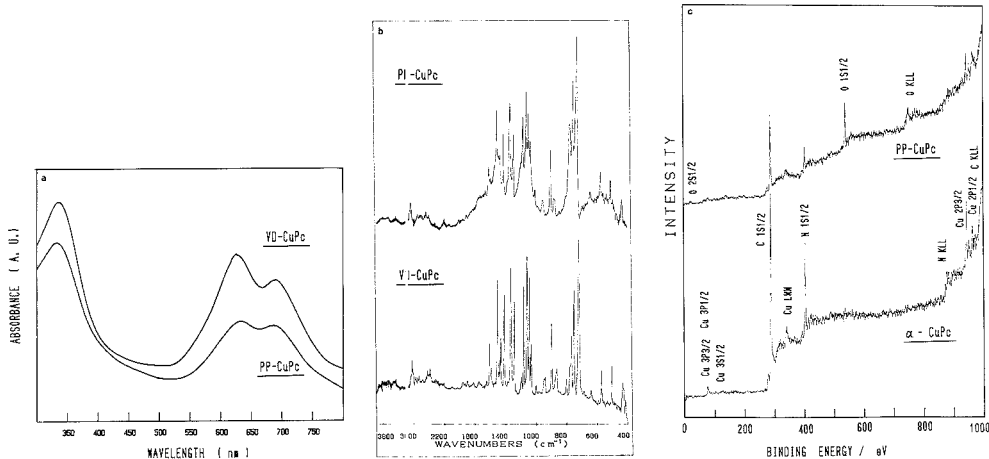
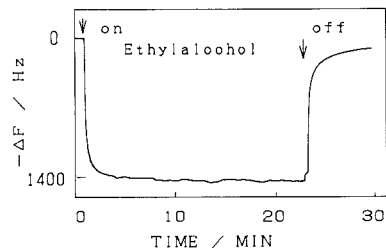


Figure 3. Characterization of the plasma-polymerized film. Here, pp-CuPc means the plasma-polymerized Cu Pc, and  $\alpha$ -CuPc and VD-CuPc stand for pure Cu Pc and a vapor-deposited film of Cu Pc, respectively. (a) UV and visible spectra of plasma-polymerized (lower) and vapor-deposited film (upper). The spectra are shifted vertically for clarity. (b) FT-IR spectra. The higher spectrum is the plasma-polymerized, and the lower is the vapor-deposited film. (c) ESCA spectra of plasma-polymerized (upper) and starting pure Pc (lower). ESCA spectra (using Mg K  $\alpha$ ) were obtained with a VG ESCA 3 (VG Scientific, Sussex) with vacuum of  $1 \times 10^{-9}$  Torr ( $1.33 \times 10^{-7}$  Pa) and X-ray power of 120 W (10 mA, 12 kV). The assignment of ESCA peaks is shown.



**Figure 4.** Typical example of time course of a frequency decrease by the application of  $2.78 \times 10^4$  ppm of ethyl alcohol. At the time shown by "on", the flow of air containing ethyl alcohol was begun, and at the time shown by "off", ethyl alcohol was purged by a stream of air.

due to C-H stretching near  $3000 \text{ cm}^{-1}$ , C-H bending at  $1740\text{--}1370 \text{ cm}^{-1}$ , N-H bending near  $1600 \text{ cm}^{-1}$ , and C=N stretching at  $1460\text{--}1500 \text{ cm}^{-1}$  are observed, but they are broadening. The ring structure of Pc is reserved in the plasma-polymerized film.

The ESCA (electron spectroscopy for chemical analysis) spectrum (Figure 3c) was essentially the same as that of the starting pure Pc when widely scanned spectra were compared. Detailed comparison showed the presence of  $\text{O}_{1s}$  in the plasma-polymerized film and the appearance of a component of  $\text{C}_{1s}$  with a higher energy level (data not shown), suggesting the presence of an oxidized carbon chain. Oxygen may be coming from air; plasma-polymerized polymer has radicals, which react with  $\text{O}_2$  or  $\text{H}_2\text{O}$  in air to form OH or COOH groups after the polymer is removed from the reaction bell jar (23). From these facts, we may conclude that the film formed retains the essential features of Pc, although some oxidation may occur.

Osada and his colleagues (24) reported a SEM (scanning electron microscope) photograph of plasma-polymerized Pc ( $\times 3000$ ), revealing that the polymerized membrane had a flat smooth surface. The measurement for the surface roughness with the method of Taly-Step showed that the surface roughness was within 3%. Although their photograph was obtained with the film coated on flat glass, it is likely that the surface of the film coated on the quartz crystal is smooth. This is reasonable because the plasma polymerization proceeds so as to plug depression of the surface (23). The surface of a plasma-polymerized tetraphenylborate membrane formed on a Millipore filter paper was smooth according to the SEM photograph (25), although a Millipore filter has rough surfaces.

**Response of Plasma-Polymerized PC.** Figure 4 shows typical data of frequency decrease in response to ethyl alcohol at a concentration of  $2.78 \times 10^4$  ppm. (Here, ppm is defined as  $10^{-6}$  mol per 1 mol of air as carrier gas.) The decrease reached a steady value about 4–5 min after the onset. Purging of ethyl alcohol with air reversed the frequency change. The rate seemed to be somewhat slower than that of the onset, and the kinetic trace appeared to have two components. The extent of the frequency changes was  $1400 \pm 70$  ( $n = 5$ ).

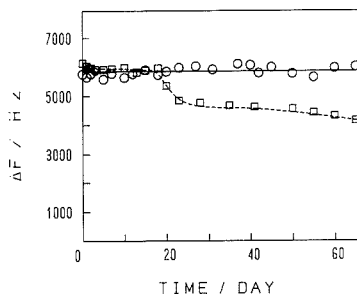
The frequency decreases caused by adsorption of ethyl alcohol ( $2.78 \times 10^4$  ppm) were measured by varying the amount of Pc on the crystal. Here, the amount of Pc was estimated from the frequency change due to polymerization on the crystal surface, assuming that a decrease of 0.633 Hz corresponded to 1 ng of adsorption, as described in the Experimental Section. The linear relation held up to  $30 \mu\text{g}$  of Pc (data not shown), indicating that the amount of adsorbed ethyl alcohol is proportional to the volume of plasma-polymerized Pc.

Table I shows the frequency change brought about by the ethanol sorption to various coating materials on a crystal

**Table I. Comparison of Responses to Ethyl Alcohol When Various Coating Materials Are Used on the Crystal<sup>a</sup>**

film material	$\Delta F$ , Hz	film material	$\Delta F$ , Hz
plasma-polymerized Pc	1400	plasma-polymerized	60
evaporated Pc	1420	naphthalene	
polystyrene	600	plasma-polymerized	950
poly(vinyl chloride)	500	tetraphenylborate	
		none	20

<sup>a</sup> Amounts of coating materials were kept constant at  $20 \mu\text{g}$ . None means the quartz surface without any treatment. Experiments were done with a flow type cell. The concentration of ethanol was  $2.78 \times 10^4$  ppm, and the flow rate was 2.7 L/min.



**Figure 5.** Long lifetime of plasma-polymerized film on quartz. The frequency changes of the oscillator with plasma-polymerized Cu Pc (open circles) and of that with vapor-deposited Pc film (open squares) in response to  $1.04 \times 10^5$  ppm ethyl alcohol are plotted against the days. After 20 days the response of the deposited film had decreased while no damage to the plasma-polymerized film was observed. The amounts of Cu Pc in both films were  $25 \mu\text{g}$ .

surface. The amounts of coating materials remained constant at  $20 \mu\text{g}$ , confirming the benefits of Pc as an adsorption material.

**Long Lifetime of Plasma-Polymerized Film.** As described in the Introduction, plasma-polymerized film is expected to be long-lived. Figure 5 shows that this expectation proves to be true. Frequency changes of the oscillator with plasma-polymerized Pc and of that with vapor-deposited Pc film in response to  $1.04 \times 10^5$  ppm ethyl alcohol were plotted against days. During these experiments (performed at  $30^\circ\text{C}$ ), both films were subjected to a daily vapor application and a purge with air (5 L/min). After 20 days, the response of the oscillator with vapor-deposited film was lowered, perhaps due to the loss of Pc, while the response of the plasma-polymerized oscillator remained the same for as long as 60 days. The average of the response of the plasma-polymerized oscillator for 60 days was  $5852.5 \pm 151.9$  (mean  $\pm$  standard deviation).

**Sensitivity and Partition Coefficient.** Figure 6 shows the linear relationship between frequency change and gas concentration observed when the flow type cell is used. For chemicals whose evaporation velocity is slow, the flow cell method was not applicable, so we used the batch cell. With this type cell, however, changing of the concentration of test chemicals is difficult, and we therefore assumed a linear relationship between the frequency decrease and the concentration. Table II summarizes the magnitude of the frequency decrease of the crystal in response to various organic chemicals. The second column from the right represents the response sensitivity (Hz/ppm), which means the magnitude of the frequency change per 1 ppm. This table indicates that the sensitivity ranges from 670 to 0.001 Hz/ppm and that the present crystal system responds well to benzyl alcohol, nitrobenzene, aniline, naphthalene, benzoic acid, phenol, diphenyl, *n*-pentyl alcohol, *n*-octyl alcohol, *n*-decyl alcohol,

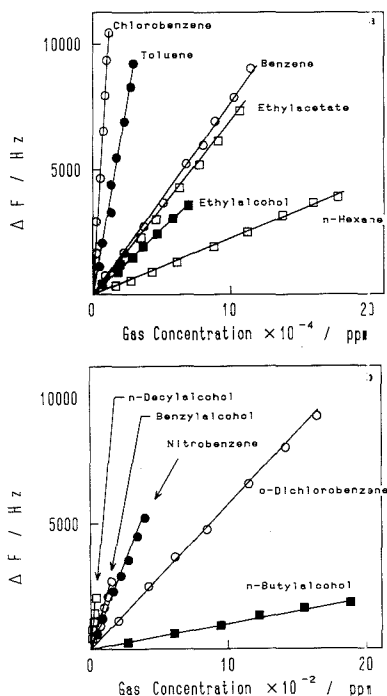


**Figure 6.** Linear relationship between frequency decrease and gas concentration. Organic solvents used are noted.

$\beta$ -ionone, vanillin, etc. The human threshold values (in ppm) for sensation (34, 35) are as follows: benzyl alcohol, 5.5; nitrobenzene, 2.7; aniline, 70; naphthalene, 6.8; benzoic acid, 85; phenol, 5.9; *n*-octyl alcohol, 0.13;  $\beta$ -ionone, 73; vanillin,  $1.87 \times 10^{-7}$ . On the other hand, when a 10-Hz change of frequency is taken as the minimal distinguishable change, the detection limits (in ppm) of the present plasma-polymerized Pc-quartz system are as follows: benzyl alcohol, 0.58; nitrobenzene, 0.78; aniline, 0.70; naphthalene, 0.68; benzoic acid, 0.053; phenol, 0.67; *n*-octyl alcohol, 0.32;  $\beta$ -ionone, 0.015; vanillin, 0.017. Except for vanillin and *n*-octyl alcohol, the present crystal system can detect these chemicals 10 or 100 times more sensitively than man.

The definition and method of calculating the partition coefficient  $K$  were described in the Experimental Section. In Figure 7,  $\log K$  values are plotted against the carbon number of the alkanes and corresponding alcohols (Figure 7a) and against the carbon number of aromatic or ring compounds (Figure 7b). Figure 7a shows that values of the alcohols are larger than those of the corresponding hydrocarbons. For example, a value of octanol is about 178 times that of octane, even though they have the same number of carbon atoms. The differences in  $K$  between hydrocarbons and corresponding alcohols are larger as the number of carbons decreases. In Figure 7b, when the hydrogen of benzene is substituted by Cl,  $\text{OCH}_3$ , OH,  $\text{NH}_2$ , or COOH, the sensitivity increases; the difference between benzene and benzoic acid is about 1698-fold. We obtained good correlation between  $\log K$  of benzene derivatives and absolute value of Hammett numbers. It is interesting that the absolute value, not the Hammett number itself, correlates with  $\log K$ , suggesting that the polarization of adsorbing molecules is one of the important factors. Thus, molecules having polar substitutions show high

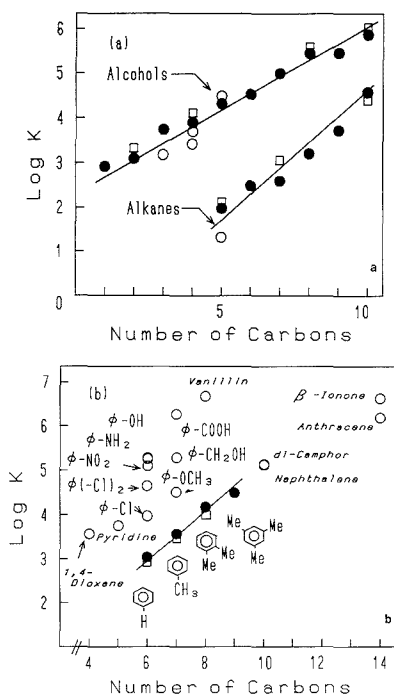


**Figure 7.** Values of  $\log K$  plotted against number of carbons. (a) Data for alkanes and alcohols. Closed circles represent normal alkanes and alcohols, while open circles represent branched ones. (b) Data for aromatics and some ring compounds. Compound names are written in the figure. Closed circles represent data for  $(\text{CH}_3)_n$ -substituted benzene ( $n = 0-3$ ). The line is a regression line for these closed circles, and it is interesting that the slope of the line in this figure is nearly equal to that of the line of alkanes in part a. The value of  $K$  was increased when the H of benzene was substituted by  $\text{CH}_3$ ,  $\text{C}_2\text{H}_5$ ,  $\text{OCH}_3$ ,  $\text{NO}_2$ ,  $\text{NH}_2$ , OH,  $\text{CH}_2\text{OH}$  and COOH. Squares in both parts a and b were obtained with vapor-deposited film.

affinity for the film. This property is not due to the plasma polymerization, because the vapor-deposited film also displays this property (squares indicate the data of evaporated Pc).

It is very interesting that the slope of the line for the alkanes is equal to that of  $(\text{CH}_3)_n$ -substituted benzene ( $n = 0-3$ ). Analysis of this phenomenon is now in progress in this laboratory. In addition, we found that the values of  $\log K$  for various compounds can correlate well with some parameters such as Hammett number, Taft number, and modified Small's number. Details will be published elsewhere.

**Comparison of Response Sensitivity with Previous Studies.** Okahata and Shimizu (10) made a device of piezoelectric quartz covered with multilayers of an amphiphatic compound for gas detection. The magnitudes of frequency decrease reported in this paper are about 10 times greater than their values. Since the film thickness and area are almost equal, the partition coefficient of plasma-polymerized Pc is 10 times larger than their values, meaning that Pc is a good adsorbent.

Sanchez-Pedreno et al. (11) investigated coating materials for detection of nitrobenzene, and various materials such as charcoal, poly(ethylene glycol), quadrol, tetrabase, and triethanolamine gave a frequency decrease of 136-140 Hz in response to 7 ppm of nitrobenzene. The present system gives 90 Hz. It is noted that the basic resonance frequency of their system was 15 MHz, and that of ours is 9 MHz. According

Table II. Frequency Change and Sensitivity to Various Organic Compounds<sup>a</sup>

chemicals	$\Delta F$	concn, ppm	sensitivity, Hz/ppm	log K	chemicals	$\Delta F$	concn, ppm	sensitivity, Hz/ppm	log K
acetic acid	16160	$2.0 \times 10^4$	0.808	4.22	ethyl cyclohexane	10801	$1.67 \times 10^4$	0.647	3.85
acetone	4674	$2.95 \times 10^5$	0.016	2.58	ethylene glycol	2901	$1.32 \times 10^2$	22.0	5.47
isoamyl alcohol	10519	$4.70 \times 10^3$	2.24	4.49	ethyl ether	7047	$7.28 \times 10^5$	0.010	2.20
<i>n</i> -amyl alcohol	5484	$3.67 \times 10^3$	1.49	4.32	<i>n</i> -heptane	1930	$6.01 \times 10^4$	0.032	2.59
aniline	7896	$5.53 \times 10^2$	14.3	5.27	1-heptanol	4760	$5.00 \times 10^2$	9.52	5.00
anisole	12297	$4.34 \times 10^3$	2.83	4.51	<i>n</i> -hexane	4194	$1.99 \times 10^5$	0.021	2.48
anthracene	779	3.47	224	6.19	1-hexene	3699	$2.43 \times 10^5$	0.015	2.34
benzene	9221	$1.32 \times 10^5$	0.07	3.04	<i>n</i> -hexyl alcohol	6053	$2.12 \times 10^3$	2.86	4.53
benzoic acid	1922	10.2	188	6.27	$\beta$ -ionone	8692	$1.30 \times 10^1$	667	6.63
benzyl alcohol	2620	$1.51 \times 10^2$	17.3	5.29	mesitylene	10416	$3.42 \times 10^3$	3.05	4.49
bicyclohexyl	9726	$1.97 \times 10^2$	49.4	5.56	methyl alcohol	3694	$1.68 \times 10^5$	0.022	2.92
<i>n</i> -butyl alcohol	4108	$8.47 \times 10^3$	0.485	3.90	methylcyclopentane	6041	$1.80 \times 10^5$	0.034	2.69
isobutyl alcohol	4437	$1.46 \times 10^4$	0.304	3.70	naphthalene	1598	$1.09 \times 10^2$	14.6	5.14
sec-butyl alcohol	4233	$2.66 \times 10^4$	0.16	3.41	nitrobenzene	5415	$4.21 \times 10^2$	12.9	5.11
alcohol					nonane	3365	$6.03 \times 10^3$	0.558	3.73
<i>n</i> -butyraldehyde	6379	$1.5 \times 10^5$	0.043	2.86	1-nonanol	1901	$3.16 \times 10^1$	60.2	5.47
<i>tert</i> -butyl alcohol	2707	$5.47 \times 10^4$	0.049	2.91	<i>n</i> -octane	2876	$1.88 \times 10^4$	0.15	3.21
DL-camphor	4330	$2.66 \times 10^2$	16.29	5.12	1-octanol	4070	$1.32 \times 10^2$	30.9	5.46
carbon	21339	$1.52 \times 10^5$	0.141	3.05	1-octene	5964	$2.29 \times 10^4$	0.26	3.45
tetrachloride					<i>n</i> -pentane	3842	$6.74 \times 10^5$	0.006	1.98
chlorobenzene	13064	$1.50 \times 10^4$	0.87	3.97	isopentane	1117	$9.05 \times 10^5$	0.0012	1.32
chloroform	5387	$2.56 \times 10^5$	0.021	2.33	$\beta$ -pentanol	4867	$1.15 \times 10^4$	0.423	3.77
cumene	9327	$6.41 \times 10^3$	1.46	4.17	$\beta$ -phenethyl alcohol	12823	$2.36 \times 10^2$	54.3	5.73
cyclohexane	8251	$6.05 \times 10^4$	0.136	2.80	phenol	13354	$8.95 \times 10^2$	14.9	5.29
cyclohexanol	3067	$1.78 \times 10^3$	1.72	4.32	phenyl ether	7419	$3.59 \times 10^4$	0.206	3.17
cyclohexane-carboxylic acid	1679	42.1	39.9	5.58	$\gamma$ -picoline	9667	$7.89 \times 10^3$	1.23	4.21
cyclohexanone	3384	$6.51 \times 10^3$	0.52	3.81	$\alpha$ -pinene	9056	$6.47 \times 10^3$	1.40	4.10
cyclohexyl-benzene	10219	78.9	130	5.99	1-propanol	6469	$2.39 \times 10^4$	0.270	3.74
cyclopentane	4732	$4.17 \times 10^5$	0.011	2.30	propionaldehyde	13231	$7.08 \times 10^5$	0.019	2.59
<i>p</i> -cymene	4401	$1.97 \times 10^3$	2.23	4.31	isopropyl alcohol	4315	$5.86 \times 10^4$	0.074	3.18
decaline	7359	$1.03 \times 10^3$	7.14	4.80	propylene glycol	3644	$1.58 \times 10^2$	23.1	5.74
<i>n</i> -decane	9274	$2.08 \times 10^3$	4.46	4.58	pyridine	9564	$2.63 \times 10^4$	0.363	3.75
1-decene	6993	$2.14 \times 10^3$	3.27	4.45	pyrogallol	250	2.33	107	6.02
<i>n</i> -decyl alcohol	1804	$1.84 \times 10$	97.9	5.88	salicylic acid	1787	2.72	657	6.76
<i>o</i> -dichlorobenzene	9651	$1.80 \times 10^3$	5.35	4.65	styrene	9353	$8.3 \times 10^5$	1.13	4.12
dichloromethane	17971	$5.74 \times 10^5$	0.031	2.65	tetrahydrofuran	5894	$2.32 \times 10^5$	0.025	2.63
1,4-dioxane	14195	$5.26 \times 10^4$	0.27	3.57	toluene	9236	$3.30 \times 10^4$	0.28	3.57
ethyl acetate	7700	$1.21 \times 10^5$	0.064	2.95	vanillin	1035	1.73	596	6.68
ethyl alcohol	3717	$7.76 \times 10^4$	0.048	3.10	water	1333	$3.13 \times 10^4$	0.043	3.46
ethylbenzene	6957	$1.25 \times 10^4$	0.557	3.81	<i>o</i> -xylene	11241	$8.76 \times 10^3$	1.28	4.17

<sup>a</sup>The concentration (ppm defined as  $10^{-6}$  mol/mol of air) was calculated from vapor pressure taken from an appropriate book (31–33), assuming the ideal gas law. The sensitivity is defined as the frequency change divided by concentration ( $\Delta F$ /ppm); i.e. it corresponds to the magnitude of frequency change per 1 ppm. The definition of the partition coefficient is referred to the text.

to Sauerbrey's equation (1), if we use a 15-MHz oscillator covered with plasma-polymerized Pc, the calculated frequency change is  $90 \times (15/9)^2 = 167$  Hz, which is somewhat larger than their value of 136–140 Hz.

Guilbault and his colleagues (8) constructed a piezoelectric toluene sensor capable of detecting 30–300 ppm toluene. A similar concentration range of toluene can be detected, although it is noted that the present system is not too sensitive to this substance (see Table II).

**Effect of the Central Metal.** Table III shows the effect of a central metal of phthalocyanine (PC) or tetraphenylporphyrin (Por) on the sensitivity of *n*-octyl alcohol, naphthalene, benzoic acid, and anisole. The values listed in this table are all positive, meaning that the presence of central metals increases K. It is very interesting that anisole is adsorbing at Pb Pc or Mn Pc about 10 times more than other Pc and that naphthalene is adsorbing at Cu Pc or Fe Pc (not Por). The reason is not clear at present.

**Concluding Remarks.** This paper shows that Pc can be plasma-polymerized successfully on the surface of piezoelectric quartz and that the film formed is very stable and adheres strongly to the surface. After 60 days of use, no damage was

Table III. Influence of the Central Metal on log K<sup>a</sup>

membrane	$\Delta \log K$			
	1-octanol	naphthalene	benzoic acid	anisole
CuPc	0.03	1.05	0.88	0.13
FePc	0.33	1.08	0.51	0.15
FePor	0.23	0.79	0.40	0.20
MnPc	0.15	0.85	0.49	1.32
CoPc	0.02	0.64	0.53	0.07
PbPc	0.04	0.4	0.31	1.32
VoPc	0.39	0.68	0.42	0.09
H <sub>2</sub> Pc				

<sup>a</sup>Influence of the central metal of plasma-polymerized Pc or Fe tetraphenylporphyrin on log K for 1-octanol, naphthalene, benzoic acid, and anisole. Differences from plasma-polymerized H<sub>2</sub>Pc are listed.

found. Barendsz et al. (19, 20), Ricco et al. (21), and Roberts et al. (22) fabricated a SAW device covered with a thin film of Pc and succeeded in obtaining a highly selective and sensitive response to halogen gases and NO<sub>2</sub> gases. A gradual decrease of the sensitivity was found, however, since operation



of the device was performed at 150 °C, and gradual loss of the film occurred, possibly due to the sublimation (17). This study suggests that the use of plasma-polymerized Pc on an SAW device may provide a good gas sensor. The next aim of the experiment is to show that plasma-polymerized Pc membrane has long life even when it is operated at 150 °C and when halogen gas and NO<sub>2</sub> gas are applied.

Many organic chemicals show sorption to phthalocyanine. Especially, plane molecules having conjugate double bonds and some polar substituting groups or higher alcohols, such as vanillin, benzoic acid, aniline, nitrobenzene, phenol, *n*-octyl alcohol, 1-nonanol, *n*-decyl alcohol, benzyl alcohol, DL-camphor,  $\beta$ -ionone, naphthalene, and anthracene, have strong affinity to plasma-polymerized Cu Pc film. A chemical having several aromatic rings is considered to be a mutagen. It has been shown that Pc and related compounds adsorb a mutagen having aromatic rings (36), which is consistent with the present data.

The preliminary results on the influence of the central metal of phthalocyanine suggest that there are certain combinations of phthalocyanine and chemicals that show different selectivity from one another. Carey and Kowalski (12) made an array of piezoelectric crystals whose selectivities for gases were different and attempted to construct a sensor that could identify both quantitatively and qualitatively. For this array, the use of piezoelectric crystals with plasma-polymerized Pc films containing various central metals would allow realization of a sensitive and stable sensor.

#### ACKNOWLEDGMENT

The authors are indebted to Y. Osada (Ibaraki University) for his guidance in plasma polymerization of Pc, to S. Kuriki (Hokkaido University) for permission to use the multiinterference thickness meter, and to Y. Sanada and T. Yokono (Hokkaido University) for permission to use their Nicolet FT-IR. We thank Toyo Ink Co. and Asada Kagaku Co. for their generous gift of ultrapure Cu Pc and other Pc, Y. Iijima, JEOL, for discussion of ESCA spectra, and T. Kawasaki, Takasago-kouryou, for teaching us the threshold values of human odor sensation. Finally, the authors express their thanks to reviewers for their invaluable suggestions and comments during the review process.

#### LITERATURE CITED

- (1) Sauerbrey, Guenter. *Z. Phys.* **1959**, *155*, 206-222.
- (2) King, William H., Jr. *Anal. Chem.* **1964**, *36*, 1735-1739.
- (3) Hlavay, Joseph; Guilbault, George G. *Anal. Chem.* **1977**, *49*, 1890-1898.
- (4) Alder, John F.; McCallum, John J. *Analyst* **1983**, *108*, 1169-1189.
- (5) Guilbault, George G.; Lu, S. S.; Czanderna, A. W. *Application of Piezoelectric Quartz Crystal Microbalances*; Elsevier: New York, 1984; Chapters 8 and 10.
- (6) Janata, Jiri; Bezegh, Andras. *Anal. Chem.* **1988**, *60*, 62R-74R.
- (7) Lai, Colin S. I.; Moody, Gwilym J.; Thomas, John D. R. *Analyst* **1986**, *111*, 511-515.
- (8) Ho, Mat H.; Guilbault, George G.; Rifetz, Bernd. *Anal. Chem.* **1980**, *52*, 1489-1492.
- (9) Ho, Mat H.; Guilbault, George G.; Scheide, Eugene P. *Anal. Chim. Acta* **1981**, *130*, 141-147.
- (10) Okahata, Yoshiro; Shimizu, Osamu. *Langmuir* **1987**, *3*, 1171-1172.
- (11) Sanchez-Pedreno, J. A. O.; Drew, Peter K. P.; Alder, John F. *Anal. Chim. Acta* **1986**, *182*, 285-291.
- (12) Carey, Patrick, W.; Kowalski, Bruce R. *Anal. Chem.* **1988**, *60*, 541-544.
- (13) Edmonds, T. E.; West, Thomas S. *Anal. Chim. Acta* **1980**, *117*, 147-157.
- (14) Elmosalamy, M. A. F.; Moody, G. J.; Thomas, J. D. R.; Kohnke, F. A.; Stoddart, J. F. *Anal. Proc.* **1989**, *26*, 12-15.
- (15) Oirschot, Th. G. J. V.; Leeuwen, D. V.; Medema, J. J. *Electroanal. Chem. Interfacial Electrochem.* **1972**, *37*, 373-385.
- (16) Sadaoka, Yoshihiko; Sakai, Yoshiro; Yamazoe, Noboru; Seliyama, Tetsumo. *Denki Kagaku* **1982**, *50*, 456-462.
- (17) Robert, von Ewyk L.; Chadwick, Alan V.; Wright, John D. J. *Chem. Soc., Faraday Trans. 1* **1980**, *76*, 2194-2205.
- (18) Chadwick, Alan V.; Dunning, Patricia V.; Wright, John D. *Mol. Cryst. Liq. Cryst.* **1986**, *134*, 137-153.
- (19) Nieuwenhuizen, Marten S.; Nederlof, Arnold J.; Barendsz, Anton W. *Anal. Chem.* **1988**, *60*, 230-235.
- (20) Nieuwenhuizen, Marten S.; Barendsz, Anton W. *Sens. Actuators* **1987**, *11*, 45-62.
- (21) Ricco, A. J.; Martin, S. J.; Zipperian, T. E. *Sens. Actuators* **1985**, *8*, 319-333.
- (22) Roberts, G. G.; Holcroft, B.; Ross, J.; Barraud, A.; Richard, J. *Bri. Polym. J.* **1987**, *19*, 401-407.
- (23) Yasuda, Hirotosugu. *Plasma Polymerization*; Academic Press: New York, 1985.
- (24) Osada, Yoshihito; Mizumoto, Akira; Tsuruta, Hiroaki. *J. Macromol. Sci. Chem.* **1987**, *A24*, 403-418.
- (25) Kurosawa, Shigeru; Kamo, Naoki; Kobatake, Yonosuke; Toyoshima, Isamu. *J. Membr. Sci.* **1989**, *46*, 157-166.
- (26) Osada, Yoshihito; Mizumoto, Akira. *J. Appl. Phys.* **1986**, *59*, 1776-1779.
- (27) Osada, Yoshihito; Ohta, Fumihiko; Mizumoto, Akira; Takase, Mitsuo; Kurimura, Yoshimi. *Nippon Kagaku Kaishi* **1986**, *7*, 866-872.
- (28) Osada, Yoshihito. *Membrane (Tokyo)* **1985**, *10*, 215-223.
- (29) Shinkai, Seiji; Ishihara, Midori; Manabe, Osamu; Mizumoto, Akira; Osada, Yoshihito. *Chem. Lett.* **1985**, 1029-1032.
- (30) Nomura, Toshiaki; Nagamune, T. *Anal. Chim. Acta* **1983**, *155*, 231-234.
- (31) Weast, Robert C.; Astle, Melvin, J. Eds. *Handbook of Chemistry and Physics*, 69th ed.; CRC Press: Boca Raton, FL, 1988.
- (32) Asahara, Syouzou, Tokura, Jinichiro, Eds. *Solvent Handbook*; Kodansha Scientific: Tokyo, 1976.
- (33) Nippon Kagakukai, Ed. *Kagaku Binran Kisoheh (Chemical Table)*, 3rd ed.; Maruzen: Tokyo, 1984.
- (34) Appell, Lois. *Am. Perfum. Cosmet.* **1964**, *79*, 25-39.
- (35) Stahl, W. H. *ASTM Data Ser. No. DS 48*, 1973.
- (36) Hayatu, Hikoya; Oka, Takanori; Wakata, Akihiko; Ohara, Yoshiko; Hayatu, Toshiro; Kobayashi, Hiroshi; Arimoto, Sakae. *Mutation Res.* **1983**, *119*, 233-238.

RECEIVED for review May 1, 1989. Accepted October 26, 1989.

# Binding Studies Using Ion-Selective Electrodes. Examination of the Picrate-Albumin Interaction as a Model System

Theodore K. Christopoulos<sup>1</sup>

Laboratory of Analytical Chemistry, University of Athens, 104 Solonos Street, Athens 106 80, Greece

Eleftherios P. Diamandis\*<sup>2</sup>

Department of Clinical Biochemistry, Toronto Western Hospital, 399 Bc thurst Street, Toronto, Ontario M5T 2S8, Canada

We are studying the binding of ligands to macromolecules by using ligand ion selective electrodes as transducers. The picrate-bovine albumin interaction is examined in detail as a model system. A picrate ion selective electrode is used to monitor the free picrate concentration directly in the presence of albumin and bound ligand. The binding parameters are estimated and the effect of protein concentration, ionic strength, pH, and temperature is studied. The experimental data are interpreted with a specially designed computer program that performs nonlinear least-squares fitting of the generalized Scatchard model with an infinite number of classes of binding sites directly to the raw potentiometric data. The binding parameters (binding constant and maximum number of ligands that can be bound), the nonspecific binding as well as their standard deviations are estimated by this program. The principles described can be used for the potentiometric study of any ligand-binder interaction.

## INTRODUCTION

The interaction of small molecules (ligands) with biological macromolecules has attracted increasing interest during the last 20-30 years because it was realized that such interactions are involved in many regulatory and defence mechanisms, in metabolic pathways and in the expression of the pharmacologic action of many drugs. More specifically, it is now well-known that most drugs, during their transport through the blood circulation, bind reversibly to blood constituents, e.g. albumin, globulins, lipoproteins, etc. This binding influences both the intensity and duration of the pharmacologic action because only the free drug is able to reach the sites of the pharmacologic action (receptors) or drug metabolism (1).

All binding studies are focused on the determination of the binding parameters i.e. (a) the maximum number of ligands that can be bound to a macromolecule and (b) the value of the binding constant. Other interesting aspects of binding are the structure of the binding sites and the forces that are involved in this process. The analytical methodology that has been applied to study binding phenomena is used primarily to measure the concentration of either the free (nonbound) or the bound ligand, usually under equilibrium conditions, in solutions-mixtures of known total concentration of both the ligand and the macromolecule (binder). These methods are either indirect or direct. In the indirect methods, the amount of bound or free ligand is measured after a physical separation of the two fractions. In the direct methods, this is not necessary because binding results in a change of a

physical property of the ligand, e.g. in the absorption or emission spectrum.

Examples of indirect methods include equilibrium (2-4) or dynamic (5) dialysis, ultrafiltration (6), gel filtration (6), and high-performance liquid chromatography (7). Examples of direct methods include absorption, fluorescence, nuclear magnetic resonance, or circular dichroism spectroscopy (2-4).

Ion-selective electrodes (ISE) are electrochemical transducers able to monitor directly the free ion activity (concentration) in a solution that contains both the free and the bound form. During the last 15 years, many studies have focused on the factors that affect the ISE response in complex biological solutions containing proteins and cells like serum and whole blood. These studies address the practical problems of measuring ions like H<sup>+</sup>, Na<sup>+</sup>, K<sup>+</sup>, Cl<sup>-</sup>, Ca<sup>2+</sup>, Mg<sup>2+</sup>, and Li<sup>+</sup> in biological fluids without or with minimal sample pretreatment or dilution. Currently, many such ions are measured routinely in biological fluids using ISE, which is now the preferred methodology over flame photometry (8, 9).

Although the results of monitoring free ion concentration in protein solutions using ISE are very encouraging, the use of such transducers in binding studies involving proteins as binders and inorganic or organic ions as ligands is very limited. The Mg<sup>2+</sup>- and Ca<sup>2+</sup> ISE have been used to study the binding of these ions to bovine and human serum albumin (10, 11). Similar studies have been published for Cu<sup>2+</sup> (12, 13). In these studies, the determination of the binding parameters was carried out either by graphical methods or by least-squares fitting of the hyperbola of the Scatchard plot to the experimental data. Similar methods were used to determine the parameters for the binding of bile acids to bovine serum albumin using an ISE for bile acids (14). An ISE for flufenamic acid has also been reported and its response studied in the presence of bovine albumin, but no binding parameters were determined (15). The ISE for dodecyl sulfate and octyl or decyl sulfate were used to study the binding of these ions to bovine albumin (16) and  $\beta$ -lactoglobulin (17), respectively. The estimation of the bound anion was based on the increase of the critical micelle concentration in the presence of the binder.

In this paper, we are examining the binding of ligands to macromolecules by using ligand ISE. In order to demonstrate the capabilities of the proposed system, we are using the picrate-bovine serum albumin interaction as a model. A picrate ISE (18) is used to monitor the free concentration of the ligand in the presence of albumin. The binding parameters are estimated, and the effect of the protein concentration, ionic strength pH, and temperature on the estimation of the binding parameters is studied.

We have also designed a computer program which performs nonlinear least-squares fitting of the generalized Scatchard model (ref 19, infinite number of classes of binding sites) directly to the raw (untransformed) experimental data, i.e.,

<sup>1</sup> Present address: Department of Clinical Biochemistry, Toronto Western Hospital, 399 Bathurst St., Toronto, ON M5T 2S8, Canada.

<sup>2</sup> Also: Department of Clinical Biochemistry, University of Toronto, 100 College St., Toronto, ON M5G 1L5, Canada.

to the pairs of electrode potential and total ligand concentration. The binding parameters and the nonspecific binding as well as their standard deviations are estimated by this program.

### EXPERIMENTAL SECTION

**Apparatus.** The picrate anion selective electrode was used with a single junction Ag-AgCl electrode as the external reference (Orion Model 90-01-00). Potential readings were obtained with a Corning Research pH/mV meter (Model 12) and recorded simultaneously on a strip-chart recorder (Radiometer) equipped with a high sensitivity unit (REA-112). The pH measurements were carried out with a combination glass electrode (Radiometer). A double-walled 50-mL beaker was used as the reaction cell. During binding studies, the temperature was kept constant ( $\pm 0.1$  °C) and the reaction mixtures were stirred with the aid of a magnetic stirrer.

**Reagents.** All chemicals used were of analytical reagent grade and deionized distilled water was used for solution preparation.

**Buffers.** The buffers used were phosphate, 0.1 M, for pH 6.5, 7.0, 7.4, 8.0, and 11.5 and borate, 0.1 M, for pH 9.0. The buffers were prepared by dissolving sodium dihydrogen phosphate or boric acid and adjusting the pH with a 10 M sodium hydroxide solution.

**Sodium Picrate Stock Solution (0.100 M).** Air-dried picric acid (22.91 g) (Fluka) was mixed with ~800 mL of water and the pH was adjusted with 10 M NaOH to 6.0. The final volume was then adjusted to 1 L with water. The solution was stored in an amber bottle at room temperature. More dilute solutions were prepared as needed, by dilution with buffer solutions.

**Bovine Serum Albumin (BSA) Solutions.** Bovine serum albumin (Cohn fraction V, albumin content 96–99 %, Sigma) was used. The albumin content of solutions is checked by weighing the residue after drying a certain volume for 2 h at 105 °C. Dilute BSA solutions for binding studies are prepared in various buffers as needed. These solutions are stored for no more than a week at 4 °C.

**Sodium Picrate–Bovine Serum Albumin Mixed Solutions.** These are prepared by mixing appropriate volumes of picrate and BSA solutions, as described in detail later.

**Procedures. Picrate-Ion Selective Liquid Membrane Electrode.** The preparation of the liquid ion exchanger and the characteristics of the picrate ion selective electrode have been described elsewhere (18). The liquid ion exchanger consists of the tetrapentylammonium-picrate ion pair, dissolved in 2-nitrotoluene (0.01 M). An Orion liquid membrane electrode body (Model 92) was used as the electrode assembly with the Millipore LCWPO 1300 PTFE porous membrane. The PTFE membrane was cut to the appropriate size and a stack of four was used to avoid any leakage of the organic phase. The internal reference solution was 0.1 M NaCl–0.01 M sodium picrate (saturated with silver chloride). When not in use, the electrode was kept in a  $10^{-2}$  M solution of sodium picrate.

**Calibration Curve of the Picrate ISE.** A 20.0-mL volume of the appropriate buffer solution is pipetted into the thermostated reaction cell, the picrate ISE and the reference electrode are immersed in it, and stirring at a constant rate is started. After 2–3 min, various increments of a  $3.00 \times 10^{-2}$  M sodium picrate solution are added. The electromotive force (emf) readings are recorded after stabilization to  $\pm 0.1$  mV (it takes about 30 s and remains constant for at least 2 min). The constant term,  $E'$ , and the slope,  $S$ , of the Nernst equation are calculated by regression analysis of the linear part of the graph.

**Potentiometric Study of the Picrate–BSA Interaction.** A 20.0-mL volume of a BSA solution (solution A) in the appropriate buffer is pipetted into the thermostated reaction cell, the picrate–ISE and the reference electrode are immersed in it, and stirring at a constant rate is started. After 2–3 min, an aliquot of a mixed solution that contains sodium picrate (0.03 or 0.1 M total concentration depending on the experiment) and BSA at a concentration equal to that of solution A is added. The volume added is such that the emf reading becomes equal ( $\pm 1$  mV) to that of the largest emf value of the linear part of the calibration curve (this value corresponds to a  $2 \times 10^{-5}$  M concentration of free picrate). Afterward, various increments of the mixed solution are added until the emf recorded reaches the lowest value of the linear part of the calibration curve (this corresponds to a  $10^{-2}$  M

concentration of free picrate). The emf readings are recorded after stabilization to  $\pm 0.1$  mV following each addition (we typically wait about 30 s but readings remain unchanged for at least 2 min after stabilization). During such binding experiments, the total BSA concentration is kept constant irrespective of the dilution that occurs due to the addition of picrate solution.

### THEORY AND CALCULATIONS

The free picrate concentration,  $F$ , after each addition, is calculated from the emf readings and the equation of the calibration curve. The bound picrate concentration,  $B$ , after each addition, is calculated from the equation

$$B = T - F \quad (1)$$

where  $T$  is the total picrate concentration after each addition.

In this work, we use the generalized Scatchard model (19) to describe the binding phenomena. The protein is considered to have an  $m$  number of distinct classes of independent and noninteracting binding sites. Class  $i$  contains an  $n_i$  number of individual sites that have the same affinity for the ligand. The site binding constant,  $K_i$ , characterizes the sites of the  $i$ th class. The concentration of bound ligand,  $B$ , is related to the above parameters as shown by eq 2 (19), where  $P_t$  is the total protein concentration. The second term of this equation takes account for the nonspecific binding of the ligand to the protein molecule,  $N_s$  being the nonspecific binding parameter (20, 21).

$$B = \sum_{i=1}^m \frac{n_i K_i F}{1 + K_i F} P_t + N_s F \quad (2)$$

After  $F$  is calculated from the calibration curve and  $B$  from eq 1, the Scatchard plot is constructed ( $B/F$  vs  $B$ ). From this plot the  $N_s$  parameter can be estimated by performing linear least-squares fitting of the  $B/F$  vs  $B$  data which are located at the last part of the plot. In this area, the plot is approximately parallel to the horizontal axis. The estimation of  $N_s$  in this manner is based on the fact that if the free ligand concentration becomes too high, the  $B/F$  ratio reaches a constant value that is equal to  $N_s$  (eq 2).

The knowledge of  $N_s$  allows for the construction of the corrected Scatchard plot, which is the plot of  $B_{\text{spec}}/F$  vs  $B_{\text{spec}}$  ( $B_{\text{spec}}$  specifically bound ligand). The value of  $B_{\text{spec}}$  is equal to  $B - N_s F$ . From the corrected Scatchard plot, approximate values for the binding parameters  $n$  and  $K$  are obtained by using the method of limiting slopes and intercepts described in detail in ref 22 assuming a model with two classes of binding sites. These graphically obtained parameters are used as initial estimates in a nonlinear least-squares fitting process that calculates the statistically "true" values. This process is described in detail below.

**Nonlinear Least-Squares Fitting of the Generalized Scatchard Model Directly to the Raw Experimental Data.** The total picrate concentration after each addition is selected as the independent variable and the emf as the dependent variable. The binding parameters and the total picrate concentration determine each time the free picrate concentration in the solution and this in turn determines the expected (calculated) emf,  $E_c$ . Because of the random errors that unequivocally accompany every analytical measurement, the observed emf,  $E_e$ , differs from the theoretically calculated one and the following equation holds:

$$E_i = (E_c)_i + e_i \quad (3)$$

where  $e_i$  is the experimental error at the  $i$ th emf measurement. The most probable values of the parameters  $n_j$ ,  $K_j$  ( $j = 1, \dots, m$ ), and  $N_s$  are those that minimize the sum of the squares of residuals.

$$\Phi = \sum_{i=1}^N w_i [E_i - (E_c)_i]^2 = \sum_{i=1}^N w_i e_i^2 \quad (4)$$

where  $N$  is the number of the experimental points and  $w_i$  is the statistical weight accompanying the  $i$ th emf measurement ( $w_i = \sigma_i^{-2}$ ,  $\sigma_i$  is the standard deviation of the  $i$ th emf value). The function  $\Phi$  is minimized when its partial derivatives with respect to the parameters become zero, i.e.

$$\frac{\partial \Phi}{\partial \theta_l} = 0 \quad \text{for } l = 1, \dots, p \quad (p = 2m + 1) \quad (5)$$

with  $\theta_l = n_l$  for  $l = 1, \dots, m$ ,  $\theta_l = K_l$  for  $l = m + 1, \dots, 2m$  and  $\theta_{2m+1} = N_s$ . Calculating the partial derivatives from eq 4 and introducing them in eq 5 give

$$\frac{\partial \Phi}{\partial \theta_l} = -2 \sum_{i=1}^N \frac{w_i e_i \partial(E_c)_i}{\partial \theta_l} \quad \text{for } l = 1, \dots, p \quad (6)$$

which can be expressed in matrix notation as

$$\mathbf{J}^T \mathbf{W} \mathbf{e} = 0 \quad (7)$$

where  $\mathbf{J}$  is the  $N \times p$  Jacobian matrix with elements  $J_{ij} = \partial(E_c)_i / \partial \theta_j$  (the symbol  $T$  as an exponent states the transpose of a matrix),  $\mathbf{W}$  is a  $N \times N$  diagonal matrix with  $W_{ii} = w_i$ , and  $\mathbf{e}$  is the  $N \times 1$  vector of the residuals  $e_i$ . Relationship 6 (or 7) is in fact a nonlinear system of  $p$  equations with  $p$  unknowns that is solved by an iterative process (23, 24). If  $\theta^{(0)}$ ,  $(\mathbf{E}c)_{T, \theta^{(0)}}$  and  $\theta$ ,  $(\mathbf{E}c)_{T, \theta}$  are the initial (guess) and the final (solution) parameter vectors, respectively, with the corresponding emf vectors, then a Taylor series expansion about  $(\mathbf{E}c)_{T, \theta^{(0)}}$  gives

$$(\mathbf{E}c)_{T, \theta} = (\mathbf{E}c)_{T, \theta^{(0)}} + \mathbf{J} \Delta \theta \quad (8)$$

where terms higher than the first order have been neglected.  $\Delta \theta$  is the parameter correction vector.

Substituting the vector  $\mathbf{e}$  from eq 3 into eq 7 yields

$$\mathbf{J}^T \mathbf{W} [\mathbf{E} - (\mathbf{E}c)_{T, \theta}] = 0 \quad (9)$$

After substituting  $(\mathbf{E}c)_{T, \theta}$  from eq 8 into eq 9 and rearrangement yields:

$$(\mathbf{J}^T \mathbf{W} \mathbf{J}) \Delta \theta = \mathbf{J}^T \mathbf{W} \mathbf{e} \quad (10)$$

Relationship 10 is a linear system of  $p$  equations with  $p$  unknowns. The correction vector can be provided by solving this system. The new parameter vector is then given by

$$\theta^{(1)} = \theta^{(0)} + \Delta \theta \quad (11)$$

When the above algorithm (Gauss-Newton) was applied for the fitting of the Scatchard model to the potentiometric binding data, it did not always converge and many times there was an increase rather than a decrease in the sum of squares of residuals during the iterative process. This happened because this algorithm does not assure that the  $(\mathbf{J}^T \mathbf{W} \mathbf{J})$  matrix will be in each iteration a positive definite. To overcome this problem, we applied the Marquardt-Levenberg modification (25) where the parameter correction vector is calculated by solving the linear system

$$(\mathbf{J}^T \mathbf{W} \mathbf{J} + \lambda \mathbf{D}) \Delta \theta = \mathbf{J}^T \mathbf{W} \mathbf{e} \quad (12)$$

where  $\lambda$  is a positive number and  $\mathbf{D}$  a diagonal matrix with elements  $D_{ii} = (\mathbf{J}^T \mathbf{W} \mathbf{J})_{ii}$ .

The iterative process has two loops. In the external one, initial parameter estimates are introduced and the vector of the expected emf values is calculated. The elements of the matrix  $\mathbf{J}$  and vector  $\mathbf{e}$  are then calculated and also the sum of the squares of residuals. Afterward, the elements of the  $(\mathbf{J}^T \mathbf{W} \mathbf{J})$  matrix and of the vector  $\mathbf{J}^T \mathbf{W} \mathbf{e}$  (eq 12) are calculated. At this point, the internal loop is started. An initial value is assigned to the parameter  $\lambda$ , the linear system (eq 12) is solved (by the Gauss-Jordan elimination method), and the correction vector  $\Delta \theta$  derived is added to the parameter values yielding better values. The new value of  $\Phi$  is then calculated and is compared with the previous one. If it is greater, then the

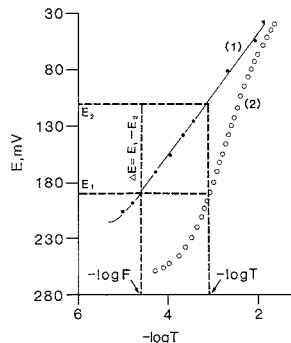


Figure 1. Calibration curves of the picrate ISE (1) and a plot of emf vs  $-\log T$  in the presence of BSA at a concentration of 32.0 g/L (2).

internal loop is repeated by increasing  $\lambda$  until an acceptable correction vector (which will decrease  $\Phi$ ) is yielded. In this case, the internal loop closes and a new external loop is started by entering the new parameter values as starting ones. The iterative process is terminated (converged) when the corrections of the parameters are less than 0.01% of their current values. An interactive computer program written in BASIC (for the IBM PC and for the AMSTRAD CPC computers) performs: the potentiometric binding data treatment, i.e., the calibration of the electrode, the calculation of the initial estimates of the binding parameters, and the nonlinear least-squares fitting. In addition, the calibration graph, the saturation plot, and the Scatchard plot are also constructed by the computer along with the corresponding calculated curves. Furthermore, the user has the option to fit several Scatchard models (variable number of classes of sites) searching for the best one without reloading the binding data.

The calculation of the expected emf value for each experimental point is carried out by first estimating the free picrate concentration as a function of the total picrate concentration and of the current values of binding parameters. This is accomplished by the Newton-Raphson approximative method (26) and is described in Appendix A. In Appendix B, the calculation of the partial derivatives of the electrode potential with respect to binding parameters is presented for the general form of the Scatchard model (infinite number of sites).

## RESULTS AND DISCUSSION

The principle of the application of ion-selective electrodes for the study of the binding of ionic ligands to macromolecules (e.g. proteins) is based on the fact that in a solution containing protein molecules, free ionic ligand, and protein bound ionic ligand, the ISE responds only to the free ionic ligand species. Because of their highly hydrophilic character, neither the protein molecules nor the protein-bound ions can penetrate into the organic solvent of the electrode membrane to cause a change in the emf.

A typical calibration curve ( $E$  vs  $-\log F$ ) of the picrate ISE as well as a plot of the emf vs  $-\log T$  in the presence of BSA are presented in Figure 1. Once the picrate binds to albumin it cannot be sensed by the electrode; thus, the observed emf is much higher in the presence of albumin (curve 2), in comparison to the same total picrate concentration and absence of albumin from the measuring solution. The theoretical slope of the emf vs  $\log T$  curve is given at any point by the derivative of the emf with respect to  $\log T$ . The following equation holds (chain rule):

$$\frac{dE}{d(\log T)} = \frac{dE}{d(\log F)} \frac{d(\log F)}{dF} \frac{\partial F}{\partial T} \frac{dT}{d(\log T)} \quad (13)$$

**Table I. Influence of the Protein Concentration on the Binding of Picrate to BSA<sup>a</sup>**

BSA, g/L	$n_1$	$10^{-3}K_1, M^{-1}$	$n_2$	$10^{-3}K_2, M^{-1}$	Ns	SD <sub>res</sub> , mV
20.0	1.64 (0.02)	39.0 (1.1)	4.7 (0.2)	0.89 (0.04)	0.27 (0.07)	0.2
32.0	1.83 (0.04)	42.1 (0.8)	4.9 (0.1)	0.92 (0.03)	0.39 (0.01)	0.1
50.0	1.70 (0.03)	37.7 (0.9)	4.4 (0.1)	0.93 (0.04)	0.59 (0.01)	0.2

<sup>a</sup>Numbers in parentheses are the standard deviations of the parameter values. <sup>b</sup>SD<sub>res</sub> is the standard deviation of residuals as defined in the text.

**Table II. Influence of Ionic Strength on the Binding of Picrate to BSA<sup>a</sup>**

[NaCl], M	$n_1$	$10^{-3}K_1, M^{-1}$	$n_2$	$10^{-3}K_2, M^{-1}$	Ns	SD <sub>res</sub> , mV
0.01	1.60 (0.04)	36.9 (1.5)	4.2 (0.1)	1.27 (0.09)	0.21 (0.01)	0.3
0.05	1.67 (0.03)	34.5 (0.9)	4.6 (0.1)	1.00 (0.05)	0.28 (0.01)	0.1
0.10	1.78 (0.02)	32.2 (0.5)	5.0 (0.1)	0.91 (0.03)	0.20 (0.01)	0.3
0.20	1.74 (0.04)	28.3 (0.8)	3.6 (0.1)	1.09 (0.09)	0.26 (0.01)	0.3

<sup>a</sup>See footnote of Table I for further explanations and abbreviations.

**Table III. Effect of pH on the Binding of Picrate to BSA<sup>a</sup>**

pH	$n_1$	$10^{-3}K_1, M^{-1}$	$n_2$	$10^{-3}K_2, M^{-1}$	Ns	SD <sub>res</sub> , mV
6.5	2.03 (0.02)	44.4 (0.9)	5.4 (0.1)	0.78 (0.03)	0.42 (0.01)	0.1
7.0	1.83 (0.02)	42.1 (0.8)	4.9 (0.1)	0.92 (0.03)	0.39 (0.01)	0.1
7.4	1.63 (0.02)	38.7 (0.8)	4.7 (0.1)	0.88 (0.04)	0.27 (0.01)	0.1
8.0	1.58 (0.01)	39.4 (0.5)	5.2 (0.1)	0.78 (0.02)	0.32 (0.01)	0.1
9.0	1.39 (0.03)	40.4 (1.3)	3.3 (1.0)	1.25 (0.08)	0.39 (0.01)	0.2
10.0	1.54 (0.05)	26.3 (1.4)	5.7 (1.0)	0.43 (0.10)	0.13 (0.01)	0.5
11.5	1.60 (0.03)	20.3 (0.7)	10.3 (0.5)	0.22 (0.02)		0.4

<sup>a</sup>See footnote of Table I for further explanations and abbreviations.

Given that  $dE/d(\log F) = S$ ,  $d(\log F)/dF = 1/2.3F$ , and  $dT/d(\log T) = 2.3T$  we have

$$\frac{dE}{d(\log T)} = S \frac{T}{F} \frac{\partial F}{\partial T} \quad (14)$$

Equation 14 is general. When no binder (BSA) is present,  $T = F$  and the slope of the  $E$  vs  $\log T$  curve equals the electrode slope. In the presence of a binder, the derivative is calculated by substituting  $T$  and  $\partial F/\partial T$  from eq A1 and A2 (Appendix A) into eq 14 which finally gives

$$\frac{dE}{d(\log T)} = S \frac{\sum_{i=1}^m \frac{n_i K_i F}{1 + K_i F} P_i + (Ns + 1) F}{\sum_{i=1}^m \frac{n_i K_i F}{(1 + K_i F)^2} P_i + (Ns + 1) F} \quad (15)$$

In eq 15, the denominator is always smaller than the numerator because the term  $1 + K_i F > 1$ . Therefore  $dE/d(\log T)$  is always greater or equal to  $S$  in absolute terms, in the presence or absence of the binder, respectively (see Figure 1, curves 2 and 1). The above equations hold only in the area of linear response of the electrode. A simple graphical way for the calculation of the free ion concentration after each addition is also shown in Figure 1. The  $B/F$  ratio (ordinate of Scatchard plot) is then directly derived from the equation

$$B/F = 10^{-\Delta E/S} - 1 \quad (16)$$

where  $\Delta E$  is shown in Figure 1 and  $S$  is the electrode slope. The binding of picrate to BSA was studied at three different protein concentrations, i.e. at 20.0, 32.0, and 50.0 g/L. Typical Scatchard plots are presented in Figure 2. It is obvious that at high picrate concentration, the plots, instead of intersecting the horizontal axis at points indicating the total concentration of binding sites, become parallel to the axis due to the non-specific binding of picrate to BSA. In Table I, we present the values of binding parameters as estimated by nonlinear least-squares fitting of the Scatchard model with two classes

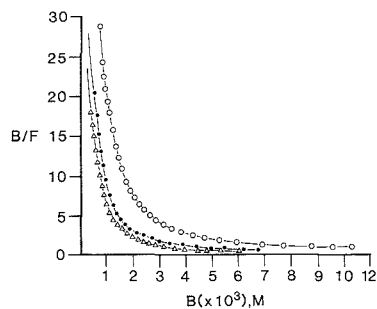


**Figure 2.** Potentiometric study of the binding of picrate to BSA at different BSA concentrations: Scatchard plots at BSA concentrations of ( $\Delta$ ) 20.0, ( $\bullet$ ) 32.0, and ( $\circ$ ) 50.0 g/L. The theoretical Scatchard curves (parameter values taken from Table I) are drawn over the experimental points.

of binding sites to the experimental data. It can be observed that the number of binding sites and the binding constants are practically independent of protein concentration. The last column of Table I shows the standard deviation of residuals calculated after the convergence of the iterative process. These numbers are of the same magnitude as the expected error in the measurement of the emf providing strong evidence that the model chosen is correct.

The influence of ionic strength on the binding was studied at a constant BSA concentration of 32.0 g/L by adding NaCl at final concentrations of 0.01, 0.05, 0.10, and 0.20 M. Scatchard plots at various ionic strengths were constructed in a manner similar to that of Figure 2. The values of binding parameters are presented in Table II. Ionic strength does not affect significantly these values. The dependence of picrate/BSA association on the pH was studied at a BSA concentration of 32.0 g/L using the appropriate buffers. Scatchard plots at various pH values were constructed in a

Table IV. Effect of Temperature on the Binding of Picrate to BSA<sup>a</sup>

Temp, °C	$n_1$	$10^{-3}K_1, M^{-1}$	$n_2$	$10^{-3}K_2, M^{-1}$	Ns	SD <sub>res</sub> , mV
10.0	1.78 (0.02)	107.5 (2.2)	4.3 (0.1)	2.99 (0.06)	0.40 (0.01)	0.2
15.2	1.83 (0.02)	83.9 (2.4)	4.2 (0.1)	2.12 (0.06)	0.23 (0.01)	0.2
20.2	1.82 (0.02)	52.6 (1.1)	4.5 (0.1)	1.51 (0.05)	0.24 (0.01)	0.2
30.0	1.72 (0.02)	40.5 (0.7)	4.2 (0.1)	1.26 (0.04)	0.20 (0.01)	0.2
40.3	1.64 (0.01)	29.9 (0.4)	3.7 (0.1)	1.04 (0.03)	0.20 (0.01)	0.1

<sup>a</sup> See footnote of Table I for further explanation and abbreviations.

manner similar to that of Figure 2. The values of the binding parameters are presented in Table III. A significant decrease of both binding constants is observed by increasing the pH above 9.0. In the pH range studied (pH 6.5–11.0), picric acid is completely dissociated ( $pK_a = 0.38$ ). The decrease in the affinity of protein for picrate by increasing pH above 9.0 is expected since at such high pH values the  $\epsilon$ -amino groups of lysine are gradually becoming deprotonated. This effect does not favor the attraction of the picrate anion to the BSA molecule. It is generally accepted in the literature that by increasing pH, the ability of albumin to bind anionic ligands decreases (27).

The effect of temperature on the binding was studied at 10.0, 15.2, 20.2, 30.0, and 40.3 °C (BSA concentration 32.0 g/L and pH = 7.4). Scatchard plots for each temperature were constructed. Analytical results are presented in Table IV. With decreasing temperature, both binding constants increase. This observation suggests that picrate binding to both classes of sites is an exothermic reaction. The number of binding sites remains practically constant.

From the results presented in Tables I–IV, it can be concluded that the nonspecific binding increases with increasing protein concentration and decreases with increasing temperature and pH reaching zero value at highly alkaline solutions (pH 11.0). Nonspecific binding can be considered as an accumulation of picrate ions on the protein surface because of weak interactions. The incorporation of a term that accounts for nonspecific binding in the general Scatchard model (eq 2) is mandatory for the fitting of the model to the data, especially at high picrate concentrations. This term has also been used previously (20, 21) when binding was studied by radioisotopic techniques. In Figure 3, the percent of bound picrate,  $100B/T$  the percent of nonspecifically bound picrate,  $100 Ns F/T$ , and the percent of specifically bound picrate,  $100(B - Ns F)/T$ , are presented as a function of the negative logarithm of the free picrate concentration. In fact, this plot shows the extent of nonspecific binding in the concentration range covered. Nonspecifically bound picrate is kept under 10% of total picrate in the range of free picrate concentration from  $2 \times 10^{-5}$  to  $3 \times 10^{-3}$  M (i.e. over a 100-fold range), then increasing rapidly to 17% of total picrate when the free concentration becomes  $10^{-2}$  M (i.e. for only a 3-fold increase in free concentration). In Figure 3, the distribution of bound picrate between the two classes of binding sites of BSA during an experiment is also shown. This is expressed as the percentage of the total picrate concentration that is bound to the first or the second class as a function of  $-\log F$ .

In Figure 4, saturation plots of BSA (i.e. plots of  $r =$  specifically bound picrate/ $P_t$  as a function of  $-\log F$ ) at 10.0 and 40.3 °C are shown. The theoretical saturation curves were also constructed by using the binding parameters from Table IV. Saturation plots have been considered (28, 29) as the most objective means for testing the completeness of the binding study and the adequacy of the concentration range covered. It has been theoretically proven (30, 31) that it is necessary to cover a range of 75% of the entire saturation curve to get adequate information for the assignment of the appropriate model to the binding data. As is shown in our experiments

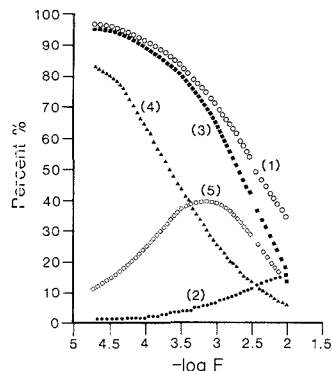


Figure 3. Graphical presentation of various fractions of bound picrate vs  $-\log F$  during the binding study: (1) percent of totally bound picrate; (2) percent of nonspecifically bound picrate; (3) percent of specifically bound picrate; (4) percent of picrate bound to the first class; (5) percent of picrate bound to the second class of binding sites.

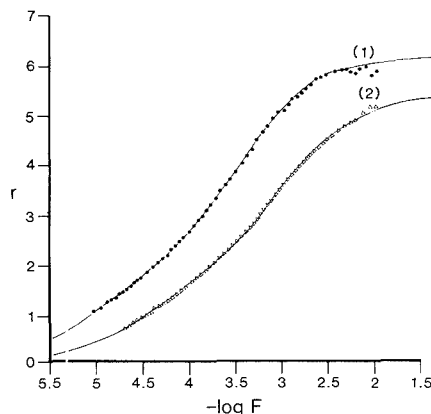


Figure 4. Plots of BSA saturation with picrate at 10° (1) and 40.3 °C (2), respectively. The theoretical saturation curves are drawn over the experimental points.

(Figure 4), a range of about 3 decades of free picrate concentration was covered. This corresponds to a wide saturation range of BSA from 16.6% to 94.9% at 10 °C and from 12.7% to 95.3% at 40.3 °C.

In the present work, the binding experiments were carried out as titrations of the protein with the anionic ligand. With this technique, we have avoided possible errors that may occur due to small changes in  $E'$  after frequent removing, washing, and reimmersing the ISE from one solution to the other. This happens when experimental protocols using various mixtures of protein–ligand are used to derive data. The presence of

BSA in the reaction mixture did not change the time needed for the stabilization of the electrode potential (to  $\pm 0.1$  mV) after each addition of picrate ( $< 30$  s). Therefore, it can be concluded that the picrate-BSA association is a rapid reaction completed in less than 30 s. In order to prove that the presence of protein does not cause any deleterious effect to either the picrate ISE membrane or the liquid junction of the reference electrode, we performed calibration curves before and immediately after binding experiments carried out at a 50 g/L BSA concentration. The values for the constant term of the Nernst equation were  $-72.1$  and  $-72.6$  mV and those for the electrode slope were  $-59.1$  and  $-59.4$  mV/decade before and after such binding experiments, respectively. These findings also suggest that there is no significant drift of the electrode response during a complete binding experiment (lasting approximately 60 min).

The contribution of BSA to the ionic strength of the measured solution can be estimated by assuming that the negative charges on the protein molecule ( $\sim 17$  at pH 7.4) (27) behave like monovalent anions (11). Therefore, a bovine serum albumin concentration of  $7.46 \times 10^{-4}$  M (50 g/L), which is the maximum concentration used in our experiments, causes an additional ionic strength of  $I = 6.3 \times 10^{-3}$  M in the measured solution. This contribution is not significant because all experiments were performed in 0.1 M buffer solutions. From these findings, it is concluded that the activity coefficient of the anionic ligand is practically the same in the presence or absence of BSA. It is thus possible to calculate the free picrate concentration in BSA solutions by directly using the equation of the calibration curve.

One contribution of the present work is that it provides a complete and statistically correct treatment of potentiometric data for studies involving the interaction of ionic ligands with macromolecules. Earlier treatments of potentiometric binding data have been based either on graphical procedures (10-12) or on least-squares treatment (13, 14) by using  $B/P$  as the dependent variable and  $F$  as the independent variable. There are many graphical approaches that are commonly used for the analysis of such data e.g. the Scatchard plot (19), the Benesi-Hildebrand plot (32), the Klotz plot (33), and the Hill plot (34). These methods facilitate transformation of the data into a straight line representation. However, a straight line only results under the simplest binding reaction mechanism and these methods do not generalize to more complicated binding models (e.g. for two or more classes of sites). In addition, the graphical analysis of results always contains some degree of subjectivity. Calculation of binding parameters by least-squares treatment is generally the recommended method. However, the choice of the dependent and independent variables is important for the purpose of satisfying statistical guidelines. A regression analysis has to be performed with the assumption that the independent variable is error-free. In the case of potentiometric data, assuming that the uncertainty in the emf measurement is  $\sigma_E$  (constant) and applying the error propagation law (35), we can calculate the uncertainties of the coordinates ( $B/F$  and  $B$ ) of the Scatchard plot as follows

$$\sigma_B = \sigma_F = \frac{2.3\sigma_E}{S} F \quad (17)$$

and

$$\sigma_{(B/F)} = \frac{2.3\sigma_E T}{S F} \quad (18)$$

where  $S$  is the electrode slope.

In Figure 5, a simulated Scatchard plot is shown along with the experimental uncertainties which are caused by an error of  $\sigma_E = 2$  mV in the measured electrode potential. The bars

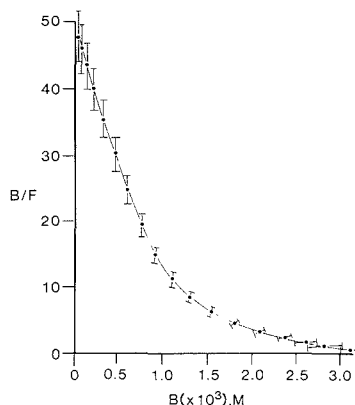


Figure 5. A simulated Scatchard plot along with the experimental uncertainties caused by an error of  $\sigma_E = 2$  mV in the emf measurement:  $n_1 = 2$ ;  $K_1 = 50\,000\text{ M}^{-1}$ ;  $n_2 = 5$ ;  $K_2 = 1500\text{ M}^{-1}$ ;  $P_1 = 4.78 \times 10^{-4}$  M.

shown correspond to 1 standard deviation on both the ordinate and the abscissa of the plot. From eqs 17 and 18 and from Figure 5, it is clear that the measurement errors appear in both the independent and the dependent variable and, also, are highly correlated and nonuniform.

For these reasons, the application of common least-squares programs (linear or nonlinear) directly to the Scatchard plot coordinate system is always statistically incorrect and often yields results which are inferior even to those obtained by graphical techniques. The plots of  $B$  vs  $F$  or  $F/B$  vs  $F$  as well as the double reciprocal plot ( $1/B$  vs  $1/F$ ) are for the same reasons inappropriate for direct regression analysis even if a simple straight line represents the experimental data.

In this work, the original (untransformed) raw potentiometric data, i.e., the electrode potential vs total ion concentration were analyzed by nonlinear least-squares treatment. In this system, the independent variable is practically error-free and the measurement error is restricted to the dependent variable (emf). We used graphical techniques (Scatchard plots) only for presentation of the data and for making initial estimates of the binding parameters. A list of the computer program with sample data and outputs can be obtained by writing to the authors.

The picrate binding to serum albumin was first studied by Teresi and Luck (36) using equilibrium dialysis. A very narrow total picrate concentration range (from  $5.0 \times 10^{-7}$  to  $2.5 \times 10^{-6}$  M) was covered. Therefore, a model of only one class of binding sites was assumed. Parameter values of  $n = 6$  and  $K = 1.26 \times 10^5\text{ M}^{-1}$  were found by a graphical technique.

Analytical application of the picrate/albumin association was first reported by the authors (37, 38). In these reports, the picrate ISE was used for the quantitative determination of albumin in plasma, serum, and whole blood but the estimation of binding parameters was not performed.

The application of ion selective electrodes for the study of the binding of ions to biological macromolecules offers a number of significant and unique advantages over the existing methodologies. First, the measurement of the free ion in the presence of the bound ion is carried out continuously without the need for separation procedures and without any disturbance of the chemical equilibrium of the system. Furthermore, binding studies can be accomplished in a wide concentration range since ISE response usually covers about 3 decades of the free ion concentration (range of  $10^{-5}$  to  $10^{-2}$  M is typical for most liquid-membrane ISE). In addition, by

the proposed "titration" technique, a large number of experimental points can be obtained in a short time (30–60 s per experimental point). Finally, this method is especially useful in cases where binding does not entail changes of the spectral characteristics of either the macromolecule and/or the ligand. A disadvantage of the proposed potentiometric method is that it does not provide direct information about the nature of the binding sites and of the interactions that are responsible for the phenomenon. It is mostly useful for the estimation of binding parameters.

The picrate-albumin association was used in the present study only as a model. The method described can be extended for any ion-macromolecule interaction. Especially, in view of the many drug ion selective electrodes that have been reported in the literature (39), we suggest the use of the above potentiometric methodology for the study of the binding of drugs to serum proteins.

#### APPENDIX

**A. Calculation of the Free Ion Concentration.** During the iterative nonlinear fitting process, it is necessary to calculate the free ion concentration corresponding to each experimental point, whenever new parameter values are derived. From the current binding parameter values and the total ion concentration at each experimental point, the free ion concentration is calculated by solving the equation

$$T = \sum_{i=1}^m \frac{n_i K_i F}{1 + K_i F} P_i + (N_s + 1)F \quad (\text{A1})$$

using the Newton-Raphson method of successive approximations (26).

We start the calculations from the last experimental point (highest total ion concentration) and use this value as initial guess. For the other points, the calculated free concentration of the previous point is taken as initial guess. The general expression of the derivative of  $T$  with respect to  $F$  at the  $i$ th point is

$$\frac{\partial T_i}{\partial F_i} = 1 + \sum_{j=1}^m \frac{n_j K_j P_{ji}}{1 + K_j F_j} + N_s \quad (\text{A2})$$

**B. General Expressions for the Partial Derivatives of the Electrode Potential with Respect to the Binding Parameters.** The expressions shown below have derived for any number of binding sites and include the case of nonspecific binding. The following equation holds (chain rule)

$$\frac{\partial E_i}{\partial \theta_j} = \frac{dE_i}{d(\log F_i)} \frac{d(\log F_i)}{dF_i} \frac{\partial F_i}{\partial \theta_j} \quad (\text{B1})$$

$$j = 1, \dots, 2m + 1$$

$$i = 1, \dots, N$$

where  $\theta_j$  are the binding parameters. Derivatization of the Nernst equation and substitution to eq B1 give

$$\frac{\partial E_i}{\partial \theta_j} = \frac{S}{2.3F_i} \frac{\partial F_i}{\partial \theta_j} \quad (\text{B2})$$

The partial derivatives of  $F$  with respect to the binding parameters are calculated indirectly as follows:

$$\frac{\partial F_i}{\partial \theta_j} = - \frac{\partial T_i / \partial \theta_j}{\partial T_i / \partial F_i} \quad (\text{B3})$$

Combination of eqs B2 and B3 gives

$$\frac{\partial E_i}{\partial \theta_j} = - \frac{S}{2.3F_i} \frac{\partial T_i / \partial \theta_j}{\partial T_i / \partial F_i} \quad (\text{B4})$$

The partial derivatives of  $T$  with respect to the parameters are calculated by derivativizing eq A1 with respect to  $n$  and  $K$ , respectively

$$\frac{\partial T_i}{\partial n_j} = \frac{K_j F_i P_{ji}}{1 + K_j F_i} \quad (\text{B5})$$

$$\frac{\partial T_i}{\partial K_j} = \frac{n_j F_i P_{ji}}{(1 + K_j F_i)^2} \quad (\text{B6})$$

The partial derivative of  $T$  with respect to  $N_s$  is

$$\partial T_i / \partial N_s = F_i \quad (\text{B7})$$

By substituting the  $\partial T_i / \partial F_i$ ,  $\partial T_i / \partial n_j$ ,  $\partial T_i / \partial K_j$ , and  $\partial T_i / \partial N_s$  from eqs A1, B5, B6, and B7, respectively, to eq B4, the following analytical expressions for the partial derivatives are obtained:

$$\frac{\partial E_i}{\partial n_j} = - \frac{SK_j P_{ji}}{2.3(1 + K_j F_j) \left[ 1 + \sum_{i=1}^m \frac{n_i K_i P_{ji}}{(1 + K_i F_i)^2} + N_s \right]} \quad (\text{B8})$$

$$\frac{\partial E_i}{\partial K_j} = - \frac{Sn_j P_{ji}}{2.3(1 + K_j F_j)^2 \left[ 1 + \sum_{i=1}^m \frac{n_i K_i P_{ji}}{(1 + K_i F_i)^2} + N_s \right]} \quad (\text{B9})$$

$$\frac{\partial E_i}{\partial N_s} = - \frac{S}{2.3 \left[ 1 + \sum_{i=1}^m \frac{n_i K_i P_{ji}}{(1 + K_i F_i)^2} + N_s \right]} \quad (\text{B10})$$

**Registry No.** Picric acid, 88-89-1.

#### LITERATURE CITED

- Reidunberg, M. M.; Erill, S. *Drug Protein Binding*; Clinical Pharmacology and Therapeutics Series Vol. 6; Praeger: New York, 1984.
- Drug-Protein Binding. In: *Ann. N.Y. Acad. Sci.* **1973**, *226* Anton, A. H.; Solomon, H. M., Ed.; collected papers of the conference on Drug Protein Binding of the New York Academy of Sciences, Jan 1973.
- Meyor, M. C.; Guttman, D. E. *J. Pharm. Sci.* **1968**, *57*, 895-918.
- Vallner, J. J. *J. Pharm. Sci.* **1977**, *66*, 447-465.
- Sparrow, N. A.; Russell, A. E.; Glasser, L. *Anal. Biochem.* **1982**, *123*, 255-264.
- Kurz H.; Trunk, H.; Weitz, B. *Arzneim.-Forsch./Drug-Res.* **1977**, *27*, 1373-1380.
- Sebile, B.; Thuand, N.; Tillement, J. P. *J. Chromatogr.* **1981**, *204*, 285-291.
- Proceedings of the Workshop on Direct Potentiometric Measurements in Blood*; Kock, W. F., Ed.; National Bureau of Standards: Gaithersburg MD, May 1983.
- Czaban, J. D. *Anal. Chem.* **1965**, *57*, 345A-356A.
- Frye, R. M.; Lees, H.; Rechnitz, G. A. *Clin. Biochem.* **1974**, *7*, 258-270.
- Andersen, N. F. *Clin. Chem.* **1977**, *23*, 2122-2126.
- Naik, D. V.; Jewell, C. F.; Schulman, S. G. *J. Pharm. Sci.* **1975**, *64*, 1243-1245.
- Mohunakrishnan, P.; Chignell, C. F. *J. Pharm. Sci.* **1982**, *71*, 1181-1182.
- Vadere, M.; Lindenbaum, S. *Int. J. Pharm.* **1982**, *11*, 57-69.
- Kiry, S.; Oda, Y.; Sasaki, M. *Chem. Pharm. Bull.* **1983**, *31*, 1085-1091.
- Birc, B. J.; Clarke, D. E.; Lee, R. S.; Oakes, J. *Anal. Chim. Acta* **1974**, *70*, 417-423.
- Kresneck, G. C.; Constantinidis, I. *Anal. Chem.* **1984**, *56*, 152-156.
- Hadijoannou, T. P.; Diamandis, E. P. *Anal. Chim. Acta* **1977**, *94*, 443-447.
- Scatthard, G. *Ann. N.Y. Acad. Sci.* **1949**, *51*, 660-673.
- Prior, R. L.; Rosenthal, H. E. *Anal. Biochem.* **1976**, *70*, 231-240.
- Munson, P. J.; Rodbard, D. *Anal. Biochem.* **1980**, *107*, 220-239.
- Klotz, I. M.; Hunston, D. L. *Biochemistry* **1971**, *10*, 3065-3069.
- Wenworth, W. E. *J. Chem. Educ.* **1965**, *42*, 96-103.
- Wenworth, W. E. *J. Chem. Educ.* **1965**, *42*, 162-167.
- Marcuardt, D. W. *J. Soc. Indust. Appl. Math.* **1963**, *2*, 431-441.
- Perrin, C. L. *Mathematics for Chemists*; John Wiley and Sons, Inc.: New York, 1970.
- Peters, T., Jr. Serum Albumin. In *The Plasma Proteins*, 2nd ed.; Putnam, F. W., Ed.; Academic Press: New York, 1975, Vol. 1, pp 133-181.
- Klotz, I. M. *Science* **1982**, *217*, 1247-1249.



- (29) Klotz, I. M. *Biopharm. Drug Dispos.* **1985**, *6*, 105-106.  
 (30) Deranleau, D. A. *J. Am. Chem. Soc.* **1969**, *91*, 4044-4049.  
 (31) Deranleau, D. A. *J. Am. Chem. Soc.* **1969**, *91*, 4050-4054.  
 (32) Benesi, H. A.; Hildebrand, J. H. *J. Am. Chem. Soc.* **1949**, *71*, 2703-2707.  
 (33) Klotz, I. M. *Arch. Biochem.* **1946**, *9*, 109-117.  
 (34) Hill, T. L. *J. Chem. Phys.* **1946**, *14*, 441-453.  
 (35) Bevington, P. R. *Data Reduction and Error Analysis for the Physical Sciences*; McGraw-Hill: New York, 1969.  
 (36) Teresi, J. D.; Luck, J. M. *J. Biol. Chem.* **1948**, *174*, 6E3-6E1.  
 (37) Diamandis, E. P.; Papastathopoulos, D. S.; Hadjiioannou, T. P. *Clin. Chem.* **1981**, *27*, 427-430.  
 (38) Christopoulos, T. K.; Diamandis, E. P. *Clin. Biochem.* **1986**, *19*, 151-160.  
 (39) Koryta, J. *Anal. Chim. Acta* **1988**, *206*, 1-48.

RECEIVED for review August 8, 1989. Accepted October 23, 1989.

## Transport of Catechols through Perfluorinated Cation-Exchange Films on Electrodes

Anna J. Tüdös, Wim J. J. Ozinga, Hans Poppe, and Wim Th. Kok\*

Laboratory for Analytical Chemistry, University of Amsterdam, Nieuwe Achtergracht 166, 1018 WV Amsterdam, The Netherlands

Steady-state amperometric and chronocoulometric experiments were carried out with a glassy carbon rotating disk electrode coated with a film of the perfluorinated ion-exchange polymer Nafion, in order to investigate the transport of anionic, cationic, and neutral catechols through the film. The distribution constants of the compounds between film and solution ( $K_d$ ) were measured, and the diffusion coefficients in the film ( $D_f$ ) were calculated. The film diffusion coefficients of catecholamines were found to be in the range (0.5 to 3.0)  $\times 10^{-7}$  cm<sup>2</sup> s<sup>-1</sup>. The selectivity constants were determined of the Nafion film for catecholamines relative to three monovalent cations Li<sup>+</sup>, Na<sup>+</sup>, and K<sup>+</sup>. The competitive effects of the buffer cations were found to decrease in the order expected from literature data on the ion-exchange selectivity of Nafion. The buffer cation concentration has no influence on the transport of neutral catechols through the film, and for anionic catechols the effect was opposite to that for cations. Other important factors for the detection in flow-through systems were also investigated, such as the influence of the film thickness, the pH, and the methanol concentration. From the results guidelines were formulated to obtain maximum selectivity for cationic analytes with Nafion-coated electrodes in liquid chromatography and flow-injection analysis.

### INTRODUCTION

Many recent studies have been devoted to the chemical modification of electrode surfaces with polymer films. In literature surveys (1, 2) the unique possibilities and the potential analytical importance of polymer modified electrodes have been emphasized. Polymer coated electrodes are used in analytical experiments for various purposes: catalysts can be immobilized on the electrode surface, reagents can be stored and released in a controlled way, or substances can be pre-concentrated in the film. However, the most straightforward application is to create a selective barrier for certain undesired substances, selectively excluding them from the electrode surface. Polymer films with incorporated ionic groups are especially suited for this purpose. The oppositely charged ions are readily transported from the solution into and through the film, whereas identically charged ions are excluded.

Nafion is a perfluorinated, sulfonated ion-exchange polymer, a trademark of Du Pont. It has been successfully used to modify electrodes for neurochemical analysis (3-6) and for

amperometric detection in liquid chromatography (7, 8). Despite of the large number of publications on Nafion electrodes the amount of analytically important data is still insufficient: few studies deal with the transport of analytically important compounds through Nafion films (9, 10), and in applied studies important parameters are often treated only qualitatively. For optimal analytical use, however, the sensitivity should be minimized for interferences and maximized for the analytes, and a quantitative study on the influence of the film on the response rate is also essential.

The sensitivity in amperometric detection for a compound is determined by the permeability of the film. The permeability is a function of two parameters, the distribution constant between the film and the solution, and the diffusion coefficient of the compound in the film. These two parameters should be determined independently, to be able to optimize the response rate, a factor contributing to peak broadening in liquid chromatography.

In the present paper, the transport is investigated of anionic, cationic, and neutral catechols through Nafion films on a rotating disk electrode. The study presented here deals with the most important factors for optimal detection in liquid chromatography and flow-injection analysis: the influence of the film thickness, the type and concentration of the buffer, the pH, and the methanol concentration of the solution. From the results obtained, guidelines are formulated for an optimal application of Nafion electrodes in flow-through systems.

### THEORY

In amperometric measurements with a film-coated electrode, with the electrode potential at a sufficiently high (or low) potential, the rate of electrochemical oxidation or reduction of a substrate in solution is determined by the rate of convective diffusion of the substrate in the solution and its diffusion through the film. The transport of substrate toward the electrode surface can be described by a two-layer model (11, 12). This model assumes a diffusion layer, a stagnant layer of solution on the surface of the electrode, and an unchanged (bulk) composition of the solution outside this diffusion layer. The steady-state current  $i_{ss}$ , as determined by the transport through the two layers, is

$$1/i_{ss} = 1/i_d + 1/i_f \quad (1)$$

where  $i_d$  is the current that would be measured without a film and  $i_f$  the current without the diffusion layer. The current in the absence of a film,  $i_d$ , is given by

$$i_d = nFAc_0D_s/d \quad (2)$$

where  $c_0$  is the (constant) bulk concentration of the substrate,  $d$  the thickness of the diffusion layer, and  $A$  the electrode surface area.

For the rotating disk electrode, as used in this study, the diffusion layer is uniform over the electrode surface; its thickness  $d$  is a function of the rotation speed of the electrode,  $\omega$ , as described by Levich (13)

$$d = 1.61D_s^{1/3}\nu^{1/6}\omega^{-1/2} \quad (3)$$

where  $D_s$  is the diffusion coefficient of the substrate in solution and  $\nu$  is the kinematic viscosity of the solution. When equilibrium is maintained at the film/solution interface, the concentration ratio over the interface is given by the distribution constant  $K_d$ . In that case  $i_t$  is given by

$$i_t = nFAK_d c_0 D_t / f \quad (4)$$

where  $f$  is the film thickness and  $D_t$  is the diffusion coefficient of the substrate in the film. The well-known Koutecky-Levich plots are obtained by measuring the steady-state current at different rotation speeds and plotting  $1/i_{ss}$  vs  $\omega^{-1/2}$ . From the slopes of these straight lines the diffusion coefficient of the substrate in solution can be calculated, while from the intercept the film-permeability ( $K_d D_t$ ) can be obtained. However,  $K_d$  and  $D_t$  cannot be obtained independently from steady-state measurements alone. Therefore, we devised a method, a modification of that used by Szentirmay and Martin (14), to measure these two parameters independently.

The distribution constant  $K_d$  can be determined by means of chronocoulometric experiments, in which the potential is stepped from a value at which no electrode reaction takes place to a value where the limiting current is reached. After the potential step is applied, initially a high current is measured, as consequence of the depletion of the substrate in the film and the diffusion layer. Subsequently, the current falls to the steady-state level. The distribution constant can be calculated from the excess charge  $q_{ex}$ , the infinite time integral of the current after subtraction of the steady-state current

$$q_{ex} = \int_0^{\infty} (i - i_{ss}) dt \quad (5)$$

It can be shown (see Appendix) that  $q_{ex}$  is given by

$$\frac{q_{ex}}{nFAc_0} = K_d f \left[ 1 - \frac{i_t}{i_t} + \frac{1}{3} \left\{ \frac{i_{ss}}{i_t} \right\}^2 \right] + \frac{1}{3} d \left[ \frac{i_{ss}}{i_d} \right]^2 \quad (6)$$

The first term on the right-hand side of eq 6 represents the depletion of the film after the potential step and the second term, the depletion of the diffusion layer. When  $K_d \gg d/f$ , the last term can be neglected. Generally, it is so small that it cannot be distinguished from the charge required to build up the potential of the electrode, as measured in blank solutions. If a series of chronocoulometric experiments are performed at different rotation speeds,  $q_{ex}$  and  $i_{ss}$  can be measured, and  $i_t$  can be calculated from the corresponding Koutecky-Levich plot.  $K_d$  is obtained by substituting these values in eq 6. Since  $K_d D_t$  is known from Koutecky-Levich plots,  $D_t$  can also be calculated. The advantage of this method to separate  $K_d$  and  $D_t$  is that there is no need for apparatus capable of sampling fast changing signals (15) and that all measurements can be made on the analyte itself (16). When the distribution of a compound between film and solution is governed by ion exchange processes, its distribution and thereby its transport through the film are both dependent upon the concentration of the buffer cation in the solution  $[M^+]_s$ . When the measurement is performed with a low substrate concentration, virtually all ion-exchange sites in the film are occupied by buffer cations. In that case  $K_d$  is given by

$$K_d = 1000K_M^i / (EW \nu [M^+]_s) \quad (7)$$

where  $K_M^i$  is the selectivity constant of the film for the analyte over the buffer cation  $M^+$ ,  $EW$  the equivalent weight of the ion-exchange polymer,  $\nu$  the volume (in  $\text{cm}^3$ ) of 1 g of dry polymer after swelling in the solution and  $[M^+]_s$  is in  $\text{mol L}^{-1}$ . When the excess charge can be determined reliably, both the distribution and the selectivity constants can be calculated.

## EXPERIMENTAL SECTION

**Apparatus.** Voltammetric measurements were carried out on a Metrohm 626 Polarorecord and a 663 VA stand equipped with a rotating disk electrode. The electrode was a 3 mm diameter glassy carbon rod in a 7 mm diameter PTFE shaft. In the belt-driven electrode shaft a second groove was scooped to increase the span of rotation speeds. Rotation speeds were measured with an optical tachometer.

Steady-state measurements were carried out at a potential of +0.8 V vs Ag/AgCl/3 M KCl. For the chronocoulometric experiments an external voltage supply (Delta Elektronika) was connected to the potentiostat, and the potential was stepped from +0.2 to +0.8 V. The currents were registered on a BD 12 integrating recorder (Kipp en Zonen).

**Reagents and Solutions.** A 5 wt % solution of Nafion EW 1100 was obtained from Aldrich. Dilutions were prepared in methanol. The concentration of these solutions was determined by titration with sodium hydroxide.

The catecholamines were used as received. Dopamine hydrochloride (DA), *dl*-norepinephrine (NE), 3,4-dihydroxyphenylacetic acid (DOPAC), and catechol (C) were obtained from Janssen Chimica, *dl*-epinephrine (E) and *DL*-DOPA from Sigma. Concentrated stock solutions were stored at 4 °C.

Buffer solutions were prepared by dissolving lithium, sodium, or potassium hydroxide in water (0.01 mol  $\text{L}^{-1}$ ) and adjusting the pH with monochloroacetic acid (pH 2.5–3.5), acetic acid (pH 4.0–5.5) and phosphoric acid (pH 6.0–7.0). The cation concentration was then varied by adding concentrated solutions of the nitrate salt. The solutions in the measuring cell (20 mL) were deoxygenated by purging with nitrogen. All experiments were performed at ambient temperature ( $19 \pm 2$  °C).

**Preparation of the Modified Electrodes.** Two basic methods have been tested to apply a thin Nafion film to the electrode, dip coating and droplet evaporation. The latter method proved to be more reproducible. Still, sometimes considerable differences were observed from one coating to another, and visual inspection showed differences in the area on which the Nafion layer was deposited. The most consistent results were obtained when a 5- $\mu\text{L}$  droplet of a diluted Nafion solution was spread out on the glassy carbon surface, and the solvent was allowed to evaporate in air at room temperature. The reproducibility did not improve by changing the volume of the applied solution, nor did it improve when the film was prepared by applying successive layers of Nafion or when the film was dried under a hot-air gun (5).

The intercept of the Koutecky-Levich plots for catechol was found to be proportional to the amount of Nafion applied for the majority of the films prepared (ca. 100). Hence, the thickness and uniformity of each layer were checked experimentally by recording the Koutecky-Levich plots for catechol. When the intercepts deviated for over 20% from the value expected for the amount of Nafion applied, the electrode was not used, and the film was wiped off with a tissue soaked in methanol. A strongly uneven coverage, or pinholes in the film, cause an increase in the slope of the Koutecky-Levich plot, as compared to the bare electrode. When the deviation of the slope exceeded 15%, the electrode was not used, either.

The film thickness was calculated from the amount of Nafion applied. On the basis of the water uptake and the density of Nafion in contact with aqueous solutions (17), a specific volume of 0.84  $\text{cm}^3$  for 1 g of (dry) Nafion was assumed.

## RESULTS

**Voltammetry.** Voltammograms were recorded in buffer at pH 4.5 using bare and coated GC electrodes. Typical examples are shown in Figure 1. After the bare electrodes were cleaned, the half-wave potentials kept shifting during use, but in the presence of the Nafion coating the wave shape

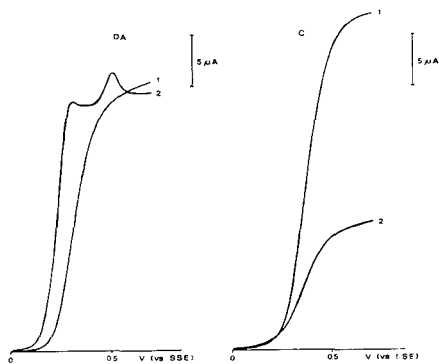


**Figure 1.** Voltammograms of dopamine (DA) and catechol (CA) at bare (1) and Nafion-coated (2) electrodes: analyte concentration,  $2 \times 10^{-5}$  mol L $^{-1}$ ; acetate buffer, pH = 4.5;  $[Na^+] = 0.10$  mol L $^{-1}$ ; rotation speed, 450 rad s $^{-1}$ ; scan rate, 2 mV s $^{-1}$ ; film thickness 0.8  $\mu$ m.

and the reproducibility improved. All the compounds could be measured at the current plateau at +0.8 V. Steady-state limiting currents were linear with the analyte concentrations in the range studied ( $5 \times 10^{-6}$  to  $5 \times 10^{-4}$  mol L $^{-1}$ ).

Koutecky-Levich plots of catechol in acetate buffer are shown in Figure 2. The plots of bare electrodes often showed a small intercept (0.0–1.0 A $^{-1}$  mol L $^{-1}$ ) depending on the history of the electrode and the concentration of the compound. This intercept was probably caused by the adsorption of reaction products on the electrode surface. At coated electrodes this phenomenon cannot be distinguished from the effects imposed by the film; hence, at low intercept values the determination of the film permeability is probably less accurate than in the case of thick films.

The diffusion coefficients of catecholamines in solution were calculated from the slopes of the Koutecky-Levich plots at bare and coated electrodes. Depending on the composition of the solution the diffusion coefficients were in the range of  $(0.55\text{--}0.60) \times 10^{-5}$  cm $^2$  s $^{-1}$ .

**Influence of the Buffer Cations.** The influence of the buffer cations was studied at pH = 4.5 with three cationic catechols (DA, E, and NE), two uncharged catechols (DOPA and C), and one which is partially anionic in the solution (DOPAC). The film permeability was determined at different Li $^+$ , Na $^+$ , and K $^+$  concentrations and is shown in Figure 3 for cationic and in Figure 4 for anionic and neutral species. In the case of cationic species, the intercepts of the Koutecky-Levich plots were proportional to the buffer cation concentration, that is, the film permeability is inversely proportional to the buffer cation concentration. Since this is expected of a competitive ion-exchange process, it may be concluded that this appears to be the major distribution mode. The permeability decreases from one catecholamine to the other in the order DA > E > NE. The competitive effect of the buffer cations decreases in the order K $^+$  > Na $^+$  > Li $^+$ , in agreement with literature data on the ion-exchange selectivity of Nafion (18).

Figure 4 shows the influence of the potassium ion concentration on  $c_0/i_t$  for noncationic catechols. Both the film permeability and the influence of the buffer concentration on it are low compared to the cationic species. The decrease of the film permeability with the buffer concentration for DOPA indicates that ion exchange plays a role. However, apparently other processes are more important. The film permeability for catechol is practically independent of the potassium concentration, whereas for DOPAC it shows a slight increase with increasing potassium concentration. Similar results were

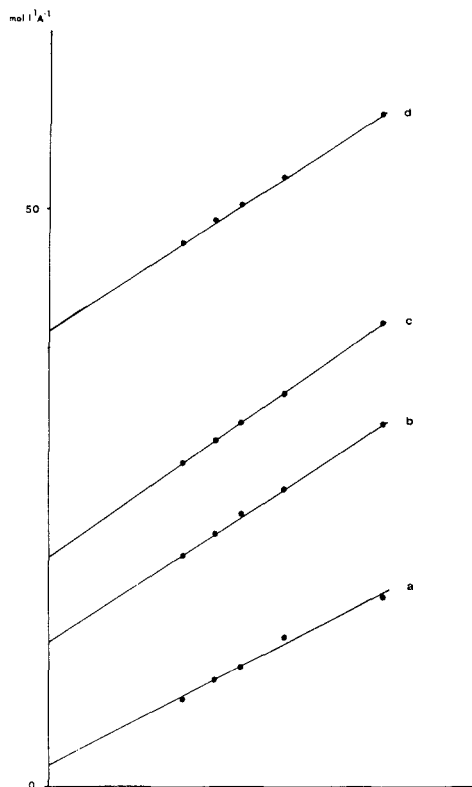


**Figure 2.** Koutecky-Levich plots of  $5 \times 10^{-5}$  mol L $^{-1}$  catechol: acetate buffer, pH = 4.5;  $[Na^+] = 0.01$  mol L $^{-1}$ ; film thickness, 0 (a), 0.8 (b), 1.6 (c) and 3.2 (d)  $\mu$ m.

obtained with lithium and sodium buffers.

**Influence of the pH.** As was shown in the previous section, the rate of transport of a compound through the film is strongly dependent on its charge. Therefore, in the case of weakly acidic or basic compounds the pH of the solution is important. The influence of the solution pH on the transport of the amino acid DOPA ( $pK_a = 2.2$ ) and on the weak acid DOPAC ( $pK_a = 4.1$ ) was studied at low and high sodium ion concentrations. The results are shown in Figure 5. In this figure the film currents are plotted to illustrate the contributions of the differently charged catechol species to the transport through the film. Below pH = 4 DOPA is readily transported through the film as a cation, and a competitive effect of the sodium ion is observed. At high pH values, where DOPA is present in the solution as zwitterion, the transport through the film is strongly decreased. Here, the sodium ion concentration is of little influence.

In the case of DOPAC the change in the film permeability with the pH is also observed at a solution pH of about 4. The film is less permeable for the anionic species (above pH 5) than for the neutral species (below pH 4). It is interesting to note, that the sodium ion concentration has little influence in the case of neutral species, while for anions the permeability increases with increasing sodium ion concentration. This may be attributed to a decrease of the repulsive forces between the DOPAC anions and the ionic sites in the film by a decrease in the zeta potentials. For catechol the film permeability did not depend on the solution pH in the range studied (2.5–7.0).

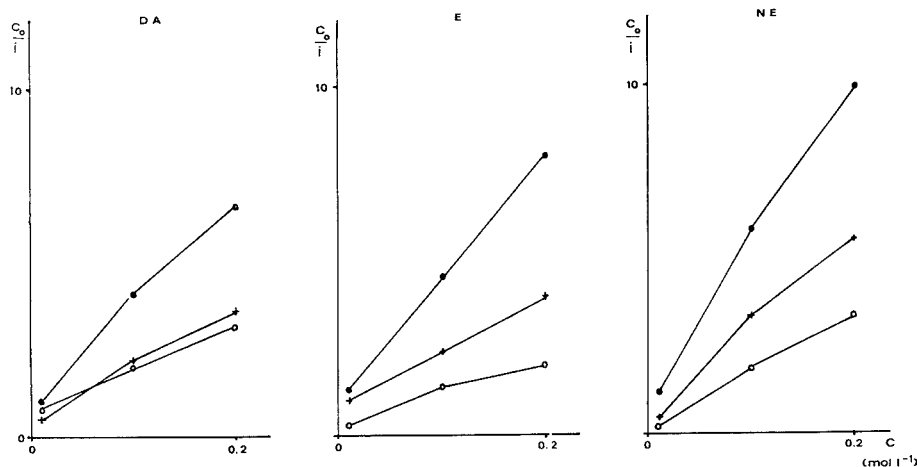


Figure 3. Influence of the buffer cation concentration on the intercepts of Koutecky-Levich plots for DA, E, and NE: analyte concentration,  $10^{-5}$  mol/L; acetate buffer, pH = 4.5; film thickness,  $3.2 \mu\text{m}$ ; buffer cation,  $\text{Li}^+$  (O),  $\text{Na}^+$  (+), or  $\text{K}^+$  (●).

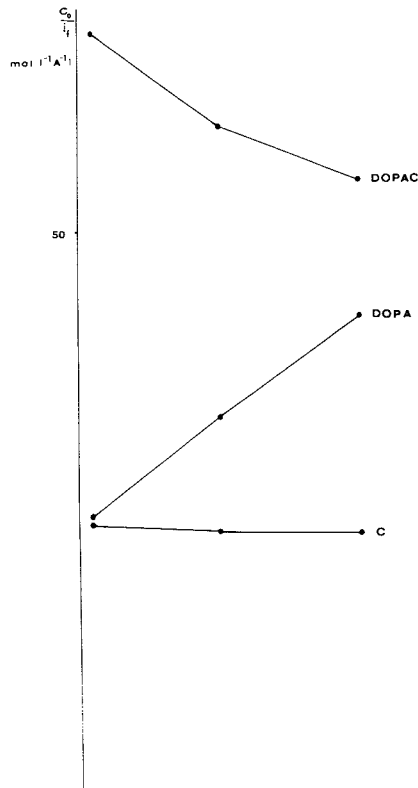


Figure 4. Influence of the potassium ion concentration on the intercept of Koutecky-Levich plots for DOPA, DOPAC, and C: analyte concentration,  $5 \times 10^{-5}$  mol  $\text{L}^{-1}$ ; acetate buffer, pH = 4.5; film thickness,  $3.2 \mu\text{m}$ .

**Influence of the Methanol Concentration.** The influence of the methanol concentration of the solution on the

stability and permeability of the Nafion film was also studied, since methanol is often used as organic modifier in reversed-phase chromatography. Depending on the method of preparation of the films, the stability is affected by organic components in the solution (19). The stability of the film was evaluated from the film permeability for catechol in aqueous buffers after rotation of the electrode in a solution containing methanol. At a methanol content of 40% (v/v) and higher, the film was rapidly stripped off from the electrode surface. In solutions up to 25% methanol content the film was stable for at least 48 h.

The film permeability for catechol and dopamine was measured in sodium acetate buffers (pH = 4.5) with 0, 10, and 20% (v/v) methanol. No significant influence of the methanol concentration was found.

**Determination of Distribution Constants and Diffusion Coefficients.** The Nafion-coated electrode was allowed to equilibrate for at least 10 min in the solution of the compound at a potential of +0.2 V, then the potential was stepped to +0.8 V. Figure 6 shows a typical time-dependent current and its integral after the potential step. The method to determine  $q_{\text{ex}}$  is also indicated. Measurements were performed with different settings of the time constant and sensitivity of the potentiostat/amplifier, while other conditions were kept constant. No influence of the potentiostat settings on the measured values of  $q_{\text{ex}}$  was found, which indicates that these values were not affected by electronic artifacts.

The chronocoulometric experiments were also performed with bare electrodes (with and without DA in solution) and with coated electrodes in blank buffer solutions. Under the above three different conditions the same blank values of  $q_{\text{ex}}$  were found, indicating that the charging of the double layer at the electrode surface was the main contribution. The charge measured (2–5  $\mu\text{C}$ ) increased with the aging of the electrode. Measured values of  $q_{\text{ex}}$  were corrected for the blank values.

The excess charge was measured at low rotation speed, where the measurement is the most reliable since  $q_{\text{ex}}$  is then relatively high and  $i_{\text{ss}}$  low. The value of  $i_{\text{ss}}/i_p$  was calculated from a Koutecky-Levich plot, and  $K_d$  could then be calculated with eq 6. At bare electrodes  $q_{\text{ex}}$  comprises the depletion of the diffusion layer. Since this charge could not be distinguished from the background loading charge in blank solutions, the term in eq 6 representing the contribution of the diffusor layer at coated electrodes was neglected, being always

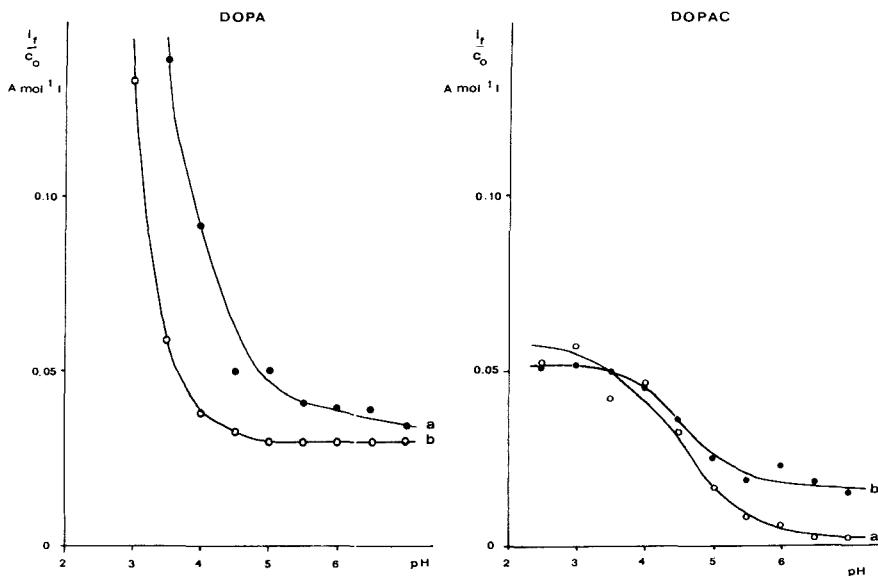


Figure 5. Influence of the solution pH on the film-permeability for DOPA and DOPAC: concentration of the compounds,  $5 \times 10^{-5}$  (DOPA) and  $10^{-4}$  mol L $^{-1}$  (DOPAC);  $[\text{Na}^+] = 0.01$  (a) and  $0.20$  mol L $^{-1}$  (b); film thickness,  $1.6 \mu\text{m}$ .

Table I. Determination of Distribution and Selectivity Constants of Catecholamines by Chronocoulometric Experiments<sup>a</sup>

cation	concn, mol L $^{-1}$	DA				E				NE			
		$q_{\text{ex}}, \mu\text{C}$	$i_{\text{ss}}/i_f$	$K_d$	$K_M^1$	$q_{\text{ex}}, \mu\text{C}$	$i_{\text{ss}}/i_f$	$K_d$	$K_M^1$	$q_{\text{ex}}, \mu\text{C}$	$i_{\text{ss}}/i_f$	$K_d$	$K_M^1$
Li $^+$	0.01	141	0.00	3210	29.7	116	0.00	2640	24.4	20	0.01	460	4.3
	0.02	80	0.01	1840	34.0	60	0.01	1380	25.5	10	0.02	230	4.3
	0.05	38	0.03	890	41.3	16	0.02	370	17.1	n.d.	—	—	—
Na $^+$	0.01	73	0.01	1680	15.5	55	0.01	1270	11.7	15	0.01	350	3.2
	0.02	35	0.02	810	15.0	29	0.02	670	12.5	7	0.03	160	3.0
	0.05	14	0.04	330	15.4	11	0.04	260	12.1	n.d.	—	—	—
K $^+$	0.01	37	0.01	850	7.9	35	0.02	810	7.5	8	0.02	190	1.7

<sup>a</sup> Concentration of catecholamines  $10^{-5}$  mol L $^{-1}$  in acetate buffer, pH 4.5.  $q_{\text{ex}}$  determined at  $53 \text{ rad s}^{-1}$ , corrected for blank value.

smaller than at bare electrodes. Since in most cases  $i_{\text{ss}}/i_f$  was small,  $q_{\text{ex}}$  was approximately equal to  $nFAK_d/c_0$  (14). Differences with this simpler method of calculation were up to 4% only. In Table I the observed  $q_{\text{ex}}$  values and the calculated distribution constants are comprised for DA, E, and NE in various buffers. From the table the following conclusions can be drawn:

1. The distribution constants are inversely proportional to the buffer cation concentration; hence ion-exchange is the major distribution process.

2. The distribution constants of the catecholamines are in the order  $\text{DA} > \text{E} > \text{NE}$ .

3. The competing effect of the buffer cations is in the order  $\text{K}^+ > \text{Na}^+ > \text{Li}^+$ .

From the distribution constants the selectivity constants have been calculated for the catecholamines over the buffer cations (Table I). The agreement over different buffer concentrations is reasonable, given the variation of the  $q_{\text{ex}}$  measurements (generally in the order of  $\pm 3 \mu\text{C}$ ). From the results it can be seen that the assumption that virtually all ion-exchange sites in the film are occupied by buffer cations was justified. In the most extreme case ( $10^{-5}$  mol L $^{-1}$  DA in  $0.01$  mol L $^{-1}$  Li $^+$ ) only 3% of the sites was occupied by the analyte cations.

The diffusion coefficients of the three catecholamines in Nafion film have been calculated from the distribution con-

Table II. Calculated Diffusion Coefficients of Catecholamines in Nafion

buffer cation	$D_f, 10^{-7} \text{ cm}^2 \text{ s}^{-1}$		
	DA	E	NE
Li $^+$	0.53	1.02	2.99
Na $^+$	0.87	1.14	2.52
K $^+$	0.94	0.82	2.78

stants and the film permeabilities at different buffer ion concentrations (Table II). The diffusion coefficients do not depend significantly on the type of the buffer cation. The diffusion coefficient of the less strongly bound NE is higher than those of DA and E.

It was also attempted to measure the distribution constant of catechol. However, this proved to be difficult, since the excess charge is only slightly different from the loading charge in blank solutions. The distribution constant of catechol was found to be approximately 4. From the distribution constant a film diffusion coefficient of  $2 \times 10^{-7} \text{ cm}^2 \text{ s}^{-1}$  can be calculated. However, these values indicate merely the order of magnitude.

## DISCUSSION

The mutual selectivity constants of Nafion for the buffer cations were derived from two types of measurements. First, they were calculated from the influence of the buffer cation

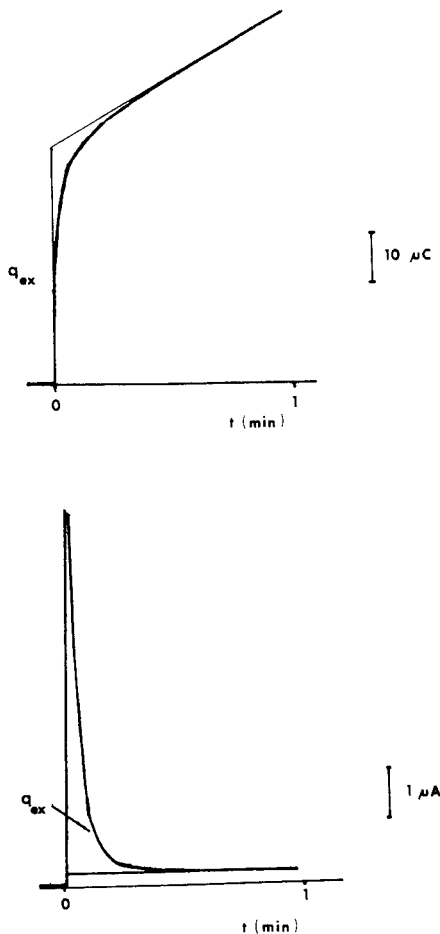


Figure 6. Time-dependent current and charge curves after a potential step, and determination of  $q_{ex}$ :  $10^{-5}$  mol L $^{-1}$  DA in acetate buffer, pH = 4.5;  $[Li^+] = 0.02$ ; film thickness, 3.2  $\mu$ m.

concentrations on the film permeability for catecholamines in steady-state measurements, as derived from the slopes of the plots in Figure 3. Second, they were calculated from the influence of the cations on the equilibrium film concentrations of the catecholamines in chronocoulometric measurements (Table I). The calculated selectivity constants are given in Table III. The relative selectivity of the Nafion films for Li $^+$ , Na $^+$ , and K $^+$  can be compared with literature values (18). Generally, the values found in our study are lower than those of Yeager and Steck. Since their measurements were more direct, their values are probably more accurate.

In two recent studies on the measurement of the diffusion coefficients of catecholamines in Nafion, values of about  $2 \times 10^{-9}$  cm $^2$  s $^{-1}$  were published, almost 2 orders of magnitude lower than the values obtained in our experiments. In the first study (9), chronoamperometric measurements were carried out, from which  $K_d D_f^{1/2}$  was obtained, while  $K_d$  values were obtained independently. The reported  $K_{iNa}$  values were 1500 for NE and 5000 for DA, about 300 times larger than our results. In the second study (5), the diffusion coefficient of dopamine in Nafion was obtained from response rate measurements in

Table III. Mutual Selectivity Constants of Buffer Cations in Nafion

method	compound	$K_{Li}^K$	$K_{Li}^{Na}$	$K_{Na}^K$
steady state	DA	2.3	1.3	1.8
	E	4.0	1.8	2.2
	NE	2.7	1.6	1.7
chronocoulometric	DA	4.1	2.1	1.9
	E	3.2	2.0	1.6
	NE	2.5	1.3	1.9
literature (18)	-	6.9	2.1	3.3

a flow-through system. With a fast-potential sweep technique the concentration of dopamine in a Nafion film was sampled close to the electrode surface. Sampling was fast enough to avoid disturbance of the concentration in the film. The permeation of dopamine in the film after a change of the dopamine concentration in the flowing solution was measured, and from this rate  $D_f$  was calculated. While the response time was calculated the contribution of the transport through the diffusion layer was neglected. However, this is not allowed under all conditions. Even if the response rate of the diffusion layer alone (as measured at a bare electrode) is very high, transport through the diffusion layer may be a limiting factor for the accumulation in the film. This effect can cause a considerable contribution to the response time, which is proportional to  $K_d$  (20). This also explains the decrease of the calculated diffusion coefficient when the buffer concentration decreased: both  $K_d$  and the coupling contribution to the response time increased. Other studies support the observation that the diffusion coefficients in the film are in the order of  $(1-2) \times 10^{-7}$  cm $^2$  s $^{-1}$ , rather than  $2 \times 10^{-9}$  cm $^2$  s $^{-1}$ . It can be derived (20) that in flow-through detection the contribution to band broadening of a film on an electrode is given by

$$\sigma_t^2 = \gamma f^4 / D_f^2 \quad (8)$$

where  $\gamma$  is a constant ranging from 1/90 for low values of  $K_d$  to 1/6 for analytes with high  $K_d$ . Experimentally observed contributions to band broadening (7, 8) are much smaller than is expected for compounds with a film diffusion coefficient of  $D_f = 2 \times 10^{-9}$  cm $^2$  s $^{-1}$ . For instance for a 2- $\mu$ m film (7) a  $\sigma$  between 2 and 8 s should have been found, where a negligible contribution to peak broadening was reported.

## CONCLUSIONS

One of the primary conclusions resulting from this study is that the importance of the buffer cation concentration for the permeability of Nafion films on electrodes should not be underestimated. The selectivity for cations compared to neutral or anionic compounds cannot be accounted for by the differences in diffusion coefficients in the film, but it is mainly the result of the differences in distribution constants at the film/solution interface. In some analytical applications the solution composition is fully restricted (such as in vivo measurements). However, optimization is often possible if the composition can be chosen within certain limits (e.g., in flow-injection analysis). The following guidelines can be used to obtain maximum selectivity for cationic analytes.

1. Low buffer concentration improves both the film permeability for cationic compounds and the shielding efficiency for anionic compounds.

2. Lithium buffer salts are preferred over sodium or potassium salts.

3. A proper choice of the solution pH results in an improved shielding of the electrode from interfering compounds which are converted into anions. The appropriate solution pH can be derived from the  $pK_a$  value of the interfering compound in solution.

**Table IV. Calculated Influence of the Buffer Composition on the Selectivity of a Nafion-Coated Electrode in Flow-Through Detection<sup>a</sup>**

compound	$i_{ss}/i_d$	
	0.20 mol L <sup>-1</sup> K <sup>+</sup>	0.01 mol L <sup>-1</sup> Li <sup>+</sup>
DA	0.77	0.99
E	0.73	0.99
NE	0.68	0.99
DOPA	0.23	0.26
DOPAC	0.13	0.02
C	0.43	0.43

<sup>a</sup>Film thickness: 2 μm. Buffer pH = 7.

4. Methanol may be added to the solution up to 25% (v/v) without reducing the stability of the film (for the E/W 1100 Nafion used in this study). The methanol content of the solution is of little influence on the selectivity.

5. When a fast response of the coated electrode is important, this limits the thickness of the film that can be applied. For instance, in order to obtain a band-broadening contribution in liquid chromatography of less than 0.01 s<sup>2</sup> for a compound with  $D_f = 10^{-7}$  cm<sup>2</sup> s<sup>-1</sup>, the film thickness should not exceed 3 μm.

To illustrate the utility of the above considerations, the influence of the buffer composition has been calculated on the selectivity of the Nafion film in flow-through detection. A mean diffusion layer thickness of 10 μm has been assumed, which is a realistic value for commercially available flow-through electrochemical detectors if the liquid flow rate is 1 mL min<sup>-1</sup>. In Table IV the calculated  $i_{ss}/i_d$  values are given for the cationic compounds, representing the ratio of the peak areas at coated and bare electrodes. It can be seen that the sensitivity for catecholamines improves if a 0.20 mol L<sup>-1</sup> potassium buffer is replaced by a 0.01 mol L<sup>-1</sup> lithium buffer. The leakage of (DOPAC) anions through the Nafion film will be strongly diminished at the same time.

## APPENDIX

**Derivation of Equation 6.** To obtain the relation between  $q_{ex}$  and  $K_d$  the differential equations describing the diffusion of the substrate in the diffusion layer and the film have to be evaluated. When  $x$  is the distance from the electrode surface and  $c_f$  and  $c_s$  denote the substrate concentrations in the film and the diffusion layer, respectively, these equations are

$$0 < x < f, \quad \frac{\delta c_f}{\delta t} - D_f \frac{\delta^2 c_f}{\delta x^2} = 0 \quad (9a)$$

$$f < x < f + d, \quad \frac{\delta c_s}{\delta t} - D_s \frac{\delta^2 c_s}{\delta x^2} = 0 \quad (9b)$$

If equilibrium is reached before the potential step, the initial conditions are

$$t = 0, 0 < x < f, c_f = K_d c_0$$

$$t = 0, f < x < f + d, c_s = c_0$$

The boundary condition for the electrode surface after a potential step to a sufficiently high value is

$$x = 0, c_f = 0$$

and for the outer surface of the diffusion layer

$$x = f + d, c_s = c_0$$

The assumption that the transport of substrate over the film-diffusion layer interface is not rate-determining leads to

an equilibrium condition for the interface

$$x = f, c_f = K_d c_s$$

The conservation of mass gives a final boundary condition

$$x = f, D_f \frac{\delta c_f}{\delta x} = D_s \frac{\delta c_s}{\delta x}$$

The current is given by

$$i(t) = nFAD_f \left( \frac{\delta c_f}{\delta x} \right)_{x=0} \quad (10)$$

Transformation of eq 9a and 9b to the Laplace domain, with the initial and boundary conditions stated above, yields differential equations which can be solved to give the Laplace transform of the current

$$\bar{i}(s) = nFAK_d c_0 \frac{D_f^{1/2} \cosh p_1 s^{1/2} + q_2 \cosh p_2 s^{1/2}}{s^{1/2} q_1 \sinh p_1 s^{1/2} + q_2 \sinh p_2 s^{1/2}} \quad (11)$$

$$p_1 = \frac{f}{D_f^{1/2}} + \frac{d}{D_s^{1/2}} \quad p_2 = \frac{f}{D_f^{1/2}} - \frac{d}{D_s^{1/2}}$$

$$q_1 = 1 + K_d \frac{D_f^{1/2}}{D_s^{1/2}} \quad q_2 = 1 - K_d \frac{D_f^{1/2}}{D_s^{1/2}}$$

The Laplace transform of the steady-state current  $i_{ss}$  (eq 1) is

$$\bar{i}_{ss}(s) = nFAK_d c_0 \frac{D_f D_s}{s (K_d d D_f + f D_s)} \quad (12)$$

Back-transformation of these formulas to the time domain is not necessary. For any transformable function  $f(t)$  the infinite time integral can be written as (21)

$$\int_0^{\infty} f(t) dt = \lim_{s \rightarrow 0} \bar{f}(s) \quad (13)$$

By subtraction of eq 12 from eq 11, series expansion of the hyperbolic terms, and taking the limit for  $s \rightarrow 0$ , the excess charge is obtained

$$q_{ex} = nFAK_d c_0 \frac{\frac{1}{3} D_s^2 f^3 + K_d D_f D_s f^2 d + K_d^2 D_f^2 f d^2 + \frac{1}{3} K_d D_f^2 d^3}{(K_d D_f d + D_s f)^2} \quad (14)$$

Substitution of eqs 1, 2, and 4 in eq 14 and rearrangement yield the convenient expression for  $q_{ex}$  of eq 6.

## ACKNOWLEDGMENT

The authors are grateful to Applikon BV (Schiedam, The Netherlands) for providing the Metrohm equipment.

## LITERATURE CITED

- Murray, R. W. In *Electroanalytical Chemistry*; Bard, A. J., Ed.; Marcel Dekker: New York, 1984; Vol. 13.
- Murray, R. W.; Ewing, A. G.; Durst, R. A. *Anal. Chem.* **1987**, *59*, 373A.
- Gerhardt, G. A.; Oke, A. F.; Nagy, G.; Moghaddam, B.; Adams, R. N. *Brain Res.* **1984**, *290*, 390.
- Rice, M. E.; Oke, A. F.; Bradberry, C. W.; Adams, R. N. *Brain Res.* **1985**, *340*, 151.
- Kristensen, E. W.; Kuhl, W. G.; Wightman, R. M. *Anal. Chem.* **1987**, *59*, 1752.
- Hulthe, P.; Hulthe, B.; Johannessen, K.; Engel, J. *Anal. Chim. Acta* **1987**, *198*, 197.
- Ji, H.; Wang, E. J. *Chromatogr.* **1987**, *410*, 111.
- Wang, J.; Tuzhi, P.; Golden, T. *Anal. Chim. Acta* **1987**, *194*, 129.
- Nagy, G.; Gerhardt, G. A.; Oke, A. F.; Rice, M. E.; Adams, R. N.; Moore, R. B., III; Szentimay, M. N.; Martin, C. R. *J. Electroanal. Chem.* **1985**, *188*, 85.
- Lawson, D. R.; Whiteley, L. D.; Martin, C. R.; Szentimay, M. N.; Song, J. I. *J. Electrochem. Soc.* **1988**, *135*, 2247.
- Gough, D. A.; Leyboldt, J. K. *Anal. Chem.* **1979**, *51*, 439.
- Ikeda, T.; Schmelz, R.; Denisevich, P.; Willman, K.; Murray, R. W. *J. Am. Chem. Soc.* **1982**, *104*, 2683.

- (13) Levich, V. G. *Physicochemical Hydrodynamics*; Prentice-Hall: Englewood Cliffs, NJ, 1962.
- (14) Szentirmay, M. N.; Martin, C. *Anal. Chem.* **1984**, *56*, 1898.
- (15) Marrese, C. A.; Miyawaki, O.; Wingard, L. B., Jr. *Anal. Chem.* **1987**, *59*, 248.
- (16) Ewing, A. G.; Feldman, B. J.; Murray, R. W. *J. Phys. Chem.* **1965**, *89*, 1263.
- (17) Mauritz, K. A.; Hora, C. J.; Hopfinger, A. J. *Polym. Prepr. (Am. Chem. Soc., Div. Polym. Chem.)* **1978**, *19*, 324.
- (18) Yeager, H. L.; Steck, A. *Anal. Chem.* **1979**, *51*, 862.
- (19) Mocre, R. B.; Martin, C. R. *Macromolecules* **1988**, *21*, 1334.
- (20) Kok, W. Th.; Tüdös, A. J.; Poppe, H. *Anal. Chim. Acta* **1989**, *228*, 31.
- (21) Laa, E. T. van der *Chem. Eng. Sci.* **1955**, *7*, 187.

RECEIVED for review December 1, 1988. Accepted November 3, 1989.

## Thin-Layer Chromatography with Supersonic Jet Fluorometric Detection

Totaro Imasaka, Katsunori Tanaka, and Nobuhiko Ishibashi\*

*Faculty of Engineering, Kyushu University, Hakozaki, Fukuoka 812, Japan*

A mixture sample is developed by a silica gel on a flexible thin-layer chromatograph (TLC) sheet. This is mounted on a sliding sheet roller attached to a supersonic jet nozzle. The first dye laser beam (275 nm) is introduced from a small through-hole to desorb the chemical species on the TLC sheet. The vaporized sample is entrained into a carrier gas of argon, and the gas is then expanded into a vacuum to form a supersonic jet. The sample molecule is detected by fluorescence induced by the second dye laser beam (366–375 nm). This technique allows direct measurements of the excitation spectrum and the chromatogram for the sample developed on the TLC sheet. The amount of sample used for recording a spectrum is 4.4  $\mu\text{g}$ . The detection limits are  $\sim 10$  ng in spectrometric and chromatographic measurements.

In the environment there are many chemical species with similar structures, whose toxicities drastically change by slight modification of the chemical structure. Therefore, a selective analytical method is essential in their determination. Supersonic jet (SSJ) spectrometry provides a useful means for this purpose, because of sharp line structure in the spectrum (1–3). It has been used for selective determination of polycyclic aromatic hydrocarbons (PAHs) and biological molecules with similar structures. However, there are so many chemical species in the environment that combination with a separation technique is sometimes necessary prior to the measurement.

SSJ spectrometry is a flowing analytical technique, and it is possible to combine it with chromatography. In current works, gas chromatography (GC) is successfully used for this purpose. Methods based on fluorescence (FL) detection (4–8) and multiphoton ionization (MPI) (9–11) have been reported, and picogram quantities of PAHs have already been determined (7). For nonvolatile or thermally labile molecules, liquid chromatography (LC) based on supercritical fluid sample introduction has been used (12). More recently, supercritical fluid chromatography (SFC) is used, instead of LC, for sample separation (13, 14). The assignment of the chemical species is performed by measuring a fluorescence spectrum with an optical multichannel analyzer (8) or by measuring a mass spectrum with a time-of-flight mass spectrometer (MS) (11),

during the time period when the sample passes through the detector. This approach allows reliable assignment of the chemical species from the well-resolved fluorescence or mass spectrum. Supersonic jet spectrometry combined with chromatography has great selectivity, but it has an inevitable disadvantage described below.

In current SSJ spectrometry, a pulsed dye laser is used for excitation or multiphoton ionization of the molecule, because of the wide tuning range and high peak power of the laser. The repetition rate of the pumping laser, e.g. an excimer laser, is practically limited to 10–100 Hz. It is difficult to measure the excitation spectrum in the short time period when the eluents transit a chromatograph detector. Thus only the specific molecule, whose spectral parameters are known prior to the measurement, can be detected with great selectivity, making it difficult to apply chromatography/SSJ spectrometry to unknown samples.

In this study we use thin-layer chromatography (TLC) for sample separation in SSJ spectrometry to measure the excitation spectrum and the chromatogram simultaneously. The sample is deposited at the bottom of the chromatograph sheet in a straight line, and it is developed by a solvent. At an appropriate  $R_f$  value (the ratio of migration distances for the sample to the solvent), the sample is vaporized by the first dye laser beam. The molecules are entrained in a carrier gas, which is expanded into a vacuum to form a supersonic jet. The sample is detected by fluorescence induced by the second dye laser beam. The excitation spectrum is measured by scanning the position of laser desorption (LD). A similar approach using MPI/MS is reported elsewhere (15). However, a portion of the TLC sheet is cut out and attached on the sample holder for laser desorption. Thus the sample location should be known prior to the measurement. The present analytical technique allows repetitive measurements of the excitation spectrum by scanning the position of the TLC sheet, and then it is applicable to unknown samples.

### EXPERIMENTAL SECTION

**Apparatus.** A laser ablation/supersonic jet nozzle was originally developed for the studies of metal clusters by Smalley and co-workers (16, 17). In the present study the nozzle is modified for the application to the sample developed on the TLC sheet. The nozzle structure is shown in Figure 1, which is essentially a combination of the specially designed component described below and the pulsed nozzle (pulse width,  $\sim 1$  ms) used in our gas-phase experiment (18). A flexible TLC sheet (100 mm long, 61 mm wide) is mounted on a sliding sheet roller (diameter, 20

\* Author to whom correspondence should be addressed.



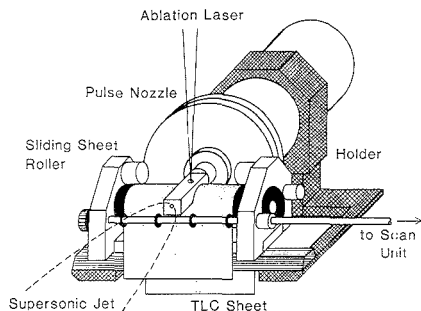


Figure 1. Supersonic jet nozzle for thin-layer chromatograph detection.

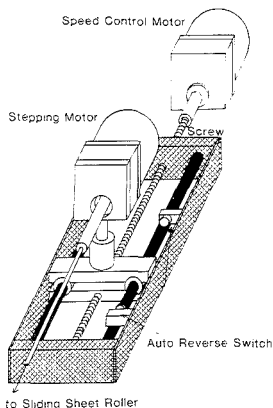


Figure 2. Driving unit for translation and rotation of TLC sheet attached to supersonic jet nozzle.

mm) supported by ball bearings (THK Bearing), which is rotated with gears (Kyoikusha) attached to the ends of two stainless steel rods (diameter, 3 mm). O-rings are fitted to this shaft to contact with the TLC sheet softly. Two ball bearings (THK Bearing) are attached to fit the TLC sheet on the roller, whose holder is mounted on the stage, which is smoothly translated by ball bearings (THK Bearing). A desorption laser beam is introduced from a small through-hole (i.d., 1 mm) to vaporize the sample on the TLC sheet. The curvature of the nozzle head surface to contact with the TLC sheet is designed to be 11 mm. The separation between the nozzle head and the TLC sheet is adjusted to 0.2 mm.

Figure 2 shows a driving unit for translating and rotating the sliding sheet roller. This is performed by rotating the stainless steel rod by using a stepping motor (Oriental Motor) mounted on the stage, which is translated by rotating a screw with a speed control motor (Oriental Motor). Two switches are positioned at both ends to limit the translational distance. The electric circuit for controlling the motors is designed in this laboratory. When the stage arrives at the end switch, the speed control motor stops working during 0.6 s, and the stepping motor rotates the shaft five steps, corresponding to 0.4 mm on the TLC sheet. The speed control motor starts moving again backward to change the scanning direction. A typical translational speed is 20 mm/min. This scan controller is installed outside the vacuum chamber, and the shaft is sealed with an O-ring.

A block diagram of the experimental apparatus is shown in Figure 3. After an argon gas is injected into the nozzle throat (i.d., 1.5 mm), the first dye laser pumped by the second harmonic of a Nd:YAG laser (Quantel, YG581C-20, TDL50, UVX-2, DCC-3, 20 Hz) is fired to vaporize the sample on the TLC sheet. The laser beam is reflected by a dielectric coated mirror and is exactly focused on the sample surface by a lens (focal length, 30 cm). The

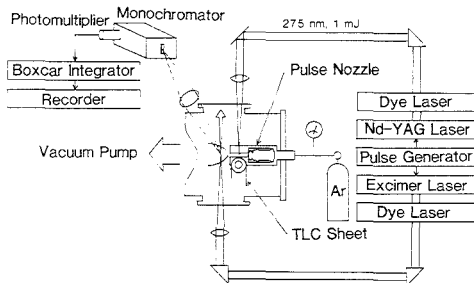


Figure 3. Experimental apparatus for TLC/LD/SSJ/FL.

beam position was visually confirmed by looking at it through the dielectric mirror. The laser dye used for desorption was fluorescein 27. The oscillating wavelength was adjusted to 275 nm, which was the shortest wavelength available in the present dye laser system. The pulse energy typically used was  $\sim 1$  mJ. The second dye laser pumped by an excimer laser (Lambda Physik, EMG102MSC, FL2002, 5 mJ) is synchronously fired at 130  $\mu$ s after the first dye laser. This is focused by a lens (focal length, 30 cm) 10 mm away from the top of the nozzle throat. The vacuum chamber is evacuated by a pumping system described elsewhere (19). Fluorescence from the sample is measured by a monochromator (Jasco, CT-100, 400 groove/mm) equipped with a photomultiplier (Hamamatsu, R928). The typical slit width used was 2 mm, corresponding to a spectral resolution of 4.8 nm. The signal is measured by a boxcar integrator (NF Circuit Design Block, BX-530A), the typical gate width being 1  $\mu$ s. The output signal is displayed by a chart recorder (Hitachi, 056).

**Reagents.** The PAHs used in this study, 1-chloroanthracene, 2-chloroanthracene, 9-chloroanthracene, and 9,10-dichloroanthracene, were purchased from Aldrich. The PAH 9-methylanthracene was supplied from Nakarai. The laser dyes BBQ, PBD, and fluorescein 27 were obtained from Exciton. The laser dye 7D4MC was purchased from Eastman Kodak. The TLC sheet (Merck, Kieselgel 60, normal phase) for sample separation consists of a thin silica gel layer (0.2 mm) on a polyester film. Nitrogen dioxide, which was used for an investigation of the cooling effect, was purchased from Takachiho.

**Procedure.** The sample was dissolved in chloroform and was deposited in a straight line at the bottom of the TLC sheet with a glass capillary. The sample was developed 50 mm with a solvent such as *n*-hexane. This was air-dried and was attached to the sliding sheet roller. After the nozzle was installed in the vacuum chamber, the shaft for translation and rotation of the roller was connected to the motor. The stagnation pressure of the argon gas was adjusted to 200 Torr throughout this experiment.

## RESULTS AND DISCUSSION

**Cooling Effect.** The TLC sheet is flexible but cannot be bent sharply into a U-shape. The nozzle throat becomes longer than the bending diameter, as shown in Figure 3. The cooling effect due to jet expansion can be degraded by increasing the length of the nozzle throat; a hydrodynamic flow becomes a molecular flow, which may substantially increase the jet temperature. First, the cooling effect was investigated by changing the length of the nozzle throat, using  $\text{NO}_2$  as a sample; an excitation spectrum was measured by monitoring the  $\nu_2$  band at around 455 nm. The procedure for the calculation of the rotational temperature from the line profile is described in detail elsewhere (18). The rotational temperature obtained was 3.4–4.1 K for nozzle throat lengths of 0, 1, 12, 22, and 39 mm. This fact is consistent with a calculated translational temperature of 3 K obtained by assuming direct jet expansion from the nozzle. Thus, it is tentatively concluded that a nozzle throat shorter than 40 mm induces a minor effect in rotational cooling. In this study the length of the nozzle throat is designed to be 29 mm, promising sharp spectral lines in the SSJ spectrum.

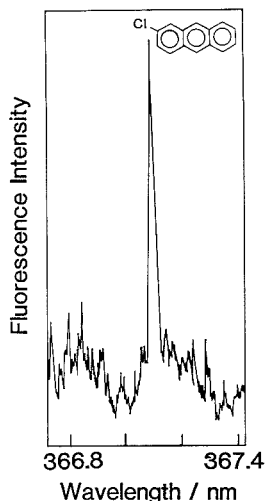


Figure 4. Supersonic jet excitation spectrum for 2-chloroanthracene adsorbed on TLC. Fluorescence is monitored at 387.0 nm.

**Spectral Features.** Supersonic jet excitation spectra were measured for 1-, 2-, and 9-chloroanthracene, 9-methylanthracene, and 9,10-dichloroanthracene adsorbed on the TLC sheet. Figure 4 shows the spectrum for 2-chloroanthracene, which is known as a thermally labile molecule to form a polymerized tar at an elevated temperature (12). A rather poor signal to noise ratio (S/N) is due to the low fluorescence quantum yield of 2-chloroanthracene. The line widths of the 0-0 transition peak observed for the above five compounds were 1.9–2.8  $\text{cm}^{-1}$ . Amirav et al. calculated the rotational temperature of anthracene to be 15 K from a line width of 3  $\text{cm}^{-1}$  (20). Thus it is implied that the molecules are sufficiently cooled by jet expansion, at least to 15 K.

**Sensitivity.** The time period required for the measurement of an excitation spectrum was 15 min. After the sample was laser-desorbed, the TLC sheet was detached from the nozzle. A zigzag trace was found on the TLC sheet, which was 0.1 mm wide and 366 mm long. By extraction of 9,10-dichloroanthracene adsorbed on the TLC sheet into chloroform, a quantity of sample in a unit area was calculated by measuring the concentration with a conventional fluorescence spectrometer. The result indicates that the density of the sample molecule is 0.12  $\mu\text{g}/\text{mm}^2$ . During the measurement of an excitation spectrum, 4.4  $\mu\text{g}$  of sample is calculated to be consumed. By a single laser shot 0.24 ng of sample ( $6 \times 10^{11}$  molecules) is desorbed in the present condition, which is slightly less than the values reported elsewhere:  $3 \times 10^{13}$  molecules in MPI spectrometry (21) and  $2 \times 10^{12}$  molecules for laser-ablated monomers from a polymer surface (22). In TLC/MPI/MS the detection limits are reported to be  $\sim 12$  ng for indole-3-acetic acid and  $\sim 3$  ng for imipramine, which are obtained by averaging the signals over 10 pulses (1 s) (15). These values are comparable to a detection limit of  $\sim 10$  ng for 9,10-dichloroanthracene obtained in this study, which is estimated from a desorbed amount of sample during the time constant (0.24 ng  $\times 20$  Hz  $\times 5$  s) and the S/N ratio of the spectrum ( $S/N = 7$ ).

**Background Signal.** The sensitivity was determined by several sources of background emission. Strong light scatter originated from particulates ablated from the TLC gel, but could be reduced to negligible levels by using a fluorescence monochromator. Photoemission induced by laser breakdown

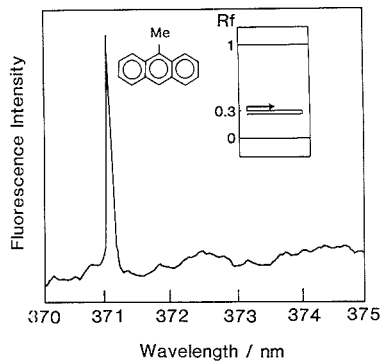
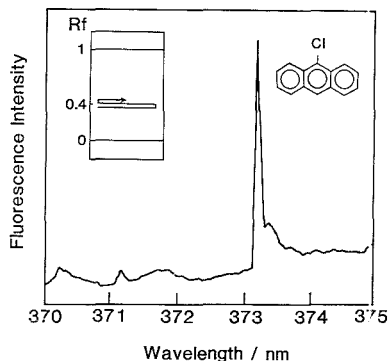


Figure 5. Supersonic jet excitation spectrum for chemical species located at  $R_f = 0.3$  in TLC. Fluorescence is monitored at 393.5 nm. A mixture sample of 9-methylanthracene and 9-chloroanthracene is developed by *n*-hexane.

lasted 20  $\mu\text{s}$  even at the fluorescence detection port, but it could be also reduced to negligible levels by temporal discrimination. Long-lived photoemission continued more than 130  $\mu\text{s}$  after the desorption laser pulse. The photoemission intensity was not critical to the excitation and fluorescence wavelengths. This was reduced by using a narrow gate width, but it was still difficult to remove completely even at a gate width of 1  $\mu\text{s}$ . It is probably due to fluorescence from chemicals adsorbed on the small particulates ablated from the TLC gel. More gentle laser ablation, e.g. by using an infrared  $\text{CO}_2$  laser, may reduce formation of particulates, but this approach was not investigated in this study due to unavailability of the equipment.

**Timing of Two Laser Pulses.** The dependence of the signal intensity on the time period between the firing of the two dye lasers was not investigated quantitatively, due to a poor S/N ratio of the signal. However, the largest signal providing a cooled spectrum was observed only when the timing was exactly adjusted to 130  $\mu\text{s} \pm 2$  ns. This fact implies that the sample is localized in the jet pulse and is focused within a short time period. This is consistent with a sample pulse width of  $\sim 4$   $\mu\text{s}$  observed in the previous studies of LD/SSJ and LA/SSJ (22, 23). As pointed out, this is advantageous for improving the sensitivity since the amount of the sample on the TLC sheet is quite limited. In current SSJ spectrometry, it is necessary to use at least several milligrams of sample to optimize experimental conditions. This amount sometimes exceeds a fatal dose for a heavily toxic compound. It is noted that the sample remaining on the TLC is safely recovered after the measurement. Therefore, even a toxic sample could be measured with negligible levels of contamination in the laboratory.

**TLC Sample.** The sample on the TLC sheet was developed by *n*-hexane, and the SSJ spectrum was measured at specified  $R_f$  values. The excitation spectra recorded for the mixture sample of 9-methylanthracene and 9-chloroanthracene are shown in Figures 5 and 6. The wavelength of the fluorescence monochromator was adjusted to 393.5 nm to monitor vibronic bands, at which fluorescence from both the components could be detected within a spectral resolution of 4.8 nm. When the excitation spectrum is recorded at  $R_f = 0.3$ , a single peak appears at 371.16 nm, which corresponds to the 0-0 transition for 9-methylanthracene. When the measurement is carried out at  $R_f = 0.4$ , a single peak appears at 373.25 nm corresponding to the 0-0 transition for 9-chloroanthracene. No other peaks are observed in this narrow spectral range. As demonstrated, this method allows the measurement of the



**Figure 6.** Supersonic jet excitation spectrum for chemical species located at  $R_f = 0.4$  in TLC. The experimental conditions are identical with those in Figure 5.

excitation spectrum for the chemical species separated by chromatography. This is a distinct advantage of TLC/LD/SSJ over the other techniques combining SSJ with GC, SFC, or LC. This figure of merit may allow the application of this method to unknown samples.

SSJ spectrometry using no chromatograph separation has some difficulties in the assignment of the chemical species in the mixture sample, since there are many possible spectral patterns by a combination of the spectrum. The present TLC technique provides additional selectivity in SSJ spectrometry, and furthermore the assignment of peaks to a specific component might be performed even when the separation resolution is incomplete; if a group of peaks tends to increase or decrease in the same manner when the  $R_f$  is changed, they might be assigned to the signals originating from the same component.

Conventionally, absorption or fluorescence spectrometry has been used in the TLC detector. More recently, a laser-based TLC detector utilizing fluorescence (24, 25), thermal lens (26, 27), or mass spectrometry (28) has been reported. However, these methods sometimes suffer from poor spectral selectivity and from lack of information in the assignment. Low-temperature spectrometry has also been used in the TLC detector; fluorescence line narrowing spectrometry (FLNS) is applied to a PAH-nucleoside adduct adsorbed on a TLC plate cooled at a liquid helium temperature (29). However, the spectral lines are not completely resolved, which may be partly due to a complex structure of the adduct molecule and to the interaction between the sample molecule and the solid substrate.

**Chromatogram.** Figure 7 shows chromatograms measured by adjusting the excitation and fluorescence wavelengths to optimum values for 9-methylanthracene and 9-chloroanthracene, respectively. Only single components are observed in the chromatograms. No other signal peaks are observed at different  $R_f$  values. It indicates that these compounds are present at  $R_f = 0.3$  and  $0.4$ , respectively. In the measurement, 4.9 and 1.7  $\mu\text{g}$  of the above compounds are charged on the TLC sheet, respectively; 9-methylanthracene is slightly overcharged and is appreciably broadened. From the S/N ratio, the detection limit of 9-chloroanthracene is estimated to be  $\sim 10$  ng, which is similar to the case in the measurement of the excitation spectrum. This is comparable to the values for naphthalene derivatives separated by GC using a conventional (noncapillary) separation column combined with a SSJ fluorescence detector (4). The separation resolution is rather poor at present, but it may be improved by using a reverse-phase sheet, though it is not commercially available yet.

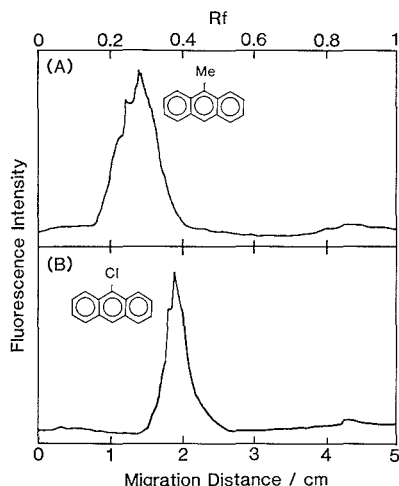


**Figure 7.** Chromatograms for mixture sample of 9-chloroanthracene and 9-methylanthracene. The excitation and fluorescence wavelengths (nm) are (A) 371.16, 390.6 and (B) 373.25, 393.5.

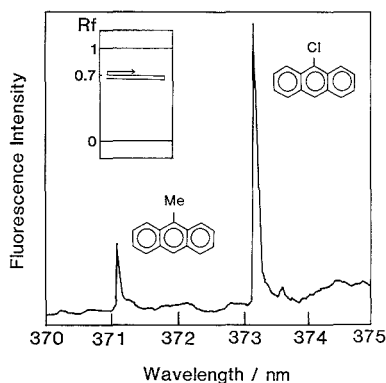


**Figure 8.** Supersonic jet excitation spectrum for chemical species located at  $R_f = 0.7$  in TLC. Fluorescence is monitored at 393.5 nm. The sample is developed by the mixed solvent of *n*-hexane and chloroform (2:1).

Further improvement may be obtained by using high-performance thin-layer chromatography (HPTLC).

**Resolution on Excitation Spectrum.** Since the real sample contains many chemical species, it is sometimes difficult to resolve all the components by chromatography. Even in such cases, it is possible to resolve the components on the excitation spectrum in TLC/LD/SSJ spectrometry. Figure 8 shows the excitation spectrum measured for the mixture sample developed by the mixed solvent of *n*-hexane and chloroform (2:1). In this condition, 9-chloroanthracene and 9-methylanthracene are not resolved on the TLC sheet. In room-temperature spectrometry they provide almost identical excitation and fluorescence spectra, and thus it is difficult to determine these components selectively by TLC equipped with a conventional fluorometric detector. As shown in Figure 8, these components are clearly resolved on the SSJ excitation spectrum, since they provide sharp 0-0 transition peaks at different wavelengths. This figure of merit may be ascribed to good spectral selectivity in TLC/LD/SSJ spectrometry.

## LITERATURE CITED

- (1) Hayes, J. M.; Small, G. J. *Anal. Chem.* **1983**, *55*, 565A.
- (2) Johnston, M. V. *TRAC, Trends Anal. Chem.* **1984**, *3*, 58.
- (3) Lubman, D. M. *Anal. Chem.* **1987**, *59*, 31A.
- (4) Hayes, J. M.; Small, G. J. *Anal. Chem.* **1982**, *54*, 1202.
- (5) Pepich, B. V.; Callis, J. B.; Danielson, J. D. S.; Gouterman, M. *Rev. Sci. Instrum.* **1986**, *57*, 878.
- (6) Pepich, B. V.; Callis, J. B.; Burnes, D. H.; Gouterman, M.; Kalman, D. A. *Anal. Chem.* **1986**, *58*, 2825.
- (7) Stillier, S. W.; Johnston, M. V. *Anal. Chem.* **1987**, *59*, 567.
- (8) Imasaka, T.; Tanaka, K.; Ishibashi, N. *Anal. Sci.* **1988**, *4*, 31.
- (9) Imasaka, T.; Shigezumi, T.; Ishibashi, N. *Analyst* **1984**, *109*, 277.
- (10) Imasaka, T.; Okamura, T.; Ishibashi, N. *Anal. Chem.* **1986**, *58*, 2152.
- (11) Imasaka, T.; Tashiro, K.; Ishibashi, N. *Anal. Chem.* **1986**, *58*, 3242.
- (12) Imasaka, T.; Yamaga, N.; Ishibashi, N. *Anal. Chem.* **1987**, *59*, 419.
- (13) Simons, J. K.; Sin, C. H.; Zabriskie, N. A.; Lee, M. L.; Goates, S. R. *J. Microcal. Sep.* **1989**, *1*, 200.
- (14) Goates, S. R.; Sin, C. H.; Simons, J. K.; Markides, K. E.; Lee, M. L. *J. Microcal. Sep.* **1989**, *1*, 207.
- (15) Li, L.; Lubman, D. M. *Anal. Chem.* **1989**, *61*, 1911.
- (16) Powers, D. E.; Hansen, S. G.; Geusic, M. E.; Pui, A. C.; Hopkins, J. B.; Dietz, T. G.; Duncan, M. A.; Langridge-Smith, P. R. R.; Smalley, R. E. *J. Chem. Phys.* **1982**, *86*, 2556.
- (17) Hopkins, J. B.; Langridge-Smith, P. R. R.; Morse, M. D.; Smalley, R. E. *J. Chem. Phys.* **1983**, *78*, 1627.
- (18) Hayashi, T.; Imasaka, T.; Ishibashi, N. *Chem. Phys.* **1986**, *109*, 145.
- (19) Imasaka, T.; Fukuoka, H.; Hayashi, T.; Ishibashi, N. *Anal. Chim. Acta* **1984**, *156*, 111.
- (20) Amirav, A.; Horwitz, C.; Jortner, J. *J. Chem. Phys.* **1988**, *88*, 3092.
- (21) Li, L.; Lubman, D. M. *Rev. Sci. Instrum.* **1988**, *59*, 557.
- (22) Imasaka, T.; Tashiro, K.; Ishibashi, N. *Anal. Chem.* **1989**, *61*, 1530.
- (23) Arrowsmith, P.; de Vries, M. S.; Hunziker, H. E.; Wendt, H. R. *Appl. Phys. B* **1988**, *46*, 165.
- (24) Berran, M. R.; Zare, R. N. *Anal. Chem.* **1975**, *47*, 1200.
- (25) Bicking, M. K. L.; Kniseley, R. N.; Svec, H. J. *Anal. Chem.* **1983**, *55*, 200.
- (26) Chen, T. I.; Morris, M. D. *Anal. Chem.* **1984**, *56*, 19.
- (27) Fotio, F. K.; Morris, M. D. *Anal. Chem.* **1987**, *59*, 185.
- (28) Finney, R. W.; Read, H. *J. Chromatogr.* **1989**, *471*, 369.
- (29) Cooper, R. S.; Jankowiak, R.; Hayes, J. M.; Pei-qi, L.; Small, G. J. *Anal. Chem.* **1988**, *60*, 2692.

RECEIVED for review August 14, 1989. Accepted November 22, 1989. This research is supported by Grants-in-Aid for Scientific Research from the Ministry of Education of Japan and by Kurata Foundation.

## Optimization of Separations in Supercritical Fluid Chromatography Using a Modified Simplex Algorithm and Short Capillary Columns

Jeffrey A. Crow and Joe P. Foley\*

Department of Chemistry, Louisiana State University, Baton Rouge, Louisiana 70803

A modified simplex algorithm has been used to optimize supercritical fluid chromatography (SFC) separations of samples containing nonhomologous, nonoligomeric components. Short capillary columns are employed in the initial separations, with a transfer to a longer column for greater efficiency as needed. Two chromatographic response functions, based on peak-valley ratio or threshold resolution criteria, were found to be suitable for SFC. Two- and three-variable simplexes utilizing (i) density gradient rate and temperature, (ii) simultaneous pressure and temperature gradient rates, or (iii) initial density, density gradient rate, and temperature provided good results for the samples in this study. Convergence to the global optimum was shown for case i by restarting the simplex in another part of the parameter space. A synthetic mixture of three difficult-to-separate sesquiterpene lactones was separated by optimization on a short column using the three-parameter simplex and then transferring the method to a longer column.

### INTRODUCTION

More often than not, the initial separation of a given sample is unsatisfactory, usually because the desired resolution between all the peaks of interest is insufficient. To improve the separation in an efficient manner, an optimization procedure with well-defined goals is strongly recommended (1). The goals set may vary depending on how many peaks are of interest, the resolution required, the importance of analysis time, and other considerations. The point at which an optimization procedure is terminated depends on the quality of the separation desired; there is a distinct difference between an acceptable and an optimum separation. The decision upon which optimization is usually based takes into account a

minimum resolution in some maximum time frame (2). Many chromatographic response functions (CRF's) have been developed and used based on this idea (3, 4).

Each of the three terms in the fundamental resolution equation (5) can be optimized to improve the separation. Retention ( $k'$ ) and the selectivity ( $\alpha$ ) should first be optimized via changes in the density of the mobile phase, the temperature, and the gradient rates. Optimization of these two parameters is clearly the first step, since it will indicate if the current mobile phase/stationary phase combination is adequate for the separation being considered. The efficiency of a column,  $N$ , is determined by its length and the nature of the stationary phase, including column diameter or particle size. Given the square root dependency of resolution on  $N$ , large changes in parameters controlling  $N$  (e.g., column length or linear velocity) will result in only moderate changes in resolution and thus should only be considered if changes in the parameters controlling selectivity and retention in SFC (composition, density, temperature (or their respective gradients, if employed)) do not suffice.

Supercritical fluid chromatography (SFC) displays GC- and/or LC-like behavior, depending on both the solutes and the experimental conditions. Some components may partition by their vapor pressures while others partition by solventlike properties of the mobile phase (6). As the experimental conditions are changed, the behavior of some or all of these components may be reversed. Elution order may also depend on such properties as basicity and steric hindrance (7). Finally, many of the parameters that control retention and selectivity are moderately to highly synergistic (8). For these reasons, univariate optimization strategies (sequential optimization of one parameter at a time) or intuitive approaches are often ineffective in locating a true optimum (3), hence the need for a simultaneous multivariate approach in order to obtain the best possible separation.

Historically, SFC has largely been used for the separation of homologous or oligomeric series of compounds (particularly those without chromophores), and methods for these types of separations are relatively easy to develop intuitively. However, as SFC is applied more frequently to samples with diverse, nonhomologous components, it is clear that a better optimization strategy (or theory) will be necessary.

The sequential simplex method is a multivariate optimization procedure that uses a geometrical figure called a simplex to move throughout the response surface in search of the optimum set of experimental conditions (9). The simplex has been successfully used in various forms of chromatography, particularly high-performance liquid chromatography (10-12) and gas chromatography (13-16). To our knowledge, however, the present study represents the first application of the simplex method to SFC. In the present work we investigate the ability of a simplex algorithm to optimize SFC separations. First, the simplex method is used with a synthetic test mixture for initial assessment of the procedure, and then it is applied to some difficult-to-separate sesquiterpene lactones using a more rigorous three-parameter optimization.

### THEORY

**Simplex Algorithm.** In the simplex method, the number of initial experiments conducted is one more than the number of parameters (temperature, gradient rate, etc.) to be simultaneously optimized. These initial experiments establish the vertices of a geometric figure (simplex), which will subsequently move through the parameter space in search of the optimum. Once the initial simplex is established, the vertex with the lowest value is rejected, and a new point is found by reflecting the simplex in the direction away from the rejected vertex. In this way the simplex proceeds toward the optimum set of conditions. Details on the simplex algorithm are available elsewhere (3, 4, 9, 17-19).

Some advantages of the simplex method include the following: (1) little chromatographic insight is required, (2) computational requirements (relative to other statistical strategies) are minimal, and (3) any number of parameters may be considered. Some disadvantages of the simplex algorithm are (1) a large number of experiments may be required to find an optimum, (2) little insight into the response surface is provided, and (3) a local rather than a global optimum may be found (3). With respect to the latter deficiency, the chances of finding a global optimum are enhanced by using a modified simplex which allows other operations besides reflection, such as expansions and contractions. The chances of a mistaking a local optimum for the global optimum are also reduced by restarting the simplex in a different region of the parameter space. If the same optimum is found after restarting the simplex, it is probable that the global optimum has been found.

**Response Functions.** For chromatographic optimization, it is necessary to assign each chromatogram a numerical value, based on its quality, which can be used as a response for the simplex algorithm. Chromatographic response functions (CRFs), used for this purpose, have been the topic of many books and articles, and there is a wide variety of such CRFs available (3, 4, 20, 21). The criteria employed by CRFs are typically functions of peak-valley ratio, fractional peak overlap, separation factor, or resolution. After an extensive (but not exhaustive) survey, we identified two CRFs that are straightforward and easy to use. We intentionally avoided the more complicated CRFs that include factors of maximum analysis time, minimum retention time, or other arbitrary weighting factors. As discussed by Schoenmakers (3), these complex CRFs are neither as versatile nor as desirable as previously believed. The "multiple" weighting factors of these CRFs can usually be reduced to a single weighting factor

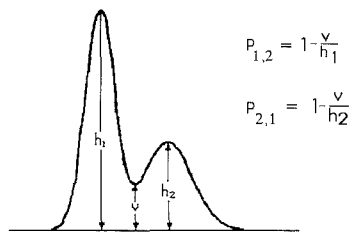


**Figure 1.** Illustration of the peak-valley ratio measurement used for the optimization process. See eq 2 for the response function used in conjunction with this criterion.

simply by rearrangement of the CRF.

The first CRF we considered uses a threshold criterion based on resolution between peaks ( $R_{s,min}$ ), given the equation

$$\text{CRF-1} = \frac{1}{k_w} \begin{cases} R_{s,min} \geq x \\ = 0 & R_{s,min} < x \end{cases} \quad (1)$$

In eq 1,  $k_w$  is the capacity factor for the last peak (retention time may be used instead), and  $R_{s,min}$  is the minimum acceptable resolution set arbitrarily by the user. CRF-1 favors chromatograms with a resolution greater than an arbitrary value "x" for all peaks in the shortest amount of time possible. For chromatograms where  $R_{s,min} < x$  for any pair of peaks, the response is set to zero. If the resolution between all pairs of peaks is greater than x, the response is set equal to  $1/k_w$ . Thus as analysis time decreases, the response function value increases provided that the resolution does not fall below the threshold value. For our analyses,  $R_{s,min}$  was chosen to be unity. A different value may be more appropriate in some instances.

An inherent problem with CRF-1 is its inability to distinguish between chromatograms with a resolution below the threshold. All such chromatograms would have a value of zero, among which the algorithm could not differentiate. A more continuous CRF may therefore be desirable in some instances.

The second CRF we considered is a continuous one based on the ratio of peak height to valley depth. There are several ways in which this ratio can be implemented, and the specific method we used, first introduced by Christophe (22), is illustrated in Figure 1. The resulting CRF is

$$\text{CRF-2} = \frac{\Pi(P_{i,i-1}P_{i,i+1})^{1/2}}{t_w} \quad (2)$$

where, for the  $i$ th peak,  $P_{i,i-1} = 1 - (v_{i-1}/h_i)$  and  $P_{i,i+1} = 1 - (v_{i+1}/h_i)$  (see Figure 1).

CRF-2 also favors short analysis times and well-resolved peaks. There is no threshold value for resolution, and the compromise between resolution and analysis time is not as well-defined as in CRF-1. Inclusion of analysis time in the denominator of an objective function may result in the loss of some information, compensated for by a rapid analysis time (23). It is important to note, however, that as peaks become overlapped CRF-2 decreases rapidly, as shown in Figure 2, and it is unlikely that a short analysis time will compensate for poor resolution (3). This is true only to a point, however, as the peak-valley ratio utilized by CRF-2 does not diminish to an appreciable extent until the resolution falls below a value of 1 to 1.25. If a minimum resolution is an absolute requirement, it is probably better to use a threshold criterion such as that introduced earlier so that the desired resolution is set by the user.

**Solvent Peak.** A common problem in SFC is the separation of the solvent peak and the first peak of interest. For reproducibility and quantitation, it is important to separate the peaks of interest from the highly asymmetric, tailing

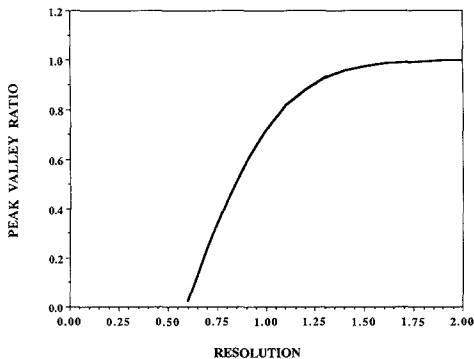


Figure 2. Relationship between resolution and peak-valley ratio as calculated from the equation  $P = 1 - 2 \exp(-2R_s^2)$ . See ref 3 for details.

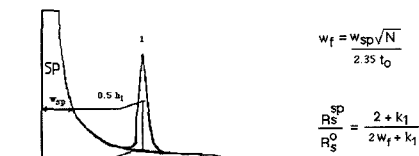


Figure 3. Illustration of the method for determining resolution between the solvent peak and the first peak of interest. The method was taken and modified from that introduced by Schoenmakers et al. (24). See eqs 3 and 4 in text.

solvent peak. If CRF-1 or any other CRF that uses resolution ( $R_s$ ) is employed, a procedure suggested by Schoenmakers et al. (24) and modified in our laboratory can be used to measure the resolution between the solvent peak and the first solute peak.

Schoenmakers' calculation uses the width of each peak measured at 13.5% relative to the solute peak and a weighting factor proportional to the width of the solvent peak. Our modification is the measurement of both peak widths at 50% relative to the solute peak instead of at 13.5%. We have found the former measurement significantly easier because it more readily avoids problems caused by (i) potential base-line disturbances on the lower part of the solvent peak tail resulting from the start of a gradient or (ii) imprecise peak width measurements resulting from low signal-to-noise ratios (i.e., near the limit of detection).

In order to be equivalent to Schoenmakers' original expression, our modification requires that the coefficient in the denominator of the weighting factor expression be reduced from 4 to 2.35. Our modifications are shown in eq 3 and in Figure 3. In eq 3,  $w_{sp}$  is the width of the solvent peak

$$w_f = \frac{w_{sp} N^{1/2}}{2.35 t_0} \quad (3)$$

measured at 50% relative to the solute peak,  $N$  is the plate count of the column, and  $t_0$  is the retention time of the solvent peak. The solute peak used to calculate the efficiency will obviously affect the value of  $w_f$ , and should typically have a  $k'$  value between two and four. Note that if the solvent peak was ideal (symmetric instead of tailed),  $w_f$  would be unity. For broader solvent peaks,  $w_f$  becomes larger. The resolution between the solvent peak and first analyte peak ( $R_s^{SP}$ ) is calculated by

$$R_s^{SP} = \frac{2 + k_1}{2w_f + k_1} R_s^O \quad (4)$$

where  $R_s^O = \Delta t_R / W_{\text{solute}}$  and  $k_1$  is the capacity factor for the solute peak.

Note that no such modifications for the solvent peak are generally necessary for CRFs that employ a peak-valley ratio, since the overlap is measured directly and no assumptions are made concerning peak shape. As the first solute peak becomes more overlapped with the solvent tail, the peak-valley ratio will rapidly decrease toward zero and give rise to an unfavorable response.

**Increasing  $N$ .** For a new sample, the time required for analysis must include the development of the method for separation. In the case of SFC, a great amount of time can be saved by performing the method development with a very short column (25). This can be done efficiently in combination with the modified simplex algorithm described above. Additional time will of course be saved if this short column proves to be sufficient, once the conditions are optimized, for the final analysis. If the current column does not provide the required efficiency, the resolution can be increased by a factor  $y$  via a  $y^2$  increase in column length. If a gradient is being used, the gradient rate should be decreased appropriately. Assuming that  $\ln k$  vs the variable of interest (density, pressure, or temperature) is linear, the gradient rate should be decreased by  $y^2$  (23). Note that although an increase in column length results in a proportional increase in analysis time, hours of analysis time have already been saved by first optimizing the separation on a short column.

If the separation is still unsuitable after optimization of the experimental conditions and column length, selectivity must be optimized further by changing the stationary phase, the type of column, or the mobile phase by changing it or adding a modifier.

## EXPERIMENTAL SECTION

**SFC System.** The chromatographic system consisted of a Model 501 supercritical fluid chromatograph (Lee Scientific, Salt Lake City, UT) with the flame ionization detector (FID) set at 375 °C. The instrument was controlled with a Zenith AT computer. A pneumatically driven injector with a 200-nL or a 500-nL loop was used in conjunction with a splitter. Split ratios used were between 5:1 and 50:1 depending on sample concentration and the chosen linear velocity, while the timed injection duration ranged from 50 ms to 1 s. We found that variation of both the split ratio and the injection time allowed greater control over the amount of solute transferred onto the column. Data were collected with an IBM-AT computer using Omega-2 software (Perkin-Elmer, Norwalk, CT). The simplex program and the response function calculation programs were written in TrueBASIC (TrueBASIC, Inc., Hanover, NH). The capillary columns used were a 0.55-m, a 1-m, and a 3-m SB-Biphenyl-30 (30% biphenyl, 70% methyl polysiloxane), with a 50- $\mu$ m internal diameter and a film thickness of 0.25  $\mu$ m. The mobile phase was SFC grade carbon dioxide (Scott Specialty Gases, Baton Rouge, LA). Linear velocities were 1.5 and 2.0 cm/s through the 50- $\mu$ m frit restrictor, estimated from the retention time of methane at 100 atm and 100 °C. To prevent plugging, the 15- $\mu$ m split restrictor was run out of the oven into a vial of methylene chloride. This was important in the analysis of the more polar sesquiterpene lactone sample (vide infra). Density was held constant until the solvent had eluted, at which point a gradient program was initiated.

**Samples.** Two samples were used to test the simplex method. Sample 1 was a synthetic test mixture consisting of six low-to-medium molecular weight solutes (acetophenone, propiophenone, bicyclohexyl, biphenyl, undecylbenzene, and benzophenone) of varying polarity and functionality dissolved in HPLC grade hexane. An injection duration of 100 ms was used with this sample. Sample 2 was a synthetic mixture of three sesquiterpene lactones (glaucolide A, burrodin, and psilostachyin A) dissolved in HPLC grade methylene chloride. An injection duration of 200 ms was used in conjunction with this sample.

**Simplex Algorithm.** The modified simplex algorithm was based on that used by Nelder and Mead (27) except that any vertex obtained through a contraction that had the worst response

Table I. Results of Two-Parameter Simplex, Run 1

vertex	density rate, (g/mL)/min	temp, °C	response (eq 2)	$t_w^a$ , min	simplex movement	retained vertices
1	0.075	75	0.150	6.51	—	—
2	0.123	88	0.186	5.00	—	—
3	0.088	123	0.122	4.52	—	—
4	0.110	40	$-\infty^b$	—	reflection	1,2
5	0.094	102	0.175	4.84	$c_w$ contraction	1,2
6	0.142	115	0.187	3.93	reflection	2,5
7	0.175	135	0.0601	3.45	expansion	2,5
8	0.172	101	0.205	3.85	reflection	2,6
9	0.211	100	0.205	3.67	expansion	2,6
10	0.229	128	$-\infty$	—	reflection	6,9
11	0.150	98	0.199	4.24	$c_w$ contraction	6,9
12	0.218	83	0.201	3.94	reflection	9,11
13	0.279	85	$-\infty$	—	reflection	9,12
14	0.182	95	0.221	3.99	$c_w$ contraction	9,12
15	0.174	112	0.193	3.68	reflection	9,14
16	0.207	90	0.234	3.69	$c_w$ contraction	9,14
17	0.179	84	0.227	4.11	reflection	14,17
18	0.204	80	0.227	3.97	reflection	14,17

<sup>a</sup> $t_w$  is the retention time of the last eluting peak. <sup>b</sup>This value is given to conditions that are outside the boundary limits.

was kept and the next-to-worse vertex was rejected instead. This avoids massive contractions which often reduces the parameter space too quickly (see ref 9). Experimental conditions for the initial vertex are chosen intuitively by the user; the remaining vertices of the initial simplex are calculated by the algorithm using a user-specified step size. Boundary conditions for the parameter space were specified according to instrumental limitations or arbitrarily, but with rational user judgement. When the simplex algorithm moved outside the set boundaries, a response value of negative infinity was given to that coordinate. Peak and valley heights were measured from the chromatograms on screen using the data collection system and a program was written to calculate the peak-valley ratio response function from these values. The response function value was subsequently used in the simplex program.

## RESULTS AND DISCUSSION

**Two-Variable Simplex.** While the simplex algorithm can be performed with any number or kind of parameters, the number of experiments required for convergence to an optimum rapidly increases as more parameters are considered (3). Also, since the number of parameters changing is larger, the response surface is more complex, i.e., with more local optima, and thus a global optimum may be more difficult to find. For these reasons it is advisable to limit the parameters to the ones believed to be important in the optimization process. For SFC, these include density (or pressure), temperature, mobile phase composition, and gradient of each. To reiterate, the key to a rapid optimization for a given separation is to consider only the most important variables.

In our first attempts at SFC optimization we considered only two parameters: density gradient and column temperature. The boundary limits for this simplex were 0.01–0.4 (g/mL)/min for the density gradient rate and 40–200 °C oven temperature. The linear velocity for this simplex was approximately 1.5 cm/s. Sample 1 described earlier was used to test the optimization procedure. Table I gives the experimental conditions and value of the response function (CRF-2) at each vertex of the simplex. The amount of peak overlap can be ascertained by multiplying the response in the tables by  $t_w$  (see eq 2). Also note that the "retained vertices" column refers to the vertices kept just prior to the generation of the current vertex. Figure 4 illustrates the movement of the simplex algorithm and the evolution of the CRF. When the simplex algorithm chose conditions outside the boundary limits, a very negative response value was given to that coordinate. This can be seen in the tables and in the response progress figures where negative columns indicate this very

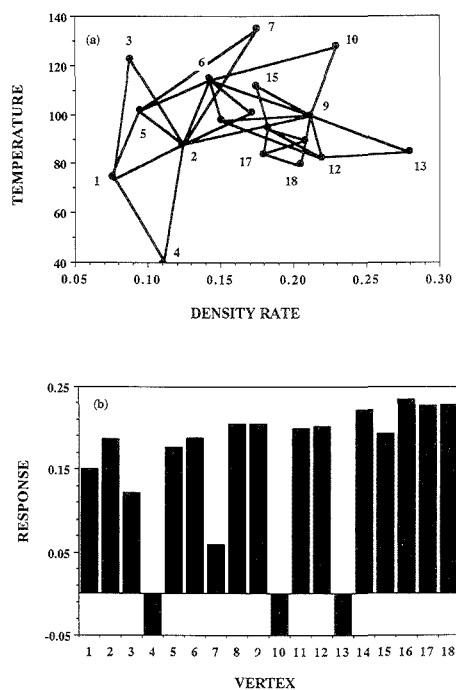


Figure 4. First simplex optimization of density gradient rate and column temperature performed on the test mixture, showing (a) simplex movement and (b) response progress.

negative response. Chromatograms for selected vertices in the simplex are shown in Figure 5. The simplex was terminated after a good separation was obtained under 4 min. The best result was obtained at vertex 16, at a density gradient of 0.207 (g/mL)/min and an oven temperature of 90 °C, as seen in Figure 5d.

Given the possibility of finding a local rather than a global optimum, the simplex was restarted from another region of the parameter space by using the same boundary limits and linear velocity as before. The data for this second simplex are given in Table II. Figure 6 shows the simplex movement

Table II. Results of Two-Parameter Simplex, Run 2

vertex	density rate, (g/mL)/min	temp, °C	response (eq 2)	$t_w^a$ , min	simplex movement	retained vertices
1	0.150	50	0	—	—	—
2	0.247	63	0.103	4.36	—	—
3	0.176	98	0.215	4.26	—	—
4	0.272	111	— <sup>b</sup>	—	reflection	2,3
5	0.181	65	0.171	5.17	$c_w$ contraction	2,3
6	0.110	101	0.164	5.02	reflection	3,5
7	0.144	91	0.202	4.10	$c_w$ contraction	3,5
8	0.139	124	0.122	3.75	reflection	3,7
9	0.170	80	0.201	4.50	$c_w$ contraction	3,7
10	0.202	87	0.236	3.80	reflection	3,9
11	0.231	85	0.223	3.93	expansion	3,9
12	0.237	103	0.211	3.53	reflection	3,11
13	0.220	97	0.239	3.49	$c_w$ contraction	3,11
14	0.275	84	—	—	reflection	11,13
15	0.201	95	0.123	3.87	$c_w$ contraction	11,13

<sup>a</sup>  $t_w$  is the retention time of the last eluting peak. <sup>b</sup> This value is given to conditions that are outside the boundary limits.

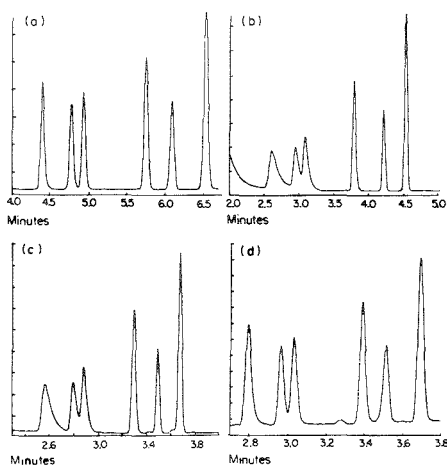


Figure 5. Four chromatograms from the first two-parameter simplex: (a) vertex 1, (b) vertex 3, (c) vertex 15, (d) vertex 16. Components are, from left to right, hexane (solvent), acetophenone, propiophenone, bicyclohexyl, biphenyl, undecylbenzene, and benzophenone. See Table I for conditions and response values for these chromatograms. Signals corresponding to tallest peaks were (a) 26, (b) 44, (c) 48, and (d) 17.2  $\mu$ A.

and the progression of the CRF values. The best response was obtained at vertex 13, with a density gradient of 0.22 (g/mL)/min and an oven temperature of 97 °C. The response at vertex 13 (0.239) is essentially equivalent to that at vertex 16 (0.234) in the first simplex (cf. Tables I and II). The somewhat faster convergence of the second simplex is explained by its larger initial step sizes, thus requiring less time to reach the optimum region. Nonetheless, since both trial runs converged to essentially the same conditions, it is highly probable that the global optimum has been reached.

From Tables I and II it can be seen that the last vertices in the simplex are not always the ones with the best response. This is due to the fact that once an optimum region is reached, the simplex begins to "circle" the optimum. At this point it is advisable to discontinue the simplex, as many experiments could be wasted in the close vicinity of the optimum (3). In our view, whenever a set of experimental conditions that provides the desired separation within the maximum specified analysis time has been found, the optimization procedure (method development) can be halted. Although we feel that

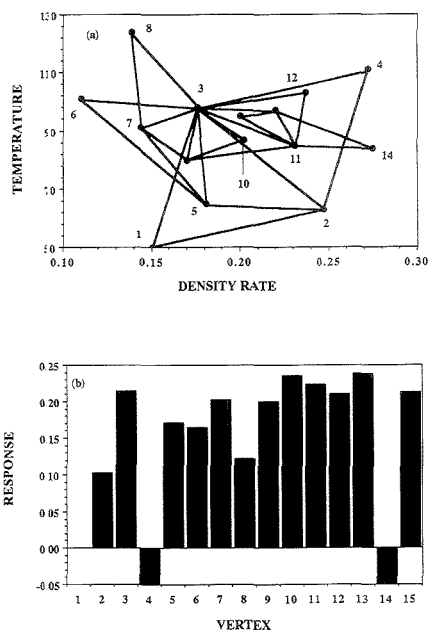


Figure 6. Second run for the simplex optimization of density gradient rate and column temperature performed on the test mixture, showing (a) simplex progress and (b) response progress.

this is the most practical criterion for ending a simplex, other more rigorous criteria for simplex termination are also available. One such criterion is based on a comparison of the relative change in the various experimental conditions (17). For the last three vertices of the first simplex (Table I), the relative standard deviation for the density rate and temperature are 8% and 6%, respectively. Although somewhat higher than desirable, we believe these data indicate that the predicted optimum for density rate and temperature are close to the true optimum.

Whereas a linear density gradient at constant temperature may result in a more predictable solvent strength program, asymptotic density gradients have been shown to give a better separation for the later-eluting oligomeric peaks of higher molecular weight samples (28), particularly when a temperature gradient is performed simultaneously (29). Unfortu-



Table III. Results of Two-Parameter Simplex, Simultaneous Gradients

vertex	pressure rate, atm/min	temp rate, °C/min	response (eq 2)	$t_w^a$ , min	simplex movement	retained vertices
1	30	20	0.263	3.61	-	-
2	69	25	0.326	2.62	-	-
3	40	39	0.283	3.15	-	-
4	79	44	$-\infty^b$	-	reflection	2,3
5	42	26	0.283	3.23	$c_w$ contraction	2,3
6	71	12	0.332	2.59	reflection	2,5
7	86	-1.7	$-\infty$	-	expansion	2,5
8	97	11	0.296	2.33	reflection	2,6
9	83	15	0.341	2.47	$c_c$ contraction	2,6
10	85	1.6	$-\infty$	-	reflection	6,9
11	73	19	0.333	2.59	$c_w$ contraction	6,9
12	85	22	0.342	2.47	reflection	9,11
13	93	27	0.345	2.38	expansion	9,11
14	103	23	0.325	2.31	reflection	9,13
15	80	20	0.344	2.51	$c_w$ contraction	9,13
16	90	33	0.338	2.42	reflection	13,15
17	85	19	0.331	2.46	$c_w$ contraction	13,15
18	98	26	0.338	2.36	reflection	13,17

<sup>a</sup>  $t_w$  is the retention time of the last eluting peak. <sup>b</sup> This value is given to conditions that are outside the boundary limits.

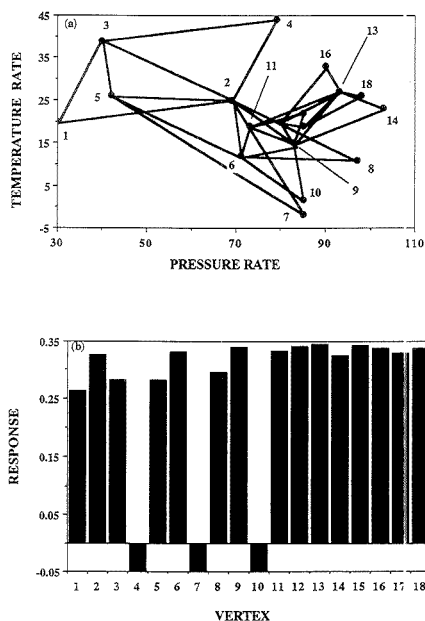


Figure 7. Simplex optimization using two simultaneous gradients (pressure and temperature) performed on the test mixture, showing (a) simplex progress and (b) response progress.

nately, asymptotic gradients are more tedious to generate experimentally, and this disadvantage would be exacerbated during the course of a simplex run. Fortunately, however, asymptotic density gradients can usually be approximated by a linear pressure program. Thus in order to consider the possible benefits of optimizing these variables, a third simplex algorithm was run by using simultaneous linear pressure and temperature gradients on this same test mixture used in simplex runs 1 and 2. The boundary limits for this simplex were 5–150 atm/min and 5–40 °C/min. The data for this simplex are given in Table III. Figure 7a shows the simplex progress, and the CRF evolution is shown in Figure 7b. Two chromatograms for this optimization are shown in Figure 8.

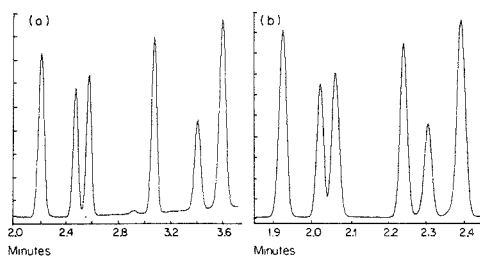


Figure 8. Two chromatograms from the simultaneous gradient simplex: (a) vertex 1 and (b) vertex 13 (best response). See Table I for conditions and response values for these two chromatograms. Signals corresponding to tallest peaks were (a) 22 and (b) 52 pA.

Figure 8a is the chromatogram obtained for the initial vertex, while Figure 8b is the chromatogram for vertex 13, at which the best response was obtained. The major improvement observed is about a 33% reduction in analysis time. For separations to be transferred to a longer column, this reduction of analysis time becomes very significant. For this separation, a higher linear velocity of 2 cm/s was used, resulting in a shorter analysis time than that observed in Figure 5, and thus higher response function values. The temperature gradient reduced peak tailing (cf. Figure 5 and 8) and allowed closer peak spacing without overlap, also contributing to the shorter analysis time.

**Three-Variable Simplex.** While the above optimizations provide a useful graphical representation of the simplex progress, the initial density (or pressure) is also an important parameter that should be considered in SFC optimizations. We have found that, other factors being equal, the starting density determines the highest initial temperature that can be used without merging the first solute peak and the solvent peak. For this reason the starting density was also included as a parameter in the simplex.

This three-variable simplex algorithm was employed to optimize the separation of a sesquiterpene lactone sample. One of the largest groups of plant products, sesquiterpene lactones possess great biological activity and are useful in many medical and agricultural capacities (30). Separation techniques often used for these compounds include column liquid chromatography, gas chromatography (GC), and reversed-phase high-performance liquid chromatography (HPLC).

Table IV. Results of Three-Parameter Simplex

vertex	initial density, g/mL	density rate, (g/mL)/min	temp, °C	response (eq 2)	$t_w^a$ , min	simplex movement	retained vertices
1	0.250	0.100	60	0.132	4.74	-	-
2	0.486	0.171	84	0	-	-	-
3	0.309	0.383	84	$-\infty^b$	-	-	-
4	0.309	0.171	154	0	-	-	-
5	0.387	-0.089	115	$-\infty$	-	reflection	1,2,4
6	0.329	0.265	91	0.0901	2.09	$c_w$ contraction	1,2,4
7	0.401	0.186	2	$-\infty$	4.74	reflection	1,2,6
8	0.332	0.175	116	0	1.73	$c_w$ contraction	1,2,6
9	0.121	0.189	95	$-\infty$	-	reflection	1,6,8
10	0.395	0.175	86	0.157	2.06	$c_w$ contraction	1,6,8
11	0.317	0.186	42	$-\infty$	-	reflection	1,6,10
12	0.328	0.177	98	0.055	2.41	$c_w$ contraction	1,6,10
13	0.320	0.037	71	0.129	4.66	reflection	1,10,12
14	0.315	0.031	47	$-\infty$	-	reflection	1,10,13
15	0.325	0.141	85	0.131	2.73	$c_w$ contraction	1,10,13
16	0.326	0.241	83	0.128	2.43	reflection	1,10,15
17	0.322	0.088	74	0.146	3.52	$c_w$ contraction	1,10,15
18	0.319	0.101	62	0.163	3.76	reflection	1,10,17
19	0.316	0.082	50	0	-	expansion	1,10,17
20	0.440	0.143	88	0	-	reflection	10,17,18
21	0.298	0.111	67	0.182	3.73	$c_w$ contraction	10,17,18
22	0.231	0.025	49	$-\infty$	2.73	reflection	17,18,21
23	0.354	0.138	77	0.136	2.85	$c_w$ contraction	17,18,21
24	0.365	0.107	75	0.141	2.47	reflection	17,18,23
25	0.317	0.060	64	0.143	2.38	reflection	17,18,24
26	0.273	0.059	58	0.128	2.31	reflection	17,18,25
27	0.342	0.095	71	0.131	2.51	$c_w$ contraction	17,18,25
28	0.338	0.130	74	0.147	2.42	reflection	17,18,27
29	0.310	0.117	69	0.130	2.46	reflection	17,18,28
30	0.334	0.101	70	0.133	2.36	$c_w$ contraction	17,18,28

<sup>a</sup>  $t_w$  is the retention time of the last eluting peak. <sup>b</sup> This value is given to conditions that are outside the boundary limits.

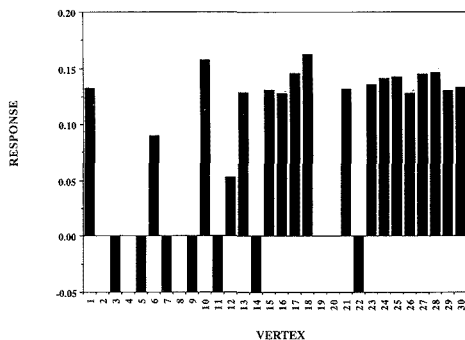


Figure 9. Response progress for the three-parameter simplex on the sesquiterpene lactone sample.

None of these methods, however, has proven to be completely satisfactory. Classical column chromatography does not always provide the needed resolution, GC analysis may result in thermal degradation of the sample, and HPLC is limited by the lack of a sensitive universal detector.

For these reasons, SFC would appear to be a promising alternative for the separation of these compounds. To our knowledge, the present study represents the first separation of this class of compounds by SFC. Although somewhat polar and perhaps more amenable to a modified  $\text{CO}_2$  mobile phase, at least some sesquiterpene lactones can be separated with pure  $\text{CO}_2$  (vide infra).

For the optimization of the sesquiterpene sample, a 55-cm SB-Biphenyl-30 column with an internal diameter and film thickness of 50 and 0.25  $\mu\text{m}$ , respectively, was used for the separation. Boundary limits were 0.2–0.5 g/mL (initial den-

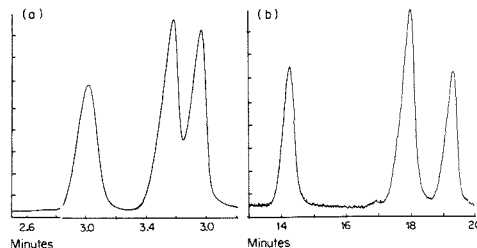


Figure 10. Chromatograms from the sesquiterpene lactone sample optimization for (a) the separation with the best response from the simplex (vertex 18) and (b) the separation after transfer to the 3-m column. Conditions for chromatogram a are given in Table III and for chromatogram b were 0.319 g/mL initial density, 0.01 g/mL/min gradient and 62 °C oven temperature. Components are, from left to right, psiosotachyin A, burrodin, and glaucolide A. Signals corresponding to tallest peaks were (a) 44 and (b) 16 pA.

sity), 0.01–0.4 (g/mL)/min (density gradient rate), and 50–200 °C (temperature). Table IV gives the experimental parameters used in the simplex and the responses for the vertices; simplex movement was not shown due to the difficulty of graphically representation of a three-dimensional figure in two dimensions. Figure 9 shows how the CRF evolved as the simplex progressed. After 30 vertices the simplex was terminated, with vertex 18 giving the best response with initial density of 0.319 g/mL, a 0.101 (g/mL)/min density gradient after solvent elution, and an oven temperature of 62 °C. Figure 10a shows the optimized chromatogram for this short column.

**Increasing  $N$  for the Final Separation.** We have found that it is worthwhile to have several different lengths of columns on hand so that the efficiency can be varied as necessary once the selectivity and retention have been op-

timized. From Figure 10a it is clear that the 55-cm column does not provide sufficient resolution for this sesquiterpene lactone sample. The resolution in this chromatogram is about 0.4 for the last two peaks. Transferring the method to a 300-cm column, an increase in length of 5.5, should increase  $R_s$  by a factor of  $5.5^{1/2}$  to a value near unity. The corresponding gradient rate to use would be  $(0.101 \text{ (g/mL)/min})/5.5 = 0.018 \text{ (g/mL)/min}$ . To achieve a resolution greater than unity, we employed a slightly lower gradient rate of  $0.010 \text{ (g/mL)/min}$ . Note that we intuitively selected this lower gradient rate for the final separation to provide a slightly higher resolution. The resulting separation is shown in Figure 10b. A decrease in the signal to noise ratio is apparent here, resulting from longer analysis times which decrease the peak heights.

**Response Functions.** The continuous CRF used above (CRF-2) proved to be the most efficient and successful of all the CRFs we examined. Calculation of CRF values was quick and straightforward, aided by a simple, yet effective, computer program. As can be seen from Figure 5, however, and as stated in the theory section, continuous CRFs do compromise resolution with analysis time up to a point. If a threshold CRF with  $R_{s,\text{min}} = 1.5$  (e.g., CRF-1) been used in the first simplex instead of the continuous CRF-2, vertex 16 would not have been the best set of conditions but would rather have received a value of zero because of peaks two and three (see Figure 5). The simplex would have obviously taken a different course dictated by that criterion.

If column efficiency is constant throughout an optimization procedure, a useful parameter to use in eq 1 instead of  $R_s$  would be the separation factor  $S$ , defined as (31)

$$S = \frac{t_2 - t_1}{t_1 + t_2} \quad (5)$$

Equation 5 has the advantage of easily being obtained from the chromatogram and is related to resolution in the following manner:

$$R_s = S \frac{N^{1/2}}{2} \quad (6)$$

Unfortunately we cannot always assume that the column efficiency will be constant for all peaks in a chromatogram, or for chromatograms run under different conditions. As shown by Snyder, et al. (32), the bandwidth of a peak observed in gradient elution is reduced compared to that obtained under nongradient conditions. The factor by which the bandwidth is reduced is usually a function of gradient steepness and is also determined by the instantaneous value of  $k'$  as the solute leaves the column. This reduction in bandwidth cannot be estimated under nongradient conditions, so that in order to correctly use the separation factor approach, bandwidths for each chromatogram under different gradient conditions would have to be calculated. In general, it is easier to measure resolution directly using eq 7

$$R_s = \frac{t_2 - t_1}{w_{\text{avg}}} \quad (7)$$

where  $t_1$  and  $t_2$  are the retention times and  $w_{\text{avg}}$  is the average width of the peaks at the base line. For pairs of peaks with resolution obviously greater than that desired, a measurement is not needed for threshold CRFs like CRF-1.

**Solvent Peak.** The anticipated problem of separating the first solute peak from the solvent peak was solved by using a response function which severely penalizes such overlap. Since gradients were initiated immediately after the solvent had eluted, analyte peaks on or near the tail of the solvent peak were broad because they were eluted under nongradient conditions. Figure 5b demonstrates this effect. Since the

peaks eluting under nongradient conditions are not focused, the relative height of the valley is greater and the chromatogram is thus penalized. When the first solute peak elutes late enough to be truly influenced by the gradient, it will receive a better value from the response function. Our results indicate that it requires less than 1 min of gradient conditions for the first solute peak to be sharp and well-separated from the solvent.

Since the length of time necessary to elute the solvent will change depending on initial conditions, it may be difficult to determine the hold time needed. Although it is reasonable to use the longest hold time that will be encountered for any one chromatogram for all the chromatograms considered, doing this will penalize those chromatograms in which the solvent elutes well before the end of the set hold time. A better approach is either to manually start gradients once the solvent has eluted or to run a solvent blank before each sample to determine the hold time. Alternatively, if the linear velocity could be accurately predicted, the elution time of the solvent for a given set of experimental conditions could be predicted, assuming the solvent was more or less unretained ( $k' = 0$ ). A more sophisticated solution would be the use of a data feedback system to start the gradients once the detector signal returns to a given value after solvent elution.

## CONCLUSIONS

A systematic method development scheme is clearly desirable for SFC, and as we have shown in the present work, the modified simplex algorithm is a promising approach to the optimization of SFC separations. By use of a short capillary column and first optimizing the selectivity and retention, rapid separations are possible in the development stage, with the potential of optimizing efficiency later if needed. This saves hours of analysis time, especially if the short column proves to be sufficient for the final separation. Confidence that the global optimum has been found is provided by the convergence to the same conditions of two simplexes started at different points within the parameter space.

Since our report represents the first application of the simplex algorithm in SFC, there are many avenues open for development. Although we have demonstrated the potential of simplex optimization in SFC and have shown how it can be successfully implemented, additional studies focusing on the selection of the best combinations of experimental parameters to optimize are clearly warranted. Other opportunities for research include the extension of the simplex method to packed columns and modified mobile phases and a detailed evaluation of other response functions not examined in the present study. Finally, other optimization strategies, such as a grid search (33), factorial design (34), or window diagrams (35) may also prove to be useful.

## ACKNOWLEDGMENT

The authors gratefully acknowledge N. H. Fischer and his group for providing the sesquiterpene lactones.

## LITERATURE CITED

- (1) Snyder, L. R.; Glajch, J. L.; Kirkland, J. J. *Practical HPLC Method Development*; Wiley: New York, 1986.
- (2) Watson, M. W.; Carr, P. W. *Anal. Chem.* **1979**, *51*, 1835-1842.
- (3) Schoenmakers, P. J. *Optimization of Chromatographic Selectivity*; Elsevier: Amsterdam, 1986.
- (4) Berridge, J. C. *Techniques for the Automated Optimization of HPLC Separations*; Wiley: Chichester, England, 1985.
- (5) Snyder, L. R.; Kirkland, J. J. *Introduction to Modern Liquid Chromatography*; Wiley: New York, 1979.
- (6) Chester, T. L.; Innis, D. P. *HRC CC, J. High Resolut. Chromatogr. Chromatogr. Commun.* **1985**, *8*, 561-566.
- (7) Ashraf-Khorassani, M.; Taylor, L. T. *J. Chromatogr. Sci.* **1988**, *26*, 331-336.
- (8) Smith, Roger M., Ed. *Supercritical Fluid Chromatography*; Royal Society of Chemistry: London, 1988.
- (9) Deming, S. N.; Morgan, S. L. *Anal. Chem.* **1973**, *45* (3), A278-A283.
- (10) Berridge, J. C.; Morrissey, E. G. *J. Chromatogr.* **1984**, *316*, 69-79.

- (11) Berridge, J. C. *J. Chromatogr.* **1982**, *244*, 1-14.  
 (12) Balconi, M. L.; Sigon, F. *Anal. Chim. Acta* **1986**, *191*, 299-307.  
 (13) Dose, E. V. *Anal. Chem.* **1987**, *59*, 2420-2423.  
 (14) Morgan, S. L.; Deming, S. N. *J. Chromatogr.* **1975**, *112*, 267-285.  
 (15) Morgan, S. L.; Jacques, C. A. *J. Chromatogr. Sci.* **1978**, *16*, 500-504.  
 (16) Bartu, V.; Wicar, S.; Scherpenzeel, G. J.; Leclercq, P. A. *J. Chromatogr.* **1986**, *370*, 219-234.  
 (17) Jurs, P. C. *Computer Software Applications in Chemistry*; Wiley: New York, 1986.  
 (18) Deming, S. N.; Parker, L. R., Jr. *CRC Crit. Rev. Chem.* **1978** (September), 187-202.  
 (19) Shavers, C. L.; Parsons, M. L.; Deming, S. N. *J. Chem. Educ.* **1979**, *56* (5), 307-309.  
 (20) Wegscheider, W.; Lankmayr, E. P.; Budna, K. W. *Chromatographia* **1982**, *15* (8), 498-504.  
 (21) Debets, H. J. G.; Bajema, B. L.; Doornbos, D. A. *Anal. Chim. Acta* **1983**, *151*, 131-141.  
 (22) Christophe, A. B. *Chromatographia* **1971**, *4*, 455-458.  
 (23) Smits, R.; Vanroelen, C.; Massart, D. L. Z. *Anal. Chem.* **1975**, *273*, 1-5.  
 (24) Schoenmakers, P. J.; Naish, P. J.; Hunt, R. J. *Chromatographia* **1987**, *24*, 579-587.  
 (25) Crow, J. A.; Foley, J. P. *HRC CC, J. High Resolut. Chromatogr. Chromatogr. Commun.* **1989**, *12*, 467-470.  
 (26) Snyder, L. R. In *High-Performance Liquid Chromatography: Advances and Perspectives*; Horvath, C., Ed.; Academic Press: New York, 1980; Vol. 1, pp 208-316.  
 (27) Nelcer, J. A.; Mead, R. *Computer J.* **1965**, *7*, 308-313.  
 (28) Fjellisted, J. C.; Jackson, W. P.; Peadar, P. A.; Lee, M. L. *J. Chromatogr. Sci.* **1983**, *21*, 222-226.  
 (29) Later, D. W.; Campbell, E. R.; Richter, B. E. *HRC CC, J. High Resolut. Chromatogr. Chromatogr. Commun.* **1988**, *11*, 65-69.  
 (30) Fischer, N. H.; Olivier, E. J.; Fischer, H. D. *Fortschr. Chem. Org. Naturst.* **1979**, *38*, 47-390.  
 (31) Ober, S. S. In *Gas Chromatography*; Coates, V. J.; Noebels, H. J., Fagron, I. S., Eds.; Academic Press: New York, 1958; pp 41-50.  
 (32) Snyder, L. R.; Dolan, J. W.; Gant, J. R. *J. Chromatogr.* **1979**, *165*, 3-33.  
 (33) Svoboda, V. *J. Chromatogr.* **1980**, *201*, 241-252.  
 (34) Kong, R. C.; Sachok, B.; Deming, S. N. *J. Chromatogr.* **1980**, *199*, 307-321.  
 (35) Lau, R. J.; Purnell, J. H. *J. Chromatogr.* **1975**, *112*, 71-79.

RECEIVED for review August 14, 1989. Accepted November 3, 1989. J.P.F. gratefully acknowledges support provided by grants from the Exxon Education Foundation and the LSU Center for Energy Studies. J.A.C. is the recipient of an LSU Alumni Federation Fellowship.

## Determination of Iodine in Oyster Tissue by Isotope Dilution Laser Resonance Ionization Mass Spectrometry

J. D. Fasset\* and T. J. Murphy

Center for Analytical Chemistry, National Institute of Standards and Technology, Gaithersburg, Maryland 20899

The technique of laser resonance ionization mass spectrometry has been combined with isotope dilution analysis to determine iodine in oyster tissue. The long-lived radioisotope,  $^{129}\text{I}$ , was used to spike the samples. Samples were equilibrated with the  $^{129}\text{I}$ , wet ashed under controlled conditions, and iodine separated by coprecipitation with silver chloride. The analyte was dried as silver ammonium iodide upon a tantalum filament from which iodine was thermally desorbed in the resonance ionization mass spectrometry instrument. A single-color, two-photon resonant plus one-photon ionization scheme was used to form positive iodine ions. Long-lived iodine signals were achieved from 100 ng of iodine. The precision of  $^{127}\text{I}/^{129}\text{I}$  measurement has been evaluated by replicate determinations of the spike, the spike calibration samples, and the oyster tissue samples and was 1.0%. Measurement precision among samples was 1.9% for the spike calibration and 1.4% for the oyster tissue. The concentration of iodine determined in SRM 1566a, Oyster Tissue, was 4.44  $\mu\text{g/g}$  with an estimate of the overall uncertainty for the analysis of  $\pm 0.12 \mu\text{g/g}$ .

Iodine is an essential trace element for man. Its accurate measurement in foods is vital to understanding human dietary intake and verifying that minimum daily allowances are observed, especially in restricted diets such as infant formulations. Isotope dilution mass spectrometry (IDMS) is an inherently accurate technique (1), a "definitive method" for which systematic errors can be thoroughly evaluated. In general, the quantity of an element is determined by IDMS by measurement of the change in isotopic ratio that is produced by adding a calibrated amount of an enriched isotope

of the element to the sample. As such, the technique can only be used for elements with more than one isotope. Iodine has only one stable isotope in nature,  $^{127}\text{I}$ . However, the radioisotope  $^{129}\text{I}$  is long-lived (half-life,  $1.59 \times 10^7$  years) and available. Thus, the accurate measurement of I in biological and botanical matrices by using IDMS is made possible.

Mass spectrometric methods have been developed both to measure isotope ratios of iodine for IDMS and to measure ultratrace amounts of  $^{129}\text{I}$  in the environment, which is typically at levels  $10^{-6}$  to  $10^{-12}$  of stable  $^{127}\text{I}$ , itself at part-per-million levels in botanical and biological material. A negative thermal ionization (TIMS) technique has been developed by Heumann et al. They have used IDMS to determine I in salt, chemicals, food, and water (2-4). A second negative thermal ionization technique has been published by Delmore in which lanthanum hexaboride is cataphoretically deposited onto a rhenium ionization filament. This filament treatment lowers the work function of the rhenium and results in high ionization efficiency and measurement sensitivity for iodine (5). Delmore's technique was adapted in our laboratory and used to determine iodine in SRMs 1572 (Citrus Leaves) and 1549 (Powdered Milk) by IDMS (6).

Secondary ionization mass spectrometry (SIMS) was initially investigated to measure  $^{129}\text{I}$  (7). Ion sputtering ionization, as is done in SIMS, is also used in accelerator mass spectrometry (AMS), which has achieved the lowest detection limits for  $^{129}\text{I}$  (8). AMS effectively eliminates the limiting background of isobaric molecular interferences which are observed in both secondary ionization and thermal ionization mass spectrometry. The detection of  $^{129}\text{I}$  in the environment after the Chernobyl reactor accident is an example of AMS capabilities (9).

Laser resonance ionization mass spectrometry (RIMS) has been studied in our laboratory for possible application to  $^{129}\text{I}$

measurement (10). A relatively simple, single-color resonance ionization scheme (two-photon resonance + one-photon ionization) was shown to be both efficient and moderately selective. The practical application of RIMS to the problem of  $^{129}\text{I}$  measurement is impeded by the difficulties in achieving high sample utilization efficiencies while using a combination of pulsed lasers and continuous thermal atomization. These experiments did serve to demonstrate that long-lived ion beams of moderate intensity could be generated from nanogram quantities of iodine. Thus, RIMS appeared capable of being used straightforwardly with IDMS to determine part per million levels of iodine in biological and botanical materials.

We report here the results of an IDMS analytical project for determination of iodine in SRM 1566a, Oyster Tissue, using ID-RIMS. This project included the calibration of the  $^{129}\text{I}$  spike for concentration and isotopic composition; the determination of iodine analytical blank; the analysis of previously certified material, SRM 1549 (Powdered Milk); and the analysis of the new SRM material.

## EXPERIMENTAL SECTION

**Reagents.** High-purity reagents, produced by subboiling distillation (11) at NIST and stored in Teflon bottles, were used in this study. Ammoniacal cyanide solution was prepared by passing 50 mL of a solution containing 1 g of KCN followed by 10 mL of high-purity water through an acid-cleaned cation exchange column and collecting the eluate, containing dilute HCN, in 40 mL of 2 mol/L  $\text{NH}_4\text{OH}$ .

**Isotopic Spike.** The isotopic spike was SRM 4949A, Iodine-129 Radioactivity Standard, obtained from the Office of Standard Reference Materials, NIST, Gaithersburg, MD. A solution of this material was prepared in a Teflon bottle and made alkaline by the addition of sodium carbonate. The solution was calibrated by ID-RIMS against high-purity potassium iodide and contained  $(4.181 \pm 0.081) \times 10^{-8}$  mol/g (1s,  $n = 6$ ). The measured spike ratio,  $^{127}\text{I}/^{129}\text{I}$ , was  $0.1579 \pm 0.0013$  (1s,  $n = 5$ ) or atom fraction content of 0.1364 for  $^{127}\text{I}$  and 0.8636 for  $^{129}\text{I}$ .

**Chemistry.** Duplicate samples of about 1 g, accurately weighed, were taken from each of three different bottles of SRM 1566a, Oyster Tissue. A third sample was taken from each bottle and dried for 48 h in a vacuum desiccator (160 Torr,  $2.1 \times 10^4$  Pa) at room temperature over magnesium perchlorate. The percentage weight loss of each sample was used to correct the sample weight to dry weight for each sample from the corresponding bottle. (Weight losses ranged from 1.9 to 2.3%.)

Each sample was transferred to a 250-mL bottle made of Teflon-FEP and spiked with a weighed quantity of  $^{129}\text{I}$  solution. The spiked samples were wet ashed by heating with 15 mL of fuming nitric acid (90%  $\text{HNO}_3$ , ACS reagent grade. This procedure retains iodine by oxidation to iodate while destroying the organic matrix. Once red fumes of nitric oxide were no longer produced, 5 mL of perchloric acid was added to each solution. The solutions were heated to complete the oxidation. Each solution was then diluted with about 10 mL of high-purity water and transferred to a 40-mL centrifuge tube. The insoluble matter (mainly  $\text{KClO}_4$ ) was removed by centrifugation followed by decantation. Iodate was then reduced with 5 mL of hydrazine sulfate solution (2 g of hydrazine sulfate/100 mL of water). The resulting iodide was coprecipitated with chloride by the addition of 1 mL of 0.01 mol/L HCl and 1 mL of 0.005 mol/L silver nitrate solution. The mixed  $\text{AgCl-AgI}$  precipitate was allowed to stand overnight in the dark and separated by centrifugation, washed, and dissolved in ammoniacal cyanide solution. Ten milliliters of 2.5 mol/L  $\text{HNO}_3$  was added to reprecipitate  $\text{AgCl-AgI}$ . The precipitate was again separated by centrifugation and dissolved in ammoniacal cyanide for mass spectrometric analysis at about 20  $\mu\text{g}$  of I/mL.

**Instrumentation.** The RIMS instrument has been previously described in detail (12, 13). The system consists of a pulsed, 10-Hz laser system capable of producing 3 mJ of UV radiation ranging from 260 to 306 nm, a 60° radius-of-curvature magnetic sector thermal source mass spectrometer with an ion multiplier detection system, and a transient digitizer to accumulate the pulsed ion flux. The mass spectrometer is fully automated with respect to magnet

switching, laser wavelength scanning, and data acquisition from the transient digitizer. For iodine, a 30-cm quartz lens is used to focus the laser to a 200- $\mu\text{m}$ -diameter beam waist in front of the sample filament.

**Sample Filaments and Sample Loading.** Tantalum filaments, 6.2 mm  $\times$  1.3 mm  $\times$  0.025 mm, in which a shallow groove had been formed, were used to dry the samples. A 5-mL aliquot of the sample solution was dried on the sample filament (100 ng of I) for each individual mass spectrometric determination.

## RESULTS AND DISCUSSION

The ultimate purpose of this work was to determine the concentration of iodine reliably in oyster tissue by using isotope dilution mass spectrometry. There were two main components to this work: chemical and instrumental. Chemical procedures were developed to ensure equilibration of the spike with the sample and to separate the iodine in a form suitable for measurement. Laser mass spectrometric procedures were investigated for accurate and precise isotopic ratio measurement.

**Chemistry.** The accuracy of IDMS is totally reliant upon the isotopic equilibration of the spike isotope with the natural element in the sample. Thus, loss of analyte from the sample (or the spike added) before equilibration is achieved cannot be tolerated. Once equilibration occurs between the isotopes, loss of the element can be tolerated, since it is the isotopic ratio that defines the original concentration. The key step is dissolving the sample and bringing the spike and natural isotopes to the same oxidation state with no elemental loss.

The equilibration of the spike isotope and natural  $^{127}\text{I}$  was studied by using radioactive  $^{129}\text{I}$  (half-life, 60.1 days) as a tracer isotope and by monitoring the radioactivity during the chemical processing steps. A quantity of  $^{129}\text{I}$  was added to each sample so that sufficient  $\gamma$ -ray counts over background were observed in reasonable counting periods (a few minutes). Various methods of wet ashing the organic matrix and oxidizing iodide to iodate were investigated. Fuming nitric acid solubilized the sample while retaining and oxidizing the iodide. Dissolution could be accomplished overnight on a hot plate; addition of perchloric acid and further heating completed the process. Once the samples were oxidized, a slow loss of iodine was observed. However, samples that suffered variable losses of iodine at this stage were analyzed and the precision of the measured results for concentration indicated that equilibration had been achieved.

The  $^{129}\text{I}$  tracer experiments indicate that after the final recovery steps, reduction of iodate to iodide and coprecipitation with chloride, 70–85% of the iodine is recovered in the experiment.

**Resonance Ionization.** The ionization potential of iodine is 84 340  $\text{cm}^{-1}$  (10.25 eV) and the first electron excited state is 54 633  $\text{cm}^{-1}$ . These parameters dictate the choice of a resonance ionization scheme that uses readily generated UV radiation: a three-photon process, where the absorption of two photons is required to reach the discrete electronic level for iodine and absorption of the third photon results in ionization, a so-called 2 + 1 process. The utility of the generalized 2 + 1 process in resonance ionization has been addressed and experimental results shown for Au, Bi, Ca, Cu, Mg, Y, Ta, and Zr (14) using visible wavelengths. We have previously used this scheme to demonstrate RIMS for both Be (15) and C (16) using UV wavelengths. Roughly half of the elements in the periodic table are suitable for resonance ionization using the 1 + 1 single-color scheme with wavelengths between 260 and 355 nm. The addition of the 2 + 1 resonance ionization scheme expands significantly the number of elements that can be resonantly ionized using a single tunable laser system.

The efficiency of the 2 + 1 process has been examined for C and for other elements (14, 16). Both theory and experiment have demonstrated that the sensitivity of the process can be

high for selected transitions. In general, the 2 + 1 scheme will require higher laser intensities than resonance ionization schemes in which all excitation steps are resonantly enhanced. In our experiment, the higher laser intensity is achieved by the insertion of a 30-cm focal length lens that increases the laser fluence in front of the sample filament by a factor of 400, at a cost of decreasing the geometrical overlap with the atom cloud thermally desorbed from the filament. Although we have not measured the efficiency of this arrangement experimentally, ionization efficiency is not the limit to sensitivity in the IDMS determinations described here. The analytical blank provides the sensitivity limit in our measurements.

We have previously reported on the spectroscopy for iodine using our experimental system, examining the wavelength range 278–310 nm (10). The most intense signals were observed at 279.7 and 298.2 nm. These wavelengths correspond to two-photon transitions from the ground state of iodine to levels at 71 501.5 and 67 062.1  $\text{cm}^{-1}$ . The 298.2-nm wavelength is analytically more useful, being both more sensitive and selective than the 279.7-nm wavelength.

Isotope effects must be considered in any RIMS measurement process (17). Even when isotope shifts and hyperfine splitting of resonant levels are expected to be small relative to the laser bandwidth, accurate measurement of isotope ratios cannot be assumed. Fairbank et al. have observed anomalous ratios for Sn and Mo (18). They attribute their observations to the redistribution of population between ground- and excited-state magnetic sublevels by the resonance radiation. We have examined wavelength-dependent effects on iodine isotope ratios in two ways, using the enriched iodine spike. First, we scanned the laser wavelength for both isotopes and ratioed the results. Second, we measured isotope ratios at wavelengths on both sides of the resonance maximum. Neither experiment showed a significant isotope effect.

Our previous investigations have shown that a number of iodine-containing molecular species are formed in addition to iodine atoms during heating in the mass spectrometer. The formation of these species affects the sample utilization efficiency, but the generation of adequate signals was not a problem here. There exists a much larger nonresonant background at 279.1 nm than at 298.2 nm. This nonresonant background has been ascribed to dissociation and ionization of these iodine-containing species, which occurs more efficiently for the lower wavelength, more energetic photons. The typical ratio of resonance to nonresonance signal at 298.2 nm was 100.

**Memory.** One of the problems previously noted for iodine analysis using thermal ionization mass spectrometry is instrumental memory (6). This memory is caused by the relatively high vapor pressures of iodine-containing species that are desorbed into the source of the mass spectrometer. The presence of gas-phase iodine species is readily observed using RIMS since iodine signals can be detected without heating of the sample filament. In thermal ionization, the need for having a hot, ionizing filament (1000 °C) increases the likelihood of desorbing iodine which has been deposited on source components. Practically, the problem is avoided by more frequent cleaning of the source of the mass spectrometer, especially between samples of disparate isotopic ratios.

The temperature used in heating the sample filament in RIMS is not measurable with an optical pyrometer and is probably less than 550 °C, the melting point of AgI. Thus, memory is expected to be less of a problem for RIMS relative to TIMS. The lower precision for ratio measurement in RIMS makes the observation of memory less obvious. However, when the spike ( $^{127}\text{I}/^{129}\text{I} = 0.1579$ ) was run immediately after a set of samples ( $^{127}\text{I}/^{129}\text{I} \sim 7$ ), the measured ratio was about 4% high. Baking the source with a blank tantalum filament

Table I. Analysis of Oyster Tissue, SRM 1566a

bottle/ sample	weight, g	run no.	ratio	<i>I</i> , $\mu\text{g/g}$	av
1-1	1.200 73	29	3.001	4.486	4.477
		31	2.990	4.468	
1-2	1.038 65	27	2.404	4.455	4.424
		33	2.373	4.393	
2-1	1.180 93	25	3.187	4.420	4.380
		34	3.132	4.340	
2-2	1.008 84	24	2.853	4.376	4.376
3-1	0.993 26	28	2.462	4.518	4.478
		32	2.422	4.439	
3-2	0.907 45	30	2.785	4.529	4.529
				av	4.444
				std dev	0.061
				RSD	1.4%

(2000 °C) was effective in eliminating any observable cross contamination among samples, and this precaution was taken between sets of samples with disparate ratios.

**Fractionation.** Isotopic fractionation in the thermal vaporization process is often the limiting source of measurement precision in thermal ionization. We have assessed the extent of isotopic fractionation by dividing the ratio measurements made for each mass spectrometric run into two equal time periods. The average relative difference between the first and second halves of measurement was 0.00% (95% confidence limit,  $\pm 0.34\%$ ). Thus, isotopic fractionation is not significant relative to the other sources of measurement uncertainty.

**Isotope Dilution Results.** The isotope dilution experiment required characterization of the  $^{129}\text{I}$  spike, both isotopic analysis and concentration measurements, as well as the measurement of iodine in the oyster tissue samples and the chemical blank for the procedure. In addition, the previously certified material Powdered Milk, SRM 1549, was analyzed as a check sample to verify the accuracy of the technique. Replicate isotopic measurements were made in the experiment to assess the variability of mass spectrometric measurement. A total of 40 mass spectrometric runs were made (excluding set up runs) consisting of 5 measurements of the isotopic composition of the spike, 10 measurements made on 6 spike calibration samples, 13 measurements made on 6 Oyster Tissue and 3 Powdered Milk samples, and 6 blanks. Typical internal measurement imprecision among ratios was 1% (2 standard deviations of the mean of 50 ratios); the range was 0.55–2.1%. Ratio measurement precisions for replicates were 1.1% relative standard deviation with 4 degrees of freedom for the spike calibration samples and 1.0% relative standard deviation with 4 degrees of freedom for the oyster tissue samples. The relative standard deviation was 0.9% for measurement of the spike (five determinations). Thus, ratio measurement precision is consistently about 1.0%.

Six blanks were determined. These were deliberately overspiked but gave results ranging from 8 to 14 ng. An average blank of 11 ng was subtracted from the isotope dilution results, representing an adjustment of 0.2–0.25%. The results for sample analysis are summarized in Table I.

Since the spike calibration, spike, and samples were mass spectrometrically determined in an identical fashion, any systematic error due to instrumental discrimination will be cancelled. The uncertainty is dominated by the instrumental measurement precision. The between-bottle variance is larger than the within-bottle variance, but the small number of degrees of freedom makes it difficult to attach significance to this observation. An uncertainty which combines the imprecision of the spike calibration and sample measurement by summing twice their standard errors has been assigned. The result is  $4.44 \pm 0.12 \mu\text{g/g}$  (2.7% relative).

Three samples of Powdered Milk, SRM 1549, with a certified iodine concentration of  $3.38 \pm 0.02 \mu\text{g/g}$  were also analyzed. The results,  $3.44 \pm 0.10 \mu\text{g/g}$  ( $1s, n = 3$ ), were in good agreement with the certified value.

### CONCLUSIONS

Any new analytical technique requires extensive validation before it will be accepted by the analytical community. ID-RIMS was used previously to determine iron in water (SRM 1643b) and serum (SRM 909) as part of the certification programs for these materials (19). Furthermore, a considerable number of osmium and rhenium determinations in geological materials, elemental concentrations by isotope dilution as well as naturally varying Os isotopic compositions, have been made (20–22). Here we have expanded the demonstrated capabilities of the RIMS instrument to another element, iodine, while at the same time providing further evidence for precision and accuracy of the generalized ratio measurement process.

Thermal ionization measurements of iodine can be done with both high precision (6) and with high sample utilization efficiency, i.e., ions generated per atoms in the sample (5). The ratio measurement imprecision of RIMS of about 1% that has been demonstrated here is greater than that of TIMS, but still very useful for IDMS measurements. Since the samples are prepared essentially in the same way for RIMS and TIMS, it is probable that the variability is due to the pulsed ionization/measurement process. The advent of new lasers and detection schemes for RIMS promises to reduce this variability. Although the ionization efficiency for RIMS may be high (ions generated per atom in the laser beam), the sample utilization efficiency will remain low when using a pulsed laser with a continuous source of atoms such as a thermal filament. Since a nanogram of iodine represents a  $5 \times 10^{12}$  atoms, this duty cycle loss (a factor of about  $10^{-5}$ ) can be tolerated. The measurement limit for iodine by isotope dilution is presently the 10-ng chemical blank.

The single-filament, sample loading procedure used in RIMS is simpler than the triple filament procedure, which requires preparation of a LaB<sub>6</sub> treated ionization filament. The preparation and maintenance of this ionization filament

are critical to both the sensitivity and precision of the TIMS measurement (6). And, as discussed above, source memory should be able to more easily controlled using a single, low-temperature vaporization procedure. Thus, there are practical advantages for RIMS relative to TIMS.

Registry No. I, 7553-56-2.

### LITERATURE CITED

- Fassett, J. D.; Paulsen, P. J. *Anal. Chem.* **1989**, *61*, 643A–649A.
- Heumann, K. G.; Schindlmeier, W. *Fresenius' Z. Anal. Chem.* **1982**, *312*, 595–599.
- Heumann, K. G.; Seewald, H. *Fresenius' Z. Anal. Chem.* **1985**, *320*, 493–497.
- Schindlmeier, W.; Heumann, K. G. *Fresenius' Z. Anal. Chem.* **1985**, *320*, 745.
- Delmore, J. E. *Int. J. Mass Spectrom. Ion Phys.*, **1982**, *43*, 273–281.
- Gramlich, J. W.; Murphy, T. J. *J. Res. NIST* **1989**, *94*, 215–220.
- McHugh, J. A.; Stevens, J. F. *Anal. Chem.* **1972**, *44*, 2187.
- Elmore, D.; Phillips, F. M. *Science* **1987**, *236*, 543.
- Paul, M.; Fink, D.; Hollos, G.; Kaufman, A.; Kutschera, W.; Magaritz, M. *Nucl. Instrum. Methods Phys. Res.* **1987**, *B29*, 341–345.
- Fassett, J. D.; Walker, R. J.; Travis, J. C.; Ruegg, F. C. *Anal. Instrum.* **1988**, *17*, 69–86.
- Kuehner, E. C.; Alvarez, R.; Paulsen, P. J.; Murphy, T. J. *Anal. Chem.* **1972**, *44*, 2050–2056.
- Fassett, J. D.; Moore, L. J.; Travis, J. C.; Lytle, F. E. *Anal. Chem.* **1983**, *55*, 765–770.
- Fassett, J. D.; Walker, R. J.; Travis, J. C.; Ruegg, F. C. *Int. J. Mass Spectrom. Ion Processes*, **1987**, *75*, 111–126.
- Apel, E. C.; Anderson, J. E.; Estler, R. C.; Nogar, N. S.; Miller, C. E. *Appl. Opt.*, **1987**, *26*, 1045–1050.
- Clark, C. W.; Fassett, J. D.; Lucatorto, T. B.; Moore, L. J.; Smith, W. W. *J. Opt. Soc. Am. B* **1985**, *2*, 891–896.
- Moore, L. J.; Fassett, J. D.; Travis, J. C.; Lucatorto, T. B.; Clark, C. W. *J. Opt. Soc. Am. B* **1985**, *2*, 1561–1565.
- Miller, C. M.; Fearey, B. L.; Palmer, B. A.; Nogar, N. S. In *Resonance Ionization Spectroscopy 1988*; Lucatorto, T. B., Parks, J. E., Eds.; Institute of Physics: Bristol, 1989; pp 297–300.
- Fairbank, W. M. Jr.; Spaar, M. T.; Parks, J. E.; Hutchinson, J. M. R. In *Resonance Ionization Spectroscopy 1988*; Lucatorto, T. B., Parks, J. E., Eds.; Institute of Physics: Bristol, 1989; pp 293–296.
- Fassett, J. D.; Powell, L. J.; Moore, L. J. *Anal. Chem.* **1984**, *56*, 2228–2233.
- Walker, R. J.; Fassett, J. D. *Anal. Chem.* **1988**, *58*, 2923–2927.
- Walker, R. J.; Morgan, J. W. *Science* **1989**, *243*, 519–522.
- Lambert, D. D.; Morgan, J. W.; Walker, R. J.; Shirey, S. B.; Carlson, R. W.; Zientak, M. L.; Koski, M. S. *Science* **1989**, *244*, 1169–1174.

RECEIVED for review September 15, 1989. Accepted November 20, 1989.

# Dual-Beam, Light-Scattering Interferometry for Simultaneous Measurements of Droplet-Size and Velocity Distributions of Aerosols from Commonly Used Nebulizers

R. H. Clifford, Izumi Ishii, and Akbar Montaser\*

Department of Chemistry, George Washington University, Washington, D.C. 20052

G. A. Meyer

Analytical Sciences, Building 1897, Dow Chemical Company, Midland, Michigan 48667

Dual-beam, light-scattering interferometry is introduced for simultaneous measurement of droplet-size and droplet-velocity distributions. The technique was tested in the characterization of tertiary aerosols produced by five nebulization systems (a pneumatic, an ultrasonic, and three frit-type nebulizers) used in inductively coupled plasma spectrometry. In general, the Sauter mean diameter ( $D_{3,2}$ ) of tertiary aerosol produced by frit-type nebulizer was smaller than those of ultrasonic and pneumatic nebulizers. At higher injector gas flow,  $D_{3,2}$  was reduced for the pneumatic nebulizer but was increased for the ultrasonic nebulizer. At the same injector gas flow rate, droplets move slightly faster if helium is used as injector gas instead of argon. For all practical purposes, the  $D_{3,2}$  values measured for tertiary aerosol with dual-beam, light-scattering interferometry are comparable to the same data obtained by laser Fraunhofer diffraction. Compared to laser Fraunhofer diffraction, the proposed technique possesses two unique advantages. First, droplet velocity distribution can be measured. Second, spatially resolved information on droplet-size and velocity distributions may be obtained directly and rapidly.

## INTRODUCTION

Sample solutions are commonly converted into aerosols by nebulizers for introduction to excitation sources in atomic spectrometry. The importance of understanding fundamentals of aerosol generation and transport in order to improve analytical performances of atomic spectrometry has been summarized in recent reports (1-3). Ideally the performance of sample introduction systems should be optimized with predictive model(s). Such models (3) may be developed either theoretically or empirically. The accuracy of a model in predicting fundamental parameters for any nebulizer is closely tied to the ability to measure the same parameters accurately. Thus, improved diagnostic techniques are required to establish an extensive data base for testing new models or for advancing established ones (3).

Thus far, the most frequently used parameters for correlating aerosol properties (1-3) to analytical performance have been transport efficiency, mass of analyte reaching the atomizer per second, droplet-size distributions, and the solvent load. In essence, droplet-size distribution is the primary measure affecting the magnitudes of other parameters and, ultimately, the analytical signal. The most appropriate term to describe droplet size distribution is the mass median diameter. For pneumatically produced aerosol (1, 2), mass median diameter is approximately equal to the Sauter mean

diameter: (volume-to-surface-area ratio diameter).

The techniques (1, 2) used in analytical atomic spectrometry to estimate droplet diameter include microscopic measurements, measurement with horizontal elutriators and cascade impactors, and measurements with devices based on optical scattering. Cascade impactors have often been used in droplet sizing (1, 2), but compared to the optical scattering techniques, the process is time-consuming. Also, for cascade impactors and certain light scattering techniques (1, 2), aerosol must be drawn by a vacuum for droplet sizing. The presence of a vacuum enhances evaporation of the solvent and all droplets decrease in size. Light scattering techniques (3-5) based on Fraunhofer theory are not intrusive to the aerosol, but spatially resolved information on droplet size may be difficult to obtain, and no data on velocity of various droplets are attainable. Such information is important to an analytical spectroscopist, especially when a highly polydisperse aerosol is probed.

In this report, we introduce dual-beam, light-scattering interferometry for simultaneous measurement of droplet-size and droplet velocity distributions of nebulizers used in atomic spectrometry. In the section to follow, the principle of technique is briefly reviewed along with the instrumentation required for the measurements. Advantages and limitations of the proposed technique vs other particle sizing techniques are also discussed. The proposed technique is used to characterize tertiary aerosol from pneumatic, ultrasonic, and frit-type nebulizers. As far as we know, this is the first technique that has been used for measuring droplet size and velocity simultaneously to obtain a complete description of the aerosol droplet-size distribution.

## PRINCIPLE OF THE TECHNIQUE

Dual-beam, light-scattering interferometry has extensive applications in the characterization of sprays in many fields, particularly in study of fuel spray combustion (6, 7). Detailed discussion on theoretical description of the concept and the experimental setup is given elsewhere (6, 7). Because this report constitutes the first application of the technique in diagnostic studies of nebulizers used in atomic spectrometry, it would be relevant to briefly review the principle behind these measurements.

Figure 1A shows the typical schematic of the optical system used in dual-beam, light-scattering interferometry. In general, the instrument is similar to a laser Doppler velocimeter (8-12), except that scattered light is detected at a large angle with two or more photodetectors placed behind a common aperture at fixed distances (7). For the instrument used in this work, three photomultiplier tubes (PMTs) are used. Radiation from a laser is split into two beams, the beams are focused and crossed over a very small measurement volume to be examined. As the droplets pass through the intersection of the two laser beams, scattering occurs and temporal and spatial fre-

\* To whom correspondence should be addressed.



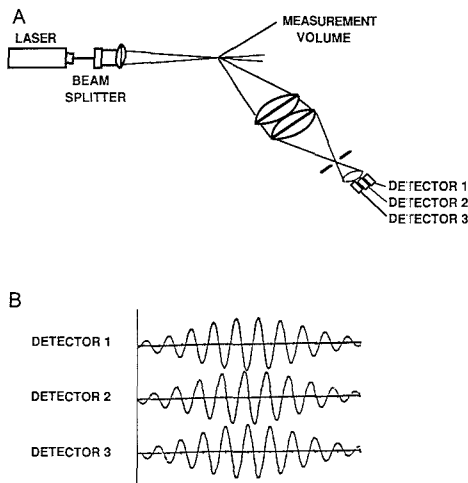


**Figure 1.** (A) Schematic of a dual-beam, light-scattering interferometer; (B) Doppler burst signals illustrating the phase shift between detectors. From ref 7, with permission.

quencies of the droplets are recorded. The scattered radiation produces an interference pattern which appears to move at the Doppler difference frequency. This temporal frequency depends on droplet velocity, laser wavelength, and the angle of the laser beams. The spatial frequency of the scattered interference fringe pattern is inversely proportional to the droplet diameter, but it is also a function of laser wavelength, beam intersection angle, the index of refraction for the droplet, and the location of the detector. As shown in Figure 1B, all detectors generate similar Doppler burst signals, but with a phase shift, as the fringes pass in front of them at the Doppler difference frequency. The phase shift is proportional to the fringe spacing and the droplet size.

For the instrument used in this study, three detectors are used to (a) expand the dynamic range for droplet size measurement and (b) minimize measurement ambiguity, especially when polydisperse aerosols are probed. For polydisperse aerosol, phase shifts exceeding  $360^\circ$  may occur which is misinterpreted as less than  $360^\circ$ . Thus, the use of a third detector eliminates such uncertainties. The overall size range of this technique is 0.5 to 10 000  $\mu\text{m}$  as compared to approximately 0.5 to 600  $\mu\text{m}$  for the laser diffraction system (3-5).

In view of the current popularity of the laser Fraunhofer diffraction (3-5) for droplet sizing, a comparison of the unique features of this technique and those of dual-beam, light scattering interferometry is relevant. The former does not measure droplet velocity, and the droplet-size distribution represents a line-of-sight integral measurement. To sample the entire cross section of the aerosol with laser diffraction, either the nebulizer must be scanned relative to the laser beam while light-scattering data are recorded (13) or that laser beam should encompass an aerosol cross section with uniform intensity. Alternatively, the lateral line-of-sight data may be Abel inverted to obtain spatially resolved information. For the dual-beam, light scattering interferometry, a very small volume ( $\sim 3 \times 10^{-5} \text{ cm}^3$ ) of the aerosol is probed. To obtain distribution for the entire cross section of the aerosol, the nebulizer must be scanned across the measurement volume, and an average weighted by the number flux and the geometry of the spray calculated (13). As discussed in a later section, one must not assume that the droplet sizes measured with the two techniques are comparable. The size distribution in laser

diffraction technique is sensitive to the relative number of droplets per unit volume, while the response of the proposed technique is proportional to the number of droplets per unit time per unit area (droplet flux). Fortunately, data obtained with the dual-beam, light scattering technique may be easily transformed for comparison with data from the laser diffraction technique.

## EXPERIMENTAL SECTION

**1. The Dual-Beam, Light-Scattering Interferometer.** The instrument used in this work for simultaneously measuring droplet-size and velocity distributions was the phase/Doppler particle analyzer (PDPA) manufactured by Aerometrics, Inc. (Sunnyvale, CA). This instrument was developed based on studies by Bachalo and Houser (7). A Compaq computer was used in our work for data acquisition and data treatment.

The parameters measured by PDPA include particle size (0.5-10 000  $\mu\text{m}$ ; dynamic range of 35:1 at any one configuration; 50 uniform size classes), particle velocity (up to 200 m/s; 50 uniform velocity classes), and sample volume cross-section for each size class. Size and velocity accuracies of 4% and 1%, respectively, are reported by the manufacturer for this instrument. Because the maximum particle number density measured with this instrument is  $10^6$ , we experienced problems in characterizing nebulizers that generate a large number of droplets.

The software for PDPA provides several types of information. These include size and velocity histograms, mean values and statistical mean diameters, probe volume size, number density, volume flux, and cumulative data plots of particle and volume. In addition, experimental data may be fitted to distribution functions and size-velocity correlation plots may be obtained. Because the PDPA response is proportional to droplet flux, PDPA software may be used to transform the particle size data for comparison with the results from laser diffraction experiments. As this paper constitutes the first publication on the application of dual-beam, light-scattering interferometry to commonly used nebulizers for atomic spectrometry, our discussion shall focus on droplet-size and velocity distributions. For the sake of comparison with the results obtained with laser diffraction (3-5), emphasis shall be placed on Sauter mean diameter and span in the characterization of aerosol. The importance of the two parameters in understanding the fundamental of aerosol generation and transport has been discussed extensively (1-3).

**2. Nebulization Systems Investigated.** Tertiary aerosol from five nebulization systems used in inductively coupled plasma (ICP) spectrometry were probed to obtain droplet-size and velocity distributions. Both Ar and He injector gases were used for all nebulizers. Aerosol was typically probed as it exited the spray chamber through a 12 mm long tube having an inside diameter of 7 mm. Ideally, the tertiary aerosol must be probed at the exit port of the injector tube of the ICP torch. This was not feasible, however, because of condensation of aerosol at the cold tip of the injector tube.

The nebulizers evaluated included a concentric pneumatic nebulizer, an ultrasonic nebulizer, and three frit-type nebulizers (14). The pneumatic nebulizer (TR-50-A1, J. Meinhard Associates, Santa Ana, CA) was made especially for use with He injector gas by the manufacturer. It was used in conjunction with a Scott double-pass spray chamber. Sample uptake rate and injector gas flow rate were changed from 0.1 to 1.0 mL/min and from 0.5 to 1.0 L/min, respectively. The ultrasonic nebulizer (Model UNPS-1, RF Plasma Product, Kresson, NJ), equipped with a spray chamber, was operated at 1.4 MHz with a forward power of 45 W. No desolvation system was used. The ranges for the sample uptake rate and the injector gas flow rate were 0.3-2.7 mL/min and 0.5-2.0 L/min, respectively. Because of the tremendous density of the aerosol by the ultrasonic nebulizer (USN), direct aerosol measurement was not feasible, and therefore, the aerosol had to be directed to the probing site with 7-ft Tygon tubing that had an inside diameter of 8 mm.

The glass frit-type nebulizers consisted of a disk-shaped glass frit nebulizer (DGFN), an externally pressurized cylindrical glass frit nebulizer (EPCGFN), and an internally pressurized thimble glass frit nebulizer (IPTGFN) described in detail elsewhere (14). The sample uptake rate and the injector gas flow rate were

changed from 0.05 to 1.0 mL/min and from 0.5 to 2.0 L/min, respectively, for these nebulizers. All data reported here are based on approximately 5000 particles examined for each nebulization condition.

A peristaltic pump (Minipulse 2, Gilson Medical Electronics, Middleton, WI) was used to deliver sample to all nebulizers. A mass flow controller (Model 8200 Matheson Gas Products, East Rutherford, NJ) was used to control the injector gas flow.

## RESULT AND DISCUSSION

To characterize the tertiary aerosol from the nebulizers, we used the Sauter mean diameter, designated as  $D_{3,2}$ , as the primary parameter. The parameter is defined as the volume-to-area ratio for the entire particle field and is obtained for the following equation (1-3):

$$D_{3,2} = \frac{\sum_{i=1}^N n_i d_i^3}{\sum_{i=1}^N n_i d_i^2}$$

where  $N$  is the total number of droplet classes (50 bins for this instrument),  $n_i$  is the counts for each droplet class  $i$ , and  $d_i$  is the diameter for size class  $i$ . All the data presented here were obtained by probing a very small ( $\sim 10^{-5}$  cm<sup>2</sup>) cross section of the tertiary aerosol emerging from the center section of the tube mounted at the exit port of the spray chamber. Thus, to a first approximation, we have assumed that tertiary aerosol is distributed uniformly across the exit tube having an inside diameter of 7 mm. Such an assumption may not be valid for the primary aerosol (13).

**1. Effect of Injector Gas Flow and Sample Uptake Rate on Sauter Mean Diameter.** Figure 2 shows the effect of the injector gas flow and sample uptake rate on the  $D_{3,2}$  for five nebulizers operated with two injector gases. Three notable observations are made. First, as the aerosol gas flow increases for both argon and helium injector gases,  $D_{3,2}$  decreases at all uptake rates for the pneumatic nebulizer. For example,  $D_{3,2}$  is reduced from 5.6 to 4.6  $\mu\text{m}$  as the Ar injector gas is increased from 0.5 to 1 L/min for an uptake rate of 1 mL/min. For the He injector gas,  $D_{3,2}$  is 5.9 and 4.9  $\mu\text{m}$  at 0.8 and 1.0 L/min, respectively, at the same uptake rate. Compared to the results obtained for helium, the values for  $D_{3,2}$  are also smaller when argon is used as the injector gas. These observations on the injector gas flow and gas type are in agreement with the trends noted by others (3-5) for primary and tertiary aerosol. Apparently, at higher gas velocities and with heavier injector gases, smaller droplets are produced because of the greater kinetic energy of the injector gas.

The second observation is concerned with the ultrasonic nebulizer which exhibits a trend for  $D_{3,2}$  contrary to that of a pneumatic nebulizer. For the USN,  $D_{3,2}$  values are increased at higher injector flow for both injector gases and, generally, at most uptake rates. This increase in  $D_{3,2}$  with gas flow for the USN may be attributed to the occurrence of a greater number of collisions between droplets, especially at high droplet number densities, thus leading to the recombination of small droplets. Also, as expected, the  $D_{3,2}$  values for the USN are smaller than those of the pneumatic nebulizer, especially when He injector gas is used.

The third observation is associated with the frit-type nebulizers. The trend in  $D_{3,2}$  does not agree with either the pneumatic or the ultrasonic nebulizer. The  $D_{3,2}$  values seem independent of injector gas flow rate. For DGFN and EPCGFN, the use of helium seem to reduce the  $D_{3,2}$  values as compared to argon. For the IPTGFN, the reverse trend is observed. At uptake rates less than 0.4 mL/min and at 1 L/min, the  $D_{3,2}$  values for IPTGFN are smaller than those measured for DGFN and EPCGFN. These were the conditions used in our previous (14) study for analytical measurements.

Examination of the data shown on Figure 2 reveals a weak linear dependence between  $D_{3,2}$  and sample uptake rate, es-

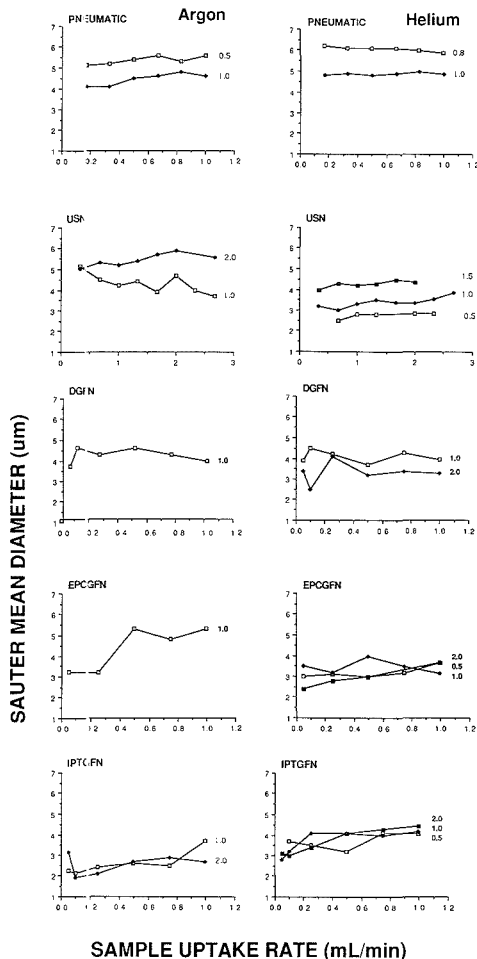


Figure 2. Effects of injector gas flow and type and sample uptake rate on the Sauter mean diameter of tertiary aerosol produced by five nebulization systems.

pecially for the pneumatic and ultrasonic nebulizers. For the frit-type nebulizers, this dependence exhibits an erratic behavior. To explain this behavior, size-volume histograms are presented in Figure 3 for the pneumatic and ultrasonic nebulizer and the IPTGFN. These data were obtained at an uptake rate of 1 mL/min (for pneumatic and USN) and 0.1 mL/min (for IPTGFN) and for the injector gas flow of 1 L/min. As expected, the broadest distribution is observed for the pneumatic nebulizer when Ar injector gas is used. The narrowest distribution is noted for the ultrasonic nebulizer using He injector gas. For IPTGFN, the distribution is narrow at the left end of the histogram, but very large droplets, representing a large volume percentage of aerosol, are also observed. Similar histograms are observed for DGFN and EPCGFN. To eliminate the large droplets from the tertiary aerosol, the spray chamber must be modified for frit-type nebulizers by adding a baffle in the spray chamber. With this change, lower  $D_{3,2}$  values are expected for the frit nebulizers.

Another parameter that is useful in aerosol characterization is the spar, which illustrates the breadth of the distribution

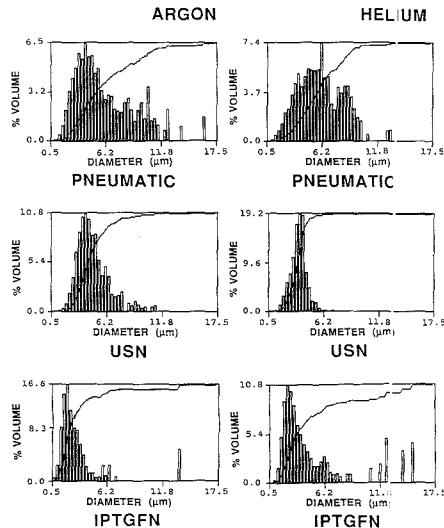


Figure 3. Size-volume histograms for tertiary aerosol of three nebulization systems. The continuous lines represent the cumulative volume of aerosol.

Table I. Values of Span Measured by Dual-Beam, Light-Scattering Interferometry for Five Nebulization Systems<sup>a</sup>

nebulizer type	sample uptake rate, mL/min	span <sup>b</sup>	
		Ar	He
A. Single Run			
USN	1	1.0	0.5
Meinhard	1	1.6	1.1
DGFN	0.05	2.7	2.3
EPCGFN	0.05	1.5	1.0
IPTGFN	0.05	1.7	2.5
B. Multiple Runs			
USN	0.3-1.0	0.9-1.4	0.5-0.8
Meinhard	0.2-1.0	1.3-1.7	1.1-1.2
DGFN	0.05-1.0	1.5-2.7	2.2-2.7
EPCGFN	0.05-1.0	0.1-2.8	1.0-1.4
IPTGFN	0.05-1.0	1.7-6.6	2.2-3.4

<sup>a</sup>All measurements were conducted at an injector gas flow of 1 L/min. The numbers listed under multiple run for span reflect the ranges observed and not necessarily the span at a particular uptake rate. <sup>b</sup>Span =  $(D_{90} - D_{10})/D_{50}$  where  $D_{10}$ ,  $D_{50}$ , and  $D_{90}$  refer respectively to droplet diameters below which 10, 50 and 90% of the cumulative aerosol volume are found (3).

(3). Table I shows values for span measured for five nebulization systems using both argon and helium as the injector gas. Compared to other nebulizers, span for the frit-type nebulizer is the greatest.

**2. Effect of Injector Gas Flow and Sample Uptake Rate on Droplet Mean Velocities.** Particle velocity is an important parameter in the optimization of plasma sources. At higher velocities, the residence time of droplets in a plasma will decrease, and this may lead to incomplete atomization, especially when the gas temperature of a plasma (15) is not as high as an Ar ICP.

Figure 4 shows the effect of injector gas flow and sample uptake rate on the mean velocity of the droplets. Mean velocity is independent from uptake rate but, as expected, changes linearly with the injector gas flow rate. The most

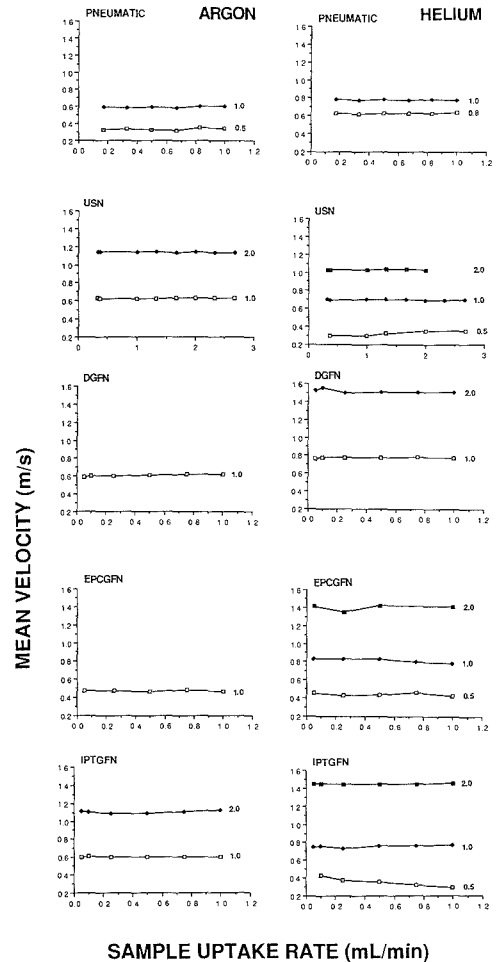


Figure 4. Effects of injector gas flow and type and sample uptake rate on the mean velocity of tertiary aerosol produced by five nebulization systems.

significant effect on mean velocity is noted when injector gas type is changed. Droplets in the helium gas stream travel faster than those transported with argon. At a sample uptake rate of 1 mL/min and an injector flow gas of 1 L/min, mean velocities of 0.595 and 0.772 m/s are measured for droplets produced by the pneumatic nebulizer when the injector gas is argon and helium, respectively. Under the same conditions for an USN, mean velocities of 0.622 and 0.703 m/s were obtained with Ar and He injector gases, respectively. The mean velocities were 0.604, 0.598, and 0.467 m/s for Ar and 0.751, 0.763, and 0.827 m/s for He at an uptake 0.05 mL/min for the IPTGFN, DGFN, and EPCGFN, respectively.

Another useful parameter for the tertiary aerosol is the velocity distribution of the droplets. Knowledge of this information is significant if different droplets move at varying velocities, and therefore, evaporation-atomization-excitation processes in a plasma could occur at different locations for various droplets. Figure 5 shows droplet size-velocity distributions for a pneumatic nebulizer when argon and helium injector gases are used. For this device, a greater variation

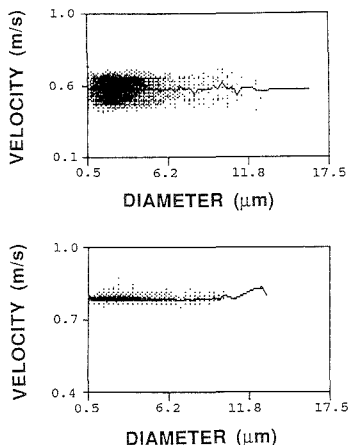


Figure 5. Size-velocity distribution for tertiary aerosol for pneumatic nebulizer using argon (top) and helium injector gas.

in droplet velocity is noted when argon injector gas is used as compared to helium.

The availability of size-velocity distribution has an additional benefit. If the number of droplets in each size class is divided by the average velocity of the droplets in the same class, then the  $D_{3,2}$  values may be compared to those obtained by the laser diffraction technique (13). For the tertiary aerosol, no significant change in  $D_{3,2}$  values were noted by us after this conversion. For example, the  $D_{3,2}$  values measured by the proposed technique for the pneumatic nebulizer were  $4.6 \mu\text{m}$  for an argon injector gas. When the number of droplets in each class was divided by average velocity of droplets in the same class, a Sauter mean diameter of  $4.5 \mu\text{m}$  was obtained. This correction for velocity distribution resulted in less than 2% change in the  $D_{3,2}$  value for the pneumatic nebulizer. Similar trends were observed for helium injector gas and also for other nebulizers. For such small droplets this observation should always be true because almost all droplets move at nearly the same velocity. Thus, for all practical purposes, Sauter mean diameters measured for tertiary aerosol with dual-beam, light-scattering interferometry are comparable to the same data obtained by laser diffraction (5). This statement is valid only if there is no spatial variation in the droplet sizes as assumed in this study. Demonstration of this assumption and the characterization of the primary aerosol are the subjects of our future studies.

### CONCLUSIONS

Dual-beam, light-scattering interferometry was used to measure simultaneously droplet-size and droplet velocity

distribution of tertiary aerosol produced by five nebulizers used in ICP spectrometry. The principle of the proposed technique, instrumentation required for the measurements, and advantages and limitations of this technique vs other particle sizing techniques were also discussed.

The nebulizers investigated included a pneumatic nebulizer, an ultrasonic nebulizer, a disk-shaped glass frit nebulizer, an externally pressurized cylindrical glass frit nebulizer and an internally pressurized thimble glass frit nebulizer. In general, the Sauter mean diameter of tertiary aerosol produced by the frit-type nebulizer is smaller than those of ultrasonic and pneumatic nebulizers. At higher injector gas flow,  $D_{3,2}$  is reduced for the pneumatic nebulizer but is increased for the ultrasonic nebulizer. For the pneumatic and the thimble frit nebulizers, the  $D_{3,2}$  value is increased as the injector gas is changed from argon to helium. At the same injector gas flow rate, droplets move faster if helium is used as injector gas instead of argon. For all practical purposes, the  $D_{3,2}$  values measured for tertiary aerosol with dual-beam, light-scattering interferometry are comparable to the same data obtained by laser Fraunhofer diffraction.

### ACKNOWLEDGMENT

We thank H. Tan of GWU and M. J. Houser of Aerometrics, Inc., for their assistance during the course of this work. Constructive comments by Lee G. Dodge, Southwest Research Institute, San Antonio, TX, are greatly appreciated.

Registry No. Helium, 7440-59-7; argon, 7440-37-1.

### LITERATURE CITED

- Gustavsson, A. Liquid Sample Introduction into Plasmas. In *Inductively Coupled Plasma in Analytical Atomic Spectrometry*; Montaser, A., Golightly, D. W., Eds.; VCH: New York, 1987.
- Browner, R. F. Fundamental Aspects of Aerosol Generation and Transport. In *Inductively Coupled Plasma Emission Spectroscopy, Part II*; Boumans, P. W. J. M., Eds.; John Wiley & Sons: New York, 1987.
- Canals, A.; Wagner, J.; Browner, R. F.; Hernandez, V. *Spectrochim. Acta* **1988**, *43B*, 1321-1335.
- Mohamad, N.; Fry, R. C.; Wetzel, D. L. *Anal. Chem.* **1981**, *53*, 639-645.
- Routh, V. W. *Spectrochim. Acta* **1986**, *41B*, 39-48.
- Bachalk, W. D. *Appl. Opt.* **1980**, *19*, 363-370.
- Bachalk, W. D.; Houser, M. J. *Opt. Eng.* **1984**, *23*, 583-590.
- Farmer, W. M. The Interferometric Observation of Dynamic Particle Size, Velocity and Number Density. Ph.D. Thesis, University of Tennessee, 1973.
- Farmer, W. M. *Appl. Opt.* **1972**, *11*, 2603-2612.
- Lesinsk, J.; Boulos, M. I. *Plasma Chem. Plasma Process.* **1988**, *8*, 113-132.
- Lesinsk, J.; Boulos, M. I. *Plasma Chem. Plasma Process.* **1988**, *8*, 133-144.
- Sakuta, T.; Boulos, M. I. *Rev. Sci. Instrum.* **1988**, *59*, 285-291.
- Dodge, L. G. *J. Propulsion Power* **1988**, *4*, 490-496.
- Clifford, R. H.; Montaser, A.; Sinex, S. A.; Capar, S. G. *Anal. Chem.* **1989**, *61*, 2777-2784.
- Chan, S.; Montaser, A. *Spectrochim. Acta* **1987**, *42B*, 591-597.

RECEIVED for review August 9, 1989. Accepted November 29, 1989. This research was sponsored by the U.S. Department of Energy under Grant No. DE-FG05-87-ER-13659.

# Kinetic Approach to the Measurement of Chemical Oxygen Demand with an Automated Micro Batch Analyzer

Purnendu K. Dasgupta\* and Kaj Petersen

Department of Chemistry and Biochemistry, Texas Tech University, Lubbock, Texas 79409-1061

An automated micro batch analyzer utilizes pressurized reservoirs of concentrated  $\text{H}_2\text{SO}_4$ ,  $\text{K}_2\text{Cr}_2\text{O}_7/\text{HgSO}_4$ , and  $\text{AgNO}_3$  that are equipped with microprocessor-driven high-speed on/off valves. The sample (460  $\mu\text{L}$ ) is blown in to a glass-filled PTFE reaction cavity provided with a temperature programmable heater. Silica optical fibers continuously monitor the disappearance of dichromate in the reaction mixture in a total volume of  $\leq 1.7$  mL with mixing provided by magnetic stirring. The continuous monitoring approach not only provides the equilibrium absorbance but also provides information on the rate of oxidant consumption and thus on the nature of substances contributing to the chemical oxygen demand (COD). The system can also be configured to study reaction rates as a function of temperature and to thus further characterize the oxidant consuming constituents. In the rapid testing mode, the instrument can process  $\sim 13$  samples/h, using a 3-min measurement time at 140  $^\circ\text{C}$  with a limit of detection of approximately 10 ppm COD. All sample compounds studied undergo oxidation by dichromate in a rate process that is first order each with respect to the oxidant and the substrate. On the basis of this observation, observed temporal oxidation profiles may be extrapolated to estimate the oxidant consumption at equilibrium.

## INTRODUCTION

In the area of water and wastewater analysis the measurement of chemical oxygen demand (COD) is one of the most important and most frequently used. A search of *Chemical Abstracts* (CA) shows over 3600 entries under this keyword since 1967 with present rate of citations in excess of 200 annually (volumes 109 and 110). Along with the measurement of biochemical oxygen demand (BOD), total oxygen demand (TOD), total organic carbon (TOC), and dissolved organic carbon (DOC), the measurement of COD is particularly important for the characterization of industrial and municipal effluents and their treatment. The origin of the BOD test is traced back to Frankland in 1870 and Dupré in 1884 (1). Its broad intent was to determine the extent to which a waste sample would consume oxygen and thereby affect the ecosystem receiving such a discharge. Even the presently abbreviated form of the BOD test requires 5 days (2). As such, the need for a faster comparable procedure culminated in the COD test which measures the number of equivalents of an oxidant consumed. The strict propriety of both the terms of BOD and COD is questionable since neither the biota nor the chemical oxidant is specified, both of which affect the results. Although a variety of oxidizing agents—permanganate (3-13) cerium(IV) (11, 14, 15), iodate (16), Fenton's reagent (17), persulfate (18), etc.—have been investigated, strongly acidic Cr(VI) at reflux temperatures is the preferred reagent (2, 19). The term COD is appropriately parenthesized as dichromate oxygen demand in the ASTM procedure (19).

The first use of Cr(VI) in the present context dates back at least to 1926 (20) albeit the term COD does not appear in

the subject index of *Chemical Abstracts* until 1952. Numerous variations of the dichromate-based COD measurement method are in the literature (21-45). Semiautomated (32, 33) and automated versions with (34-39) and without (40-42) air segmentation as well as adaptation to a complex batch mixer (43) have been described. One commercial COD analyzer also utilizes batch mixing on a relatively large volumetric scale (44). Air-segmented COD analyzers have been used as postcolumn reactors coupled to a liquid chromatograph (35) and for continuous on-stream analysis of wastewater (38). The present practice of COD measurement (2, 19) reflects in large part the procedures recommended by Moore et al. (22) and much of the subsequent important literature has appeared in the pages of this journal (17, 23, 29, 32, 45, 46).

Under the conditions of the prescribed procedure (19), all oxidizable compounds are not oxidized to the same extent. For example, reducing sugars such as glucose are oxidized even without heating while heterocycles such as pyridine are hardly oxidized even after refluxing at 140  $^\circ\text{C}$  for 2 h. It is impractical to determine the extent of oxidation that takes place for each potential compound in a particular sample, though valiant efforts to do so have been made (17, 19, 21, 22, 29, 45-48). As an additional complication, it is not widely recognized that the rate of oxidation is first order each in dichromate and in the oxidizable substance. Thus, unless dichromate is in very large excess, the fraction of a compound substance oxidized over any given period depends on its initial concentration. Ever since the original work of McNary et al. (49), colorimetry (2, 26, 27, 30-32, 34-38) has largely replaced titration as a means of evaluating the residual Cr(VI) present after digestion. Because Cr(VI) absorbs more strongly than Cr(III), optically monitoring Cr(VI) provides the more sensitive procedure and thus represents the present preference in automated methods (35, 40-42). Such procedures preclude using a large excess of Cr(VI) which may account for significant differences in the extent of oxidation for the same compound reported for either the manual (19) or automated procedures (36, 37). In the air-segmented continuous flow analyzers, it remains unknown whether oxidation at the interfacial phase boundaries proceeds at the same rate (as volatile organic compounds partition to the segmenting phase) as in bulk solution.

Presently, COD measurements yield a single number and provide no information about the substances oxidized. At best, the COD test represents "... a good balance between the value of the information gained and the speed of the analysis when compared to BOD and TOC tests" (32); at worst, it is a poor surrogate for BOD or TOC/TOD values. Many feel that the Holy Grail of quantitative oxidation of everything (COD  $\equiv$  TOD) is an inherent measure of the accuracy of the method (see e.g., refs 22, 23, 28, 45, and 50). This is perhaps why the original suggestion of Muers (51) to use  $\text{Ag}^+$  as catalyst to facilitate the oxidation of straight chain fatty acids (e.g. acetic acid) is now part of all standard procedures. Interestingly, the early English practice of an increased acid concentration, which elevates the boiling point of the reaction mixture and thus increases the extent of oxidation for some samples (43), has rarely been adopted elsewhere (37). Many others feel that COD should represent TOC rather than TOD, thus inorganic

substances that are easily oxidized by hot acidic Cr(VI) are considered interferences. Of these, chloride interference is most easily and effectively removed by complexation with  $\text{Hg}_2^{2+}$  (relatively large concentrations must be added) (18, 46); standard procedures differ as to whether sulfamic acid addition should be incorporated as a routine part of the protocol for the elimination of nitrite (2, 19), and no effective options are available to deal with ferrous iron and reduced sulfur anions, which are often important constituents of many anoxic water samples.

There are also those who believe that the COD test should indeed represent a fast surrogate BOD measurement, its originally intended purpose. At least two versions of the COD test, the rapid COD test (25) and the oxygen demand index (ODI) test (52, 53), modify the standard procedure by using shorter digestion periods and, for ODI, a lower temperature. The rapid COD method is claimed to have as good a correlation with BOD as does standard COD (54) and appears to be applicable to a large variety of wastewater samples (55). The correlation of the ODI with BOD is less convincing (26, 56). Neither, however, has been widely adopted. There are numerous studies in the literature concerning the relationship between BOD, COD, and TOC values (see ref 57 for citations). Only one conclusion appears to be generally applicable: BOD and COD are typically well correlated at any given location, although the exact relationship varies greatly from one location to another. In contrast, while TOC-COD and TOC-BOD may on occasion be even better correlated than BOD-COD, this is by no means a general occurrence (26, 58). The differences in the exact BOD-COD relationship from one type of sample to another are hardly surprising inasmuch as bacteria may be much more efficient in oxidizing some species than acidic Cr(VI) (e.g., *acetobacter* for acetate) while others (e.g., unsubstituted aromatic hydrocarbons) are significantly oxidized in the COD test but do not undergo measurable degradation in the BOD measurement. Some compounds are cytotoxic and yield "sliding" BOD values (58). The generally good COD-BOD correlation at any given location reported in the literature is more likely an indication that the nature and distribution of the species contributing to the oxygen demand remain essentially the same at the same location rather than any intrinsic relationship between the two methods.

The above discussion makes it clear that the COD value as presently measured is an operationally defined quantity with little absolute meaning. The information content is limited to a single numerical value. The importance of kinetic methods to chemical analysis constitutes the focus of a recent monograph (59). The potential value of the technique can be much greater if it is able to provide information as to not only how many total equivalents of oxidant are consumed but also the rate at which such consumption occurs. Second, in a variety of situations there is a dire need to provide the results faster than a method requiring 2 h of refluxing. Third, because of the use of toxic mercury salts and the generation of hazardous liquid wastes, it is necessary that any automated analyzer work on as small a scale as possible. In this paper, we propose an alternative for COD measurements based on the automated micro batch analyzer (AMBA) (60-62) that can fulfill the above needs.

## EXPERIMENTAL SECTION

The experimental system is shown schematically in Figure 1. Reagents (concentrated  $\text{H}_2\text{SO}_4$ , 10 mM  $\text{K}_2\text{Cr}_2\text{O}_7$  + 80 mM  $\text{HgSO}_4$ , 8% (w/v)  $\text{AgNO}_3$ ) and wash liquid (water) are contained in heavy-walled borosilicate glass bottles pressurized to 9.5 psi from a common  $\text{N}_2$  pressure source. The liquid outlet from each reservoir is connected through fast-acting all-PTFE two-way solenoid valves V1-V4 (type 075T2WNC12-32, Bio-Chem Valve corp., East Hanover, NJ). The valve outlets are in turn connected to the top of the reaction chamber RC by PTFE connecting lines

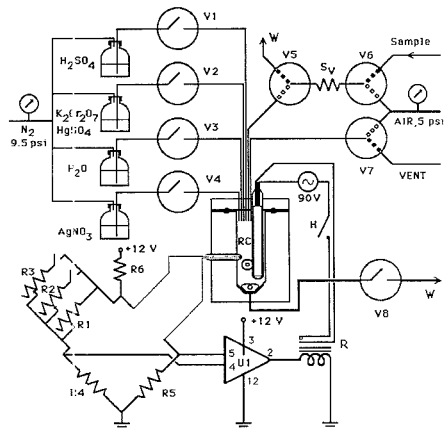


**Figure 1.** System schematic: V1-V8, inert fluid-path solenoid valves; RC, reaction chamber (see Figure 2 for details); R1-R3, adjustable resistors (R2 and R3 connected via relays), R4 = R5 = 10 k $\Omega$ , R6 = 1 k $\Omega$ ; R, temperature control relay; H, main heater relay; U1,  $\frac{1}{4}$ -LM 339.

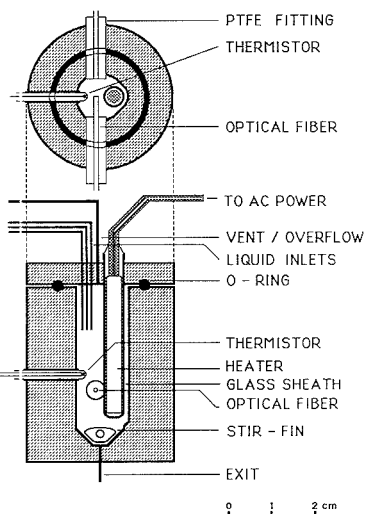


**Figure 2.** Details of the reaction chamber.

(270  $\times$  0.86, 255  $\times$  0.30, 245  $\times$  0.66, and 500  $\times$  0.30 mm for  $\text{H}_2\text{SO}_4$ ,  $\text{K}_2\text{Cr}_2\text{O}_7/\text{HgSO}_4$ ,  $\text{H}_2\text{O}$ , and  $\text{AgNO}_3$ , respectively). V5 and V6 are three-way fluorocarbon fluid path valves (type LFFX 0500200AC, the Lee Co., Westbrook, CT) used together as a loop injector where  $S_v$  represents the sample volume (60-62). Valve V7 is a three-way solenoid (Bio-Chem type 075T3W12-32) and V8 is a PTFE valve similar to V1-V4.

The heart of the system is the reaction chamber RC, machined from glass-filled PTFE. It is shown in detail in Figure 2 and the approximate scale is indicated. The reaction cavity is approximately conical at the bottom and a triangular PTFE stir-bar is trimmed to fit this shape and provide smooth stirring. All delivery/vent tubes and the heater are press-fit through undersized holes drilled in the lid. Three screws and a Viton O-ring secure and seal the lid. The tubes entering through the lid are heavily covered with black tape to prevent intrusion of stray light. One side of the circular cross section of the cavity contains a machined depression to better accommodate the cartridge heater (top view,

Table I.<sup>a</sup> Operation Sequence

time, s	V1	V2	V4	V5/V6 <sup>b</sup>	V7 <sup>b</sup> /V8	H	function
0.0-5.0				on			sample delivery
5.0-16.5		on					dichromate delivery
16.5-31.5	on						conc H <sub>2</sub> SO <sub>4</sub> delivery
31.5-211.5 <sup>c</sup>						on	heat under thermostatic control, acquire signal
211.5-216.5							continuing to read signal
216.5-223.5					on		dispose chamber contents
223.5-226.8	on		on				acid and rinse water added
226.8-232.3			on				adding more rinse water
232.3-242.3					on		dispose chamber contents
242.3-279.9	(on)		(on)		(on)		repeat above three steps twice
274.9-279.9							load sample

<sup>a</sup>Refer to Figure 1 for components. <sup>b</sup>The ports connected by the open symbols in Figure 1 are connected when valve is on. <sup>c</sup>This step can be indefinitely lengthened to extend the observation period.

Figure 2). The 1.25 × 0.125 in. cartridge heater (type C1E14, 25 W at 120 V, Watlow, Inc., St. Louis, MO) is wrapped in Al-foil to tightly fit inside 4 mm i.d. Pyrex glass sheath tubing. A glass-sealed precalibrated thermistor (type P30, 10 k $\Omega$  at 25 °C, Thermometrics, Edison, NJ) is used to monitor the temperature and provide active control via the simple resistance bridge/voltage comparator driven relay circuitry depicted in Figure 1. Referring to Figure 1, 90 V ac is applied to the heater via a main relay switch H and the temperature control circuit. Adjustable resistors R1, R2, and R3 have values of 994, 930, and 1527  $\Omega$  and the connections of R2 and R3 to the circuit are governed by relays driven by the microprocessor. The following set point temperatures are obtained in accordance with the resistors connected: R1, 101.1 °C; R1 and R2, 120.9 °C, R1 and R3, 130.6 °C; R1, R2 and R3, 142.8 °C. Some initial experiments were also conducted at a set temperature of 110.0 °C. These temperatures are referred to in rounded figures in the text.

The optical absorbance of the liquid in RC was monitored via optical fibers as shown in Figure 2. Tefzel-jacketed silica fibers (type HCN-M1000T-12, Ensign-Bickford Optics, Avon, CT), 1 mm in core diameter, were sealed into the reaction chamber with one ferrule-end and one blunt end externally threaded all-PTFE bushings (modified Omnifit fittings, Rainin, Inc., Woburn, MA). The fiber ends were ~4 mm from each other, defining the optical path length. The light source was a lens-end lamp (type L8050, 5 V 810 mA, Gilway Technical Lamps, Woburn, MA) placed behind an eight-position, logic-addressable ratcheted solenoid-driven filter wheel holding 1/2 in. interference filters. Only a single filter (15 nm band-pass at full width half maximum centered at 450 nm) was used in this work. The monochromatic light output was coupled to one end of a randomized bifurcated glass fiber bundle approximately 20 cm long with a common leg bundle diameter of ~4.5 mm (Welch Allyn, Inc., Skaneateles Falls, NY). Each of the bifurcated legs (ca. 3 mm diameter) was coupled to the 1 mm diameter silica fibers; as a consequence a major fraction of the light was lost. One silica fiber (reference arm) terminated directly in a photodiode while the second fiber terminated in the reaction chamber, RC. The exit fiber from RC was coupled to the detector photodiode. Both photodiodes were the same (type G 1115, Hamamatsu Corp., Middlesex, NJ) and the output photocurrents were fed directly into a log-ratio amplifier (type 757 N, Analog Devices, Norwood, MA). The amplifier gain was fixed at 1 V/absorbance unit. Detector signals are referred throughout the rest of the text in absorbance units (AU). The amplifier output was fed to a strip-chart recorder, generally through a digital filter (Model 1021A filter and amplifier, Spectrum, Inc., Newark, DE) using a cut-off frequency of 0.1 Hz and the unfiltered signal was sampled by an Apple IIe micro-computer with an 8-bit analog-digital converter.

The sample volume used in this work was 460  $\mu$ L (458  $\pm$  0.5  $\mu$ L, gravimetrically determined for water as sample). An identical volume of the 10 mM dichromate reagent was used (corresponding to a valve on time of 11.5 s). This choice limits the upper range of applicability to about 480 mg of COD/L. Of course, smaller sample volumes and greater Cr(VI) concentration/volume can be chosen to extend the upper limit of applicability. Following Cr(VI) addition, 940  $\mu$ L of concentrated H<sub>2</sub>SO<sub>4</sub> is added (gravimetrically measured, density 1.84 g/mL, valve on-time 15.0 s).

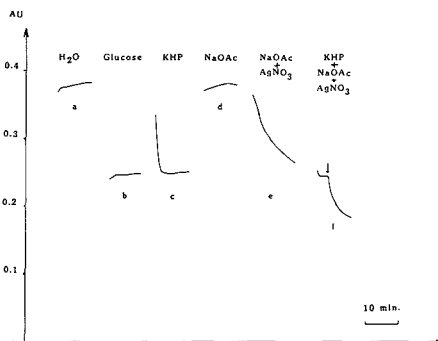


Figure 3. System output showing temporal oxidation profiles: (a) water, (b) glucose, (c) KHP, (d) CH<sub>3</sub>COONa, (e) CH<sub>3</sub>COONa with Ag<sup>+</sup> catalyst, (f) KHP + CH<sub>3</sub>COONa, Ag<sup>+</sup> catalyst added at time indicated by the arrow.

The total reaction volume is slightly smaller than the nominal sum, due to volumetric contraction. Heating is commenced immediately after H<sub>2</sub>SO<sub>4</sub> addition. An operating temperature of 140 °C is reached in under 1 min. The routine operation, a total observation time of only 3 min, starting from the commencement of heating, was used. A typical operational sequence is shown in Table I (AgNO<sub>3</sub> addition step is not shown in the table; when used, AgNO<sub>3</sub> is delivered at a rate of ~20  $\mu$ L for a 1-s valve-on time). The controller outputs were typically assigned as follows: V1, V2, V4, V5/V6, V7/V8, H, R2, R3 (slashes indicate common operation).

**Reagents.** Reagents used were of analytical reagent or reagent grade. Water used was distilled and deionized and met ASTM type I specifications.

## RESULTS AND DISCUSSION

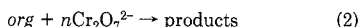
**Kinetics of Cr(VI) Oxidation.** With the rare exception of a study by Goodwin et al. (63) and two citations therein, the COD literature surprisingly does not contain any quantitative information on the reaction order involved in this reaction system for representative compounds. Potassium hydrogen phthalate (KHP) is most commonly used as a standard in COD measurement procedures (2, 19). Although the use of glucose as a standard for automated procedures has been claimed to produce analytical data that compare well with results from the standard manual procedure for a variety of water samples (12, 13, 40-42), it cannot be overemphasized that glucose is the most easily oxidized among common COD reference substances used. Figure 3 shows system outputs for water, glucose, KHP, and sodium acetate. Glucose is fully oxidized by the time data acquisition is commenced. The progress of the oxidation reaction is most clearly evident in the KHP case. There is essentially no oxidation of acetate unless silver catalyst is added. Glutamic acid behaves similarly

to acetate. In some previous laboratory intercomparisons, mixtures of glucose and glutamic acid in various proportions were used as quality control standards for COD measurements (57); it is debatable if a combination of two extremes effectively mimic the behavior of a typical sample. The general inability to define a "typical" sample undoubtedly compromises universally applicable calibration.

The oxidation rates of a number of compounds obtained by using the described reaction system were studied. These results are discussed in the following using the oxidation of KHP at 110 °C as an example. Treating the reaction solely in terms of a first-order consumption of KHP was found to lead to a poor fit of the data; moreover, the apparent reaction rate constant was a strong function of the concentration of KHP taken. Therefore, the data were treated according to the second-order rate law

$$-d[\text{Cr}_2\text{O}_7^{2-}]/dt = kn[\text{Cr}_2\text{O}_7^{2-}][\text{Org}] \quad (1)$$

where the stoichiometry of the oxidation process may be represented by



Although  $\text{H}^+$  is consumed in this reaction, it is in such large excess that this consumption is negligible relative to the total amount present. For the specific case of KHP being the organic compound oxidized,  $n$  is 5. If  $[\text{Cr}_2\text{O}_7^{2-}]_0$  and  $[\text{Org}]_0$  are the initial concentration of dichromate and the organic substance respectively, the stoichiometry (eq 2) requires that

$$[\text{Cr}_2\text{O}_7^{2-}]_0 - [\text{Cr}_2\text{O}_7^{2-}] = n([\text{org}]_0 - [\text{org}]) \quad (3)$$

The change in dichromate concentration at any given time, as represented by the left-hand side of eq 3, is directly obtained by the difference in the detector outputs between the blank signal and the sample signal at corresponding times

$$[\text{Cr}_2\text{O}_7^{2-}]_0 - [\text{Cr}_2\text{O}_7^{2-}] = (S_B - S_S)/\epsilon b = \Delta S/\epsilon b \quad (4)$$

where  $S_B$  and  $S_S$  are blank and sample detector outputs in absorbance units,  $\epsilon$  is the molar absorptivity of dichromate, and  $b$  the effective path length under the operative conditions. Substituting eqs 3 and 4 in eq 1 yields, after appropriate transpositions

$$-d([\text{Cr}_2\text{O}_7^{2-}]_0 - \Delta S/\epsilon b) / ([\text{Cr}_2\text{O}_7^{2-}]_0 - \Delta S/\epsilon b) \cdot ([\text{Org}]_0 - \Delta S/\epsilon bn) = kn dt \quad (5)$$

Equation 5 reduces to the form

$$d\Delta S / (p - \Delta S)(q - \Delta S) = (\epsilon b)^{-1} k dt \quad (6)$$

where  $p = [\text{Cr}_2\text{O}_7^{2-}]_0 \epsilon b$  and  $q = [\text{Org}]_0 \epsilon bn$ . This is readily integrated to

$$\ln [q(p - \Delta S) / (p(q - \Delta S))] = (p - q)kt / (\epsilon bn) \quad (7)$$

The quantity  $\epsilon b$  may be obtained by measuring the absorbance due to a dichromate solution of known concentration in the experimental medium at the operating temperature, relative to a blank solution (equal to the measurement solution in every respect except without dichromate). Alternatively, the quantity  $\epsilon bn$  is the slope of the calibration line obtained when the final absorbance of the reacting mixture at equilibrium (reaction time  $\geq 12$  min at 110 °C for KHP) is plotted as ordinate against the molar concentration of KHP in the final solution. The value of  $\epsilon b$  can then be computed by using the known value of  $n$ . The two approaches produced a value of  $\epsilon b$  statistically indistinguishable from each other, the mean being  $116.4 \pm 0.3 \text{ AU M}^{-1}$ . For any given calibration experiment, it is now possible to compute  $p$  and  $q$ . For 0.2, 0.5, and 1.0 mM KHP as sample (1 mM KHP = 240 mg/L COD) and  $\ln [q(p - \Delta S) / (p(q - \Delta S))]$  values were subjected to linear

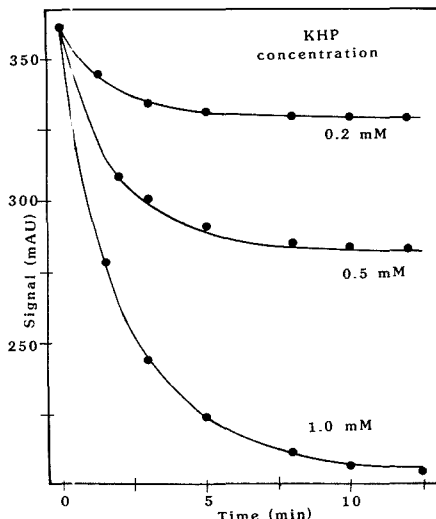


Figure 4. Second-order fit to KHP oxidation profiles.

regression against the corresponding  $(p - q)t$  values. In accordance with eq 7, the linear correlation coefficient was better than 0.99 with a near-zero intercept. The applicable rate constant,  $3.5 \text{ M}^{-1} \text{ s}^{-1}$  could be computed by multiplying the regression slope with  $\epsilon bn$ .

The above method of treating the data is relatively intolerant of errors in evaluating  $\epsilon b$ , because this error is magnified by the computing process. A superior approach is to utilize a nonlinear least-squares fitting algorithm (e.g., NLLSQ, CET research group, Norman, OK). In this approach, rough estimates of the parameters (the optimum values of which are to be determined) are initially supplied by the user. The algorithm then determines the optimum values by the Marquardt method (64). For the present application, we express eq 7 in a form that isolates the dependent variable  $\Delta S$

$$\Delta S = (\epsilon b([\text{Cr}_2\text{O}_7^{2-}]_0 - n[\text{Org}]_0)ye^{xkt}) / (1 - ye^{xkt}) \quad (8)$$

$$\text{where } x = [\text{Cr}_2\text{O}_7^{2-}]_0 - n[\text{Org}]_0 \quad (9)$$

$$\text{and } y = [\text{Cr}_2\text{O}_7^{2-}]_0 / (n[\text{Org}]_0) \quad (10)$$

Subjecting our experimental data to NLLSQ fitting of eq 8 results in the best fit predictions of  $\epsilon b = 116.5 \pm 0.6 \text{ AU M}^{-1}$  and  $k = 3.56 \pm 0.10 \text{ M}^{-1} \text{ s}^{-1}$ . The root mean square deviation of the predicted vs actual  $\Delta S$  values is 1.1 mAU; the excellent fit of the second-order model to the experimental data is shown in Figure 4. Not only is the predicted optimum fit of  $\epsilon b$  in excellent agreement with the experimental value, the robustness of the approach can be appreciated when the independence of the optimum fit values from the initial estimates is considered: the same optimum fit values for  $\epsilon b$  and  $k$  are produced with initial estimates in the range 20–500  $\text{AU M}^{-1}$  and 0.5–20  $\text{M}^{-1} \text{ s}^{-1}$  for these parameters, respectively.

The approach provides another benefit over standard linear regression. Some compounds, e.g., phenol, are appreciably oxidized by the time data acquisition begins. Time  $t$  in eq 8 is synchronous with the commencement of data acquisition. Therefore  $t$  in eq 8 is replaced by the term  $t + t_0$  where  $t_0$  is an adjustable parameter (typically 0.2 min) which represents the lag time between the onset of significant reaction and the commencement of data acquisition. (Of course, it is impossible to obtain reliable values if extensive oxidation has already



Table II. Statistical Summary of Calibration Results, KHP, 140 °C

time, min	2	3	4	5	8	10
linear corr coeff	1.000	1.000	0.998	0.998	0.996	0.996
slope, mAU/ppm COD in sample	0.571 ± 0.009	0.609 ± 0.010	0.631 ± 0.010	0.641 ± 0.010	0.644 ± 0.013	0.648 ± 0.013
intercept, mAU	384.4 ± 1.6	386.6 ± 1.6	388.8 ± 1.8	390.5 ± 1.7	392.1 ± 2.2	393.6 ± 2.2
std error of determination, ppm COD	9.2	9.	9.3	9.1	10.0	10.1
estimated limit of detection, <sup>a</sup> ppm COD	8.4	7.9	8.6	8.0	10.2	10.2

<sup>a</sup>Based on a *S/N* value of 3 (70). Lowest concentration in the calibration set was 24 ppm; this was well above the LOD.

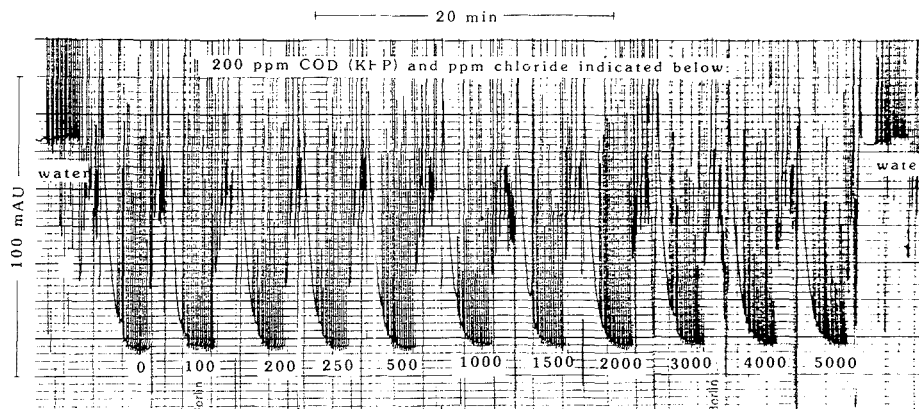


Figure 5. Typical system output on strip-chart recorder, the sample series shown indicates freedom from chloride interference. All samples represent a COD level of 200 ppm, with varying amounts of chloride (ppm Cl indicate below each trace). Noise between sample runs is due to repeated rinsing and evacuation of chamber.

occurred prior to data acquisition; this is the case for glucose). Such an approach also compensates for the time to reach the set temperature, particularly important for those compounds that display a low oxidation rate at lower temperatures but are rapidly oxidized at the set temperature. In this case,  $t_0$  is negative.

**Temperature Effect on Reaction Rate.** Despite the rudimentary temperature programming capability of the COD AMBA system, the temperature dependence of the oxidation rate for a given sample can be rapidly determined. Oxidation by acidic Cr(VI) appears to conform well to the Arrhenius equation (65). With KHP as sample (200 mg/L COD) in each case, the rate constants were determined to be  $2.51 \pm 0.08$ ,  $3.56 \pm 0.10$ ,  $6.68 \pm 0.18$ , and  $11.60 \pm 0.84 \text{ M}^{-1} \text{ s}^{-1}$  at 100, 110, 130, and 140 °C, respectively. A plot of  $\ln k$  vs the reciprocal of absolute temperature is linear with a correlation coefficient of 0.997 and an activation energy of 10.7 kcal/mol. A preexponential factor of  $4.52 \times 10^6 \text{ M}^{-1} \text{ s}^{-1}$  can be computed. Similar experimental data for phenol yield an activation energy of 3.9 kcal/mol and a preexponential factor of  $2.17 \times 10^9 \text{ M}^{-1} \text{ s}^{-1}$ . Such data for individual samples can be rapidly determined in an unattended fashion with the present instrument.

**Calibration Behavior.** The system was calibrated with three reference substances, glucose, phenol, and KHP, at a reaction temperature of 100 °C. The reaction profiles indicate that final (equilibrium absorbance) is reached in  $\approx 3$ , 8, and 15 min for glucose, phenol, and KHP, respectively. The calibration slope, expressed in terms of  $\Delta \text{mAU/ppm COD}$  in sample, was experimentally indistinguishable for the three substances,  $0.636 \pm 0.0085 \text{ mAU/ppm COD}$ . In terms of actual concentration in the reaction volume this slope is  $2.35 \pm 0.03 \text{ mAU/ppm COD}$ . Recognizing that  $1 \text{ mM K}_2\text{Cr}_2\text{O}_7$

neutralizes 48 ppm COD, the corresponding  $\epsilon b$  value is  $113 \pm 2$ . Sample carryover, measured by alternating 250 ppm COD samples with water, was  $\leq 2.5\%$ .

More detailed statistical data are listed in Table II for repeated calibration runs with KHP (seven concentrations, 0–480 ppm,  $n = 3\text{--}5$  at each concentration) for a reaction temperature of 140 °C. The reaction is essentially complete (> 99%) within 5 min. The performance parameters (linearity, standard error, LOD etc.) remain virtually the same for a reaction time of 2–10 min despite the fact that the reaction is incomplete at low concentrations. Strategies to predict the equilibrium (final) absorbance for incomplete reaction are described in a subsequent section.

**Elimination of Chloride Interference.** Other than Hg(II), the addition of Cr(III) has been suggested as a remedy for preventing the oxidation of chloride to chlorine (66). Although complexation of chloride by Cr(III) has been suggested to be the operative basis of this procedure, available equilibrium data (67) suggest that the operative factor is likely a decrease in the oxidizing ability of the dichromate due to lowering of the oxidation potential. This may also reduce the rate of oxidation of some compounds. In any case, the available data (66) do not indicate that addition of Cr(III) leads to completely satisfactory results. As such, much as it is undesirable to use toxic Hg(II), no practical alternatives are available. Addition of  $\text{HgSO}_4$  to an extent of 80.8 mM to the Cr(VI) reagent in our system enables it to handle samples containing 5000 ppm chloride without interference. Typical recorder output indicating freedom from chloride interference is shown in Figure 5.

**Slow Oxidations: Extrapolated Equilibrium Values.** Obviously, samples for which oxidation proceeds slowly represent the more challenging situations. In a single point

measurement, the option is limited to determining the residual Cr(VI) concentration after a specified period of time. In the present case, termination of the measurement period can be user specified a priori or be governed by a microcomputer based data acquisition device which terminates the measurement as the rate of change of absorbance falls below some user-selected threshold. Most importantly, the final portion of the rate profile can be processed to predict final equilibrium values. The final few minutes of the temporal profile of the dichromate concentration can be subjected to standard curve-fitting algorithms (including NLLSQ) without specific knowledge of the substrate concentration or the oxidation rate constant but assuming a second-order rate law. Other approaches previously described in this journal may also be potentially applicable (68, 69). Oxidations of glutamic acid or acetate proceed slowly even with a silver catalyst. On selected 10-min runs of replicate 200 ppm (COD) glutamate samples and 15-min runs of 175 ppm (COD) acetate samples, we were able to obtain predicted equilibrium results of  $191 \pm 19$  and  $168 \pm 20$  ppm ( $n = 6$  each), respectively, from experiments in which oxidation was obviously incomplete. These experiments were conducted with three concentration levels of silver catalyst, and despite the different oxidation rate in each case, the overall agreement is reasonable. Future work is aimed at extending this approach to multicomponent mixtures using a more sophisticated algorithm.

**Component Performance.** The overall system performance of the analyzer is controlled by the individual performance characteristics of a number of different components in the analyzer. These include detector precision, detector linearity, volumetric reproducibility of reagent addition, and the reproducibility of the temporal temperature profile. Note that the apparent optical absorbance of an acidic Cr(VI) solution is a function of the solution temperature. This likely stems more from a change in refractive index and dimensional changes of the cell rather than a real change in molar absorptivity of dichromate itself.

With only water in the reaction chamber at room temperature, the reproducibility of the detector output upon repeated evacuation and filling of RC was largely governed by the intrinsic detector noise. Considering the nature of the optical fiber coupling used, the observed peak-to-peak noise level (0.6 mAU) was quite acceptable. The detector output was linear ( $\leq 1\%$  deviation) with dichromate concentration at least up to 1.2 AU. Because all experiments were conducted with a maximum absorbance background of 0.4 AU (all specified absorbance values refer to water at room-temperature as the zero level), detector linearity is not expected to be a significant limiting factor.

In a conventional continuous flow analysis system, pumping concentrated  $H_2SO_4$  with peristaltic pumps at a constant rate over extended periods represents a major problem. Even with so-called "acid-resistant" pump tubing, it was found necessary to replace tubing every 3–4 h (42). Pneumatic delivery via inert valves therefore represents a very useful solution. The ability to use undiluted  $H_2SO_4$  as a reagent also permits its large heat of hydration to be exploited toward raising the reaction temperature. With all components initially at room temperature, the internal temperature reaches 70 °C immediately following  $H_2SO_4$  addition. Also, to make this addition procedure reproducible, the addition sequence involves adding the concentrated acid to the aqueous sample + Cr(VI)/ $HgSO_4$ . In the absence of auxiliary heating, the temperature rapidly drops, however. The reactor vessel has considerable thermal mass and glass-filled PTFE is a much better thermal conductor than PTFE. More efficient use of the heat input to the system (whether electrically or chemically generated) is warranted to attain the desired reaction temperature more

quickly from the start of a given determination cycle as well as to achieve fast thermal equilibration of the entire system during start up. External insulation, not used in this study, should be helpful.

With all reagents added and with water as sample, the absorbance reproducibility of the system was measured at  $t = 3$  min (solution temperature is  $\sim 50$  °C, heater off). Overall reproducibility was judged adequate, the detector output was  $348 \pm 2.4$  mAU (relative standard deviation 0.7%,  $n = 8$ ). With the heater turned on and a set temperature of 140 °C, the reproducibility was measured at  $t = 2, 5, 8$  and 10 min; the respective signal outputs were  $380 \pm 2, 385 \pm 3, 388 \pm 4,$  and  $389 \pm 4$  mAU, 0.5–1.0% in relative standard deviation. The slight increase in the mean background absorbance between  $t = 2$  and 10 min is not due to lack of attainment of the set temperature for the reaction mixture (the temperature sensor indicates this occurs long before 2 min) but due to slow changes in the system, possibly dimensional changes due to thermal expansion. This does not constitute a source of error per se because the behavior of the sample is always interpreted with reference to a blank. As these data indicate, the blank behavior is reproducible. Note also that the change in background absorbance as a function of solution temperature is highly nonlinear—in going from 50 to 120 °C,  $\Delta A$  is only 15 mAU while the change is nearly 20 mAU in going from 120 to 140 °C.

**Heating Considerations and Noise Sources.** A further reduction of reaction volume from ca. 1.6–1.7 mL was precluded primarily by the heater. However, since the present study was completed, we have been able to fabricate heaters of the same wattage with a total volume of <30% of that used in this work. Initially we attempted to heat the solution by resistive heating (ac) of a platinum coil (0.1 × 250 mm) immersed in it. Although a much smaller heater could be fabricated in this manner, it was not possible to use such a heater in the present system because even at relatively low applied voltages the surface temperature of the platinum wire is high enough to cause self-decomposition of the Cr(VI) solution. The self-decomposition of acidic Cr(VI) solutions at high temperatures (even without the benefit of any catalytic effects, as may be present with a heated platinum wire) is well documented in the literature (54). No matter what heater design is chosen material compatibility with the extremely aggressive reaction conditions is the foremost consideration.

By far the most important noise source in the detector output is the turn on/off spikes caused by the heater thermostat relay. The result is that the signal of interest represents an envelope below the noise spikes as in Figure 5. This does not constitute a real deterrent in data interpretation, albeit the noise represents a nuisance in aesthetic terms. Proportional, rather than on-off temperature control should eliminate this noise. We chose, however, to omit it through appropriate software. Since the data acquisition begins at a time before the thermostat switches, the initial data has no noise in it. Because the type of noise encountered is abrupt spikes, the software looks at successive data points (acquisition rate 16 points/s) and ignores the most recent one if it represents a sudden (e.g., by 25%, extent user-specified) change from the previous datum. The net result is the transformation of raw data as shown in Figure 6A to that in Figure 6B.

Powering the heater at voltages significantly above 90 V causes bubbles at the heater surface and leads to optical noise. The same happens at reaction temperatures  $\geq 150$  °C. Both of these limitations could be removed with a higher  $H_2SO_4$  content of the reaction mixture which would raise the boiling point.

**Operating Considerations.** COD measurements are often used for reporting to regulatory agencies. Even a minor de-

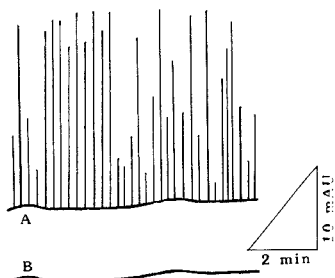


Figure 6. Examples of noise spike removal by software manipulation: (A) raw data; (B) postsoftware treatment.

violation from procedures prescribed by a regulatory agency such as the U.S. EPA requires that the new procedure must undergo an equivalency testing program of set protocol before the new procedure can be approved for regulatory purposes. We hope to report on results of such tests in the future. Meanwhile, COD measurements are routinely used also in a large number of treatment facilities, especially those involved with sewage and wastewater, to follow the course of the treatment process. In wastewater treatment facilities of a chemical/petrochemical complex, the effluent from a large number of individual plants is typically treated at a single central location. The major concern is to quickly detect the occurrence of an "upset" and thence to identify the particular manufacturing plant responsible for the increased COD and take appropriate corrective action. Broader information than that represented by a single measurement value is particularly useful in such cases. It is obvious that a measurement protocol (with or without added  $\text{Ag}^+$ ) as shown in Table I not only is capable of providing information of at least the same value as the rapid COD or ODI tests faster, it can also provide additional information on the rate of sample oxidation. Individual plant effluents have characteristic oxidation rates and under "upset" conditions a single plant is often by far the dominant contributor to the COD. Therefore, such kinetic information, especially if coupled to a temperature effect measurement, may be all that is needed to tentatively identify the malfunctioning plant. With complex samples, one protocol that yields a lot of information involves beginning with a 3-4 min measurement period without the silver catalyst. The catalyst is added at the end of this period and the course of the reaction is followed for another 4 min. Thus, this procedure provides demand levels as well as rate information on both the "normal" and "argentoactive" regions. Figure 3f illustrates this for a mixture of KHP and sodium acetate. It is for this reason we prefer a separate  $\text{Ag}^+$  reagent. For both acetate and glutamate, it has been observed that the oxidation rate continues to increase with an increase in the amount of  $\text{AgNO}_3$  added in the range 10-40 mg (50  $\mu\text{L}$  of 2-8% solution), albeit the gain is minimal in going from 20 to 40 mg. We have chosen to use  $\text{AgNO}_3$  for this purpose because of its much greater solubility relative to  $\text{Ag}_2\text{SO}_4$ . As such, relatively concentrated solutions can be used and volumetric dilution resulting from the  $\text{Ag}^+$ -reagent addition can be minimal. In control experiments with KHP standards and blanks, we have observed no effects of  $\text{AgNO}_3$  on the equilibrium absorbance value, i.e., nitric acid does not appear to participate as an oxidant in the presence of excess dichromate. Of course, if the separate  $\text{Ag}^+$ -reagent addition strategy is not used,  $\text{Ag}_2\text{SO}_4$  can be dissolved in the requisite amount directly in the sulfuric acid reagent.

## CONCLUSIONS

The determination of COD is both a diagnostic and regu-

latory measure in the treatment and disposal of municipal and industrial effluents. The approach described herein represents a fast convenient automated procedure that provides much more information than single value measurements. The total volume of reagents consumed per sample can be favorably compared to presently existing methods. Although the total number of samples that can be processed per unit time is not larger than efficient manual methods involving in-tube batch-mode digestion and photometric measurement, the minimum processing time for a sample can be much faster. The instrument is well-suited as an on-line analyzer or in conjunction with autosamplers. A simple inexpensive auto-sampler suitable for this application has been described (62). Although the instrument operates in a vented fashion, it should be easily possible either to operate the instrument under mildly pressurized conditions (2-3 atm) or to provide a microsize reflux condenser.

## LITERATURE CITED

- Phelps, E. B. *Stream Sanitation*; Wiley: New York, 1944; pp 65-66.
- American Public Health Association. *Standard Methods for the Examination of Water and Wastewater*, 16th ed.; APHA: Washington, DC, 1985; pp 525-538.
- Japan Industrial Standard JIS K 0102, 1974.
- Benson, H. K.; Hicks, J. F. G., Jr. *Ind. Eng. Chem. (Anal. Ed.)* **1931**, *3*, 30-31.
- Haupt, H. *Vom Wasser* **1935**, *10*, 60-77.
- Kashkin, M. L.; Karasik, R. M. *Med. Exp. (Kharkov)* **1940**, *4*, 9-13.
- Matubara, T. *Mitt. Med. Akad. Kioto* **1940**, *28*, 563-575.
- Klein, L. J. *Proc. Inst. Sewage Purif.* **1941**, 174-191.
- Lovett, M. J. *Proc. Inst. Sewage Purif.* **1941**, 194-195.
- American Public Health Association. *Standard Methods for the Examination of Water and Wastewater*, 9th ed.; APHA: Washington, DC, 1946; p 122.
- Nasr, M. S.; MacDonald, D. G. *Pulp Pap. Can.* **1975**, *76*, 91-93.
- Korenaga, T.; Ikatsu, H. *Analyst* **1981**, *106*, 653-662.
- Korenaga, T.; Ikatsu, H.; Moriwake, T. *Bull. Chem. Soc. Jpn.* **1982**, *55*, 2622-2627.
- Bezel, L. J. *J. Appl. Chem. USSR (Engl. Transl.)* **1945**, *18*, 361-366.
- El-Dib, M. A.; Ramadan, F. M. J. *Sanit. Eng. Div., Am. Soc. Civ. Eng.* **1966**, *92*, 97-101.
- Dzydzio, A. M. *Vodosnabzh. Sanit. Tekh.* **1938**, *8/9*, 117-125.
- Medalia, A. I. *Anal. Chem.* **1951**, *23*, 1318-1320.
- Gilmour, C. M.; Merryfield, F.; Burgess, F.; Punkerson, L.; Carswell, K. *Purdue Univ., Eng. Bull., Ext. Ser.* **1960**, *106*, 143-149.
- American Society for Testing and Materials. *Methods D1252-83*. In *Annual Book of ASTM Standards*, ASTM: Philadelphia, PA, 1984; Vol. 11.01, pp 62-68.
- Adeney, W. E.; Dawson, B. B. *Sci. Proc. R. Dublin Soc.* **1926**, *18*, 199-202.
- Ingols, R.; Murray, P. E. *Water Sewage Works* **1948**, *95*, 113-117.
- Moore, W. A.; Kroner, R. C.; Ruchhoff, C. C. *Anal. Chem.* **1949**, *21*, 953-956.
- Moore, W. A.; Ludzack, F. J.; Ruchhoff, C. C. *Anal. Chem.* **1951**, *23*, 1297-1300.
- Jenkins, S. H.; Harkness, N.; Hewitt, P. J.; Snaddon, X. V. M.; Ellerker, R.; Divito, B.; Dee, H. J. *Proc. Inst. Sewage Purif.* **1965**, *6*, 533-565.
- Jeris, J. S. *Water Wastes Eng.* **1967**, *4*(5), 89-91.
- Shriver, L. E.; Young, J. C. J. *Water Pollut. Control. Fed.* **1972**, *44*, 2140-2147.
- Chaudhuri, N.; Niyogi, S.; De, A.; Basu, A. J. *Water Pollut. Control Fed.* **1973**, *45*, 537-541.
- Wolff, C. J. M. *Water Res.* **1975**, *9*, 1015.
- Himebaugh, R. R.; Smith, M. J. *Anal. Chem.* **1979**, *51*, 1085-1087.
- Bulletins TCOOD and ACOD; O. I. Corporation: College Station, TX, 1986, 1987.
- Methods for Chemical Analysis of Water and Wastes*; EPA 600/4-79-020; U.S. Environmental Protection Agency. Environmental Monitoring and Support Laboratory: Cincinnati, OH, 1979.
- Jirka, A. M.; Carter, M. J. *Anal. Chem.* **1975**, *47*, 1397-1402.
- Edwards, S. J.; Allen, M. *Analyst* **1984**, *109*, 671-672.
- Adelman, M. H. In *Automation in Analytical Chemistry. Technicon Symposia 1966*; Mediad, Inc.: White Plains, NY, 1967; pp 552-556.
- Zuckerman, M. M.; Molof, A. H. In *Advances in Automated Analysis. Technicon International Congress 1969*; Mediad, Inc.: White Plains, NY, 1970; Vol. II, pp 121-124.
- Haines, G. D.; Anselm, C. D. In *Advances in Automated Analysis. Technicon International Congress 1969*; Mediad, Inc.: White Plains, NY, 1970; Vol. II, pp 159-162.
- Tift, E. C.; Cain, B. E. In *Advances in Automated Analysis. Technicon International Congress 1972*; Mediad, Inc.: Tarrytown, NY, 1973; Vol. VIII, pp 11-15.
- Stanley, G. H. In *Advances in Automated Analysis. Technicon International Congress 1972*; Mediad, Inc.: Tarrytown, NY 1973; Vol. VIII, pp 17-21.
- Fleet, B.; Ho, A. Y. W.; Tenygi, J. *Analyst* **1972**, *97*, 321-333.
- Korenaga, T. *Bull. Chem. Soc. Jpn.* **1982**, *55*, 1033-1038.
- Korenaga, T.; Ikatsu, H. *Anal. Chim. Acta* **1982**, *141*, 301-309.

- (42) Appleton, J. H. M.; Tyson, J.; Mounce, R. P. *Anal. Chim. Acta* **1986**, *179*, 269-278.
- (43) Harkness, N.; Hey, A. E.; Willetts, D. G. *Water Pollut. Control* **1972**, *71*, 261-277.
- (44) Model 304 COD Analyzer Bulletin; Tonics, Inc.: Watertown, MA, 1988.
- (45) Moore, W. A.; Walker, W. W. *Anal. Chem.* **1956**, *28*, 164-167.
- (46) Dobbs, R. A.; Williams, R. T. *Anal. Chem.* **1963**, *35*, 1064-1067.
- (47) Buzzell, J. C.; Young, R. H. F.; Ryczman, D. W. *Behavior of Organic Chemicals in the Aquatic Environment. Part II. Dilute Systems*; Manufacturing Chemists Association: Washington, DC, 1968; p 34.
- (48) Chudoba, J.; Dalesicky, J. *Water Res.* **1973**, *7*, 663-668.
- (49) McNary, R. R.; Dougherty, M. H.; Wolford, R. W. *Sewage Ind. Wastes* **1957**, *29*, 894-900.
- (50) Foulds, J. M.; Lunsford, J. V. *Water Sewage Works* **1968**, *115*, 112-115.
- (51) Muers, M. M. J. *Soc. Chem. Ind.* **1936**, *55*, 717.
- (52) Westerhold, A. F. *Digester* **1965**, *22* (1), 4-11.
- (53) Westerhold, A. F. *Digester* **1965**, *22* (2), 18-22.
- (54) Wells, W. N. *Water Sewage Works* **1970**, *117*, 123-129.
- (55) McLean, D. A.; Spicher, R. G. *Proc. Ind. Waste Conf.* **1973**, *28*, 1017-1024.
- (56) Reynolds, J. F.; Gollner, K. A. *Water Sewage Works* **1974**, *121*, 31-34.
- (57) Cooper, W. J.; Young, J. C. In *Water Analysis*; Minear, R. A.; Keith, L. H., Eds.; Academic Press, New York, 1984; Vol. III.
- (58) Ford, D. L.; Eller, J. M.; Gloyna, E. F. *J. Water Pollut. Control Fed.* **1971**, *43*, 1712-1723.
- (59) Mottola, H. A. *Kinetic Aspects of Analytical Chemistry*; Wiley: New York, 1988.
- (60) Swelleh, J. A.; Lopez, J. L.; Dasgupta, P. K. *Rev. Sci. Instrum.* **1988**, *59*, 2f09-2615.
- (61) Swelleh, J. A.; Dasgupta, P. K. *Anal. Chim. Acta* **1988**, *214*, 107-119.
- (62) Ping, L.; Dasgupta, P. K. *Anal. Chem.* **1990**, *62*, 85-88.
- (63) Goodwin, A. E.; Cabbiness, D. E.; Mottola, H. A. *Water, Air, Soil Pollut.* **1977**, *8*, 467-478.
- (64) Marquardt, D. W. *J. Soc. Ind. Appl. Math.* **1963**, *11*, 431-441.
- (65) Frost, A. A.; Pearson, R. G. *Kinetics and Mechanism*, 2nd ed.; Wiley: New York, 1961; p 22.
- (66) Thompson, K. C.; Mendham, D.; Best, D.; de Casseras, K. D. *Analyst* **1986**, *111*, 483-485.
- (67) Sillen, G.; Martell, A. E. *Stability Constants of Metal-ion Complexes*; Special Publication no. 17; The Chemical Society: London, 1964; p 276.
- (68) Williams, G. R.; Tolbert, L. M.; Holler, F. J. *Anal. Chem.* **1982**, *54*, 256-230.
- (69) Holler, F. J.; Calhoun, R. K.; McClanahan, S. F. *Anal. Chem.* **1982**, *54*, 755-761.
- (70) American Chemical Society Committee on Environmental Improvement. *Anal. Chem.* **1980**, *52*, 2242-2249.

RECEIVED for review June 21, 1989. Accepted November 22, 1989. This research was supported by a cooperative research agreement with the Dow Chemical Company, U.S.A.

## Optimization of Multienzyme Flow Reactors for Determination of Acetylcholine

P. Chandrani Gunaratna and George S. Wilson\*

Department of Chemistry, University of Kansas, Lawrence, Kansas 66045

Immobilized enzyme reactors have been used with high-performance liquid chromatography (HPLC) and electrochemical detection to detect acetylcholine and choline in brain tissue samples. Acetylcholine and choline eluting from the LC column are introduced into a reactor containing immobilized acetylcholinesterase, which hydrolyzes acetylcholine to choline. The product is converted by a second enzyme, choline oxidase, to hydrogen peroxide, which is determined amperometrically. Several novel immobilization techniques including immobilization through enzyme-specific antibodies were used to immobilize these enzymes to retain maximum activity. Improved detection limits were observed when the enzymes were immobilized through the avidin-biotin linkage. Better sensitivity and detection limit were obtained when both enzymes were immobilized together on the same support through the avidin-biotin linkage than when they were separately immobilized and used in two columns. The post-column system was applied to brain tissue extracts.

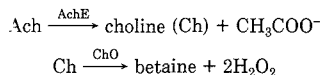
### INTRODUCTION

Acetylcholine (Ach), the main neurotransmitter in the cholinergic neurotransmitter system, is found in mammalian brain tissues. Determination of Ach and Ch levels in the brain is very important due to the significant role it plays in neuropsychiatric diseases (1). Increasingly sensitive assay techniques are required to measure the low concentrations of Ach and Ch in the brain.

\*To whom correspondence should be addressed.

Several physicochemical methods are available for the determination of Ach. These methods include GC-MS (2) and radiometric assays (3). However, these techniques are associated with time-consuming, complicated procedures and require expensive equipment. Recently, immobilized enzyme reactors (IMERs) have been used with high-performance liquid chromatography (HPLC) and electrochemical (EC) or chemiluminescence detection to assay Ach (4-7). These methods are now gaining popularity.

Use of IMERs utilizing HPLC with EC detection is based on the separation of Ach from brain tissue extracts by reverse-phase HPLC, passing the effluent through acetylcholinesterase (AchE) and choline oxidase (ChO) immobilized reactors, followed by the amperometric detection of hydrogen peroxide produced by the following reaction scheme:



However, the IMERs are not without problems. One major limitation is the loss of enzyme activity in the immobilization step due to either the binding of the enzyme to the support through or near its active site or binding in an orientation such that the active site is inaccessible. Performance of the IMER depends on the properties of the enzyme immobilized. For example, in our system AchE is more durable than ChO and can be immobilized without losing activity. ChO is very sensitive to its environment, and any change in the immediate environment surrounding the enzyme can cause a significant loss in activity.

Various methods of immobilization have been used in our studies to retain the maximum activity of the enzymes. These

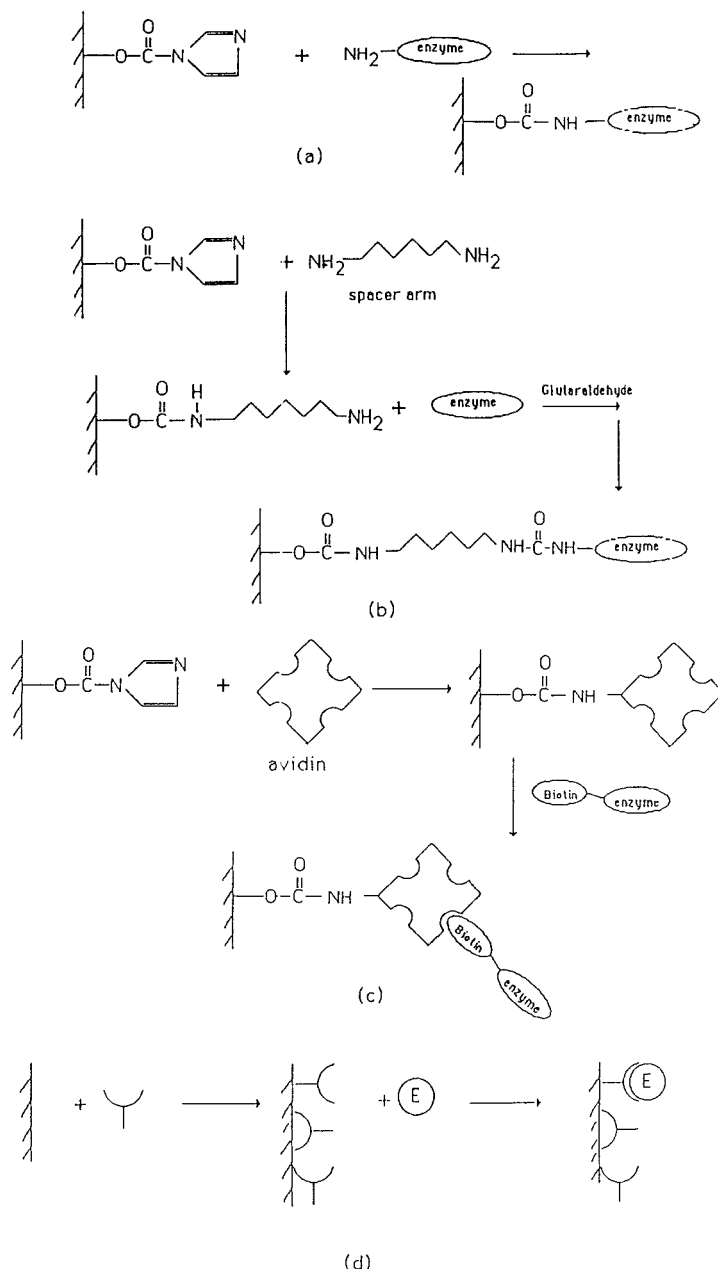


**Figure 1.** Schematic representation of various immobilization methods: (a) direct, (b) spacer arm, (c) avidin-biotin linkage, (d) antibodies.

methods include immobilization of enzyme (a) directly, (b) through a spacer arm, (c) through avidin-biotin complexation, and (d) through antibodies specific to the enzymes. These are illustrated in Figure 1.

To overcome the limitations caused by direct immobilization, the enzyme can be immobilized through a spacer arm that couples to the enzyme at a specific distance from the active site, thereby allowing the substrate to access the active

site effectively. Lengthening the spacer arm localizes the enzyme farther from the solid support, making it free to interact with substrate. A particularly well-suited system for this purpose is the avidin-biotin linkage. Avidin has a high affinity for biotin (dissociation constant  $10^{-15}$  M), and the binding of avidin to biotin is undisturbed by extreme pH or change in ionic strength. The enzyme can be immobilized through the avidin-biotin linkage as shown in Figure 1c.

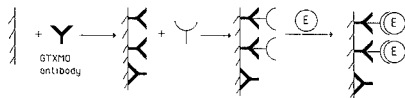


**Figure 2.** Schematic representation of site-directed antibody immobilization: immobilized antibody goat-anti-mouse IgG, Fc specific.

It has been shown that it is possible to immobilize enzymes while retaining high activity through immobilized antibodies specific to the enzyme (8). In this case, it is important to immobilize the antibody efficiently in order to couple a maximum amount of enzyme. When antibodies are coupled to the support, they can bind in various orientations as shown in Figure 1d. It is important to promote coupling through the Fc region of the antibody molecule in order to avoid attachment through an amino group near the antigen binding site (Figure 2).

Immobilizing enzymes through antibodies has the advantage of easy regeneration of the enzyme once its activity is lost. It is very convenient to immobilize new enzyme on an antibody column just by washing off the old enzyme and injecting a new aliquot of the enzyme. This allows the user to regenerate the column within minutes.

### EXPERIMENTAL SECTION

**Materials.** Acetylcholine (Ach) chloride, choline (Ch) chloride, AchE type III (electric eel) and ChO (*Alcaligenes*), triethylenetetramine tetrahydrochloride (TETA), 4-aminopyridine, and tetramethylammonium chloride (TMA) were purchased from Sigma Chemical Co. (St. Louis, MO). Sodium octyl sulfate (SOS) was purchased from Eastman Kodak (Rochester, NY). Avidin was purchased from Calbiochem Behring (San Diego, CA). NHS-LC-Biotin and CDI activated Reactigel HW-65 were obtained from Pierce Chemical Co. (Rockford, IL). Ethylhomocholine (Ehc) iodide (internal standard for Ach and Ch) was synthesized (4) from 3-(dimethylamino)-1-propanol and iodethane, both obtained from Aldrich (Milwaukee, WI). Goat-anti-mouse Fc specific antibodies were purchased from Organon Teknika-Cappel (Malvern, PA). Mouse myeloma cell line P3/NS1/1-Ag4-1 (ATCC No. TIB 18) for the preparation of hybridomas was obtained from American Type Culture Collection (Rockville, MD). All other reagents used were of analytical grade. Solutions were prepared in water obtained from a Barnstead Nanopure II system. The buffers used in the flow injection analysis (FIA) system were additionally filtered through 0.45- $\mu$ m filters. Brain (striatum) tissue samples obtained from microwave-killed or decapitated Sprague-Dawley mice were a generous donation from LeRoy Blank of the University of Oklahoma.

**Apparatus.** A Shimadzu LC-6A liquid chromatographic system consisting of a SCL-6B controller, LC-6A pump, SIL-6B autoinjector, FCV-2AH high-pressure switching valve, and CR4A integrator (all from Shimadzu Corporation, Kyoto, Japan) and a BAS LC-4B amperometric detector (BioAnalytical Systems, West Lafayette, IN) coupled to a LC-17AT flow-through thin-layer electrochemical cell were used. The complete HPLC system is shown in Figure 3. An Altex Nucleosil C-18, 5- $\mu$ m, 0.46  $\times$  15 cm (Alltech Associates, Deerfield, IL) reverse-phase column was used with a Brownlee guard column (Applied Biosystems, Santa Clara, CA) for HPLC separations. A Shimadzu 160 UV-vis spectrophotometer was used for the spectrophotometric measurements. The stainless steel columns used to make IMERs were purchased from Upchurch Scientific, Inc. (Oak Harbor, WA).

**Methods.** *Direct Enzyme Coupling to Support.* The activated HW-65 gel (1 mL) was washed according to the manufacturer's instructions. The enzyme (2 mg/mL) was dissolved in 0.1 M carbonate buffer (pH 9.35), and the solution was mixed with the prewashed gel by mechanical inversion for 30 h at 4 °C. The coupled gel was then allowed to settle, and the supernatant was removed. The collected gel was then washed on a glass frit, first with 2 M Tris buffer and then with 0.1 M phosphate buffer (PB, pH 7.4) three times, and stored in the same buffer. The protein content in the supernatant and the washings was determined by the BCA assay (9).

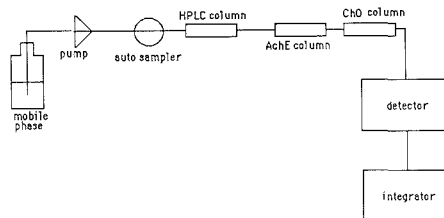


**Figure 3.** Schematic diagram of the HPLC/IMER system.

*Enzyme Coupling through a Spacer Arm to the Support.* A solution of triethylenetetramine tetrahydrochloride (TETA) (150 mg/15 mL) in 0.1 M carbonate buffer was mixed with 2 mL of unwashed gel by mechanical inversion for 48 h at 4 °C. The coupled gel was then washed with 0.1 M PB pH 8.5. The enzyme (2 mg/mL) was then cross-linked to TETA-gel with 100  $\mu$ L of 0.1% glutaraldehyde. The reaction mixture was allowed to react at room temperature for 2 h by mechanical inversion. The coupled gel was then washed with 0.1 M PB pH 8.5 and stored in the same buffer for further use.

*Enzyme Coupling through Avidin-Biotin Linkage.* Avidin (6 mg/mL) was dissolved directly in 0.1 M carbonate buffer (pH 9.35), and the solution was mixed with 2 mL of prewashed gel by mechanical inversion for 30 h at 4 °C. The coupled gel was washed and stored in 0.1 M PB. The biotinylated enzyme was prepared by reacting NHS-LC-Biotin (6 mg) and ChO (5 mg) in 1 mL of 0.05 M carbonate buffer (pH 8.0) for 2 h at 4 °C. The reaction mixture was then dialyzed against two volume changes of 0.1 M PB (pH 7.4) to remove the excess biotin. The same procedure was followed for AchE except that 2 mg of AchE and 2.4 mg of biotin were used in 0.5 mL of 0.05 M carbonate buffer. The biotinylated enzyme was then allowed to react with the avidin-coupled gel for 2 h at room temperature. The gel was then washed and stored in 0.1 M PB as before.

*Antibody Coupling to Support.* A solution of mouse monoclonal anti-enzyme antibody (5 mg/mL) in 0.1 M carbonate buffer (pH 9.35) was mixed with 2 mL of prewashed gel for 42 h at 4 °C by mechanical inversion. The coupled gel was first washed with one volume of 2 M Tris buffer (pH 8) and then one volume of 0.01 M phosphate-buffered saline (PBS, pH 7.2) and finally with 0.01 M PBS (pH 7.4). The washed gel was then stored in the same buffer containing 0.02% azide until further use. The goat-anti-mouse Fc specific antibody was coupled to the support by the same procedure.

*Preparation of Monoclonal Antibodies.* Murine monoclonal antibodies specific to ChO and AchE were prepared by the method of Kohler and Milstein (10). Six to eight week old female Balb/C mice were immunized intraperitoneally with 20  $\mu$ g of antigen. Two weeks later, the mice were again immunized intraperitoneally. The mice were then boosted with the antigen 48 h before the fusion. The splenocytes were fused with NS1 mouse myeloma cells. The positive wells were screened by an enzyme-linked immunosorbent assay (ELISA) method. The monoclonal antibodies to both acetylcholinesterase (19D) and choline oxidase (F2D1A6) were of the IgG1 subclass. Monoclonal antibodies in large quantities were obtained from the ascites fluid. The antibodies were then purified first by ammonium sulfate precipitation and then by ion exchange chromatography with 300 mM NaCl in 10 mM Tris buffer (pH 8.0) gradient elution (11). The IgG fraction was collected, concentrated, and then dialyzed against 0.1 M PB (pH 7.4).

*Sample Preparation.* Striatum tissue were homogenized in 1.0 mL of 0.1 M perchloric acid containing 2 nmol of ethylhomocholine and centrifuged at 12000g for 10 min. The pH of the supernatant was adjusted to 4.0 by adding about 40  $\mu$ L of 4 M potassium acetate, and the solution was centrifuged at 12000g for 10 min. The supernatant was directly injected into the HPLC system.

**Standards and Solutions.** Acetylcholine and choline stock solutions (0.1 M) were prepared in 0.02 M citrate-phosphate buffer (pH 4.0) weekly and stored at 4 °C. Dilutions were daily made in the reaction buffer from these standards. The reaction buffer

for the assay was 0.2 M PB (pH 8.5) containing 1 mM disodium ethylenediaminetetraacetic acid ( $\text{Na}_2\text{EDTA}$ ). The same amount (2 nmol/mL) of Ehc, the internal standard, was added to the standards as well as to the samples. The mobile phase was 0.1 M potassium dihydrogen phosphate containing 1.2 mM TMA, 0.372 g EDTA, and 10 mg/L SOS. The pH was adjusted to 7.0 by adding 5 N KOH. For the AchE antibody bound-free studies, the carrier buffer was 0.1 M PB (pH 7.4) and the eluting buffer was 0.1 M PB (pH 2.2). For ChO antibody studies, the carrier buffer was the same as the reaction buffer and the elution buffer was 0.2 M PB (pH 2.2). The IMER column was  $0.21 \times 4.0$  cm. These columns were packed with coupled gels as described elsewhere (8).

ChO activity on the support was measured by the method of Ikuta et al. (12) with some modifications. The reagent mixture, which consisted of 1% 4-aminoantipyrine, 1% phenol, 2.1% choline chloride, and horseradish peroxidase in 0.1 M Tris buffer (pH 8.0), was added to a known amount of ChO immobilized support and incubated at room temperature for 10 min. The reaction was stopped by adding ethanol. The absorbance of the supernatant was measured at 500 nm. Reagent added to an equal volume of pure gel was used as a blank.

## RESULTS AND DISCUSSION

The two enzymes used here, ChO and AchE, have very different characteristics. ChO is a monomer with a molecular weight of 72000 (13) and contains a flavin adenine dinucleotide group as the active site. AchE exists as a dimer usually containing two tetrameric sets of catalytic subunits (14). AchE has a very high turnover number (15) and a high specific activity. ChO has a very low intrinsic turnover rate and specific activity compared to AchE.

Performance of the immobilized ChO column was always evaluated before it was used in conjunction with an immobilized AchE column. First, the ChO column was used in the FIA system to detect choline standards. When the ChO column was found to be satisfactory, it was used with an AchE column to detect Ach standards.

When ChO was coupled to the support directly ( $O_{DC}$ ), the performance of the column was very poor. In this case, it was found that the activity of ChO on the support was very low even though 72% of added ChO was bound to the support. In other words, the ChO lost virtually all of its activity (about 99%) during the coupling step.

When both enzymes were coupled through the spacer arm ( $O_{SC}$  for ChO and  $E_{SC}$  for AchE), the detection limit of the assay was found to be about 2 pmol for choline. The assay is less sensitive for Ach than for Ch. It was found that when AchE was cross-linked to the spacer arm, the amount of coupling was less (53%) than when coupled directly (72.5%). Therefore, AchE was coupled directly. The enzyme activity of both AchE and ChO IMERs was lost after about a week.

The enzymes coupled through avidin-biotin ( $E_{AVC}$  for AchE and  $O_{AVC}$  for ChO) retained the highest activity, and enhanced sensitivity was observed. The detection limit in this case was 100 fmol ( $10^{-8}$  M). The columns can be used continuously for about 2 weeks without losing activity.

To enhance the sensitivity, both  $E_{AVC}$  and  $O_{AVC}$  were packed in the same column in the following different configurations: (a) well-mixed, (b) packed as two separate bands, and (c) packed in several small alternate bands. Configurations a and c both gave broad peaks for the analysis; configuration b did not show any improvement. In fact, the current was lower for b than when  $E_{AVC}$  and  $O_{AVC}$  were packed in two columns.

To achieve increased sensitivity, the biotinylated enzymes were mixed and allowed to couple to the avidin-bound support in the same mixture. This support ( $E/O_{AVC}$ ) was packed in a column and used in the FIA system. This configuration showed greatly improved sensitivity, and the detection limit was lowered 10-fold (10 fmol). A wide linear range of detection was observed. This compares with a previously reported

detection limit of about 100 fmol (5). This result is not unexpected, as previous studies have shown that attaching two enzymes in a multienzyme system to the same support results in enhanced efficiency (15). This is because if the two enzymes are in intimate contact, the local concentration of the first product is higher, leading to an increased rate for the second step.

**Immobilization through Antibodies.** Use of antibodies to immobilize enzymes has not been widely applied due to the difficulties in obtaining monoclonal antibodies (MABs). Preparation of MABs is time-consuming and expensive. The advantages of their use, however, outweigh the difficulties associated with them. Immobilized antibodies are stable for several months if stored properly at 4 °C in a buffer containing an antibacterial agent such as sodium azide. Immobilizing the enzyme through an antibody-antigen reaction is extremely simple.

When each antibody was mixed in excess in solution with its respective enzyme antigen, no inhibition of the enzyme activity was observed, suggesting that the antibodies do not block the active site of the enzyme. However, when immobilized antibody to ChO was reacted with soluble ChO, about 30% of the enzyme activity was inhibited. This may be due either to the nonspecific adsorption of the enzyme on the support or to the crowding of the support with too many antibody molecules.

Antibodies to both ChO and AchE were immobilized on the support as described above. The enzymes were immobilized by injecting an aliquot of enzyme solution in carrier buffer. The bound and free fractions were evaluated for different injection volumes and different enzyme concentrations to establish an optimum concentration and injection volume. The two antibody columns were studied separately.

AchE antibody shows high affinity toward the AchE enzyme. The AchE antibody was coupled to the support ( $AA_{DC}/E$ ) directly and used with an  $O_{AVC}$  IMER in the FIA system. AchE solution (25  $\mu\text{L}$  of 0.2 mg/mL solution) was injected into the column before it was connected to the  $O_{AVC}$  IMER so that the free fraction of AchE would not nonspecifically adsorb on the  $O_{AVC}$  IMER and give a response for Ach. The detection limit was 100 fmol, and the linear range was from  $10^{-8}$  to  $10^{-6}$  M. The same sensitivity was observed when the AchE antibody was immobilized through goat-anti-mouse Fc specific IgG ( $AF_{DC}/AE/E$ ).

When ChO antibody was bound to the support and used to immobilize ChO, it was found that the enzyme binds to the antibody effectively even though it has an apparently lower binding affinity than that of the AchE antibody. Since the reaction of ChO with the immobilized antibody is not rapid, optimal attachment is best achieved by injecting small aliquots of enzyme, i.e., it is better to inject 10 aliquots of 10  $\mu\text{L}$  of 0.1 mg/mL ChO solution than to inject 100  $\mu\text{L}$  of same ChO solution. For example, when 100  $\mu\text{L}$  of 0.1 mg/mL ChO was injected, the response for 200 pmol of Ch was only 2.2 nA. When ChO was instead injected in small aliquots (10  $\mu\text{L}$ ) 10 times, the response for 200 pmol was 10.9, indicating the higher enzyme activity in the latter case. Subfemtomole quantities of Ch could be detected soon after the enzyme was injected. The response decreases with each injection of the sample until it reaches a constant value. This decrease in response could be due to nonspecifically adsorbed enzyme being slowly washed off. This was avoided by first injecting 100  $\mu\text{L}$  of 0.1 mg/mL bovine serum albumin (BSA) solution to saturate the nonspecific sites and then injecting the enzyme. The reproducibility of the method was tested by injecting samples containing known amounts of Ach, Ch, and Ehc repeatedly. The coefficients of variation of the assay are as follows: for Ach, 1.7%; for Ch, 1.1%; and for Ehc, 2.3% ( $n = 6$ ). The

**Table I. Comparison of the Immobilization Methods for the Bienzyme Reactor**

method of immobilization <sup>a</sup>	detection limit, pmol	response to 200 pmol of Ach, nA
E <sub>DC</sub> + O <sub>DC</sub> <sup>b</sup>	2000	—
E <sub>DC</sub> + O <sub>SC</sub> <sup>b</sup>	2.0	5.1 ± 0.05
E <sub>AVC</sub> + O <sub>AVC</sub> <sup>b</sup>	0.1	13.6 ± 0.26
E/O <sub>AVC</sub> <sup>c</sup>	0.01	72.4 ± 0.17
AE <sub>DC</sub> /E + AO <sub>DC</sub> /O <sup>b</sup>	0.1	10.9 ± 0.12

<sup>a</sup> Abbreviations: E, AchE; O, ChO; DC, direct coupling; SC, spacer coupling; AVC, avidin-biotin coupling; AE, antibody to AchE; AO, antibody to ChO. <sup>b</sup> Indicates two separate columns in series. <sup>c</sup> Indicates support material for two enzymes mixed.

**Table II. Comparison of Detection Limits Obtained with Different AchE Columns**

immobilization method <sup>a</sup>	detection limit, nM	% immobilized on support
E <sub>DC</sub>	10	93 ± 0.9
E <sub>SC</sub>	100	53 ± 1.7
E <sub>AVC</sub>	1	91 ± 0.5
AE <sub>DC</sub> /E	10	100

<sup>a</sup> Abbreviations: E, AchE; DC, direct coupling; SC, spacer coupling; AVC, avidin-biotin coupling; AE, antibody to AchE.

detection limit was 100 fmol. Equivalent sensitivity was seen when the ChO antibody was immobilized through goat-anti-mouse Fc specific antibodies (AFC<sub>DC</sub>/AO/O). This method in principle is superior because a common support containing this antibody can be used to immobilize the monoclonals for both enzymes.

The results obtained by all these immobilization methods are summarized in Table I. Since the experimental data obtained so far suggest that the detection limit of the assay is determined by the ChO column, experiments were carried out to study the efficiency of the AchE column independent of the ChO column, the effluents from the AchE column were collected, and the choline content was determined. Ch in the effluent, produced by the conversion of Ach as it passes through the AchE column, is converted to H<sub>2</sub>O<sub>2</sub> by adding ChO and incubating for 1 h at 37 °C. The produced H<sub>2</sub>O<sub>2</sub> is then determined electrochemically in the FIA system. The lowest concentration of Ach that could be converted by the AchE column was thus detected. AchE columns prepared by all the immobilization methods discussed before were compared, and these results are shown in Table II. The results show that in contrast to ChO, immobilized AchE has retained most of its activity during the immobilization step regardless of the immobilization method used.

These studies have shown that the activity of the ChO column defines the detection limit of the assay. To further study this, the activity of ChO on the support after immobilization was determined. These results are shown in Table III.

The data in Table III show that the ChO immobilized through avidin-biotin linkage, O<sub>AVC</sub>, has the highest activity. Enzyme activity on the supports that have ChO immobilized through the antibody is considerably higher than that of the other methods, but lower than that attained with the avidin-biotin method. Random coupling of the antibody yields a low number of properly oriented antibody molecules on the support (17), and this, along with some reduction of enzyme activity on binding, contributes to the low observed activity. Multisite attachment of the antibody molecule also lowers its antigen binding capacity. Low activity of the antibody is substantiated from the data in Table III and the amount of

**Table III. Performance of ChO Supports.**

immobtn method <sup>a</sup>	loading of ChO, mg/mL support	% uptake of ChO	immobd enzyme activ, units	% activ <sup>c</sup>
O <sub>DC</sub>	1.2 (5.5) <sup>b</sup>	85	0.015	0.32
O <sub>SC</sub>	1.0 (4.6) <sup>b</sup>	81	0.23	6.2
O <sub>AVC</sub>	2.5 (11.5) <sup>b</sup>	91	3.8	36.3
E/O <sub>AVC</sub>	2.5 (11.5) <sup>b</sup>	84	3.1	32.1
AO <sub>DC</sub> /O	0.02 (0.09) <sup>b</sup>	100	0.023	25.6
AFC/AO <sub>DC</sub> /O	0.02 (0.09) <sup>b</sup>	100	0.018	20.0

<sup>a</sup> Abbreviations: O, ChO; E, AchE; DC, direct coupling; SC, spacer coupling; AVC, avidin-biotin coupling; AO, antibody to ChO; AFC, goat-anti-mouse Fc specific antibody. <sup>b</sup> Units of enzyme in parentheses. <sup>c</sup> Percent activity on the support relative to soluble enzyme.

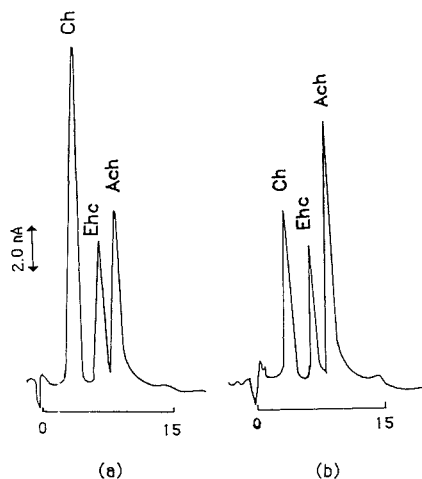


**Figure 4.** HPLC/IMER chromatograms: (a) 20  $\mu$ L of standard mixture containing 40 pmol of Ch and Ach and 40 pmol of Ehc; (b) 20  $\mu$ L of tissue extract containing 40 pmol of Ehc.

antibody immobilized. It has been estimated that only 6% of the immobilized antibody is active in effective binding of enzyme. This can be corrected by coupling Fab' fragments or by oriented coupling through the Fc region (17, 18). Since the turnover rate and specific activity of ChO are very low, a higher concentration of active enzyme in the column is required to obtain significant activity.

**Tissue Analysis.** Since E/O<sub>AVC</sub> showed the best performance, this column was used for the analysis of brain tissues. Since ChO has a pH optimum between 7.5 and 8.5 and the column material is unstable at pHs above 7.0, a compromise had to be made between the optimum pH of ChO and the column stability. Therefore the mobile phase used was 0.1 M KH<sub>2</sub>PO<sub>4</sub> containing 1.2 mM TMA, 10 mg/L SOS, and 1 mM Na<sub>2</sub>EDTA. TMA was added to the mobile phase to reduce the strong adsorption of Ach to the solid phase. But the addition of TMA shortens the lifetime of the IMER and reduces the detector response by inhibiting ChO. About 88% of enzyme activity is lost after 20 sample injections. Very well-resolved peaks were observed for a standard mixture containing Ch, Ehc, and Ach. The calibration curves obtained for Ach, Ch, and Ehc standards are linear ( $r = 0.999$  for all three analytes) in the 0.1–500-pmol range. The current response for Ehc is less than those of Ch and Ach. Typical chromatograms for a standard mixture and a sample are



shown in Figure 4. The usual neurotransmitters (dopamine, norepinephrine, and homovanillic acid) found in brain tissues gave no response in the assay system.

From the assays, the Ach content in the decapitated group was found to be  $14.3 \pm 2.1$  pmol/mg and the Ch content was  $75.7 \pm 3.4$  pmol/mg. The respective values for the microwave-killed group are  $38.9 \pm 2.6$  and  $22.8 \pm 1.8$  pmol/mg. The data are presented as the mean  $\pm$  standard error of the mean and  $n = 5$ . These results are in agreement with the published values (5). The values show that Ch concentration is high in decapitated brain tissue either due to the conversion of some Ach to Ch as a consequence of the action of residual AchE in the tissue or due to the release of membrane-bound Ch.

### CONCLUSIONS

In conclusion, we have demonstrated that effective immobilization of enzymes can be achieved through antibodies or the avidin-biotin complex. Highest activity of the immobilized enzymes was attained by the latter immobilization method. The extended spacer arm of biotin allows more efficient access to the enzyme molecule and is effective in reducing the steric hindrances associated with binding. It is also much easier to control the extent of covalent coupling of biotin to the enzyme. This system cannot be regenerated, which is a disadvantage. The immobilization through antibodies has the added advantage of easy and quick regeneration of the IMEF. The quick regenerating ability of the column is very useful, specially for tissue analysis where the TMA in the mobile phase inhibits the ChO. Optimization of antibody activity and site density, possibly with the use of spacer arms and/or coupling of Fab' fragments, may give a more satisfactory performance. Because of the inherently low specific activity of ChO and its sensitivity to its environment, the enzyme system will need to be regenerated frequently. Thus the use of antibody coupling is well worth the additional effort. A selective and sensitive method has been developed for the detection of Ach and Ch at femtomole levels. The sensitivity of the method

can further be enhanced by improving the antibody immobilization procedures to obtain increased response, and such work is currently in progress.

### ACKNOWLEDGMENT

We thank Rohan Wimalasena and Dilbir S. Bindra for their assistance in the preparation of monoclonal antibodies and Uditha de Alwis for helpful discussions.

### LITERATURE CITED

- (1) Davis, Kenneth L.; Berger, Philip A. *Brain Acetylcholine and Neuropsychiatric Disease*; Plenum Press: New York, 1979.
- (2) Newton, M. W.; Ringdahl, B.; Jenden, D. J. *Anal. Biochem.* **1983**, *130*, 88-94.
- (3) McCarna, R. E.; Stetler, J. J. *Neurochem.* **1977**, *28*, 669-671.
- (4) Potter, P. E.; Meek, J. L.; Neff, N. H. J. *Neurochem.* **1983**, *41*, 182-194.
- (5) Asano, M.; Miyauchi, T.; Kato, T.; Fujimori, K.; Yamamoto, K. *J. Liq. Chromatogr.* **1986**, *9*, 199-215.
- (6) Israel, M.; Lesbats, B. *Biolumin. Instrum. Appl.* **1985**, *2*, 1-11.
- (7) Damsma, G.; Westerink, B. H. C.; Horn, A. S. J. *Neurochem.* **1985**, *45*, 1649-1652.
- (8) De Alwis, U.; Wilson, G. S. *Talanta* **1989**, *36*, 249-253.
- (9) Wiechelman, K. J.; Brawn, Robert D.; Fitzpatrick, J. D. *Anal. Biochem.* **1988**, *175*, 231-237.
- (10) Kohler, G.; Milstein, G. *Nature* **1975**, *256*, 495-497.
- (11) Goding, J. W. *Monoclonal Antibodies: Principles and Practice*; Academic Press: New York, 1983; pp 100-115.
- (12) Ikuta, S.; MaTaura, K.; Imamura, S.; Misaki, H.; Horitsu, Y. *J. Biochem.* **1977**, *82*, 157-163.
- (13) Ohta-Fukuyama, O.; Miyake, Y.; Emi, S.; Yamano, T. *J. Biochem.* **1980**, *88*, 197-203.
- (14) MacPhee-Quigley, K.; Vedvick, T. S.; Taylor, P.; Taylor, S. S. *J. Biol. Chem.* **1986**, *261*, 13565-13570.
- (15) Zubay, Geoffrey L. *Biochemistry* Macmillan Publishing Co.: New York, 1989; p 271.
- (16) Mosbach, K.; Mattiasson, B. *Methods in Enzymology*, Vol. XLIV; Academic Press: New York, 1976; pp 453-478.
- (17) Matson, Robert S.; Little, Michael C. *J. Chromatogr.* **1988**, *458*, 67-77.
- (18) Cress, M. C.; Ngo, T. T. *Am. Biotechnol. Lab.* **1989**, *7*, 16-19.

RECEIVED for review August 9, 1989. Accepted November 28, 1989. We gratefully acknowledge support from the National Institutes of Health (GM 40038).

## CORRESPONDENCE

### Multichannel Electrochemical Detection System for Flow Analysis

Sir: Electrochemical detection in flow systems has been widely used for trace analysis of electroactive materials (1). The most common method is amperometric detection with a single disk (or plate) electrode maintained at constant potential. However, this method only provides poor information on the electrochemical properties of a species to be detected. Recently, much attention has been focused on electrochemical flow-through voltammetric detection with scanning potentials in order to obtain three-dimensional information (time, potential, and current). This method usually requires a rapid potential scan to catch species flowing in and out of the detector, resulting in increases in the background due to charging current and also in distortion of the voltammetric shape. To overcome this problem, several techniques have been reported, including square-wave voltammetry (2-9), staircase voltammetry (10-12), normal (12) and differential pulse (13) techniques, microdisk or microwire voltammetry (12, 14, 15), and a combination of voltammetric and amperometric detection (16, 17).

In this paper, we report on multichannel electrochemical detection in flow systems using a microelectrode array. The microelectrode array consisted of an assembly of independent microband electrodes held at different potentials. The currents flowing in the individual electrodes were collected to obtain three-dimensional results. This detection system was used for flow injection analysis (FIA).

### EXPERIMENTAL SECTION

Ferrocenylmethyl alcohol (FMA) was synthesized by reducing ferrocenecarboxaldehyde (Aldrich) with NaBH<sub>4</sub> and recrystallized twice from heptane. (Ferrocenylmethyl)trimethylammonium perchlorate (FA<sup>+</sup>ClO<sub>4</sub><sup>-</sup>) was prepared from its iodide salt (Aldrich) by using sodium perchlorate and was recrystallized from water.

The microelectrode array was fabricated (18) by conventional photolithography using a Shipley photoresist (Microposit 1400-31) on a glass plate sputtered with a thin gold film (film thickness: 200 nm). Figure 1 shows a schematized illustration of the array electrode. The array consisted of 16 microband electrodes. Only a part of this, shown in Figure 1 as a square, was exposed to the

Table I. Various Three-Dimensional Detection Systems

method	equiv scan rate, V/s	time, s <sup>a</sup>	potntl resolution, mV	detection lim (compd)	ref
this study (16 channel)	2.8 <sup>b</sup>	0.027	50	4 × 10 <sup>-7</sup> M, 2 × 10 <sup>-11</sup> mol (FMA, FA <sup>+</sup> )	
	2.8 <sup>b</sup>	0.27	10	4 × 10 <sup>-7</sup> M, 2 × 10 <sup>-11</sup> mol (FMA, FA <sup>+</sup> )	
voltammetric/ampereometric	2.0	0.375	-	3.7 × 10 <sup>-12</sup> mol (gentisic acid)	18
open tubular	1.0	0.75	10	10 <sup>-8</sup> M (hydroquinone)	16
square wave	1.0	0.75	10	10 <sup>-7</sup> M (N-nitroproline)	2
staircase	0.5	1.5	5	5 × 10 <sup>-12</sup> mol (catecholamines)	9
	1.25	0.6	5	10 <sup>-11</sup> mol (phenanthrenequinone)	12
	0.6	1.25	10	10 <sup>-12</sup> mol (catecholamines)	11
differential pulse	0.5	1.5	50	1.9 × 10 <sup>-12</sup> mol (norepinephrine)	13
	0.03	25	50	10 <sup>-7</sup> M (acetaminophen)	14

<sup>a</sup>Time required to obtain a voltammogram over the potential range of 750 mV. <sup>b</sup>Calculated by dividing the potential range (750 mV) by the data acquisition time.

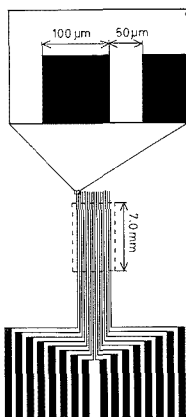


Figure 1. Schematized illustration of the microelectrode array used in this study. The area inside the square was exposed to the solution.

solution. The remainder was covered with photoresist to avoid leakage of the solution. Each band exposed to the solution was 0.1 mm in width and 7 mm in length. The flow-through cell was basically same as that used in previous studies (18, 19). The electrode array was held in the flow-through cell by a Teflon spacer (thickness: 0.1 mm). The flow channel was 4 mm wide and 12 mm long, and the total cell volume was 4.8 μL. The auxiliary electrode was a glassy carbon disk mounted in the opposite wall. An Ag/AgCl reference electrode was placed in a downstream compartment.

The multipotentiostat with 16 independent working electrode terminals was made in our laboratory. The basic circuit of the potentiostat is shown in Figure 2. The 16 responses from the current-to-voltage converters in the multipotentiostat were drawn into two-channel multiplexers, and the resulting two sets of eight signals were digitized successively by a eight-channel analog-to-digital (12 bit) converter system (Stanford Research Systems, Model SR245). All these instruments were controlled by an NEC 9801 VX2 personal computer with an 80286 central processing unit and an 80287 coprocessor. The program for instrument timing and data acquisition was written in Turbo Pascal with binary data transfer.

The FIA measurements were conducted with a JASCO 880-PU pump, an injector with a 50-μL sample loop, and the multipotentiostat connected with the flow-through cell. A stainless steel tube (10 m × 0.25 mm i.d.) was placed between pump and loop injector to serve as a pulse damper. The mobile phase was 0.1 M Na<sub>2</sub>SO<sub>4</sub> aqueous solution, and a flow rate of 1 mL min<sup>-1</sup> was used.

## RESULTS AND DISCUSSION

Figure 3a illustrates a typical three-dimensional FIA result for a mixture of 25 nmol of FMA and 25 nmol of FA<sup>+</sup> observed

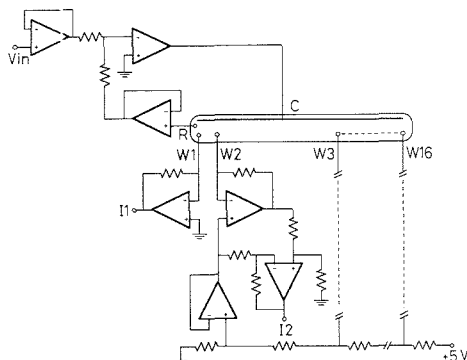


Figure 2. Basic circuit of the multipotentiostat: W<sub>1</sub>-W<sub>16</sub>, working electrodes; R, reference electrode; C, counter electrode.

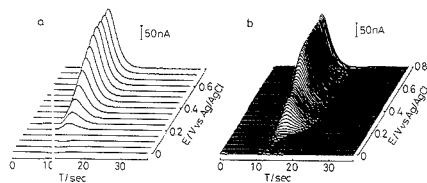
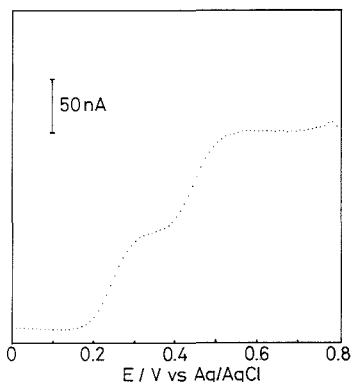


Figure 3. Three-dimensional FIA results for a mixture of 2.5 nmol of FMA and 2.5 nmol of FA<sup>+</sup>: (a) 16-channel detection; (b) 80-channel detector.

by 16-channel detection with a potential resolution of 50 mV. In this case, the potential applied to the array ranged from 0 to 750 mV vs Ag/AgCl and the potential of each microband electrode differed by 50 mV from that of the adjacent electrode. The oxidation peaks for the two ferrocenes appear at 15 s. Since the half-wave potentials for the two ferrocene derivatives differ by ca. 0.2 V, two plateaus are seen at the peak time. Unlike potential scanning methods (2-15), this 16-channel detection system does not suffer from the undesired effect of charging current, since the potentials for the individual electrodes were held at constant values. A series of currents from 16 electrodes provides a hydrodynamic voltammogram. The voltammogram is acquired within a short period; in the present 16-channel detection, 27 ms.

The resolution in terms of potential can be improved by applying small stepping potential to the 16 microband electrodes. Figure 3b shows the three-dimensional FIA result of a mixture of two ferrocenes observed by 80-channel detection with a potential resolution of 10 mV. In this case, a five-step potential staircase of 10-mV step height was applied to the



**Figure 4.** Hydrodynamic voltammogram for a mixture of 2.5 nmol of FMA and 2.5 nmol of FA<sup>+</sup>. The voltammogram was obtained from a cross section of Figure 3b at the peak time.

individual microband electrodes. Thus, the current responses at 80 different potentials were obtained in one cycle. The currents at the 16 microband electrodes were sampled at least 20 ms after each potential step to eliminate the influence of charging current. The collection and displaying of 80 current signals at different potentials were completed in 0.27 s.

The hydrodynamic voltammogram for this mixture can easily be obtained from a cross section at various times. Figure 4 shows the hydrodynamic voltammogram obtained from the cross section at the peak time of Figure 3b. The voltammogram has two stairs corresponding to the oxidation of two ferrocenes; the first for FMA and the second for FA<sup>+</sup>. The half-wave potentials for FMA and FA<sup>+</sup> were identical with those observed in cyclic voltammetry. The concentration of the ferrocenes can be determined from the height of the steady-state currents. Since each microband electrode has a different potential, cross talk between the electrodes may occur. However, the influence of the cross talk was negligible in this case. The steady-state currents for both ferrocenes linearly increased with concentration over the range 0.1 nmol ( $2 \times 10^{-6}$  M) to 200 nmol ( $4 \times 10^{-5}$  M). The detection limit ( $S/N = 2$ ) was 20 pmol ( $4 \times 10^{-7}$  M).

The results obtained in the present study are summarized in Table I, together with those in flow analyses with the potential scanning detections reported in the literature. The equivalent scan rates in the present method were calculated by dividing the potential range (750 mV) by data acquisition times. Table I also lists the time required to obtain a voltammogram over the potential range of 750 mV. The comparison demonstrates that the present system, especially with 16-channel detection, is superior to the potential scanning

methods in terms of the data acquisition time for voltammograms. Thus, the present system will be particularly suitable for three-dimensional detection by FIA with small injection volumes. Although the detection limit is not satisfactory at the present stage, it will be decreased by improving the flow cell construction and the circuits of the potentiostat. Various applications to biological samples in FIA and liquid chromatography as well as efforts to further refine the technique are now underway in our laboratory.

#### ACKNOWLEDGMENT

We thank Dr. J. R. Selman, a visiting professor of our faculty, for helpful suggestions. This study has been partly supported by Grant-in-Aid for Scientific Research (Nos. 01470076 and 01850175) from The Ministry of Education, Science and Culture, Japan.

#### LITERATURE CITED

- (1) Kissinger, P. T. *Laboratory Techniques in Electroanalytical Chemistry*; Kissinger, P. T., Heineman, W. R., Eds.; Marcel Dekker: New York, 1984; Chapter 22.
- (2) Samuelsson, R.; O'Dea, J.; Osteryoung, J. *Anal. Chem.* **1980**, *52*, 2215-2216.
- (3) Wang, J.; Ouziel, E.; Yarnitzky, C.; Ariel, M. *Anal. Chim. Acta* **1978**, *102*, 95-112.
- (4) Last, J. A. *Anal. Chem.* **1983**, *55*, 1509-1512.
- (5) Scanlon, J. J.; Flaqueur, P. A.; Robinson, G. W.; O'Brien, G. E.; Strock, P. E. *Anal. Chim. Acta* **1984**, *158*, 169-177.
- (6) Reardon, P. A.; O'Brien, G. E.; Sturrock, P. E. *Anal. Chim. Acta* **1984**, *162*, 175-185.
- (7) Thomas, M. B.; Msimanga, H.; Sturrock, P. E. *Anal. Chim. Acta* **1985**, *174*, 287-191.
- (8) Owens, D.; Sturrock, P. E. *Anal. Chim. Acta* **1986**, *188*, 269-274.
- (9) Kounaves, S. P.; Young, J. B. *Anal. Chem.* **1989**, *61*, 1469-1472.
- (10) Owens, D. S.; Johnson, C. M.; Sturrock, P. E.; Jaramillo, A. *Anal. Chim. Acta* **1987**, *197*, 249-256.
- (11) Gunasingham, H.; Tay, B. T.; Ang, K. P. *Anal. Chem.* **1987**, *59*, 262-266.
- (12) Caudill, W. L.; Ewing, A. G.; Jones, S.; Wightman, R. W. *Anal. Chem.* **1983**, *55*, 1877-1881.
- (13) Wang, J.; Dewald, H. D. *Anal. Chim. Acta* **1983**, *153*, 325-330.
- (14) White, J. G.; Claire, R. L. S., III; Jorgenson, J. W. *Anal. Chem.* **1986**, *58*, 293-296.
- (15) White, J. G.; Jorgenson, J. W. *Anal. Chem.* **1986**, *58*, 2992-2995.
- (16) Lunte, C. E.; Ridgway, T. H.; Heineman, W. R. *Anal. Chem.* **1987**, *59*, 761-766.
- (17) Lunte, C. E.; Wheeler, J. F.; Heineman, W. R. *Anal. Chim. Acta* **1987**, *200*, 101-114.
- (18) Matsue, T.; Aoki, A.; Abe, T.; Uchida, I. *Chem. Lett.* **1989**, 133-136.
- (19) Matsue, T.; Aoki, A.; Uchida, I.; Osa, T. *Bull. Chem. Soc. Jpn.* **1987**, *60*, 3591-3595.

Tomokazu Matsue\*  
Atsushi Aoki  
Eiji Ando  
Isamu Uchida\*

Department of Molecular Chemistry and Engineering  
Faculty of Engineering  
Tohoku University  
Aoba, Sendai 980, Japan

RECEIVED for review August 7, 1989. Accepted November 13, 1989.

## Lanthanum Hexaboride Electron Emitter for Electron Impact and Electron-Induced Dissociation Fourier Transform Ion Cyclotron Resonance Spectrometry

*Sir:* Ribbon filaments of either tungsten or rhenium have been used as electron sources for electron impact ionization studies by Fourier transform ion cyclotron resonance spectrometry (FT-ICR) for a number of years. Unfortunately, these filaments are also a major source of down time for these instruments. The primary reason for filament failure is me-

chanical instability resulting in twisting which, in turn, results in a loss of electron throughput due to breakage or misalignment. This twisting is a result of the torque imposed on the filament as a relatively high current (3-4 A) runs perpendicular to the strong magnetic fields employed in many of these instruments. These problems are intensified on in-

struments that use superconducting magnets. In addition, ribbon filaments require considerable power (work functions for W and Re on 4.55 and 4.96 eV, respectively) and operate at high temperatures (ca. 2500 °C) causing heating of the cell and concomitant outgassing. One solution to both of these problems is to mount the filament external to the field as in recent commercial systems.

LaB<sub>6</sub> cathodes (work function 3.5 eV) have been successfully used as thermionic electron emitters (1) in a number of devices including scanning electron and scanning tunneling microscopes and X-ray sources. These emitters have been successfully interfaced with both quadrupole and sector mass spectrometers operated in both chemical ionization (CI) and electron impact (EI) modes (2, 3). They offer several benefits over tungsten-rhenium filaments including (i) decreased power consumption (a few watts) (4), (ii) lower temperature operation (<2000 °C), (iii) increased thermal/mechanical stability, (iv) very tightly focused beams (0.5 mm to 2–3 μm (3)) with current densities of up to 100 A cm<sup>-2</sup> (5), and (v) low evaporation rate (operating at 10 A/cm<sup>2</sup>, the evaporation rate is about 10<sup>-8</sup> g cm<sup>-2</sup> s<sup>-1</sup> (4)) resulting in long emitter lifetime. A 10-fold increase in electron emitter lifetime was observed for a LaB<sub>6</sub> cathode over a rhenium filament operated at conditions generic to CI and EI ionization in quadrupole and sector mass spectrometers (2). In addition, LaB<sub>6</sub> emitters like tungsten and rhenium emitters are inert to repeated exposure to the atmosphere while cool.

There are two principal disadvantages to using LaB<sub>6</sub> electron emitters as electron sources for ionization in mass spectrometry. Namely, these cathodes (i) are expensive with respect to rhenium or tungsten counterparts, and (ii) show chemical sensitivity to electronegative species. It is thought that electronegative atoms (such as O and Cl) bind to the surface increasing the work function and reducing the electron emission. Poisoned cathodes can normally be cleaned by increasing the operating temperature for a short period of time to volatilize the oxidized LaX species (3). Surface oxidation reduces emitter lifetime in direct proportion to the amount of material that is poisoned, and exposure to high pressures (>10<sup>-6</sup> Torr) of oxidizing gases is, therefore, discouraged.

In this note, we discuss the use of a LaB<sub>6</sub> cathode as an electron source for electron impact Fourier transform ion cyclotron resonance spectrometry (FT-ICR). The feasibility of routine use of these emitters is considered in terms of projected lifetime and chemical sensitivity. Because the extremely high electron flux densities can be obtained by these emitters, we have also examined their use for electron induced ion dissociation.

### EXPERIMENTAL SECTION

All experiments were performed on an ICR system built at TAMU and equipped with a Nicolet 1280 computer. The instrument is equipped with a 3-T superconducting magnet (Oxford). The instrument has been described in detail previously (6).

The LaB<sub>6</sub> cathode used for this work (Model ES-423-BF, Kimball Physics) has a circular single crystal plane emitting surface 0.33 mm in diameter (Figure 1). The emitter is mounted in a custom ceramic holder in order to support the cathode rigidly in the magnetic field and to protect it from damage (see Figure 2). The cathode support also holds an extraction lens. The LaB<sub>6</sub> emitter, lens, and holder are mounted as one unit to a trap plate of the ICR cell. The cathode is floated at the desired ionizing potential (10 to -70 V) and electrons are gated to the cell by pulsing the extraction plate from 5 V below to 5 V above this potential.

### RESULTS AND DISCUSSION

LaB<sub>6</sub> cathodes are superior to tungsten and rhenium filaments for most applications, but it was not known if such emitters could withstand the high magnetic fields used in

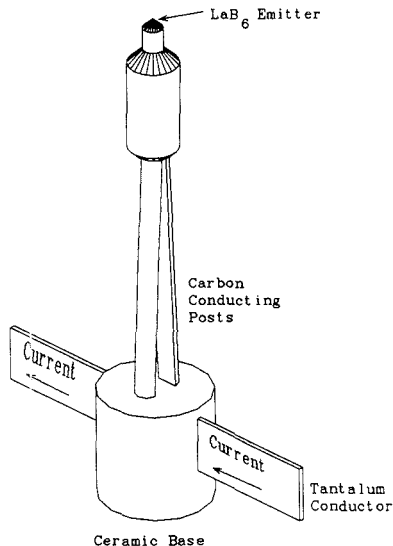


Figure 1 The Kimball Physics ES-423-BF LaB<sub>6</sub> electron emitter. Driving current flows in one tantalum conductor, up one of the conducting carbon posts, through the crystal mounting base, down the other carbon conductor post, and out of the other tantalum conductor.

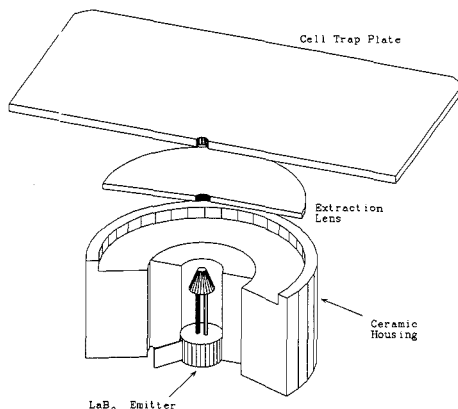


Figure 2 Section view of the electron source used in the studies reported here. The LaB<sub>6</sub> emitter is held in place by a macor receiving cup placed in a macor terminal holder. The extraction lens also fits in the emitter holder assembly.

FT-ICF. It was feared that the current flowing through the cathode would break the carbon posts supporting the crystal emitting surface due to the torque imposed by current flowing perpendicular to the high magnetic field at the emitter's tip. Experimentally, however, these concerns were found to have no basis. The cathode showed no sign of failure upon passing currents of up to 1.9 A while in the magnetic field. Emission currents of 25 nA to 200 μA were obtained on adjusting the driving current between 1.2 and 1.6 A. Outgassing of the cathode and the surrounding ceramic holder was not observed.

For these studies, the electron emitter is mounted at one end of a two-section FT-ICR cell described previously (6). Because the system is differentially pumped, the pressure in the region of the emitter could be maintained at  $2 \times 10^{-8}$  Torr

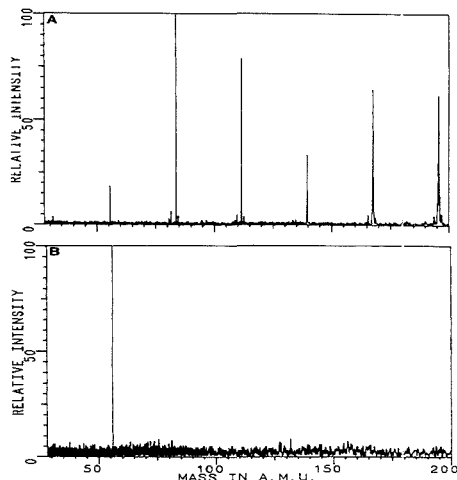


Figure 3. (A)  $\text{Fe}(\text{CO})_5$  ionized by 20-eV electrons for 200  $\mu\text{s}$ . (B)  $\text{Fe}(\text{CO})_5$  ionized by 9-eV electrons for 300 ms.

while the pressure in the ion cell (single cell mode) could be maintained at  $2 \times 10^{-8}$  or less.

The maximum current density for  $\text{LaB}_6$  emitters exceeds that for ribbon filaments by at least a factor of  $2 \times 10^5$  (5), allowing ionization periods to be very short (<60  $\mu\text{s}$ ). Ionization periods of greater than 1 ms can easily result in Coulombic space charge effects between ionized sample molecules. Excellent signal-to-noise ratio spectra were obtained for benzene for ionization periods of 60  $\mu\text{s}$  at sample pressures of  $<10^{-7}$  Torr ( $S/N = 1000$ ; 1000 signal averaged scans). In addition, increase emission current density could have serious ramifications for chemical studies, because the possibility of multiple electron interactions is increased.

As a test of multiple electron interactions, a study of electron impact ionization of  $\text{Fe}(\text{CO})_5$  was performed.  $\text{Fe}(\text{CO})_5$  was admitted to the vacuum system at a static pressure of  $2 \times 10^{-7}$  Torr. Two different ionization conditions were probed. In the first, the electron energy was set to 20 eV for a period of 200  $\mu\text{s}$  at an emission current of ca. 10  $\mu\text{A}$ . The resulting spectrum for these ionization conditions is found in Figure 3A. Note that all the  $\text{Fe}(\text{CO})_x$  ( $x = 0-5$ ) species are present in the spectrum as expected due to the fact that the appearance potentials for all members of this series are less than 20 eV (7). In the second test, the electron energy was set at 9 eV and the ionization period was set to 300 ms. Again, the emission current was maintained at ca. 10  $\mu\text{A}$ . The spectrum for these conditions (Figure 3B) shows that only  $\text{Fe}^+$  is in the cell (appearance energy (AE) ca. 15 eV). On the basis of the appearance energies for the fragment ions, only  $\text{Fe}(\text{CO})_4^+$  (AE = 9 eV) and  $\text{Fe}(\text{CO})_5^+$  (AE = 8 eV)(7) should appear in the spectrum if single electron interactions are occurring. Clearly, multiple electron interactions with  $\text{Fe}(\text{CO})_x^+$  are occurring under the latter conditions. The electron beam flux density for the spectrum in Figure 3A was approximately  $1.5 \times 10^{-3}$  electron/ $\text{\AA}$  and approximately 2 electrons/ $\text{\AA}$  for the spectrum

in Figure 3B. Multiple electron interactions have been observed to cause ion dissociation in FT-ICR studies using conventional ribbon filaments (8, 9).

The potential use of  $\text{LaB}_6$  emitters as high flux density electron sources for electron impact induced dissociation is very promising. Potential studies in this laboratory indicate that polyatomic species can be readily fragmented by using the electron beam produced by these cathodes. Significant fragmentation of benzene was observed by using ionizing electrons with nominal energies between 10 and 12 eV under high flux conditions (i.e. emission current  $>100 \mu\text{A}$ ). Under these conditions, ionization periods of  $<100 \mu\text{s}$  produced  $\text{C}_3$  and  $\text{C}_4$  fragment ions in abundance.

The lifetime of  $\text{LaB}_6$  emitters for operation at a given emission current with reference to a different emission current is given approximately by  $n^{2.45}$  (4). That is, if the emission current is decreased by a factor of 4300, then emitter lifetime increases by  $4300^{2.45}$  or  $8 \times 10^8$ . For our system, operating the emitter at  $0.023 \text{ A cm}^{-2}$  (20  $\mu\text{A}$  emission) should increase its lifetime by  $8 \times 10^8$  times over operating at  $100 \text{ A cm}^{-2}$ . On the basis of an estimated lifetime of 400 h at  $100 \text{ A cm}^{-2}$ , the projected lifetime of the  $\text{LaB}_6$  emitter in the TAMU system is approximately  $3.2 \times 10^{11}$  h without considering chemical degradation.

As mentioned above, LaX species formed by the reaction of electronegative atoms with  $\text{LaB}_6$  increase the work function, thereby poisoning the emissive properties of the cathode. To circumvent this problem, the cathode must be operated at temperatures such that the various oxidized LaX species evaporate at a rate greater than the formation rate of LaX species itself (4) decreasing the expected lifetime by orders of magnitude. Actual performance will depend strongly on the chemical environments to which the emitter is exposed; higher pressures of oxidizing species will dramatically attenuate the lifetime. We anticipate that functional lifetimes will probably not exceed 5000 h under the conditions of the FT-ICR experiment.

Registry No.  $\text{LaB}_6$ , 12008-21-8.

#### LITERATURE CITED

- (1) Lafferty, J. M. *J. Appl. Phys.* **1951**, *22*, 399-309.
- (2) Kelner, L.; Fales, H. M.; Markey, S. P.; Crawford, C. K. *Int. J. Mass Spectrom. Ion Phys.* **1982**, *43*, 249-259.
- (3) Kelner, L.; Markey, S. P.; Fales, H. M.; Cole, P. A.; Crawford, C. K. *Int. J. Mass Spectrom. Ion Phys.* **1983**, *51*, 215-223.
- (4) Crawford, C. K. *Scanning Electron Microsc.* **1979**, *1*, 19-30.
- (5) Höhn, F. J.; Chang, T. H. P.; Broers, A. N.; Frankel, G. S.; Peters, E. T.; Lee, D. W. *J. Appl. Phys.* **1982**, *53*, 1283-1296.
- (6) Kerley, E. L.; Russell, D. H. *Anal. Chem.* **1989**, *61*, 53-57.
- (7) Rosenstock, H. M.; Draxl, K.; Steiner, B. W.; Herron, J. T. *J. Phys. Chem. Ref. Data* **1977**, *6*, 1-520, 1-521.
- (8) Cody, R. B.; Freiser, B. S. *Anal. Chem.* **1979**, *51*, 547-551.
- (9) Cody, R. B.; Freiser, B. S. *Anal. Chem.* **1987**, *59*, 1056-1059.

Eric L. Kerley  
Curtiss D. Hanson  
David H. Russell\*

Department of Chemistry  
Texas A&M University  
College Station, Texas 77843

RECEIVED for review August, 24, 1989. Accepted November 22, 1989. Support for this work was provided by the NSF (CHE-8821780).

## TECHNICAL NOTES

### Elimination of Power Line Noise from Transient Signals by Selective Triggering

Emilie Lasson and Vernon D. Parker\*

Department of Chemistry and Biochemistry, Utah State University, Logan, Utah 84322-0300

Periodic noise originating from the power line is often troublesome in analytical measurements, especially at low signal levels. In recent years a great deal of effort has gone into the development of digital filters to obtain signals free of noise (1). Selection of the trigger interval (TI) can be a useful strategy to reduce the effects of periodic noise. In this paper trigger interval refers to the interval between response evoking trigger pulses. It is commonly believed that the trigger interval should not be an integer multiple of the power line frequency (2). However, Bialkowski has shown that there can be advantages to making the experimental cycle synchronous with the line frequency when a base-line subtraction procedure is used (3). Nielsen and Hammerich (4) use a triggering device with an alternating phase shift so that successive triggers are shifted by 180° relative to the line frequency. We have found that averaging signals obtained by triggering at exact selected intervals is very effective in the elimination of noise at the line frequency and the first overtone. The method is convenient, and the TI can be designed to fit the application at hand.

#### EXPERIMENTAL SECTION

**Instrumentation and Procedures.** Hewlett-Packard HP-3314A function generators were used to trigger Nicolet 310 digital oscilloscopes for recording signals. The current follower output from JS Instrument Systems Model J-1600-B potentiostats provided signals with periodic noise. Sine waves were generated with a Princeton Applied Research selective amplifier Model PAR 189. The oscilloscopes were interfaced to personal computers by using IEEE-488 interfaces. Data manipulations were carried out with FORTRAN programs.

The procedure for selecting trigger intervals involved averaging two successive oscilloscope recordings of a continuous sine wave and comparing amplitudes before and after averaging. TIs were generated with a resolution of 1 ms below 10 s and 10 ms above 10 s. No difference could be detected when triggering was performed with any of five function generators. All TIs possible with this resolution between 1 and 30 s were evaluated. This range of TI values was selected for voltammetry applications, but others outside of this range can readily be evaluated as well.

#### RESULTS AND DISCUSSION

A sample of the data generated during the trigger selection process is shown in Table I. At a trigger interval of 10.36 s the 60-Hz amplitude ratio was about 3000 and that at 120 Hz was nearly 30. A significant feature of the data is that large ratios were observed every fifth 0.01-s increment for the 60-Hz signal while large ratios appear every sixth to seventh 0.01-s increment for the 120-Hz signal. However, it was possible to find TIs, such as that at 10.36 s, where high ratios were observed for both the 60- and 120-Hz signals. For our applications we selected TI values of 1.036, 3.41, 10.36, and 27.6 s.

The effectiveness of the procedure for reducing the amplitude of periodic signals is illustrated in Figures 1 and 2. The amplitude of the sine wave (Figure 1a) was reduced by a factor of about 500 (Figure 1b) when two successive scans were averaged with a trigger interval of 10.06 s. The output of the current follower of a potentiostat at a rest potential of

Table I. Examples of Noise Reduction Factors for Various Trigger Times

trigger time/s	signal intensity ratio <sup>a</sup> at	
	60 Hz	120 Hz
10.26	747	1.3
10.27	1.1	1.0
10.28	3.3	1.3
10.29	2.6	3.3
10.30	1.1	114.8
10.31	1494	6.1
10.32	1.1	1.6
10.33	3.0	1.0
10.34	2.8	1.1
10.35	1.1	2.5
10.36	2986	28.1
10.37	1.1	11.2
10.38	3.0	2.0
10.39	3.0	1.1
10.40	1.1	1.1
10.41	1495	1.8
10.42	1.1	9.3
10.43	2.8	30.8
10.44	3.0	2.5
10.45	1.1	1.2
10.46	747	1.0

<sup>a</sup> The amplitude of the signal before averaging divided by that after averaging two scans.

0 V vs Ag<sup>+</sup>/Ag electrode in acetonitrile-Bu<sub>4</sub>N<sup>+</sup>PF<sub>6</sub><sup>-</sup> (0.1 M) is shown in Figure 2a. Averaging 20 oscilloscope traces taken at a 3.40-s interval (Figure 2b) reduced the high-frequency noise but left the 60- and 120-Hz periodic noise unchanged. Changing the TI by only 0.01 s to 3.41 s resulted in the essentially complete removal of the periodic noise (Figure 2c). The result for a TI of 3.42 s was nearly identical with that shown in Figure 2b.

Measurements over a period of several months have not revealed any significant differences in effective TI. This indicates that any instability in the line noise phase does not significantly affect the utility of the method. It is obvious that large variations in the phase would have a detrimental effect, but we have not experienced problems of this nature.

Electroanalytical chemistry is an area where elimination of power line noise can be essential for quantitative work. This is especially true when ultramicroelectrodes, which give rise to exceedingly low currents, are used in voltammetry experiments. The application of the triggering technique to linear sweep voltammetry is illustrated in Figure 3. The voltammogram recorded at 10 V/s for the oxidation of 9,10-diphenylanthracene (0.5 mM) in acetonitrile-Bu<sub>4</sub>NPF<sub>6</sub> (0.1 M) measured at a platinum disk electrode (*d* = 100 μm) is severely distorted by periodic noise (Figure 3a). Averaging 20 scans with a TI of 10.00 s followed by a fast Fourier transform (FFT) treatment (4, 5) of the data gave a voltammogram in which the 60-Hz component of the noise remained (Figure 3b). The same procedure carried out with a TI of 10.06 s gave a voltammogram free of periodic noise (Figure 3c).

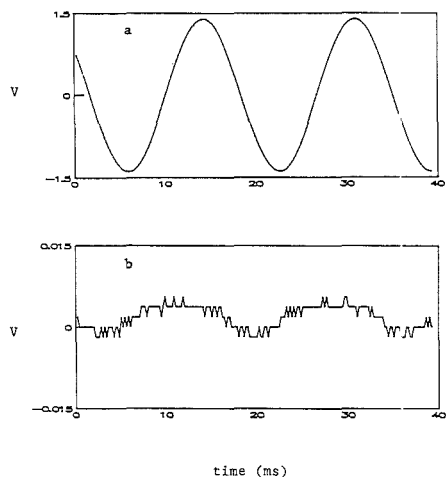


Figure 1. (a) Continuous sine wave (60 Hz) recorded on a digital oscilloscope. (b) Average of two consecutive recordings as in a with a trigger interval of 10.06 s. Note the 100-fold scale change.

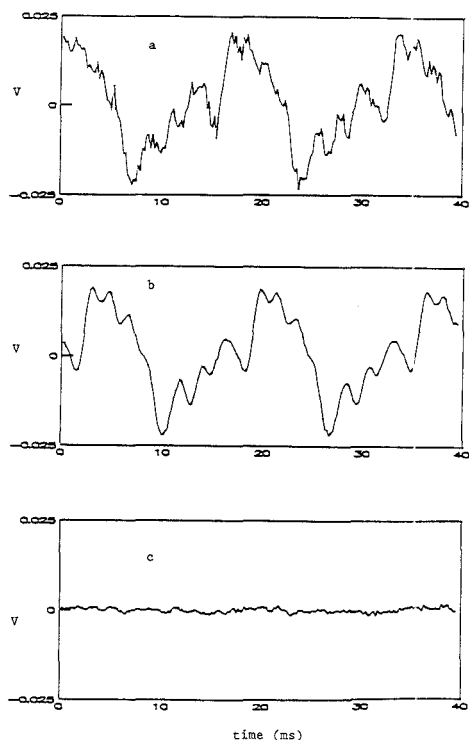


Figure 2. (a) Output from a potentiostat current follower at a constant potential in the absence of Faradaic current. (b) Average of 20 scans with a trigger interval of 3.40 s. (c) Average of 20 scans with a trigger interval of 3.41 s.

The frequency content of linear sweep voltammograms as a function of voltage sweep rate is summarized in Table II. To emphasize the effect of power line noise interference, the number of 60-Hz cycles that appear in a 1-V scan are included

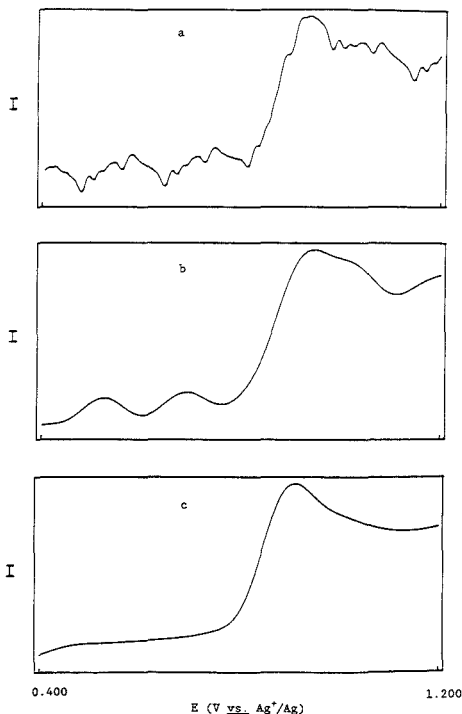


Figure 3. (a) Linear sweep voltammogram for the oxidation of 9,10-diphenylanthracene (0.5 mM) in acetonitrile- $\text{Bu}_4\text{NPF}_6$  (0.1 M) at a voltage sweep rate of 10 V/s. (b) Average of 20 scans with a trigger interval of 10.00 s after treating the data with an FFT procedure. (c) As in b with a trigger interval of 10.06 s.

Table II. Frequency Content of Linear Sweep Voltammograms

sweep rate, V/s	no. of cycles, 60 Hz/scan	freq range, <sup>a</sup> Hz	filter cutoff, <sup>b</sup> Hz
1	240	2-500	40
10	24	20-5000	400
100	2.4	200-50000	4000
1000	0.24	2000-500000	40000

<sup>a</sup>The frequency content of the linear sweep voltammogram using 512 points for a 1 V scan in the FFT procedure. <sup>b</sup>Low-pass filter cutoff used in the FFT procedure.

as well. The frequency content of the voltammetric signals in column 3 are from  $(1/NT)$  to  $(1/2T)$  where  $N$  is the number of points (512) in the FFT procedure and  $T$  is the time per point. The last column gives the FFT filter cutoff. The FFT filter is effective for voltage sweep rates of 1 V/s or less, and 60-Hz noise is not very significant at 100 V/s or higher sweep rates. The problem area is from about 1 to 50 V/s where the FFT filter cannot eliminate the noise due to significant 60-Hz components in the voltammograms. Under these circumstances, a suitably selected TI eliminates the effect of the power line interference.

Trigger intervals that give  $180^\circ$  phase shifts for successive scans may be calculated from eqs 1 and 2 where  $x$  and  $y$  are ideal trigger interval (60 Hz) =  $x(1/60) + 1/120$  (1)  
ideal trigger interval (120 Hz) =  $y(1/120) + 1/240$  (2)

integers. Equating the right-hand sides of the equations shows that  $y = 2x + 1/2$ . It is obvious that ideal TI for the two frequencies cannot be achieved simultaneously, so it is necessary to compromise. We therefore believe that our empirically based procedure for finding suitable TI cannot be greatly improved upon.

We conclude that the use of precise selected TI for repetitive recording of transient signals is a highly effective method of eliminating periodic noise. The method is especially attractive because of its simplicity and convenience of application.

#### ACKNOWLEDGMENT

We thank Dr. Stephen Bialkowski for helpful discussions.

#### LITERATURE CITED

- (1) Bialkowski, S. E. *Anal. Chem.* **1988**, *60*, 355A, 403A.
- (2) Heitja, G. M.; *Anal. Chem.* **1972**, *44*, 69A, 81A.
- (3) Bialkowski, S. E. *Rev. Sci. Instrum.* **1987**, *58*, 687.
- (4) Nielsen, M. F.; Hammerich, O.; Laursen, S. A. *Acta Chem. Scand.*, in press.
- (5) Hayes, J. W.; Glover, D. E.; Smith, D. E.; Overton, M. W. *Anal. Chem.* **1973**, *45*, 277.

RECEIVED for review August 7, 1989. Accepted October 23, 1989. The National Science Foundation (CHE-8803480) is thanked for generous support of this work.

## Real-Time Monitoring of Iodine in Process Off-Gas by Inductively Coupled Plasma-Atomic Emission Spectroscopy

Toshihiro Fujii,\* Takashi Uehiro, and Yukihiko Nojiri

National Institute for Environmental Studies, Tsukuba, Ibaraki 305, Japan

Yoshihiro Mitsutsuka and Hitoshi Jimba

Department of Chemistry, The Meisei University, Hodokubo, Hino 191, Japan

During nuclear fuel reprocessing and waste immobilization, iodine monitors are required on-line to ensure that discharged iodine is within regulation limits (1). Reliable methods are needed that are capable of measuring iodine-129 in real time at or below the maximum permissible concentration of 0.1 part per million (ppm) (v/v) in the off-gas (2). A detection capability of 0.1 ppm would make it possible to attest whether more than 99.6% radioiodine was removed. This would meet the regulation requirement of abatement facilities of the radioiodine in the nuclear fuel reprocessing plants (3). There have been a number of methods for developing such monitors (4).

Fernandez et al. (5) developed a technique that includes cryogenic sample collection, chemical form separation, quantitation by gas chromatography (GC), and isotope dilution mass spectrometry (IDMS). This technique employs negative surface ionization. They concluded that (1) less than 1 ng of  $\text{CH}_3\text{I}$  can be measured by GC, but iodine molecules must be measured by IDMS and (2) isotopic ratios of  $^{127}\text{I}/^{129}\text{I}$  as large as  $10^{-5}$  can be successfully measured on samples as small as 80 ng of iodine. However, this method is not a real-time on-line analysis.

Some on-line measurement instruments based on laser spectrometry have been tested on a laboratory scale. Baronvavski's group (6) used a He-Ne laser to detect  $^{129}\text{I}$  by an extracavity fluorescence configuration. They detected a concentration of  $^{129}\text{I}$  in air in the range of  $2 \times 10^{-7}$  mol/dm<sup>3</sup> (4.48 ppm, (v/v)) and claimed a  $^{129}\text{I}$  detection limit of about  $10^{-10}$  mol/dm<sup>3</sup>. The main disadvantage of this method is interference from nitrogen oxides ( $\text{NO}_x$ ) that are present in the off-gas streams.

Intracavity absorption spectroscopy has been used to detect very weak absorption lines in a number of atomic and molecular species (7). Hohimer and Hargis (8) used a continuous wave (CW) dye laser to detect  $^{127}\text{I}$  and  $^{129}\text{I}$  at 488 nm by intracavity absorption. They detected iodine in the concentration range  $10^{-9}$  to  $10^{-6}$  mol/dm<sup>3</sup> (22.4 to  $(2.24 \times 10^3)$  ppb (v/v)). Gales et al. (9) used a CW dye laser at 580 nm and detected a  $^{129}\text{I}$  concentration of about  $10^{-12}$  mol/dm<sup>3</sup>.

There is no doubt that a gas analyzer based upon electron impact quadrupole mass spectrometry would be very helpful to determine the amount of specific compounds known to be present in air environments. The first application of  $\text{I}_2$  detection has been reported by Matsuoka's group (10). Their results indicate a straight calibration curve for  $\text{I}_2$  peaking at  $m/z$  256 down to a 0.1-ppm (v/v) level of the standard gas sample without noticeable interferences.

As a means of atomizing an analytical sample, inductively coupled plasma (ICP) has been shown to have a remarkable adaptability for the determination of analyte concentrations with a variety of spectroscopic techniques (11). In recent years ICP has found applications in commercial instruments for atomic emission spectrometry (AES), atomic fluorescence spectrometry (AFS), and mass spectrometry (MS). Particularly the ICP-AES, the earliest of these, has come to be a comparatively mature technique due to the accumulated understanding of its function and behavior. According to this knowledge, in contrast to most elements, iodine has its most sensitive spectral lines in the vacuum ultraviolet region. Therefore, spectral lines in the vacuum region were proposed by various authors (12), the first being Kirkbright et al. (13). They purged the monochromator and optical path between the plasma torch and the entrance slit with nitrogen gases and determined a detection limit of 50 ppb for the iodine solution. These considerations led to ICP-AES being a candidate method for iodine monitoring. The advantage of ICP-AES, in principle, is that it is able not only to determine the total concentrations of both the organic and molecular radioiodines in the off-gas stream, but also to offer the potential for a real-time determination.

This paper describes a method for monitoring the gas phase of iodine by ICP emission spectroscopy. The technique uses the spectral lines in the vacuum ultraviolet region with the aid of a vacuum spectrometer. The gas sample containing iodine molecules is fed directly into the plasma.

#### EXPERIMENTAL SECTION

ICP. The equipment used will be discussed with reference to the schematic diagram shown Figure 1. The ICP atomic emission spectrometer (14) used was a vacuum instrument equipped with 45 channels for simultaneous detection. The vacuum polychro-

\* Author to whom correspondence should be addressed.



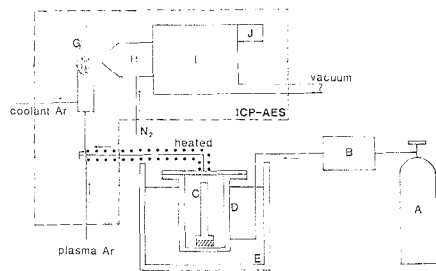


**Figure 1.** Schematics of experimental set-up: A, diluent air gas cylinder; B, thermal mass flow controller; C, diffusion tube; D, diffusion cell; E, water bath; F, T connector; G, ICP plasma; H, optical path extension tube; I, polychromator; J, PMT detector.

mator (I) was Daini Seiko's version of JY 48 PVH (Jobin Yvon, Paschen-Runge type). The main body of the polychromator was evacuated to approximately  $3 \times 10^{-3}$  Torr. The optical path extension tube (H) between the polychromator lens and the plasma discharge (G) extends into the plasma discharge and was purged with nitrogen gas at a rate of approximately 14 L/min. The PMT (J) is a photomultiplier (HAMAMATSU R-306) for the 178.28-nm iodine channel. The lowest usable wavelength for this system is limited to about 160 nm. The radio frequency (rf) generator is a product of RF Plasma Products System and is attached with an autoper control unit (APCS-3) and an automatic matching network unit (AMN-PS-1).

**Standard Gas.** Standard iodine gases were prepared by using the diffusion cell method (15). The diffusion cell (D) system was all-glass and home-built. Three different diffusion tubes (C) (10, 5.6, and 3 mm i.d.; 10 cm long) were purchased from Hokushin Corp. (Tokyo). The diffusion cell chamber was enclosed in a waterbath (E) (K4R D, MGW Lauda, West Germany) equipped with a heater that was operated by a proportional controller. The diluent air gas (reagent-grade air, Takachiho, Tokyo) entered the diffusion cell chamber via a glass flow line. The whole flow line was heated to more than 100 °C. The flow through the diffusion cell chamber was controlled and monitored by a thermal mass flow control system (B) (Model SEC-421 MKII-SS-500-4IS, STEC Corp., Kyoto, Japan), which was situated between the diffusion cell chamber and the diluent gas supply cylinder (A). The standard gas mixture leaves the cell and can be delivered to the ICP plasma for analysis through a T-shaped glass connector (F) while the argon gas flows along by way of the glass connector.

The sample gas concentration was prepared by using either a different diffusion tube or a different temperature of the water bath containing the diffusion tube. The  $I_2$  vapor concentration delivered by the diffusion cell was either determined gravimetrically or calculated from the diffusion equation (16). The agreement between the experimental and theoretical diffusion rates of iodine vapor compares favorably with a difference of less than 10%.

**Procedure.** The sample gas was directed to the ICP-AES. Iodine determination was carried out in a "profile mode" with the standard addition mode. In the profile mode, a wavelength scanning around the set wavelength could be made by moving the entrance slit along the Rowland circle under computer control (up to ca. 0.85 nm, 0.17 pm/step).

The spectrometer optimization was performed by varying the rf power and the carrier Ar gas flow rate at various sample gas flow rates.

The vacuum wavelength of 178.28 nm was taken from the most recently published tabulation (17) and was the most analytically useful emission line. Presumably, it gives a detection capability 20 times higher than that of the 206.16-nm line in the conventional ultraviolet/visible region.

## RESULTS AND DISCUSSION

**Optimization Studies.** The emission intensity of the plasma is proportional to the introduction rate of a sample (grams per second). Therefore, it is advantageous to keep the

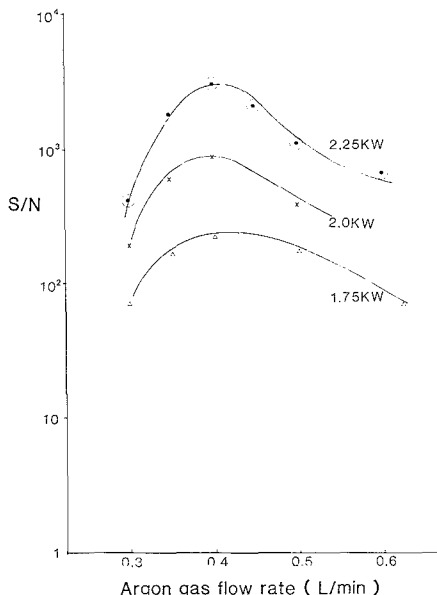


**Figure 2.** Influence of ICP rf power and plasma Ar gas flow rate on the signal to noise ratio (S/N). Data were taken at the sample gas flow rate at 400 mL/min. The ICP rf power is marked on the curve.

sample gas flow rate as large as possible in order to reduce the volume concentration of  $I_2$  to be detected. A higher sample gas flow rate would be beneficial for the detection of lower volume concentration samples. Therefore, optimization should be directed to finding the maximum sample gas flow rate, which was limited to 400 mL/min. Beyond this rate the plasma was unstable and finally was extinguished, even if the Ar flow rate and ICP rf power were varied to achieve good plasma stability.

Figure 2 shows the relationship of the signal to noise (S/N) ratio to the ICP rf power and Ar carrier gas flow rate. These results were obtained under a constant introduction rate of analyte ( $I_2$ , 12.5 ng/s), which was realized by means of the diffusion cell filled with  $I_2$ . A 400 mL/min air gas flowed through the diffusion cell in the 41 °C water bath. This setup allowed the detection of the sample gas volume concentration as low as 0.17 ppm. This study revealed that the S/N value increased with increasing rf power supplied to the ICP at the optimum Ar gas flow rate. This suggests the use of the highest power available (at present, 2.5 kW). At this level the plasma torch becomes very hot and may start to erode. Therefore, for safety reasons, the ICP was operated at no more than 2.25 kW of power.

The relationship between S/N ratio, ICP power, and Ar carrier gas flow rate was investigated as a function of air sample gas rates of 50, 100, 200, and 400 mL/min. As far as the best detection capability at the lowest  $I_2$  concentration in the air is concerned, good operational conditions should be obtained by comparing the product of the S/N value and the sample gas flow rate. In conclusion, the sample gas rate of 400 mL/min and the plasma Ar gas rate of 0.4 L/min at the 2.25-kW rf power represented optimal conditions and hence were used throughout the experiments.

**Response Characteristics.** Under the conditions described above, the following response characteristics were determined: the sensitivity, the linearity, and the detection limit (DL, the minimum detectable amount). All quantities

were examined by using the standard gas of the diffusion cell method. For these measurements, a plot of ICP response during 3-s integration was measured against the iodine concentration. When the signal is expressed in counts, this plot yields a sensitivity,  $S$ , of  $2.9 \times 10^6$  (counts/s)/ppm.

Detection response was linear over the chosen range of 0.16–11 ppm standard gases for iodine.

Three times the standard deviation of the noise measured with the sensitivity gives the DL as 0.19 ppb, which corresponds to 0.014 ng/s at the sample gas rate of 400 mL/min. This value is reasonably consistent with the following consideration. The limits of detection are reported on the order of 50 ppb (17) when the water solution of iodine is supplied to the nebulizer. On the assumption that the nebulizer efficiency to the plasma is 2% with the water sample uptake rate at 1 mL/min, we can calculate the DL for the iodine in case that the whole analyte is introduced for the analysis:

$$1 \text{ mL/min} \times 59 \text{ ng/mL} \times 0.02 \times 1/60 = 0.017 \text{ ng/s}$$

This result is in good agreement with that obtained for the DL of iodine in an air sample.

The precision of the method was determined from replicate analyses (five times) of the standard sample gas at a 0.16-ppm concentration of iodine in the air when the standard deviation was 1500 counts and the relative standard deviation was 0.2% using the peak counts.

**Concluding Remarks.** This study demonstrated that the detection of iodine by ICP-AES in a vacuum ultraviolet region meets the requirements for a real-time and sensitive monitor. The real-time determination can be realized by a plot of the integration of responses during short, i.e. seconds, periods. Scaling estimates indicate that a concentration level of 0.19 ppb (v/v) in air may be achieved. This method also offers the potential for rapid determination of total iodine in the mixture sample containing the various iodine compounds.

It should be noted that further study is needed to investigate the possible source of interference of iodine determination among air components and other off-gas components and to examine the reproducibility of signals over long periods of time.

A final note is that for actual interfacing, an ICP-AES apparatus with a high-volume sampling pump, capable of sampling directly from the fuel reprocessing plants, should be incorporated into a mobile laboratory.

#### ACKNOWLEDGMENT

We are grateful to S. Matsuoka, H. Kishi, and H. Kawano for helpful discussion and to Phillip R. Sandfur and M. L. Messersmith at Yokota Air Base for the manuscript preparation.

**Registry No.** Iodine, 7553-56-2.

#### LITERATURE CITED

- (1) United States Regulations 40 CFR 190, 1977.
- (2) Hebel, W., Cottone, G., Eds. *Management Modes for Iodine-129*; Harwood Academic Publishers: New York, 1982.
- (3) Kawano, H.; Matsuoka, S.; Fujii, T.; Tsuchiya, M.; Fumoto, H.; Kishi, H. *Mass Spectrosc.* **1986**, *34*, 249.
- (4) Moine, R. *Monitoring of Radioactive Effluents from Nuclear Facilities*; Proceedings of the International Symposium on the Monitoring of Radioactive Airborne and Liquid Releases from Nuclear Facilities, Portoroz, Yugoslavia, Sept 1977; International Atomic Energy Agency: Vienna, 1978; p 181.
- (5) Fernandez, S. J.; Rankin, R. A.; McManus, G. J.; Nielson, R. A. *Proc. 18th IOA Air Cleaning Conf.* **1985**, *2*, 1318.
- (6) Baranavskii, A. P.; McDonald, J. R. *NRL Memo. Rep.* **1977**, No. 3514.
- (7) Peterson, N. C.; Kurylo, M. J.; Braun, W.; Bass, A. M.; Keller, R. A. *J. Opt. Soc. Am.* **1971**, *74B*, 61.
- (8) Hohimer, J. P.; Hargis, P. J., Jr. *Anal. Chem.* **1979**, *51*, 930.
- (9) Goles, R. W.; Fukuda, R. C.; Cole, M. W.; Brauer, F. P. *Anal. Chem.* **1981**, *53*, 776.
- (10) Matsuoka, S.; Ito, Y. *Iodine Analysis*; Tokyo University Nuclear Engineering Research Laboratory Report (Japanese), UTNL-R-0174/43, 1984.
- (11) Fasse, V. A.; Kniseley, R. N. *Anal. Chem.* **1974**, *46*, 1110A.
- (12) Wallace, G. F. *At. Spectrosc.* **1980**, *1*, 38.
- (13) Kirkbright, G. F.; Ward, A. F.; West, T. S. *Anal. Chim. Acta* **1972**, *62*, 241.
- (14) Uehiro, T.; Morita, M.; Fuwa, K. *Anal. Chem.* **1984**, *56*, 2020.
- (15) Miguel, A. H.; Natusch, D. F. S. *Anal. Chem.* **1975**, *47*, 1705.
- (16) Altsullar, A. P.; Cohen, I. R. *Anal. Chem.* **1960**, *32*, 802.
- (17) Nygaard, D. D.; Leighty, D. A. *Appl. Spectrosc.* **1985**, *39*, 9968.

RECEIVED for review June 5, 1989. Revised manuscript received November 15, 1989. Accepted November 20, 1989. This work was supported in part by a Grant-in-Aid for Scientific Research (No. 60880026) from the Education Ministry in Japan.

# We'll put all the ~~most~~ advances in the chemical sciences right in your hands... And you won't need to lift a finger!

## AMERICAN CHEMICAL SOCIETY STANDING ORDER PLANS

The ACS has a simple way to ensure that your library always has the chemistry titles your patrons require. It's called the ACS Standing Order Plans.

With ACS Standing Order Plans, you can save the time you'd otherwise spend on literature searches and purchase order details . . . and make certain that your library has the titles your patrons want—when they need them.

### AS EASY AS 1-2-3

You can select from three Standing Order Plans—choose one or all or a combination . . . whatever best suits your patrons' needs!

1.

#### By Series:

Advances in Chemistry Series  
ACS Symposium Series  
ACS Monographs  
Professional Reference Books  
All ACS Series

2.

#### By Single Title:

ACS Abstract Books  
ACS Directory of Graduate Research  
College Chemistry Faculties

3.

#### By Subject:

Analytical • Agricultural/Agrochemical • Biological • Biotechnology • Carbohydrate • Cellulose/Paper/Textile • Colloid/Surface • Computers in Chemistry • Electronic Materials • Environmental/Chemical Health and Safety • Food/Flavor • Energy/Fuel/Petroleum/Geochemistry • Industrial/Chemical Engineering • Inorganic • Materials Science • Medicinal/Pharmaceutical • Nuclear • Organic • Polymer/Applied Polymer Science • Physical Chemistry

PLUS FIVE NEW SUBJECT AREAS . . . Chemical Information • Directories • History • Non-Technical • Toxicology!

You tell us which Standing Order Plan (or Plans) you'd like—1, 2, 3, or a combination. Your one-time order assures prompt, automatic delivery of each new title in the plan or plans you've chosen as soon as it's published. We'll send you an invoice with your shipment. You'll have thirty days to examine each new book and (if you decide for any reason) to return it for full credit. And you may modify or cancel your Standing Order Plan at any time. It's that easy!

Make sure your chemistry resources are always complete—don't overlook a single book from the world's most respected publisher in the chemistry field. Enroll in ACS Standing Order Plans today.

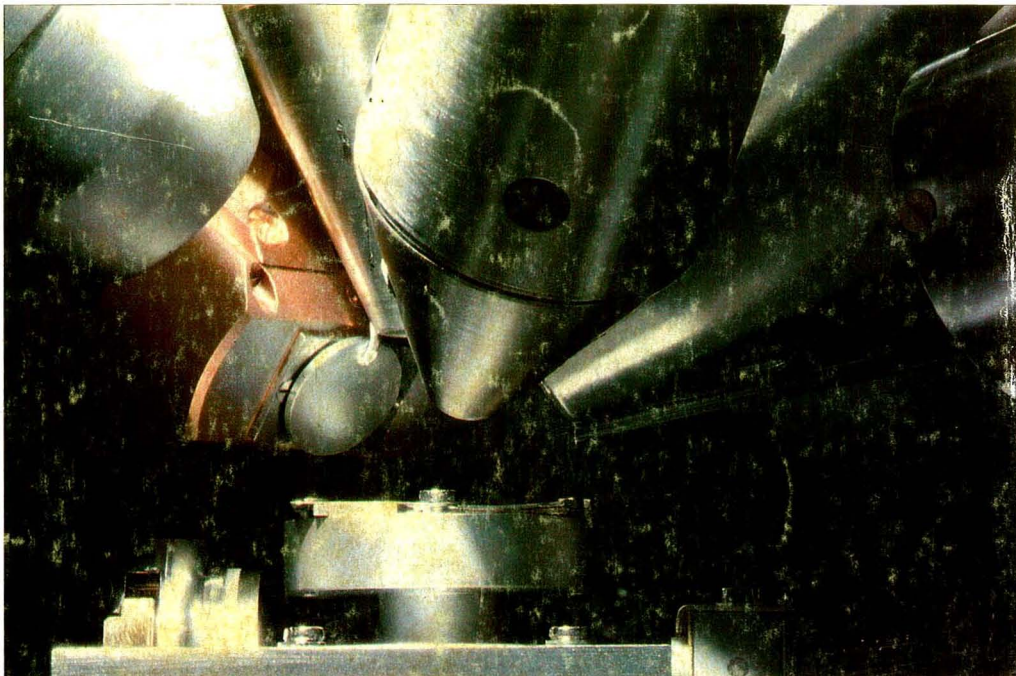
Write to American Chemical Society, 1155 Sixteenth Street, N.W.,  
Washington, DC, 20036. Or call us TOLL FREE (800) 227-5558.

25 TO  
CHOOSE  
FROM!

# GET TO THE POINT!

CD-Bonn

190.0.61.23.003.02



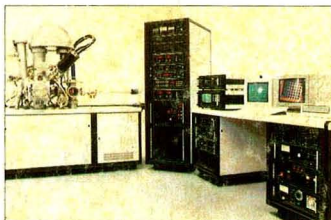
## With MAX – the Multi-Method System for High Precision Surface Analysis

When several different surface analysis methods are required to solve a problem, MAX holds the key to success. All excitation sources point to the same spot on the sample.

As an analysis proceeds step by step, one technique after another is applied, in the same system, without moving either sample or source.

- X-ray Photoelectron Spectroscopy (XPS)
- Scanning Auger Electron Spectroscopy (SAM)
- Ion Scattering Spectroscopy (ISS)
- Secondary Ion Mass Spectrometry (SIMS)
- Sputtered Neutral Mass Spectrometry (SNMS)

To find out how MAX can help you to "Get to the point", contact us at: (412) 327-5700.



Visit us at Booth 1128, Level 1  
PITTSBURGH CONFERENCE  
Javits Convention Center, N.Y.C.  
March 5–8, 1990

■ LEYBOLD VACUUM PRODUCTS INC. LAS GROUP  
5700 Mellon Road, Export, PA 15632

■ LEYBOLD AG  
Bonner Strasse 498, D-5000 Cologne 51, West Germany



*Innovative Vacuum Technology*

A Degussa Company

CIRCLE 75 ON READER SERVICE CARD